LASER ORBITAL TRANSFER VEHICLE

Project SLICK

NASA / USRA Advanced Design Program
June 1988

Department of Aerospace & Ocean Engineering
Virginia Polytechnic Institute & State University
Blacksburg, Virginia.

NASA / USRA 1988
DESIGN PROJECT

SPACE-BASED LASER-POWERED ORBITAL TRANSFER VECHICLE (PROJECT SLICK)

Department of Aerospace & Ocean Engineering
Virginia Polytechnic Institute & State University
Blacksburg,Virginia.

ABSTRACT

This report presents a conceptual design study of a laser-powered orbital transfer vehicle (LOTV). The LOTV, nicknamed SLICK (Space Laser Interorbital Cargo Kite), will be utilized for the transfer of 16000 kg of cargo between Low Earth Orbit (LEO) and either Geosynchronous Earth Orbit (GEO) or Low Lunar Orbit (LLO). This design concentrates primarily on the LEO/GEO scenario, which will have a typical LEO-to-GEO trip time of 6 days and two return versions. One version uses an all-propulsive return while the other one utilizes a ballute aerobrake for the return trip. Furthermore, three return cargo options of 16000 kg, 5000 kg (standard option), and 1600 kg are considered for this scenario. The LEO/LLO scenario uses only a standard, aerobraked version.

The basic concept behind the LOTV is that the power for the propulsion system is supplied by a source separate from the LOTV itself. For the LEO/GEO scenario the LOTV utilizes a direct solar-pumped iodide laser and possibly two relay stations, all orbiting at an altitude of one Earth radius and zero inclination. An additional nuclear-powered laser is placed on the Moon for the LEO/LLO scenario. The propulsion system of the LOTV consists of a single engine fueled with liquid hydrogen. The laser beam is captured and directed by a four mirror optical system through a window in the thrust chamber of the engine. There, seven plasmas are created to convert the laser beam energy into thermal energy at an efficiency of at least 50%. For the LEO/LLO scenario the laser propulsion is supplemented by LH2/LOX chemical thrusters.

i

ACKNOWLEDGEMENTS

PROJECT TEAM/ORGANIZATION

Project Advisor:	Dr. A. K. Jakubowski
Graduate Student:	Dan Boyer (Cost Analysis)
Team Leaders:	Jim Hornbeck John P. Keady Steve Nanney Jack Peters
Orbital Mechanics:	Andrew Crenshaw (group leader) Anthony Ferraro Dave Golden Leo H. Hoffman III Rich McNally Jack Scheible
Optics:	Steve Dowling (group leader) Dan Kubitz (group leader) Chris Hetreed Rod Maclean Dave McCulloch Steve Nanney
Propulsion:	Kevin Allinger (group leader) Rick Ellis Ken Grossman Jim Hornbeck John P. Keady Lisa Luxford Glenn Poplawski
Aerobrake:	Tim Duffie (group leader) Tim Beavers Rodney Bowersox Melanie Clay Doug Lewis Mark Roberts Brian Smith Brian Taminger
Structures:	Susan Gilley (group leader) Ken Clark Ken Duffie Mark Hametz Tim Marquart Jack Peters Clyde Simmerman
Documentation:	Steve Nanney
Model:	Anthony Ferraro Brian Smith
special aid from:	Tuan Chu

TABLE OF CONTENTS

SLICK

I am a kite high in the sky
Pursuing my orbital race
Far into outer space.
But the interesting thing
I don't glide on a string,
Only on a laser beam
Thanks to
Virginia Tech Team.

- Mary Jakubowski

1. INTRODUCTION

1.1 PROJECT BACKGROUND

One of the next major steps in NASA's Space Program is to put a
space station in orbit about the Earth. With this accomplishment
the gateway to space will be opened wider than ever, creating
many new opportunities and challenges for the Space Program. In
order to meet these opportunities and challenges, the
transportation of cargo between Low Earth Orbit (LEO) and
Geosynchronous Earth Orbit (GEO) and eventually between LEO and
Low Lunar Orbit (LLO), will be greatly needed. The most
economical way to perform these missions will most likely be
through the use of an unmanned Orbital Transfer Vehicle (OTV).

Each year the Senior class of Aerospace Engineering at Virginia
Polytechnic Institute and State University engages in a number of
year-long aerospace system design projects. For the Class of
1988, one of the major projects was the development of a
conceptual design for an unmanned Laser-powered Orbital Transfer
Vehicle (LOTV). This design concentrates primarily on the
LEO/GEO scenario and more specifically, the nonaerobraked, or all
propulsive, version of this scenario. However, an aerobraked
version for this scenario and one for the LEO/LLO scenario are
also considered.

The concept of the LOTV is based on the idea of placing the power
source for the propulsion system in a separate orbit from the
vehicle itself. For this design the power source is a direct
solar-pumped iodide laser orbiting at an altitude of one Earth
radius and zero inclination. The Laser Power Station (LPS) fires
a laser beam at the vehicle, where the beam is focused inside the
thrust chamber of the engine, creating a plasma in the flow of
the propellant. As the plasma absorbs energy from the laser
beam, it converts the laser beam energy into the thermal energy
of the propellant, which in turn causes the propellant to heat up
and expand through a nozzle to produce thrust.

The LOTV is a compromise between using as little fuel as possible
and having the smallest trip time possible. At one extreme is

the chemical OTV, which is associated with high thrust and relatively low specific impulse, resulting in short trip time and a high fuel to payload mass ratio. At the other extreme is the electric propulsion system characterized by low thrust and very high specific impulse, resulting in a low fuel to payload mass ratio but a long trip time. The LOTV has a moderately low fuel to payload mass ratio while trip time from LEO to GEO or back is still reasonable.

1.2 PRIMARY DESIGN CRITERIA

Since there is essentially no current technology on LOTV's, there were few mission requirements presented with the concept description. Table 1.1 presents the few assumptions and requirements that were established in Fall, 1987 through communications with NASA Langley. These requirements were the starting point for this design. In addition to the initial requirements, five major criteria are considered in the LOTV design process.

The most important of these criteria is to maximize the ratio of the payload mass to the propellant mass and to the dry vehicle mass. The advantages of this maximizing process are obvious. The less fuel that is required to transfer a cargo, the more economical the vehicle is, and the amount of fuel required is dependent upon how massive the vehicle is. Thus, many aspects of the design process are reiterated in order to minimize the mass of each component of the LOTV.

It is essential that a transfer vehicle have the capability to carry cargos with different masses and sizes for different missions. Otherwise, a seperate vehicle would have to be built for every different sized cargo. Furthermore, as changes occur, such as the placement of refueling stations in both GEO and LEO instead of just LEO, the vehicle should have the capability of being altered to meet these changes instead of building an

Table 1.1 Basic Assumptions and Requirements

Laser type	Direct Solar Pumped Iodide
Laser wavelength	1.315×10^{-6} m
Transmitting aperture	30 m
Window peak power density	> 25 kw/cm^2
Propellant	Hydrogen
Cargo mass	16000 kg maximum
Orbit transfer: LEO - GEO	2 - 3 weeks maximum
LEO - LLO	4 weeks maximum

2

entirely new one. Thus, the flexibility of the LOTV for cargo
and fuel capacity is essential to its feasibility.

Two more of the design criteria are the LOTV's reusability and
reliability. As mentioned before, it would not be economical to
use the vehicle once, discard it, and then build a new one.
Therefore, the reusability of all parts except, perhaps, the
aerobrake, is an important part of making the LOTV feasible for
its purpose. Obviously, the LOTV must also maintain its
reliability throughout this reusability lifetime in order for it
to be an economical method of transferring cargo.

The last of the primary design criteria essentially incorporates
all of the previous four. It is to design the LOTV so that it
can be built and operated at reasonable costs. The most
important factor in reducing costs is maximizing the mass ratios
mentioned above. By reducing the dry vehicle mass, less
propellant is required to propel the vehicle, and the less
propellant that is required to transfer the same cargo, the more
econical the LOTV is. Also, the ability to adjust the LOTV to
meet changing needs so that it can be reused many times is
extremely important in creating a vehicle that is more economical
that its competitors.

1.3 MISSION ASSUMPTIONS AND TECHNOLOGICAL REQUIREMENTS

There are two obvious but major assumptions made in order for the
LOTV to be operationsl. The first of these is that the space
station is well established for its in-space operations. Because
the LOTV will be too massive to be launched from Earth, it will
be launched in parts, requiring the availability of heavy-lift
vehicles. These parts will be taken to the space station, where
the LOTV will be assembled and launched. Thus, the space station
must be completely functional with the manpower and robotic
capability required to assemble and launch the LOTV.

The second obvious assumption is that the LOTV's power sources
are operational at the time of the LOTV's launch. First, the LPS
must be placed in its orbit of one Earth radius and zero
inclination. Furthermore, it is desirable to have two relay
stations in the same orbit as the LPS, one 120 degrees ahead of
the LPS and the other 120 degrees behind it. Although the LOTV
has the capability to operate without the relay stations, the
presence of relays removes constraints related to the line-of-
sight between the LOTV and the LPS. Also, it is assumed that the
nuclear-powered laser will be established on the Moon by the time
the LOTV is ready for lunar missions.

Since the LOTV will not be ready for missions until the early
twenty-first century, several aspects of the LOTV are highly
dependant upon technological advances made by that time. For
this design, the technology level for 2000 - 2010 has been
generally assumed. In some cases improvements in existing
technology is all that is required. For example, in order to get
large mirror surfaces to the degree of accuracy that is required

for the LOTV, large improvements will have to be made in the methods of finishing large mirrors. Also, significant advances will have to be made in the accuracy of pointing and tracking to meet the degree of accuracy required for the LOTV.

In other cases entirely new technology, specifically in the field of materials engineering, is required. Examples of this requirement can be found in both the optical and propulsion systems. First, the optical system requires new materials to make a foldable mirror that will withstand both the space environment and the stresses of being stored and redeployed every mission. Secondly, the propulsion system requires the development of new materials for the window of and the inside lining of the thrust chamber. Although the current window material has a high transmissivity, a new material with an even higher one is needed to simplify the cooling processes of the window. A reflective material that can withstand the temperatures within the thrust chamber is greatly needed to increase the efficiency of th engine as well as further simplify the necessary cooling processes.

As stated earlier, the LOTV will be assembled at the space station. Therefore, new space construction techniques will have to be developed and perfected before the LOTV is ready for use.

1.4 GENERAL MISSION SCENARIO

There are three basic scenarios for the LOTV. The initial steps of the two LEO/GEO scenarios are essentially the same. First, the LOTV will refuel and pick up cargo in LEO. Then, the LOTV will use a multi-impulse elliptical transfer to increase the apogee and then the perigee of its orbit to bring it into GEO. Then, further propulsive maneuvers will bring the LOTV to a zero degree inclination, where the payload will be dropped off and the return payload will be picked up. It should be noted here that the time required to complete these stages will be greatly decreased if two relay stations are placed in the same orbit as the LPS. This is due to the fact that without them, there will be times when the LOTV and the LPS line up with the Earth in between them. Thus, the LOTV will continue to orbit without the ability to do propulsive maneuvers until the Earth is no longer in the line-of-sight.

For the all-propulsive scenario the return trip to LEO will simply be a reverse of the LEO-to-GEO steps. However, for the aerobraked LEO/GEO scenario the plane change will not be made until the aerobraking process. The aerobraked LOTV will make propulsive maneuvers to reduce perigee until it lies within the fringes of the atmosphere. Then, the aerobrake will be deployed, friction will redue the speed of the vehicle, thereby lowering apogee, and the necessary plane change will be made to bring the LOTV back to LEO, where the return payload will be dropped off.

The LEO-to-LLO transfer consists of spiral-elliptical maneuvering into a high apogee, elliptical orbit, a trans-lunar injection

performed by two low-thrust chemical thrusters, a 22.5 degree
plane change, and an LLO injection and circularization to bring
the LOTV into the desired orbit where the payload is dropped off.
The return payload is picked up, and then the LOTV, powered by
the lunar laser, will spiral out and be aided by the chemical
thrusters into a trans-Earth injection. After the LOTV reaches
an elliptical orbit about the Earth, the same process as in the
LEO/GEO aerobraked scenario will be followed to reach LEO.

1.5 DESIGN EVOLUTION/VEHICLE CONFIGURATION

The initial LOTV design configuration was based on information
and data presented in reference 1. This configuration consisted
of a single engine with a window in the top of the thrust
chamber, a single inflatable mirror, and an aerobrake (see
figure 1.1). At this time there were only two versions, one for
the LEO/GEO scenario and one for the LEO/LLO scenario. The only
differences between these two versions were the sizes of the
various components of the LOTV. Using some conservative
assumptions on laser beam divergence through space, capture
diameters of 34 meters and 60 meters for the mirror were obtained
for the LEO/GEO and LEO/LLO scenarios, respectively. These
mirrors would focus the laser beam inside the thrust chamber in
order to form a single plasma, and they rotated about their focal
points in order to capture the beam coming in from different
directions and still reflect the beam to the same place at all
times.

At the beginning of the design process, several different
trajectories were considered for transfering from LEO to GEO.
These trajectories included the simple, near-minimum energy

FIGURE 1.1 INITIAL CONFIGURATION
WITH INFLATABLE MIRROR
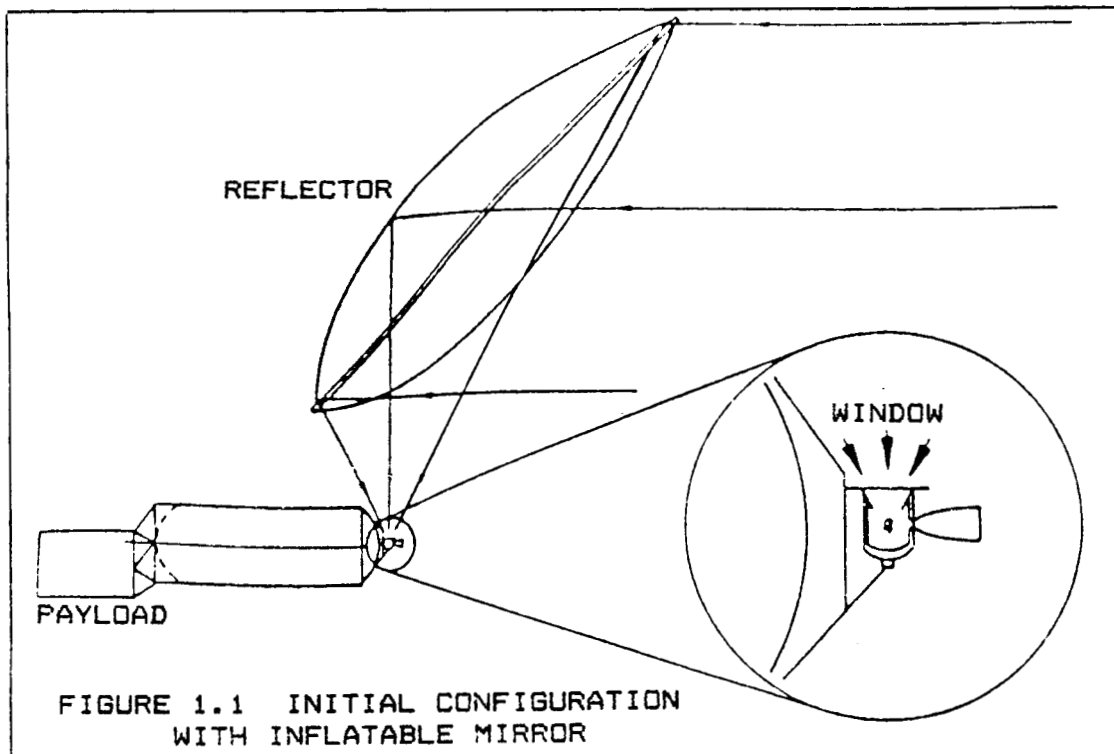
Hohmann transfer, a spiral transfer, a precessional, elliptical transfer, and a multi-impulse elliptical transfer. It turned out that the LOTV will not have enough thrust to perform the Hohmann transfer. The spiral transfer requires continuous thrusting and was therefore discarded because this would greatly limit the flexibility of the LOTV. The multi-impulse elliptical transfer was finally chosen for transfering the LOTV from LEO to GEO because it is much simpler than the precessional, elliptical transfer.

As the various components of this configuration were analyzed, the engine and mirror were both found to have rather low efficiencies. To improve the thermal efficiency of the engine, the window was moved from the top of the thrust chamber to the front. To accomodate the new location of the window, a much smaller second mirror was placed in front of the window. Now the first, or primary mirror would deflect and focus the laser beam onto the second mirror, which would in turn focus the beam inside the thrust chamber. However, it was found that a large part of the energy from the laser beam was being lost through inefficiencies in the primary mirror. Therefore, several different designs were studied in order to find a mirror of higher optical efficiency. These designs included such mirrors as the hoop-column and wrap-rib. The wrap-rib mirror was finally chosen for efficiency and ease of deployment.

Meanwhile, both a rigid and an inflatable ballute aerobrake were being studied to find the one most suitable for the LOTV. Because mass was one of the utmost considerations in this design, the rigid aerobrake was soon discarded in favor of the ballute. In order to allow for more stability and flexibility in aerodynamic performance during aerobraking, it was decided to form the ballute aerobrake from three separate bags joined together to form the single aerobrake. These individual bags will be inflated or deflated as needed to increase the vehicle stability. In order to accommodate this aerobrake design, a triangular shape was decided upon for the main structure of the vehicle. In this configuration the aerobrake would be stored in a rigid cap structure placed on the bottom of the vehicle towards the back (see figure 1.2). After the engine's final thrust before aerobraking, the cap would swing up to cover the engine, thereby protecting it for the aerobraking procedure, and the reaction control system would fire in order to turn the LOTV through 180 degrees. This procedure is necessary because the aerobrake is located at the back of the vehicle and must be on the leading side of the vehicle befor reentry. Then, the three bags would be inflated to complete the aerobrake.

As calculations of the optical system continued to be made, it was found that the surface area of the primary mirror required to redirect the beam through 90 degrees, as would be needed for the two mirror system, would be excessively large. Thus, the optical system was changed to a four mirror system supported by a 36 meter truss structure (see figure 1.2). The entire truss structure rotated on a turntable placed directly above the fourth

mirror, which was placed directly in front of the thrust chamber window. In this optical truss structure (OTS) design, a large part of the structure extended off the back of the ship when the structure was parallel to the main structure of the vehicle (figure 1.2). Calculations soon revealed that the plume coming out of the engine would quickly destroy that part of the OTS extending into the plume. Thus, the four mirror system was altered so that the OTS extended from the front of the vehicle instead of the back (see figures 1.3 and 1.4). This configuration placed the turntable and therefore the fourth mirror, as well, at the front of the vehicle.

At this time calculations revealed that an aerobrake might not actually save enough fuel on the return trip to LEO from GEO to warrant its use. Therefore, the focus of the design of the LOTV switched from an aerobraked version to a nonaerobraked, or all-propulsive, version. Only the aerobraked version was considered for the LEO/LLO scenario; however, both an aerobraked and a nonaerobraked version were considered for the LEO/GEO scenario. The major changes made in the nonaerobraked version were that the optical system no longer had to be stored and the shape of the vehicle no longer needed to be triangular. Thus, a hexagonal shape was chosen for this version to allow for better support of the fuel tanks.

Since the primary mirror of the optical system no longer had to be stored, a rigid mirror was considered in order to increase the overall efficiency of the system. Although the mass of a 34 meter diameter rigid mirror was excessively high, completely revised calculations of long distance laser beam transmission based on jitter values and optical mirror qualities projected for 2000 resulted in greatly reduced mirror sizes. As a result the 60 meter mirror was dropped; the 34 meter mirror was adopted for the LEO/LLO scenario, and work soon began on the design of an 11.5 meter rigid mirror.

Also at this time, it was realized for the aerobraked versions that to turn the ship around 180 degrees before and after aerobraking would require too much additional fuel for the reaction control system. Therefore, the original cap of the aerobrake was discarded and a new one was designed. This cap structure, as seen in figure 1.4, is also stored underneath the LOTV, but this structure was designed to slide forward and lock into the docking apparatus at the front of the vehicle. Thus, the aerobrake will already be on the leading side of the vehicle, and no control maneuvers have to be made.

Another major design change made at this time was the change to a multi-plasma engine. A seven plasma engine was chosen to increase the efficiency of the engine. This change, however, also required the window and the fourth mirror to be redesigned to have seven facets, matching the seven plasmas. The fourth mirror was changed to a variable optics mirror with a circular, center facet and six surrounding facets. As this mirror reflects the laser beam, it breaks it up into seven sections to pass

through the seven facets of the window, and each section of the beam is focused to form its corresponding plasma.

This was the last major design change made on the LOTV. The remainder of the design process consisted of an iterative procedure of making necessary corrections and evaluating the effects of these corrections on the other parts of the vehicle until a final design was achieved. Figures 1.3 and 1.4 show the final configurations of the LEO/GEO non-aerobraked and aerobraked versions, respectively.

1.6 REFERENCES

1. Jones, W. S. et al, "Laser Rocket System Analysis." NASA CR-159521, Lockheed Missiles & Space Company, 1978.

FIGURE 1.2 EARLY CONFIGURATION
WITH FOUR MIRROR SYSTEM
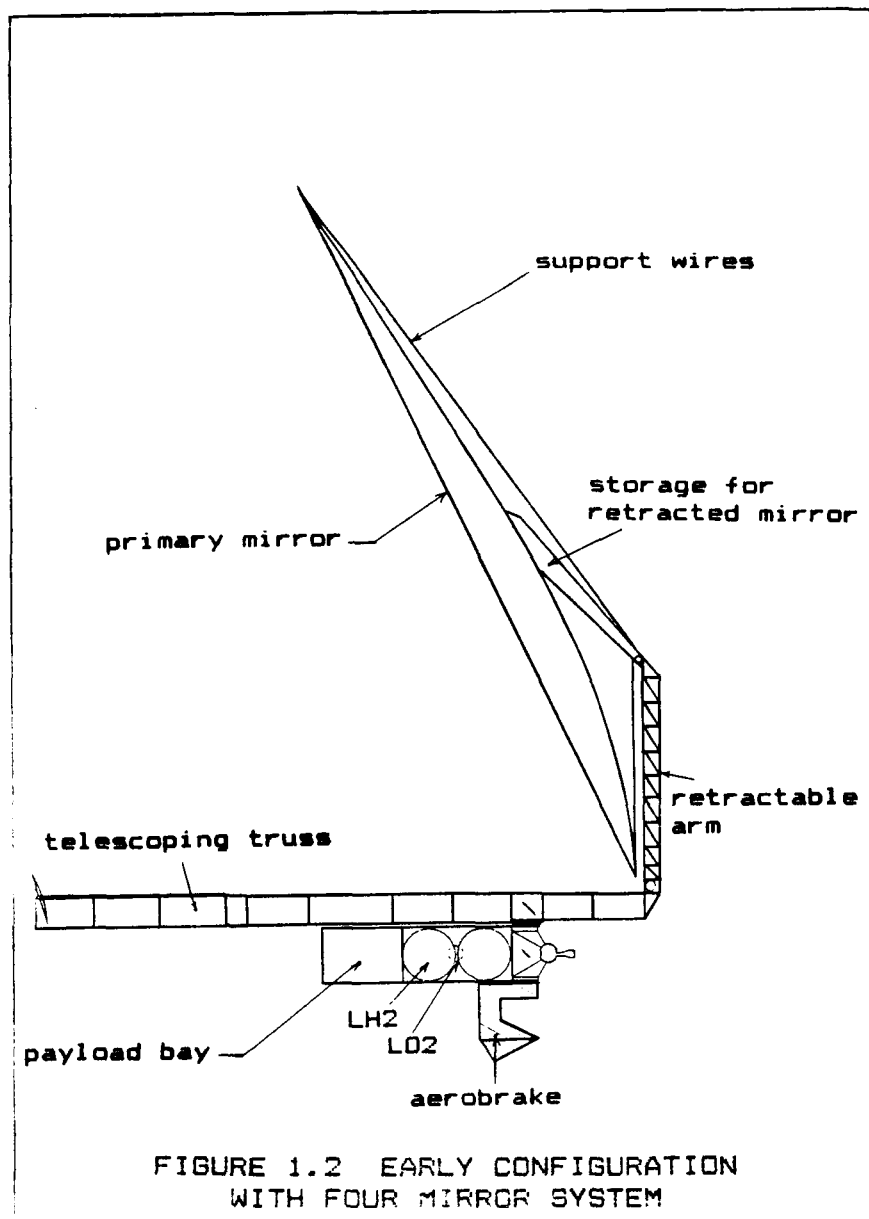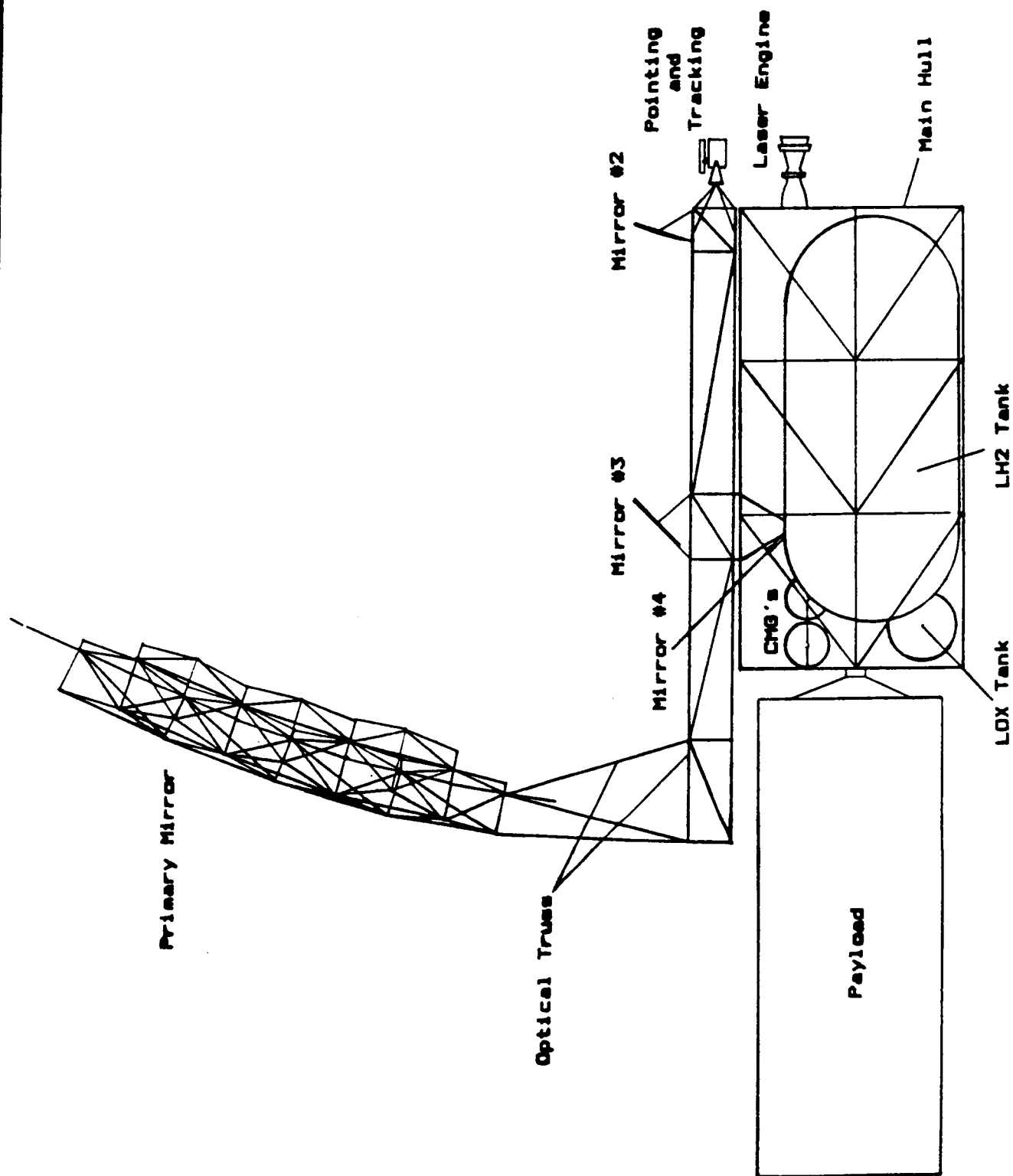
FIGURE 1.3 FINAL NON-AEROBRAKED CONFIGURATION

Primary Mirror

Optical Truss

Mirror #4

Mirror #3

Mirror #2

Pointing
and
Tracking

Laser Engine

Main Hull

LH2 Tank

CMG's

LOX Tank

Payload
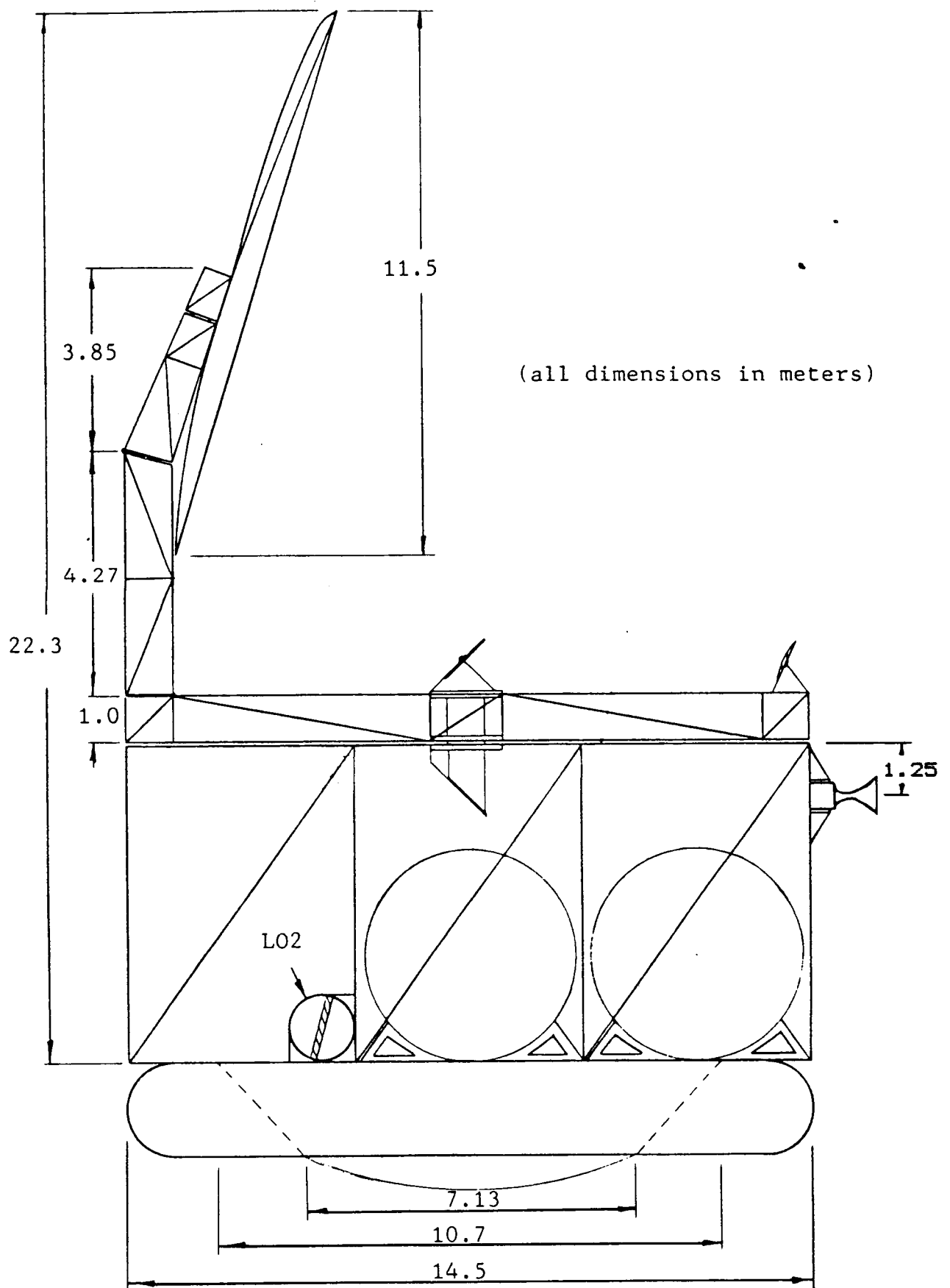
FIGURE 1.4   FINAL LEO/GEO AEROBRAKED CONFIGURATION

(all dimensions in meters)

11.5

3.85

4.27

22.3

1.0

1.25

LO2

7.13

10.7

14.5

2. ORBITAL MECHANICS

2.1 INTRODUCTION

At the commencement of the design project, the team members studying the orbital mechanics of the LOTV had not had much exposure to this subject. Therefore, the simplest transfer, a Hohmann transfer, was originally used to make some initial calculations. However, it was soon realized that the simple, near-minimum energy Hohmann transfer would require more thrust than the LOTV would be designed to produce. Thus, three low thrust trajectories were considered.

One of these trajectories, the spiral transfer, involved continuous burning. This method of transfer was soon discarded because not only did it require more energy, but it also limited the flexibility of the LOTV. The spiral transfer could only be used when special conditions had been met so that the laser could fire at all times and could reach the LOTV at all times.

Another of the trajectories allows for a great deal of flexibility because it involves burning whenever possible. This transfer utilizes ellipses, but these ellipses precess, creating very difficult calculations. Therefore, the multi-impulse elliptical transfer (see figure 2.1) was finally chosen because it retains the flexibility of the LOTV, involves much simpler calculations, and requires less energy. This transfer is a modification of the Hohmann transfer, where instead of thrusting specifically at perigee and apogee, arc burns are made through these points.

To aid in the analysis of the orbital transfer trajectories for the LEO/GEO scenarios, two computer programs were written. These programs were an invaluable aid to the analyses due to the fact that as changes were made to the LOTV, such as large mass reductions and the switch to an all-propulsive model, the analyses of the trajectories had to be recalculated each time.

Although these programs were written for LEO/GEO analyses, small adjustments were made to them in an attempt to do a preliminary analysis of the LEO/LLO scenario.

2.2 ORBITAL MECHANICS PROGRAMS

The two programs were written using different solution methods. Both simulate an orbital transfer using a multi-impulse elliptic spiral, which will be described in detail at a later point.

The first was written in the C programming language. It numerically integrates the equations of motion:

$$\frac{dr}{dt} = \bar{v} \quad \text{and} \quad \frac{dv}{dt} = \bar{a}$$

where $\bar{r}$ is the LOTV position, $\bar{v}$ is the velocity, and $\bar{a}$ is the

total acceleration due to all forces acting on the LOTV. The only forces considered are the Earth's gravity (approximated by a point mass), and the thrust due to the engine. The thrust vector is assumed to always act through the LOTV's center of mass in this analysis. These assumptions simplify the analysis enough to greatly reduce computation time, errors introduced by the integration scheme, and round-off errors due to the computer.

The second program, written in FORTRAN, uses Gauss' form of Lagrange's Planetary Equations, modified by changing the independent variable from time to true anomaly. The changes in the orbital elements are expressed as functions of true anomaly and are integrated. Time is calculated as a function of the eccentric anomaly. Many of the concepts described for the first program also hold true here. The main difference between programs is the parameters being considered. Program one analyzes the problem with the most basic concepts, Newton's laws. Program two utilizes derived equations of orbital mechanics to come up with a solution. Both codes required a great deal of time for execution. The following method was employed to further cut down on run time.

Due to the low thrust-to-weight ratio of the LOTV, impulsive thrusts at perigee or apogee cannot be use. Instead, the LOTV thrusts over an arc of the orbit beginning ahead of the optimum point and continuing past it for an equal angle (see Ref. 2.1). When the LOTV is not within this arc, the only force that needs consideration is gravity because the LOTV is not thrusting. As the LOTV finishes one such 'thrust-arc' (see Figure 2.2), we use the analytical solution to advance the LOTV to the correct position at the beginning of the next arc. By not integrating over a substantial portion of the orbit, the error inherent in the integration is also lessened to a degree.

2.3 LASER TRACKING

Constraints concerning lines-of-sight between laser and sun and laser and LOTV do not increase fuel or mass requirements. Time of transfer is greatly affected, though, possibly even doubled. A 150 km altitude limit was included to reduce the fringe effects of the atmosphere. To limit blocked lines-of-sight and increase transfer effectiveness, two relay stations are assumed to exist in the same orbit as the laser but one leading and one trailing by 120°. All previous maneuvers use the relays. Yet, even with the relays, the LOTV must roll and rotate the receiving mirror in order to capture the laser beam. The maximum roll rate of the LOTV is 6.612×10^{-6} rad/s^2 over 39.8 seconds. The maximum slew rate of the receiving mirror is 1.415×10^{-2} rad/s^2 over 14.8 seconds.

2.4 LEO - GEO - LEO TRANSFER

The first mission required by the project proposal is to transfer a payload from a LEO (radius of 6,700 kilometers and an inclination of 28.5°) to GEO at 42,000 kilometers and zero
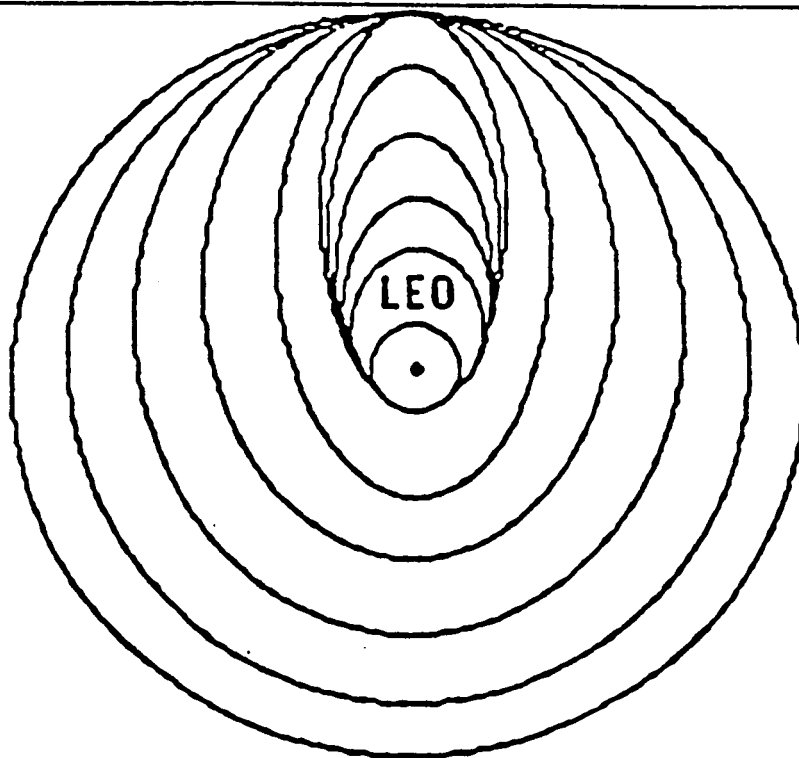
FIGURE 2.1   MULTI IMPULSE ELLIPTICAL TRANSFER

FIGURE 2.2   APOGEE AND PERIGEE THRUST ARCS

inclination (see ref. 2.2). A payload must also be returned from GEO back to LEO. Both the non-aerobraking and aerobraking analyses are discussed.

2.4.1 TRANSFER WITHOUT AEROBRAKING

The transfer method for LEO to GEO is the same for aerobraking and non-aerobraking. This maneuver first consists of perigee burns to raise the radius of apogee. When this is accomplished, the vehicle begins thrusting along apogee to circularize the orbit. After these maneuvers, the LOTV is in a circular orbit of radius 42,000 km, inclined at 28.5^o to the equator. The next maneuver will change the plane of inclination to zero by burning at the nodes of the orbit. Figure 2.3 displays the entire maneuver. For the return mission from GEO to LEO, the procedure is reversed. First, the plane change is made, followed by thrusting at apogee to reduce perigee, and finally thrust at perigee to reduce apogee and circularize the orbit.

Since ideal burns (i.e. impulsive burns exactly at apogee, perigee or the nodes) are impossible due to the low thrust-to-weight ratio, efficient thrust angles for each burn had to be found to obtain optimum performance. The accompanying graphs should be used only to ascertain trends, not to identify specific numbers. Figure 2.4 shows the important parameters of a transfer from LEO to GEO. Perigee burn arcs are shown along the horizontal axis, allowing comparison of various angles. Tradeoffs concerning delta-v, time of transfer, and number of spirals were analyzed and the optimum perigee angle was determined to be 120°. Figure 2.5 compares delta-v, time of transfer, and number of spirals to the apogee burn arc for a LEO/GEO transfer. Again, tradeoffs between each parameter show that the best apogee arc angle is 90°. The next maneuver for consideration is the plane change. Delta-v versus plane change burn arc is shown in Figure 2.6. Clearly the most advantageous burn angle for plane change at the nodes is 50°. It should be noted that half angles are shown for the burn arcs in these figures.

Three versions of the LEO/GEO scenario were examined in detail. A full payload of 16,000 kg was assumed for delivery to GEO in all three cases, but three different payloads of 16,000 kg, 5,000 kg and 1,600 kg were considered for the return trip to LEO. Maximum single burn time is 2.5 hours. Results are summarized in Table 2.1.

Figure 2.7 shows the total fuel required to deliver a payload to GEO. However, small eccentricity problems were encountered with the programs. In order to ensure the accuracy of the results, the fuel required was adjusted to make up for any uncertainties.

2.4.2 TRANSFER WITH AEROBRAKING

For this case, the optimum burn arc angles remain the same: 120° at perigee, 90° at apogee, and 50° for plane change at the nodes. In order to transfer the LOTV from LEO to GEO, the same maneuvers
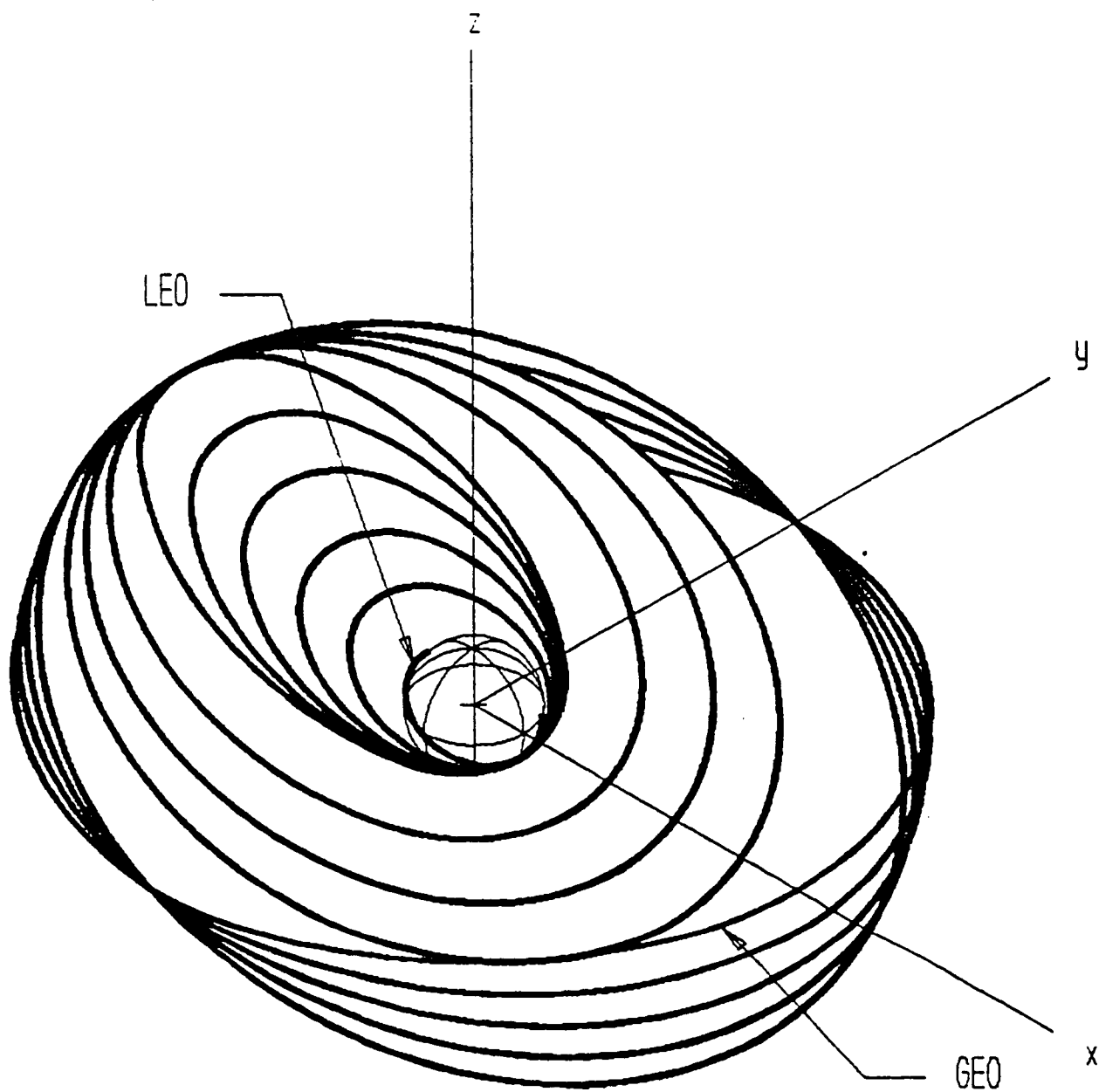
14

FIGURE 2.3   LEO-GEO TRANSFER

Table 2.1 LEO-GEO-LEO All-Propulsive Transfers

		16,000 out 16,000 back		16,000 out 5,000 back		16,000 out 1,600 back	
		out	back	out	back	out	back
initial m_o	(kg)	40,300	25,500	33,900	12,600	31,700	8,200
initial m_f	(kg)	20,200	8,500	14,000	3,750	11,000	2,500
delta-v	(km/s)	4.5	4.4	4.4	4.4	4.6	4.5
trip time	(days)	10	7	6.4	5.4	5.6	3.8
propellant used	(kg)	11,500	7,500	9,600	3,350	8,200	2,100
spirals		26	8	20	6	19	5
total burn time	(hrs)	23.5	10	19.6	6.8	17.6	4.7

are applicable to this scenario. The return to LEO , however, differs. Thrusting reduces the perigee of the orbit until it lies within the fringes of the Earth's atmosphere. Friction takes over and reduces the speed of the vehicle, thereby lowering apogee. Then only a reduced circularizing maneuver is required. Figure 2.8 displays the procedure for skipping through the atmosphere. The aerobraking maneuver will also complete the necessary plane change to return the orbital inclination to 28.5^o. LOTV velocity upon entering the atmosphere will be about 10.3 km/sec. A total delta-v of 2.4 km sec is required to enter LEO. Table 2.2 summarizes the results.

Aerobraking saves 1,500 kg of propellant. Because the actual aerobrake has a mass of 600 kg, the net savings are 900 kg. However, the problems of aerobraking the vehicle must be balanced against the mass savings.

2.5 LEO/LLO TRANSFER

The other mission considered in this report deals with cargo transportation between LEO and LLO. An altitude of 100 km as

Table 2.2 LEO to GEO

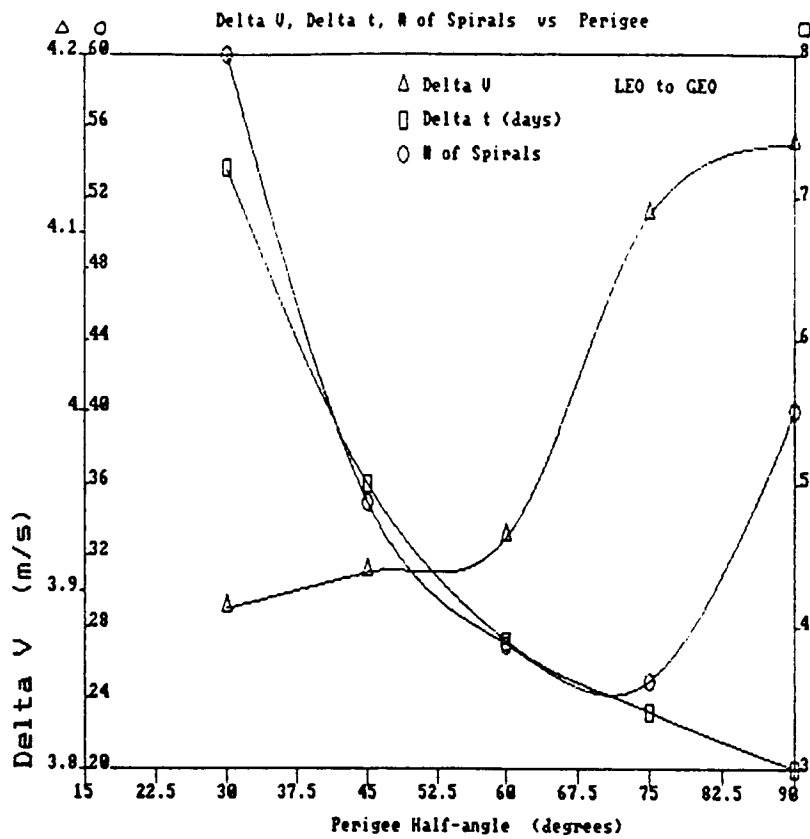|	16,000 kg out / 5,000 kg back	
	out	back
m_o	33,500 kg	11,700 kg
m_f	12,500 kg	2,400 kg
delta-v	4.6 km / s	1.58 km / s
time	7.9 days	20 hours
propellant used	9,700 kg	2,000 kg
spirals	20	4
total burn time	18.4 hours	1 hr
booster mass	600 kg	

FIGURE 2.4 LEO/GEO TRANSFER
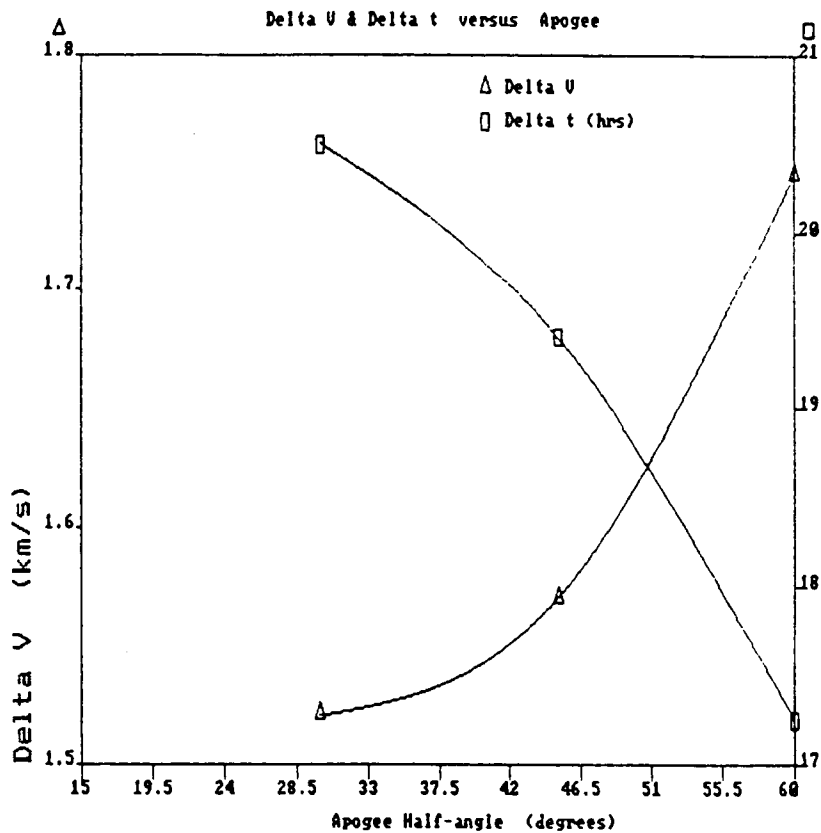PERIGEE BURN ARC COMPARISONS

FIGURE 2.5 LEO/GEO TRANSFER
APOGEE BURN ARC COMPARISONS

17
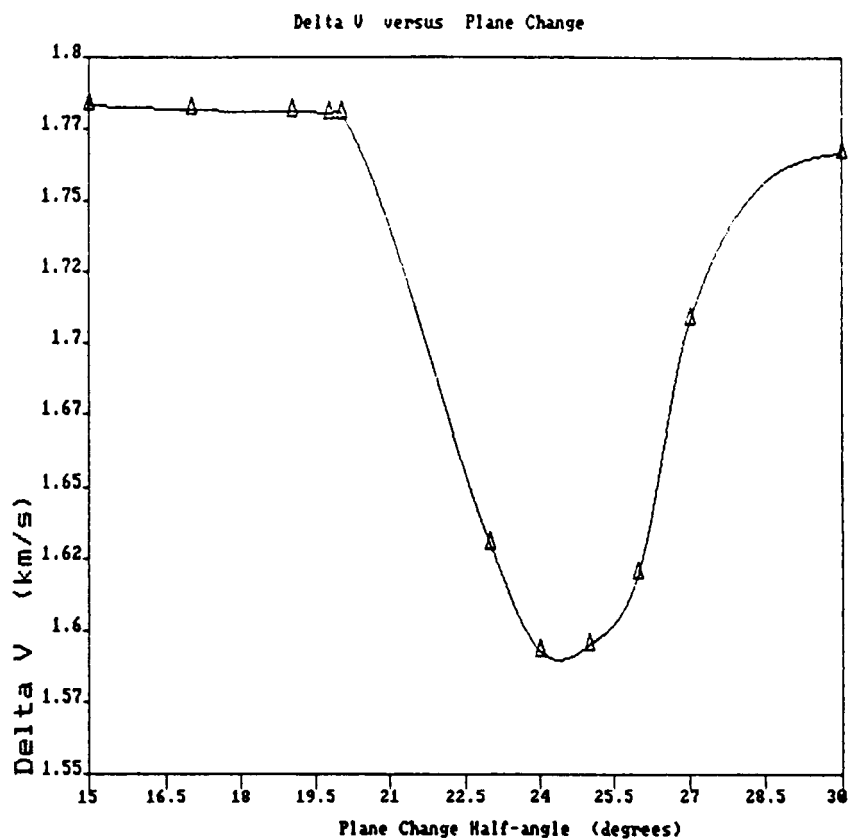
FIGURE 2.6   LEO/GEO TRANSFER
PLANE CHANGE BURN ARC COMPARISON
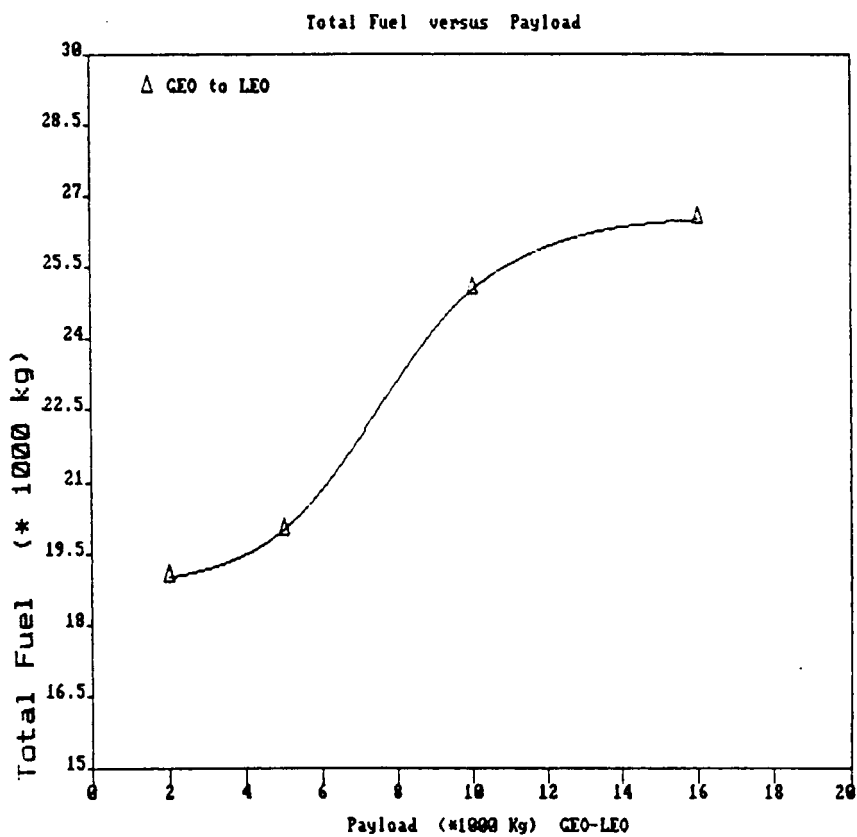
FIGURE 2.7   LEO/GEO TRANSFER
FUEL VS PAYLOAD COMPARISON

18

FIGURE 2.8   AEROBRAKED RETURN
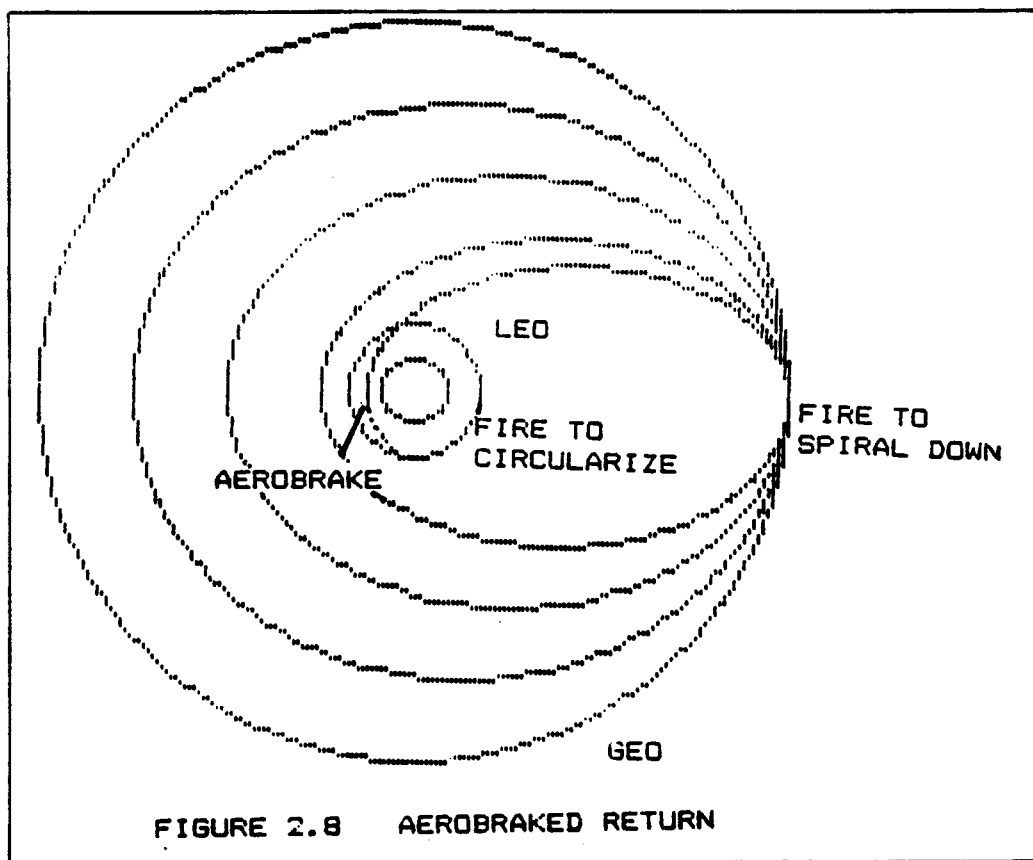
used for LLO. The patch point is a location between the Earth
and Moon where the gravitational forces from each is equal. For
simplicity, we assumed that any spacecraft on the Earth side of
the patch point would not be influenced by the Moon's
gravitational pull. Any spacecraft on the lunar side was assumed
not to feel the Earth's gravity. It lies at approximately 55,000
km from the Moon and 329,400 km from the Earth. Of extreme
importance is our assumption that a second laser station is
placed on the Moon. This is needed to perform any necessary
correctional burns and to lift the LOTV out of LLO. Chemical
thrusters were initiated into the design in order to achieve
necessary delta-v's. Only initial, approximate calculations have
been performed for this mission. Trajectories for a LEO/LLO
tranfer begin with maneuvering into a high apogee elliptic orbit,
which burns at perigee will accomplish. At the median point
between apogee and perigee, boosters will fire and set the LOTV
on an escape trajectory towards the Moon. These boosters will
also accomplish a plane change of 22.5° to match the Moon's
inclination of 6°. Figure 2.9 illustrates a transfer from
LEO-to-LLO. The optimum perigee burn arc seems to be around
120°. Many variables had to be considered to find the most
advantageous orbit at which a the chemical boosters would fire
for lunar transfer. Parameters such as booster mass, required
delta-V, distance from the Earth, and transfer time were weighed,
and the orbit selected has an apogee of 192,200 km and a perigee
of 6,700 km (radius of LEO). Figure 2.10 shows the relationships
between perigee half angle and delta-V, delta-t, and number of
spirals. The relationships between orbital radius and transfer
time and between orbital radius and delta-V are illustrated in
figures 2.11 and 2.12, respectively. The boosters will provide

19

Table 2.3 LEO to 192,200 km

m_o	40,000 kg
m_f	8,500 kg
delta-V	3.2 km/s
time	11.9 days
fuel used	8,000 kg
spirals	42
total burn time	16 hours

890 N thrust for 85 minutes, resulting in a delta-v of 170 m/s. Table 2.3 presents these results.

The LOTV reaches the patch point at a velocity of 1.556 km/s. Here, it falls under the Moon's gravity and enters a lunar hyperbolic orbit. This trajectory will bring the LOTV into a Low Lunar Orbit injection pattern where a delta-v of 1.125 km/s is necessary to circularize the orbit. Total LEO-to-LLO values can be found in Table 2.4.

This mission can put 16,000 kg of payload into LLO. We have assumed a lunar base for refueling, and, of course, a Moon-based laser to propel the LOTV back to. LEO.

2.6 LLO to LEO TRANSFER

Here, the existence of a lunar-based laser is vital to the ability of the LOTV to return to LEO. Thrusting with it's own engine at perigee over an arc of 120°, the LOTV spirals out to the patch point. Table 2.5 lists the values for this part of the transfer. Then, two boosters (445 N) fire for 24 minutes sending the LOTV on an Earth-bound trajectory. Delta-v for this chemical maneuver totals 50 m/s.

When the LOTV reaches the Earth it enters the atmosphere at 11 km/s, and loses 3.1 km/s due to friction. Figure 2.13 shows the Earth-bound trajectories. The orbit is then circularized by a pair of boosters (445 N), which add 71 m/s after thrusting for 34 minutes. Table 2.6 contains details for the entire LLO/LEO transfer.

The payload for the return consists of 5,000 kg carried externally and another 10,000 kg of liquid oxygen carried in a separated region of the main propellant tanks.

Table 2.4 LEO to LLO

m_o	36,300 kg
m_f	12,000 kg
delta-v	4.5 km/s
fuel used	10800 kg

Table 2.5 LLO to Patch Point

m_o	25,750 kg
m_f	2,000 kg
delta-v	0.69 km/s
trip time	4.2 days
no. of spirals	14
total burn time	2.1 hrs

FIRE TO CIRCULARIZE

LUNAR CAPTURE

SPIRAL OUT

PARABOLIC EARTH ORBIT
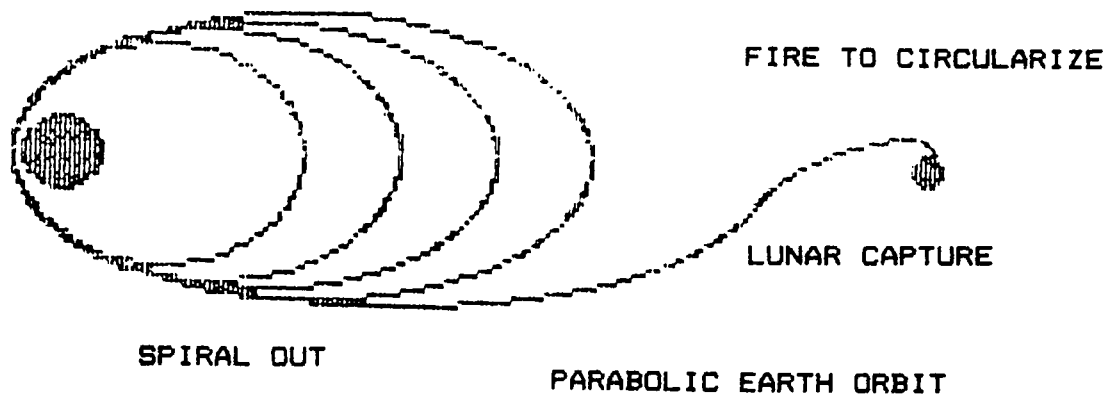
FIGURE 2.9   LEO/LLO TRANSFER

Delta V, Delta t, # of Spirals vs Perigee

△ Delta V   LEO to LLO
▯ Delta t (days)
○ # of Spirals

Delta V (km/s)

Perigee Half-angle (degrees)
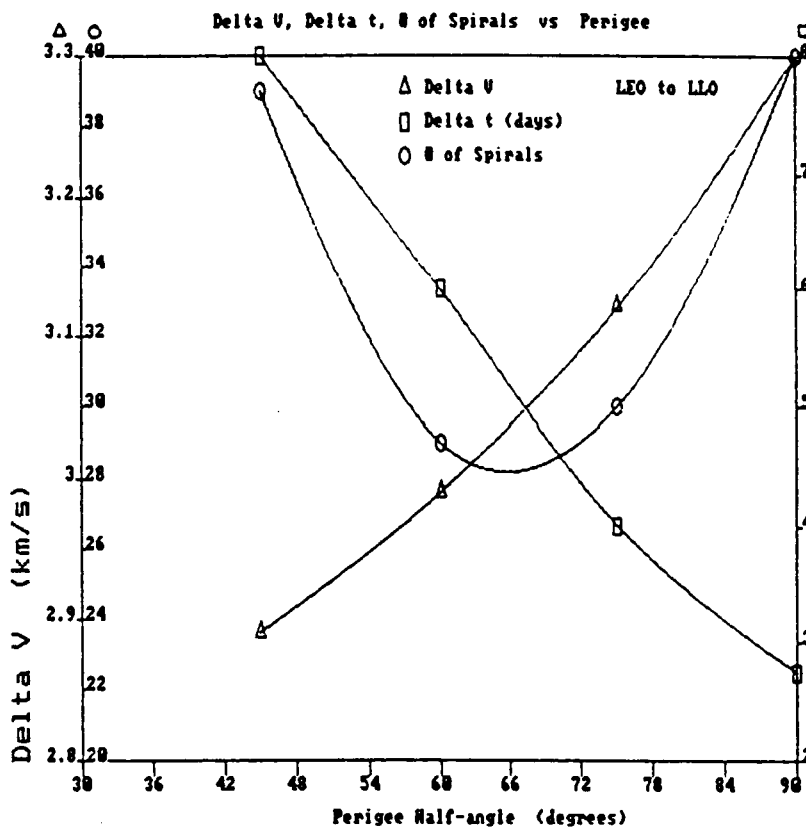
FIGURE 2.10   LEO/LLO TRANSFER
PERIGEE BURN ARC COMPARISONS

Radius versus Transfer Time

Radius (* 1000 km)
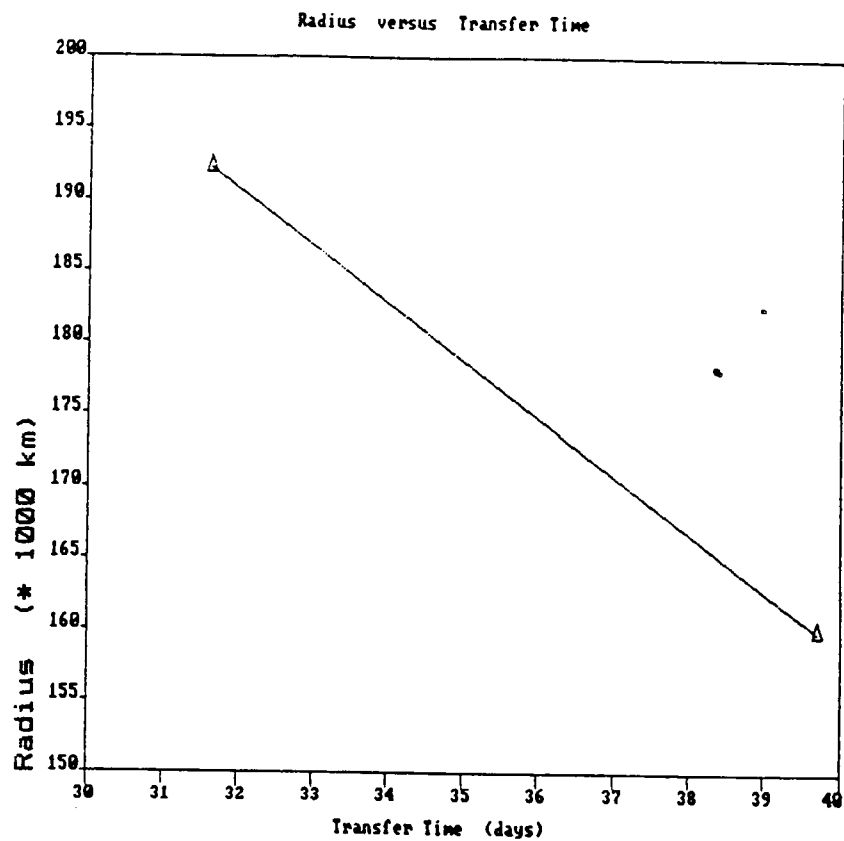
Transfer Time (days)

FIGURE 2.11   ORBIT RADIUS VS TRANSFER TIME

Radius versus Delta V

Radius (* 1000 km)
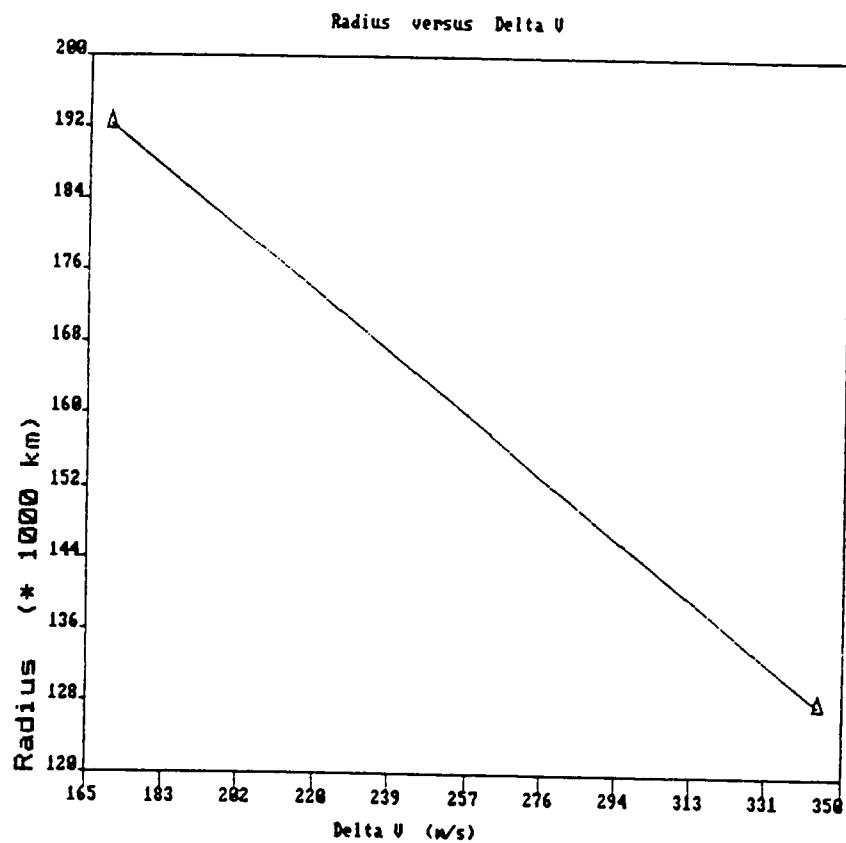
Delta V (m/s)

FIGURE 2.12   ORBIT RADIUS VS DELTA-V

22

<u>Table 2.6 LLO to LEO</u>

m_O 26,000 kg
m_f 2,000 kg
thrusted delta-v   1.9 km/s
delta-v due to aeromaneuver   3.1 km/s
payload   6,000 kg plus 10,000 kg of LOX

2.7 CONCLUSIONS

This preliminary and simple analysis shows feasibility of the LOTV trajectories discussed in this section. A more complete and accurate analysis is necessary to work out the extensive details inherent in the LOTV missions.

2.8 REFERENCES

1. Minovitch, M. A. <u>Performance Analysis of a Laser Propelled Interorbital Transfer Vehicle</u>, Phaser Telepropulsion Inc, February, 1976

2. Friedlander, A. L. <u>Interplanetary Low-Thrust Transport Capabilities</u>, Science Applications International Corporation, May, 1979

AEROBRAKE

Altitude 81 km
Valt = 11 km/s
ΔVab = 3.07 km/s

LLO

LEO

ΔVesc = 50 m/s

ΔVesc = 170 m/s

BOOSTER THRUST = 890 N
THRUST TIME = 24 MINUTES
(TWO BOOSTERS)

BOOSTER THRUST = 890 N
THRUST TIME = 85 MINUTES
(TWO BOOSTERS)

FIGURE 2.13 LLO/LEO WITH AEROBRAKE
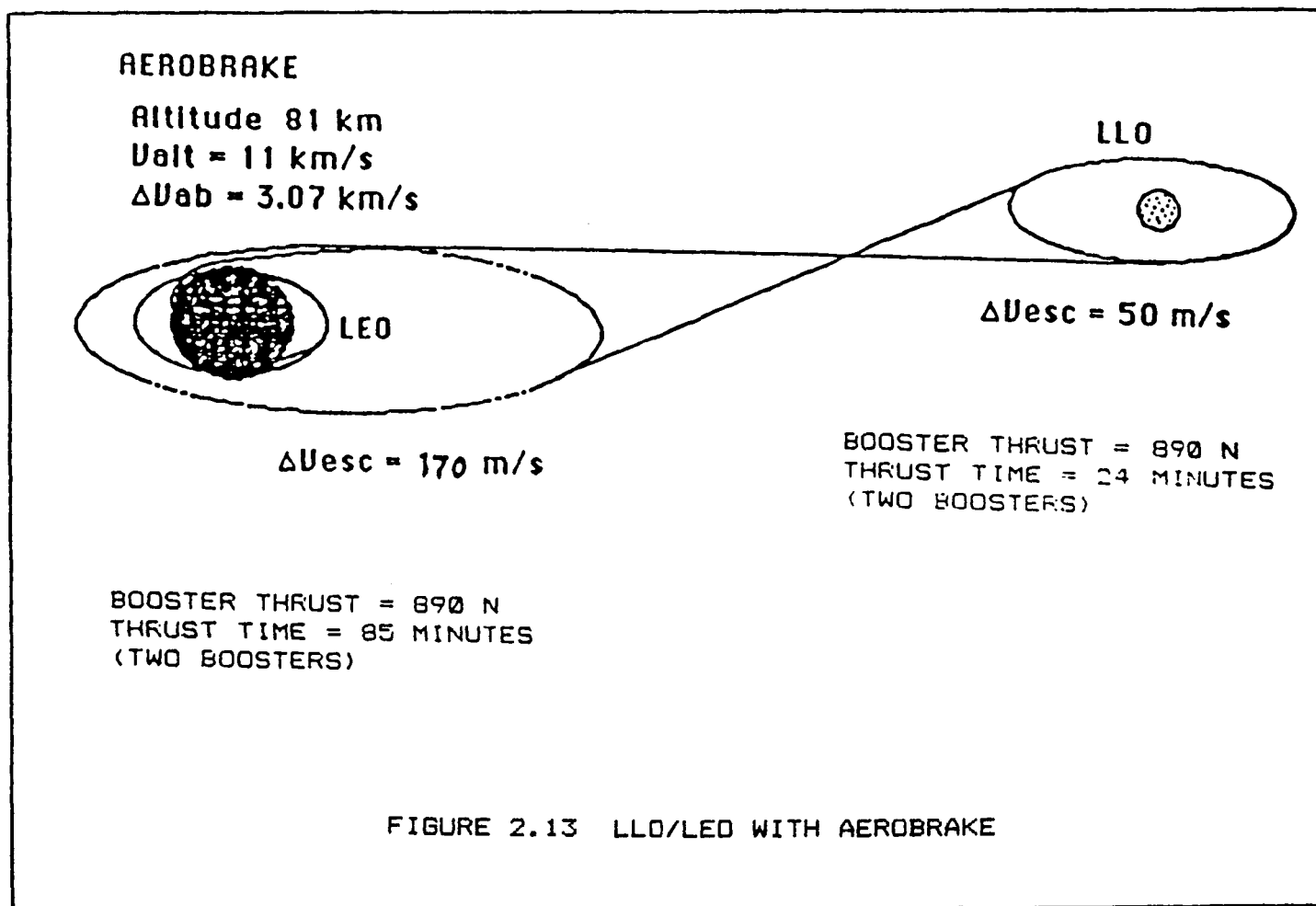
3. STRUCTURES

3.1 EVOLUTION OF THE STRUCTURAL DESIGN

The evolution of the LOTV design involved many configuration design manipulations. Throughout the design process, three separate configurations were under consideration for transfer from LEO to GEO. These included a detachable payload configuration, a combined detachable and permanent payload bay configuration, and a configuration with a triangular cross-section and attachable payload capability. Figures 3.1 and 3.2 show two such versions.

The triangular cross-section configuration for the aerobraked LOTV was chosen from these three after preliminary design analyses were completed. The major reason for this choice was that this cross-section provided the best possible distribution for the aerobrake. The main truss structure was then designed to accomodate two fuel tanks oriented lengthwise along the vehicle. After a stress analysis of the main truss, it was determined to be unstable, at which time a new design was developed.

The new truss structure was still based upon a triangular configuration, but three fuel tanks were oriented along the width of the ship, in order that more support members be added to the truss. This configuration proved to be significantly more stable and was, therefore, chosen for the aerobraked LOTVs. As a comparison to the economical usage of this configuration, a non-aerobraked configuration was also considered. Because of the added fuel requirements and the even distribution needed by a non-aerobraked system, a hexagonal cross-section was chosen with two fuel tanks oriented along the length of the vehicle.

Finally, after significant reductions in the size of the optical truss structure, size and mass reductions were also made on the overall configurations. A smaller triangular configuration with only two fuel tanks oriented along the width was chosen for the aerobraked LEO/GEO version. The only essential changes made to the non-aerobraked version were the reductions in size and mass. The triangular configuration which had already been designed with three fuel tanks oriented along the width was chosen for the LEO/LLO scenario.

3.2 MATERIALS SELECTION

Proper choice of materials is critical in the design of any truss structure. Member elements must be capable of sustaining a variety of stresses, including axial, transverse, and shear. In addition, thermal expansion, wear, and fatigue considerations must also be taken into account. Space applications dealt with herein necessitate low mass optimized with the material properties, such as strength, stiffness, and specific modulus.

Standard monolithic metals, like aluminum, were incorporated into most early space truss systems. In more recent years polymer
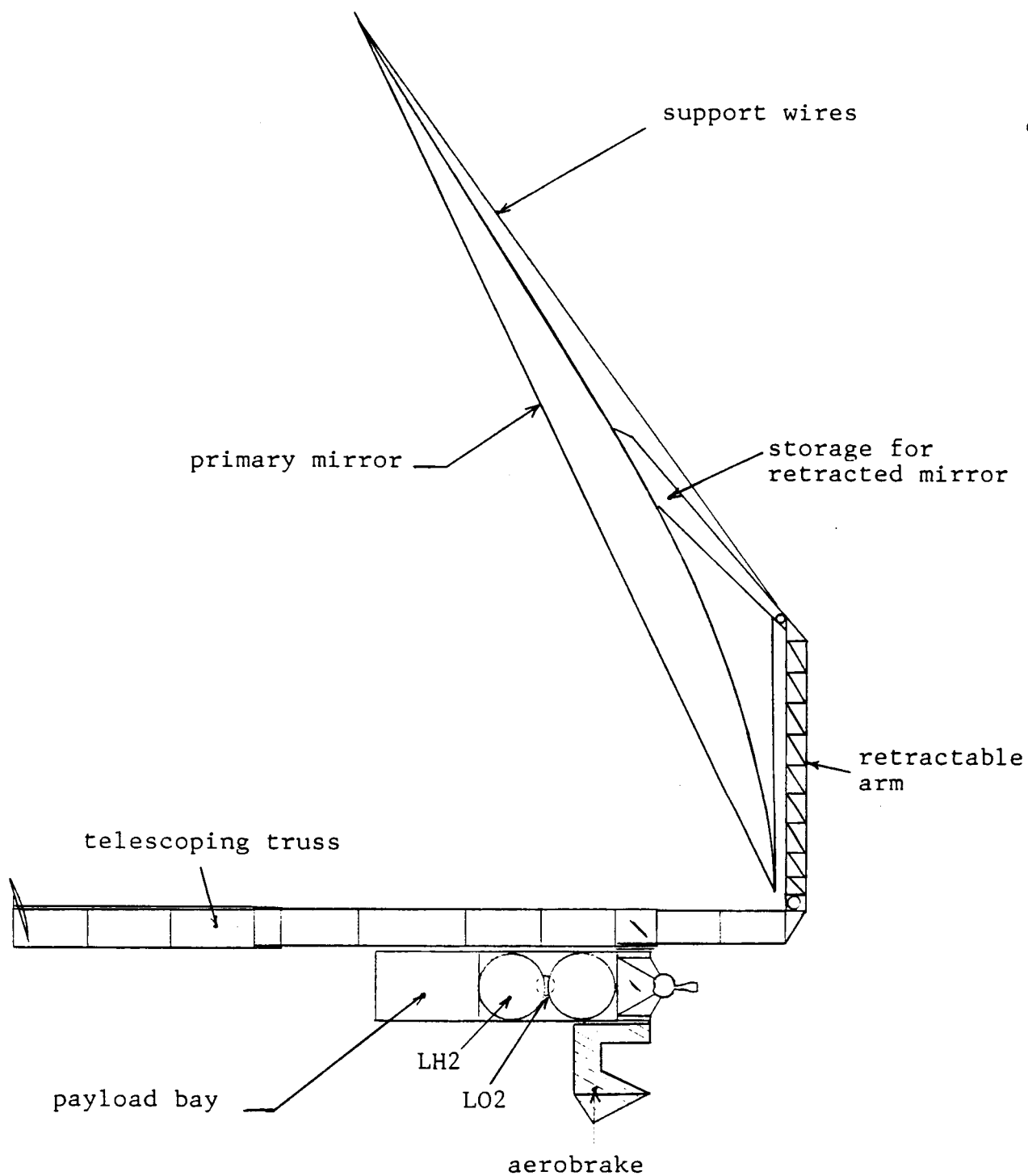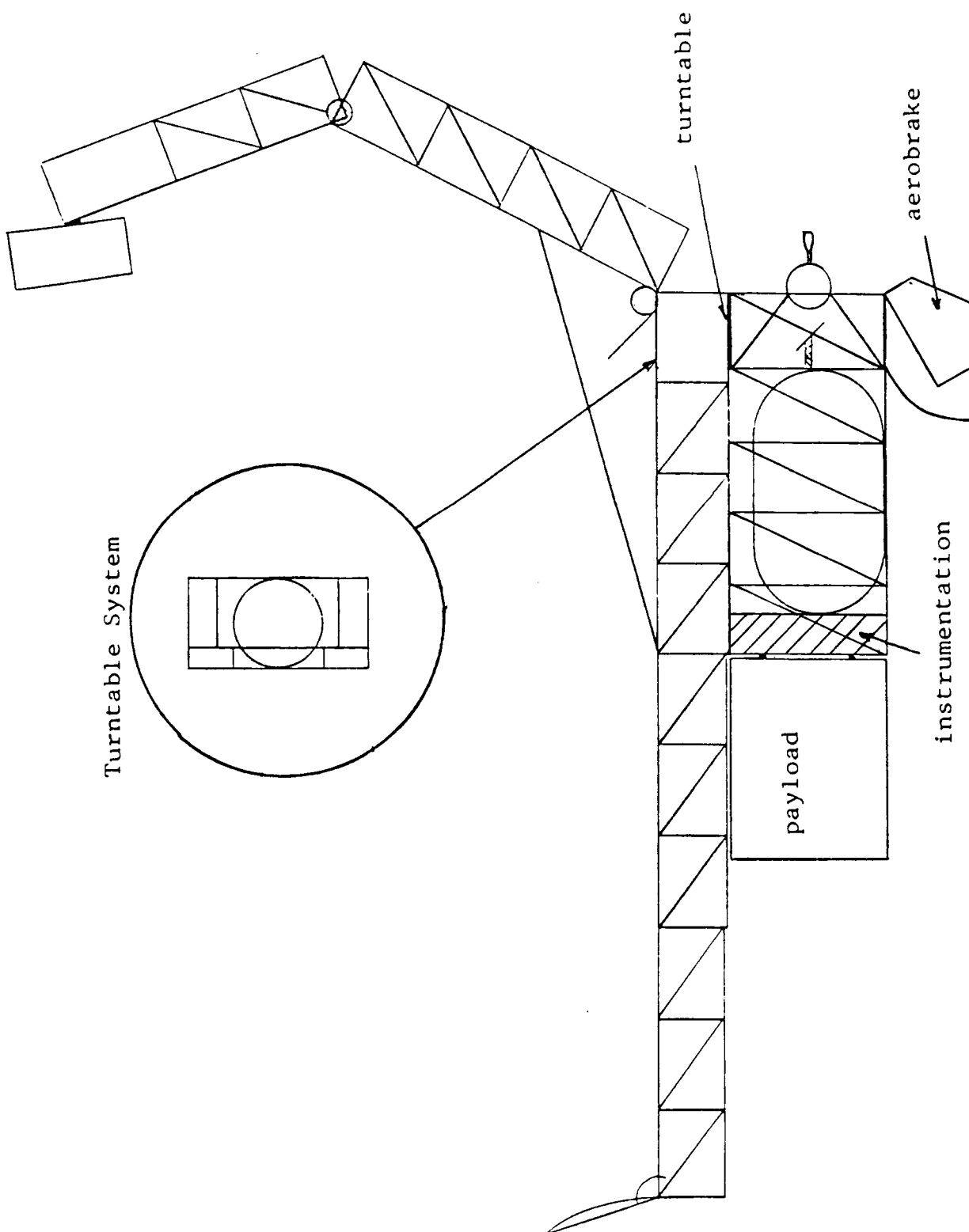
Figure 3.1   Initial Configuration

Figure 3.2 Depoloyed Mirror/Ship System

Turntable System

turntable

aerobrake

instrumentation

payload

Table 3.1 Material Properties

Property	Boron/Aluminum	Graphite/Epoxy	Aluminum
E_1 (x10^6 psi)	33.4	19.2	10.0
E_2 (x10^6 psi)	23.2	1.6	10.0
E_1/density (x10^6 in^2/s^2)	4.7	4.2	1.2
E_2/density (x10^6 in^2/s^2)	3.2	0.34	1.24
longit. strength/density (x10^3 in^2/s^2)	27.9	25.9	6.2
transv. strength/density (x10^3 in^2/s^2)	2.83	1.38	6.2

matrix composite materials, such as graphite/epoxy, and metal matrix composite materials, like boron/aluminum, have been used to take advantage of better material properties.

For the LOTV main truss structures, boron/aluminum was chosen for the truss bar elements. Metal matrix composites have many advantages over standard composite materials and monolithic metals. These include much higher strength-to-density and stiffness-to-density ratios, higher specific modulus, better fatigue and wear resistance, and lower coefficients of thermal expansion. Boron/aluminum has further advantages over graphite/ epoxy and other polymer matrix composites. Higher temperature capability, significantly higher transverse stiffness and strength, no moisture absorption, better radiation resistance, and no outgassing characterize the boron/aluminum composite. Table 3.1 compares several material properties for boron/ aluminum, graphite/epoxy, and aluminum.

Finally, boron/aluminum is currently the state-of-the-art material for many space applications. The technology for electron-beam welding of titanium end fittings has already been successfully demonstrated on the Space Shuttle. The aforementioned benefits outweigh the slightly higher material cost of boron/aluminum, especially when the consistent downward pricing trend of composite materials is taken into account. (See references 3.4 and 3.5)

3.3 NONAEROBRAKED OR ALL-PROPULSIVE CONFIGURATION

3.3.1 DESIGN CONSIDERATIONS

One of the major tradeoff criteria in the LEO/GEO LOTV design scenario is the method of return to LEO. Specifically, aerobraking and all-propulsive return trajectories and their effects on the LOTV design have been and will continue to be a major design consideration.

After investigating several preliminary aerobraked configurations, none appeared to offer a distinct mass advantage over an all-propulsive return vehicle. Furthermore, the one-mission life

of the aerobrake system and the problems of reliability and
failure prevention have caused the study of an all-propulsive
return scenario and corresponding vehicle configuration to be
given higher priority.

One of the primary constraints and limitations placed on the
design was the sizing of the OTS. Primary mirror size, based on
laser beam jitter and power distribution, as well as optical
geometry, in turn determines the OTS sizing and secondary mirror
configuration, which is detailed in the Optics section.

Since the primary function of the LOTV is the transfer of
payloads between LEO and GEO, it was decided to adapt two payload
carrying schemes as design criteria. The first scheme involves
transport of 16,000 kg from LEO to GEO and 16,000 kg on return to
LEO. This was termed Option I or the "All-Return Option."
Typically the majority of payload traffic is anticipated to be
outward to GEO, so a second scheme with an initial (LEO/GEO)
payload of 16,000 kg and a payload of 5000 kg on return, was
incorporated. This is referred to as Option II or the "Standard
Option." A third payload scheme involving a minimal return payload
of 1600 kg (Option III) was also suggested.

Another major constraint is the amount of fuel required. An
elliptical spiral transfer to GEO (with plane change) with an
all-propulsive return to LEO would require a fuel mass (liquid
hydrogen) of 20,700 kg (round trip) for Option I and 14,000 kg
for the Standard Option. Option III requires 11,700 kg fuel.
A rendezvouz/refuel operation at GEO could significantly reduce
the initial fuel requirement.

The main hull of the LOTV, which includes fuel tanks, fuel
management/pump systems, Detachable Payload Module (DPM) docking
apparatus, Control Moment Gyroscopes (CMG's), and instrumentation
for movable systems, tracking, et.al., must provide open access
between the optical system's fourth mirror and the engine window
in order to focus the laser for propulsion. Concurrently,
vehicle structural mass and fuel boil-off must be minimized. The
truss structure design must also provide good accessibility to
the fuel tanks and other internal components for maintenance.
Additionally, the structure must be able to successfully
withstand all stresses, axial, shear, torsion, and bending, which
result from forces acting on the vehicle, and the vibrational
modes of response must be stable. In the non-aerobraked scenario
the thrust (maximum thrust of 2000 Newtons) is essentially the
only force acting on the LOTV other than gravitational forces.
The low thrust nature of the propulsion system enabled the design
of a simplified, lightweight truss structure, even with a 1.5
factor of safety (3000 N maximum force) incorporated into the
stress analysis.

3.3.2 FUEL TANKS

In order to effectively minimize a weighted combination of both
fuel tank dry mass and fuel boil-off rate, a two tank configuration

<u>Table 3.2 LH2 Tank Dimensions and Masses</u>

	OPTION I	STANDARD OPTION
Diameter	4.18 m	4.0 m
Length (including caps)	10.48 m	8.5 m
Thickness	1.05 mm	1.0 mm
Dry Mass	810.00 kg	600.0 kg

for LH2 storage was chosen. Each tank is cylindrical, with spherical caps. Tank thickness was selected based on a maximum design pressure of 10 psia (safety factor of 1.5) and a dimensionless thickness/radius ratio of 0.0006 obtained from reference 3.1. A single spherical tank containing 300 kg of liquid oxygen (LO2) for reaction control will be located in the forward region of the vehicle. The tank is 0.8 m in diameter with a thickness of 0.6 mm and an overall mass of 12 kilograms. All tanks will be made of aluminum. Table 3.2 summarizes the LH2 tank dimensions and masses for each of the two payload scenarios.

Several types of tank insulation and impact protection were considered. One protection scheme included a second layer of aluminum surrounding the tanks with a layer of kevlar insulation between. Another scheme involves a "shroud mounted" aluminum protective coating fixed to the truss. Both of these schemes are far more massive than the selected alternative, a multilayer insulation (MLI)/foam blanket scheme consisting of several layers of fibrous insulation, a thin inner radiation shield, and a foam layer, all with a composite density of 2.46 kg/cub.m. The MLI protection system has a mass of 38 kg for Option I and 30 kg for the Standard Option.

3.3.3 FUEL TANK AND ENGINE SUPPORT STRUCTURE

The basic support structure for the fuel tanks consists of struts mounted from the vehicle truss structure and attached to bands encircling the fuel tanks, as shown in figure 3.3. Each strut will be mounted onto the vehicle truss structure via a band/fitting which is welded onto or integrated into the truss member (see figure 3.4). The struts will secure the fuel tanks to the structure at tangent points between the structural members and the tanks. Figure 3.5 shows a boron/aluminum band or "hoop" which encircles each fuel tank at one of two axial locations. The band has an integrated fitting identical to that on the truss member-strut connection. The smaller LO2 tank will be attached to each LH2 tank at the bands with a strut connection. The struts can be electron-welded or riveted to the fittings. Boron/aluminum will be used for all tank mounting struts and fittings. In all there will be four bands, 16 struts and 32 fittings. The total masses are as follows: hoops, 24 kg; struts, 12 kg; fittings, 22 kg for a total of 58 kg for the fuel tank support mounting for the Standard Option. The mass of the support mounting for Option I is 60 kg.

29
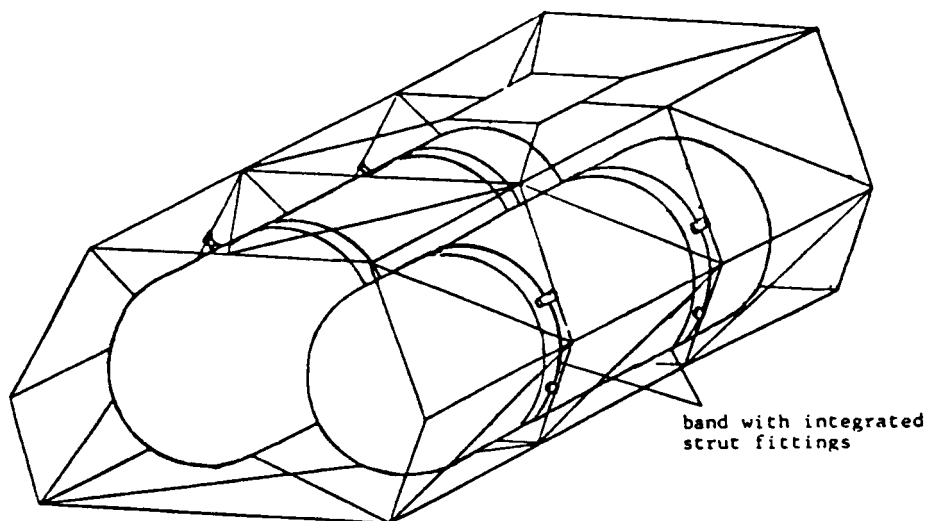
**Figure 3.3   Non-aerobraked Configuration
Fuel Tank Support Mounting System**

Note: exaggerated strut and fitting sizing for clarity
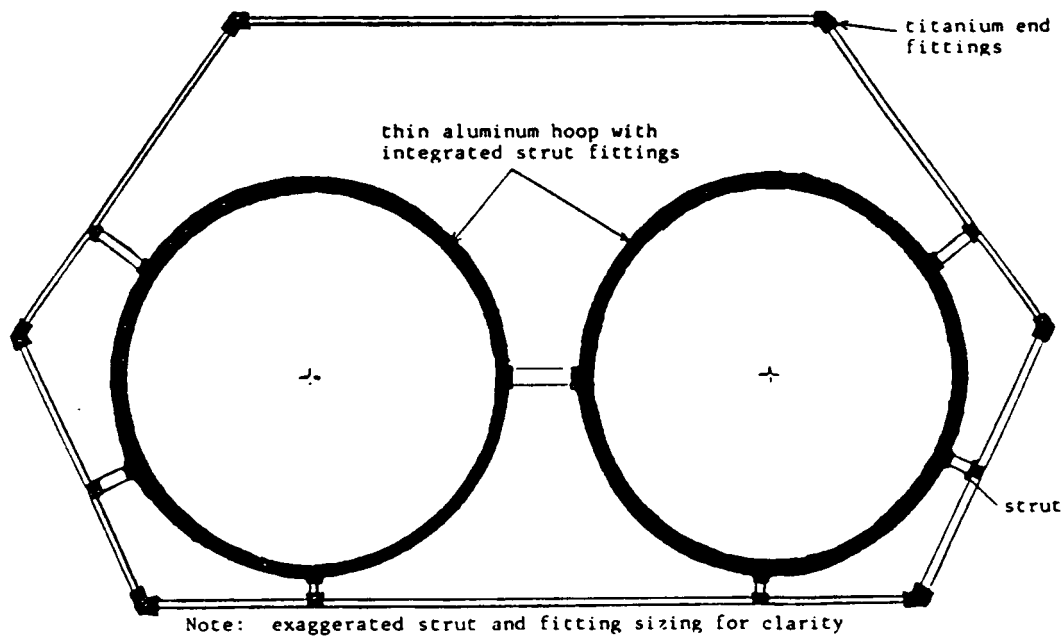
**Figure 3.4   Non-aerobraked Configuration
Cross-section with Fuel Tank Support Mounting**

30

Figure 3.5   Non-aerobraked Configuration
Band/Strut System

Figure 3.6   Non-aerobraked Configuration
Engine Support Mounting
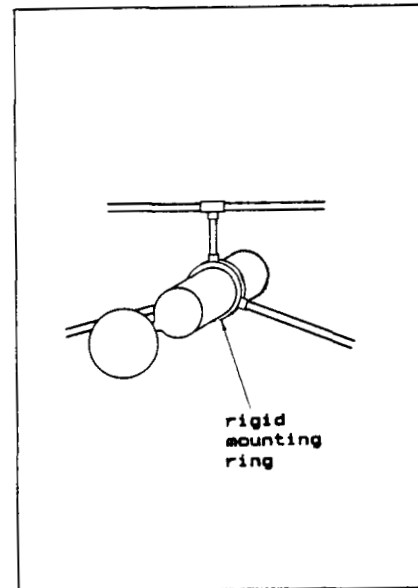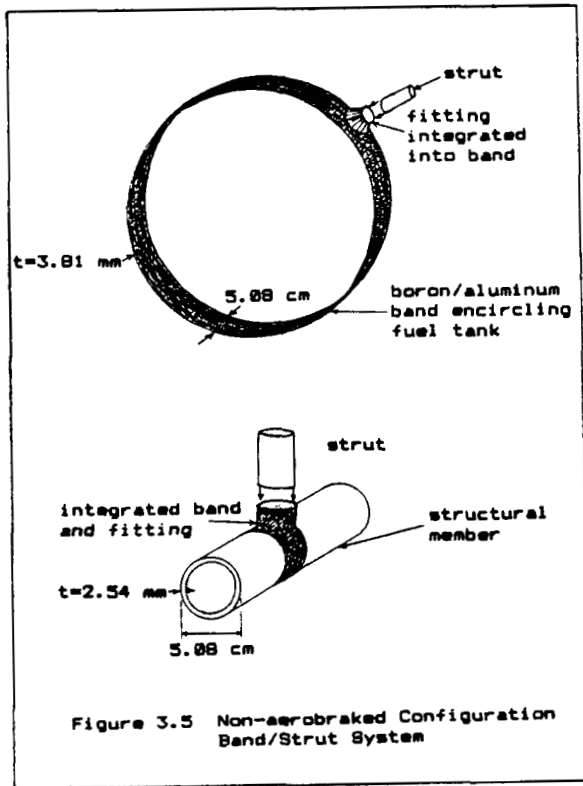
The main engine requires a much more rigid support system.   Hence
three structural members similar to those in the main truss will
be electron beam welded directly onto a rigid ring which is inte-
grated onto the engine casing.   Figure 3.6 shows a more detailed
view of the rigid mounting ring.   This system will provide a more
rigid support for the engine than the original six-member
connection, and will cause less instability problems.   It will
reduce firing and guidance error which could result from small
displacements in the engine position, as well as inefficiencies
resulting from incomplete beam transmission through the engine
window.   The total mass of the engine support mounting is 32 kg
for both options.

3.3.4 MAIN HULL AND OPTICAL TRUSS STRUCTURES

The incorporation of boron/aluminum metal matrix composite into
the truss structure significantly reduced structural mass with
respect to previous LOTV designs.   Due to its large strength to
density ratio (92 sq.cm/sq.sec) and high yield strengths in both
axial and transverse directions, a cross section of 5.08 cm outer
diameter with 3.2 mm thickness for truss members (hollow cylin-
drical members) effectively reduces structural mass to one eighth
of the original design mass, which used aluminum truss members,
while still keeping member stresses below critical levels.
Figure 3.7 shows the main truss configuration and dimensions.
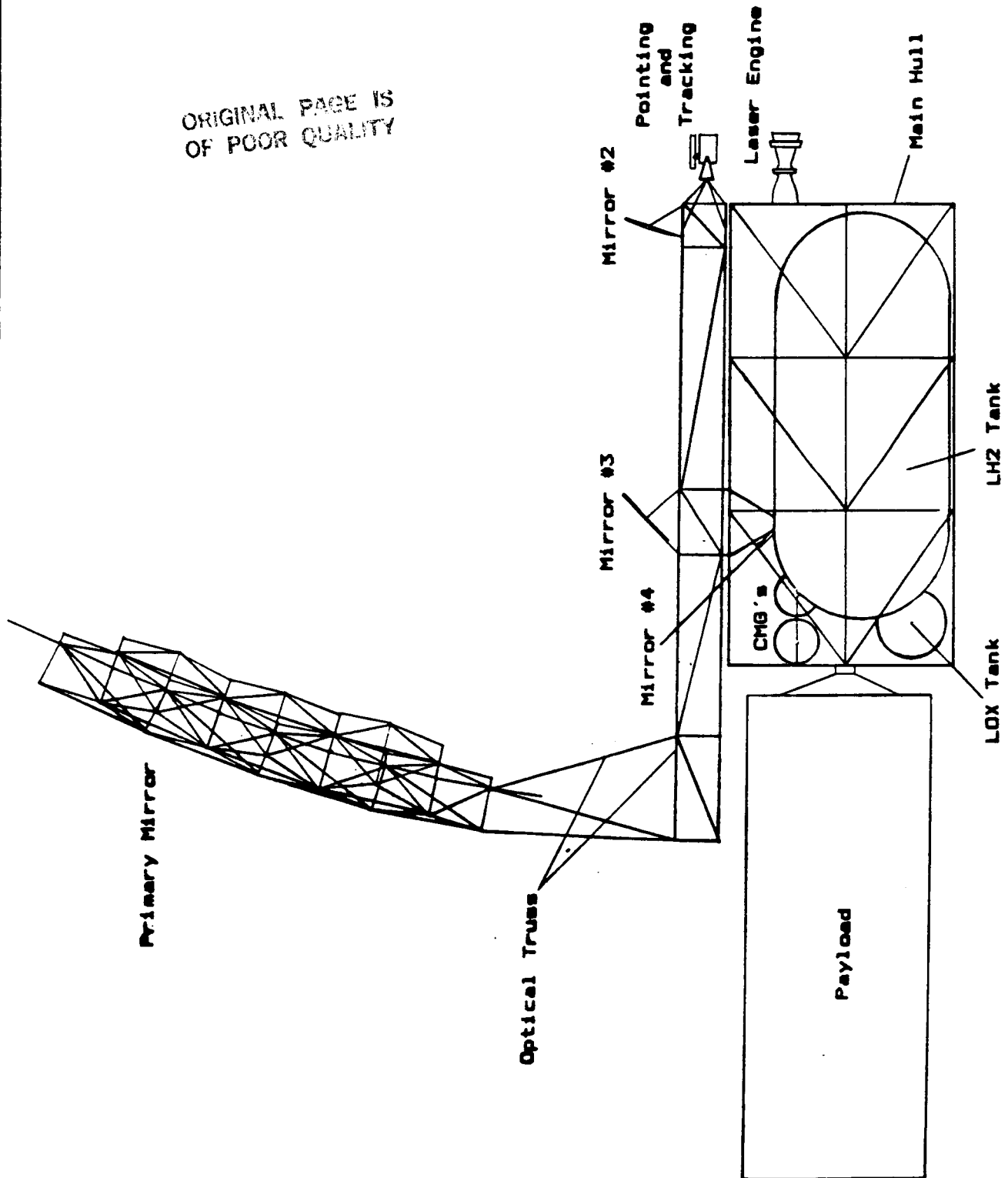
Figure 3.7 Non-aerobraked Configuration
Side View Schematic

The OTS has a main truss length of 14.5 meters, with center of
rotation located 7.25 m from the rear of the vehicle. The main
OTS frame cross section will be trapezoidal, with a 2 m upper
base, 3 m lower base, and 1 m height, with the same member cross
sectional dimensions as the main hull truss members. The
trapezoidal shape was chosen for its structural rigidity while
allowing an opening for the laser pathway between the third and
fourth mirrors. All truss members will be joined with electron
beam-cut titanium end fittings. The primary mirror arm will have
two sections, each with a 0.5 m sided equilateral triangular
cross section.

The OTS will rotate about a 2 m by 1.5 m rectangular rigid base
made of boron/aluminum with a height of 20 cm. A gearing
mechanism will drive the turntable hub which will have a 1.15 m
diameter opening to allow the laser to access the fourth mirror.
The laser pathway to the engine is located at the top of the
cross section, as shown in figure 3.7. The total mass of the
optical system is 1015 kilograms.

Throughout the life of the LOTV, the fuel tanks will inevitably
need to be removed for major servicing, repair, and/or
replacement. In order to allow for fuel tank removal, the truss
member on the front face of the vehicle, or "x-member" has been
designed to unlock and rotate up to access the tanks. Figure 3.8
shows the x-member with probe connector and four two-piece
fittings which attach it to the rest of the structure. The two
fittings at the upper corners of the member, as seen in figure
3.8, allow for rotation about a hinge, while the lower fittings
(figure 3.8) each contain two sections which lock into place and
unlock, giving the x-member freedom to rotate up into a plane
perpendicular to the front face, thus allowing the tanks to be
removed. For the Standard Option, the mass of the boron/aluminum
x-member is 16 kg, while the two-piece titanium fittings have a
mass of 10 kg, including the central probe mounting fitting.

Figure 3.8 Non-aerobraked Configuration
Cross-section with X-member
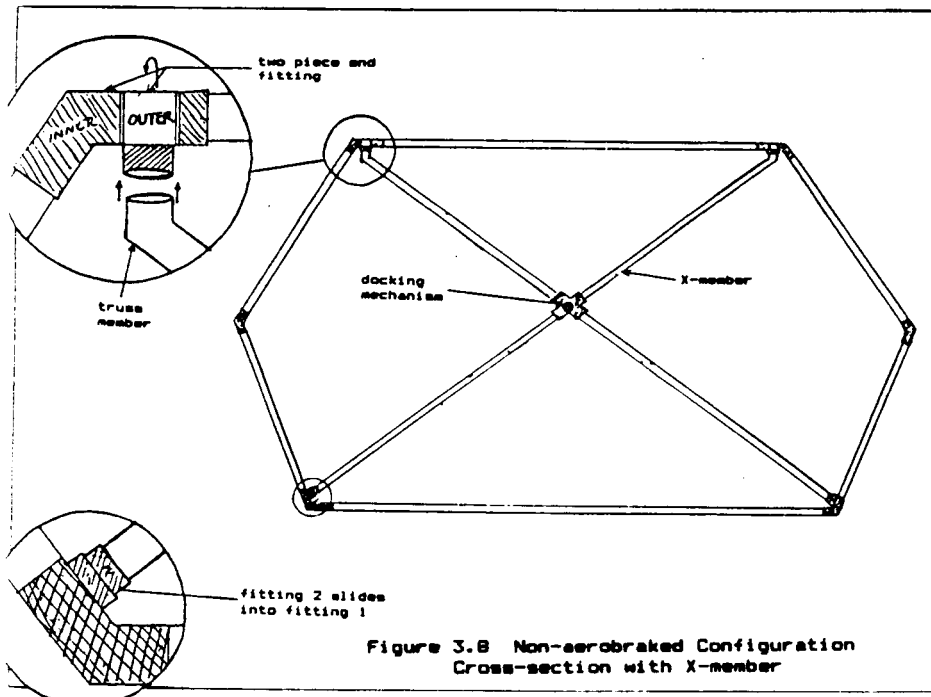
3.3.5 MASS ESTIMATES

Mass estimates for the LOTV were calculated using the following densities (see references 3.6, 3.7, and 3.8):

Aluminum	=	2800 kg/m**3
Boron/Aluminum	=	2490 kg/m**3
Titanium	=	4500 kg/m**3
Liquid Oxygen	=	1190 kg/m**3
Liquid Hydrogen	=	78 kg/m**3

Table 3.3 lists the mass estimates (in kilograms) for both payload options of the non-aerobraked LOTV.

Table 3.3 Mass (kg) Estimates - Nonaerobraked Configuration

		STANDARD	ALL-RETURN
Main Hull Structure, Engine and Tank Supports	=	486	628
Propellant Tanks	=	600	810
Primary Mirror	=	500	500
Mirrors #2, 3, and 4	=	255	255
Optical Truss Structure, Mirror Supports	=	260	260
Optical Turntable Mechanism	=	150	150
Primary Propulsion System	=	320	320 *
CMG's and R.C.S.	=	291	291
Pointing and Tracking	=	115	115
Guidance, Navigation and Control, Data Management and Communication Systems	=	200	200
Electrical Power System	=	50	50
Instrumentation	=	30	30
Detachable Payload Module	=	526	526
Docking/Connecting Apparatus	=	30	30
Vehicle Dry Mass, M_s	=	3855	4065
LEO-to-GEO Payload Mass, $M_{pl\uparrow}$	=	16000	16000
Propellant Mass at LEO (for round trip, including RCS and reserves)	=	14000	20200
OVERALL INITIAL MASS, M_{tot}	=	33855	40265
GEO-to-LEO Payload Mass, $M_{pl\downarrow}$	=	5000	16000
Propellant Mass at GEO (for return trip)	=	3750	8000
Initial Mass at GEO	=	12605	28065
Propellant Used for LEO-to-GEO Leg, $M_{p\uparrow}$	=	9600	11500
Propellant Used for GEO-to-LEO Leg, $M_{p\downarrow}$	=	3350	7500

* including propellant feed system and nozzle gimbaling system

3.3.6 CENTER OF GRAVITY MOTION AND GUIDANCE CONSIDERATIONS

Analysis of the motion of the vehicle's center of gravity throughout the mission shows cg movement to be essentially a function of mirror rotation, fuel consumption, and a step function of payload carriage (i.e., the cg moves instantaneously when the cargo is dropped off at GEO). The equations used for the center of gravity calculations are listed in Appendix A.1. A coordinate system is defined with origin at the front of the vehicle halfway up the cross section (2.6 m above the base), with x body axis, vertical y axis, and transverse z axis (see figure 3.7). The farthest forward location of the cg along the body axis is $X_{min} = 0.43$m with tanks full and primary mirror at the front of the ship. Maximum aft cg location, with payload detached at GEO, is $X_{max} = 6.68$ meters.

The vertical cg location ranges from $Y_{min} = -1.12$ m (tanks full) to $Y_{max} = 1.36$ m above the geometric center of the cross section. Transverse cg variation is a function of mirror rotation only. The optical truss system cg is 1.06 m from the axis of rotation (to the primary mirror side), causing a maximum cg shift of 0.28 meters out of the xy symmetry plane (when tanks are empty). For most of the mission $|Z|$ will be less than 10 centimeters.

Three CMG Gyroscopes will be incorporated to aid in reaction control and attitude control. Each is a 1.0 meter diameter sphere. They are mounted onto the main truss structure as shown in figure 3.7.

3.3.7 STRESS ANALYSIS AND MOMENTS OF INERTIA

A somewhat simple three-dimensional stress analysis, with the structure simply supported and a 3000 N force simulating maximum thrust (with a 1.5 safety factor) showed loadings to be within the design limits for the boron/aluminum truss members. Maximum deflections encountered were on the order of one centimeter. The analysis was carried out with a slightly modified version of "Structural Analysis Software for Microcomputers," or SASM, by B. J. Korites. SASM is an interactive package with a collection of routines which assemble a three dimensional truss structure, with dimensions and material properties input by the user, and calculate nodal displacements and member forces.

The main assumptions in the stress analysis were: (1) a statically loaded truss structure, (2) all end fittings were modeled as frictionless ball and socket joints, or nodes, which are not capable of inducing bending in the members, (3) the engine is modeled as a node, (4) a point force is applied at the engine nozzle and (5) an instantaneously applied force at the docking point is used for docking considerations. Due to the inability of more detailed routines to handle such cases as dynamic and distributed loading and structural vibration, these assumptions were necessary. However, although they are simplified, the structural analysis routines tend to give slightly high load and

Table 3.4 Moments of Inertia

	I_x	I_y	I_z
(1) Full Fuel & Payload	2.83	19.22	19.33
(2) No Fuel/Full "	1.58	11.96	12.82
(3) No Fuel/5000 kg	1.33	6.17	7.00

All moments of inertia units are 10^5 kg*m^2.

deflection estimates, thereby incorporating a built in factor of safety in the analysis.

Moments of inertia for the present configuration were obtained for several cases: (1) tanks full, full payload (16,000 kg); (2) tanks empty, full payload; and (3) tanks empty with 5000 kg payload. The component masses for the All-Return Payload Option were used, although those for the Standard Option are nearly identical with the exception of the tanks and initial fuel mass. For each of the three cases above, it was assumed that the optical system orientation is such that the primary mirror location is in the rear of the vehicle. Moments of inertia of truss members were computed separately assuming solid cylindrical shapes of equal mass, and using axis transformation equations. The mirrors were assumed to be thin disks and the fuel tanks solid cylinders with solid hemispherical caps. The propulsion system was modeled as a solid cylinder. The parallel axis theorem was used to calculate moments of inertia about an axis system centered at the vehicle cg (see Appendix A.2; reference 3.8). Table 3.4 shows moments of inertia for the LOTV for each of the three cases.

3.4 AEROBRAKED CONFIGURATIONS

3.4.1 LEO/GEO AEROBRAKED SCENARIO

3.4.1.1 Design Considerations

The major considerations in the design of the aerobraked LEO/GEO LOTV were resistance of the truss structure to stresses and a center of gravity placed as far forward as possible. The largest stresses were found to occur in front members during aerobraking. With these things in mind, the final design was chosen to be a 14.5 meter base trapezoidal ship truss (see Figure 3.9). A forward center of gravity was accomplished by placing a payload bay in front with the fuel tanks laterally placed in the back of the ship. The primary mirror was chosen to be a retractable wrapped rib mirror which, although more complicated in its deployment and storage than a rigid model, has the advantage of smaller mass.

By employing an aerobrake, return to LEO can be accomplished without the need for propulsive burns at LEO, thereby reducing

Figure 3.9 LEO/GEO Aerobraked Configuration Main Truss System
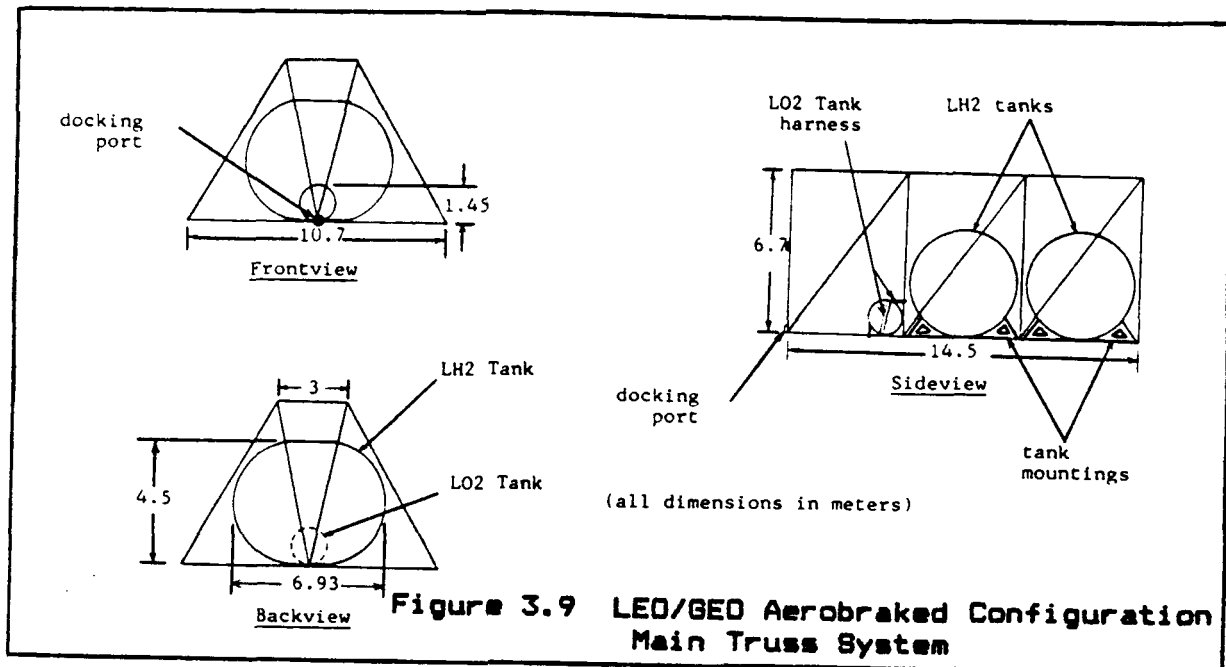
the fuel mass. The necessary fuel mass for a round trip of the standard LOTV option was estimated to be 14000 kg of liquid hydrogen. The fuel tanks are located at the front (defined during aerobraking) of the ship in order to move its center of gravity as far forward as possible. This allows better control during atmospheric flight. Also included as fuel is a spherical tank of 37 kg intended to carry the 500 kg of liquid oxygen used for in-flight maneuvering and control. Figure 3.10 gives specific tank dimensions for the LEO/GEO aerobraked ship.

The mirror system consists of a 11.5 meter diameter wrapped rib primary mirror on a 14.5 meter arm. This primary mirror collapses into its hub and therefore, may be easily stored. Also, three secondary mirrors of elliptical shape are used to direct the laser to the ship's engine. The entire system is mounted on a trapezoidal cross-section truss structure with a 3 meter base. This truss may be rotated by means of a turntable at the center of the ship. The mirror system is designed to fold down completely into a 3 meter base equilateral triangle for aerobrake purposes. Figure 3.10 shows a dimensioned sideview of the ship including the mirror system and stored aerobrake.

The hull structure, as well as the mirror structures, are designed to be completely rigid as trusses. This will allow easier in-space construction since all joints need only be pinned. All instrumentation and pump systems will be located within the main hull. The initial payload will be carried in a detachable payload module outside the main ship, while the return payload will be carried within the hull. Mass estimates, moments of inertia, and stress estimates were made using boron/aluminum as truss bar materials, while the tanks were designed to be made of aluminum, each covered with insulation and impact protection material.
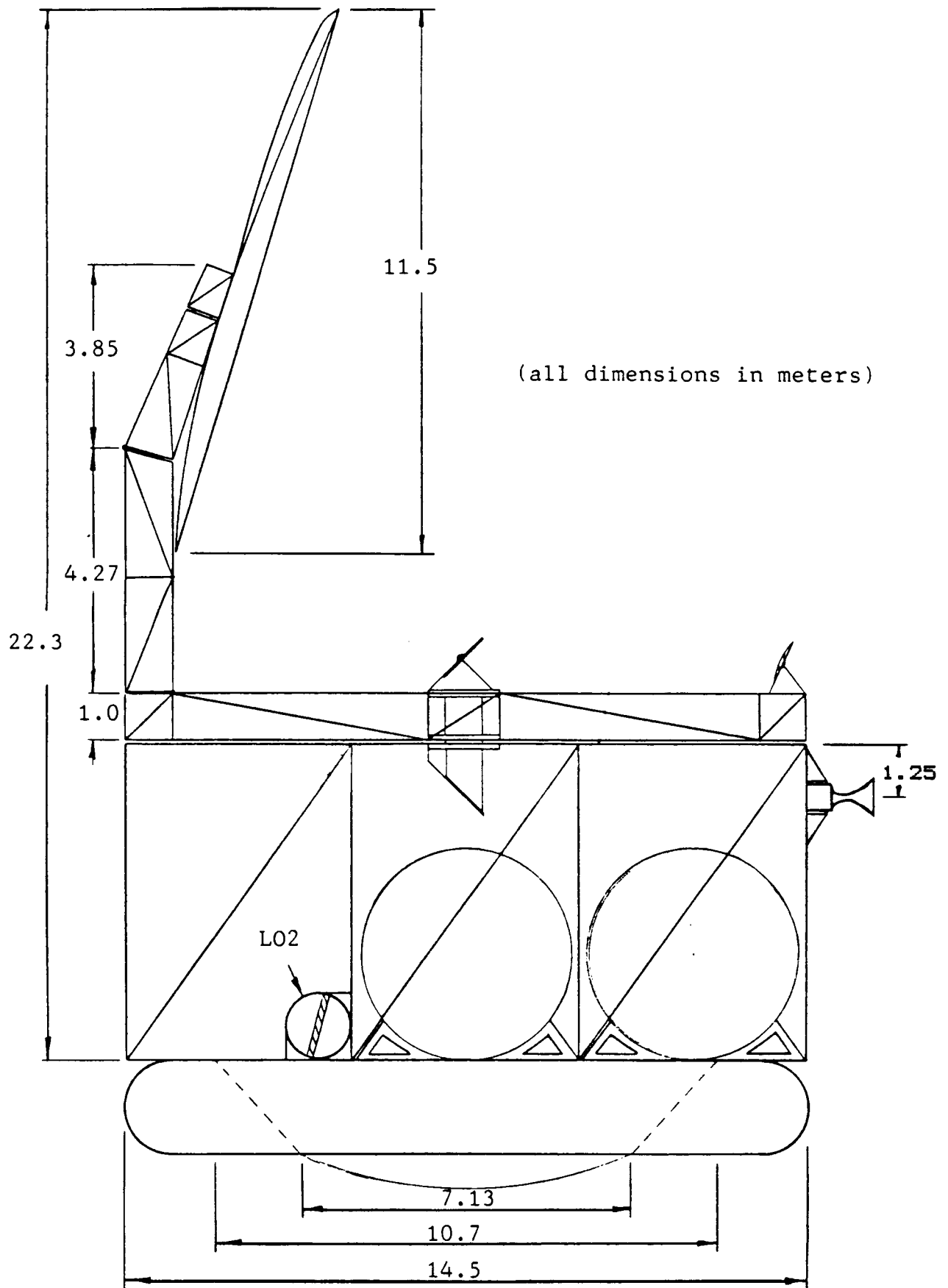
37

11.5

3.85

(all dimensions in meters)

4.27

22.3

1.0

1.25

LO2

7.13

10.7

14.5

Figure 3.10   LEO/GEO Aerobraked Configuration
Side View Schematic

38

3.4.1.2 Mass Estimates

The estimates for the masses of the ship components were obtained through the use of several assumptions. The structural masses, such as those for the fuel tanks, protection materials, truss members, detachable payload module, tank mounting systems, and end fittings were found by multiplying the material density by the material volume (see references 3.6, 3.7, and 3.8). The methods used to determine the masses of the optical, propulsive, and aerobrake systems are outlined in further detail in those specific sections of this report. Mass estimates (given in kilograms) are listed in table 3.5.

Table 3.5 Mass (kg) Estimates - LEO/GEO Aerobraked Scenario

		STANDARD	ALL RETURN
Main Hull Structure, Engine and Tank Supports	=	833	836
Propellant Tanks	=	625	750
Primary Mirror	=	200	200
Mirrors #2, 3, and 4	=	256	256
Optical Truss Structure, and Mirror Supports	=	400	400
Optical Turntable Mechanism	=	150	150
Primary Propulsion System	=	320	320 *
CMG's and R.C.S.	=	291	291
Pointing and Tracking	=	115	115
Guidance, Navigation and Control, Data Management and Communication Systems	=	200	200
Electrical Power System	=	85	85
Instrumentation	=	100	100
Detachable Payload Module	=	526	526
Docking/Connecting Apparatus	=	47	47
Aerobrake and Cap	=	695	695
Vehicle Dry Mass at LEO, $M_{s\uparrow}$	=	4843	4971
LEO-to-GEO Payload Mass, $M_{pl\uparrow}$	=	16000	16000
Propellant Mass at LEO (for round trip, including RCS and reserves)	=	12500	16400
OVERALL INITIAL MASS, M_{tot}	=	33443	37371
Vehicle Dry Mass at GEO, $M_{s\downarrow}$	=	4317	4445
GEO-to-LEO Payload Mass, $M_{pl\downarrow}$	=	5000	16000
Propellant Mass at GEO (for return trip)	=	2400	4800
Initial Mass at GEO	=	11717	25245
Propellant Used for LEO-to-GEO Leg, $M_{p\uparrow}$	=	9700	11000
Propellant Used for GEO-to-LEO Leg, $M_{p\downarrow}$	=	2000	4300

* including propellant feed system and nozzle gimbaling system

3.4.1.3 Center of Gravity and Moments of Inertia

The center of gravity locations were calculated for this ship with the mirror deployed and the aerobrake stored, and also in the aerobraking configuration (see reference 3.8). When the mirror is deployed, the center of gravity changes with the rotation of the mirror. This range may be seen as follows (all units in meters):

Beginning of mission:
$$2.262 < Xbar < 2.326$$
$$Ybar = 2.43$$
$$-0.031 < Zbar < 0.031$$

Before aerobraking:
$$3.66 < Xbar < 3.88$$
$$Ybar = 2.63$$
$$-0.116 < Zbar < 0.116$$

The center of gravity during aerobraking is as follows:

$$Xbar = 3.97$$
$$Ybar = 3.14$$
$$Zbar = 0.00$$

The corresponding moments of inertia are as follows (in kg*m):

$$I_x = 65,314$$
$$I_y = 207,153$$
$$I_z = 271,180$$

Several assumptions were made in the calculations of the moments of inertia. First, the optical turntable was assumed to consist of two thin, rectangular plates. Also, all four mirrors were treated as thin disks and the engine as a cylinder. The liquid hydrogen fuel tanks were designed to be cylindrical with spherical caps, but for the calculations were assumed to be right circular cylinders. The mountings were then added as small rectangles. Finally, the aerobrake was modelled as a short cone.

3.4.1.4 Stress Analysis

Stress analysis results were found by using a modified form of the "Structural Analysis Software for Microcomputers" by B. J. Korites. This particular software uses a series of programs designed to interact with each other giving a more powerful system than would a single code. These programs include the following: MCAT, which stores material properties; MESH, which creates a 3-dimensional mesh of nodes and members; MODEL, which adds restraints to the mesh and recalls material properties; and TRUSS, which calculates node deflections and member loads from a specified loading scheme on the restrained mesh. The analysis of the aerobraked structure is based on the assumptions of a statically loaded truss and point loads at 4 nodes, shown in figure 3.11. Since no software was available to accomodate dynamic analysis or distributed loads, these assumptions were necessary. However, since these assumptions should cause only

LEO-LLO Scenario

LEO-GEO Scenario

13m

10.7m

Figure 3.11 Forces Used for Aerobraked
Configuration Stress Analysis

1.45

docking
port

Frontview

LO2 tank harness

LH2 tanks

6.06

19

docking
port

Sideview

mounting
brackets

LH2 tank

6

4.6

LO2 tank

13

Backview

(all dimensions in meters)

Figure 3.12 LEO/LLO Aerobraked Configuration
Main Truss System
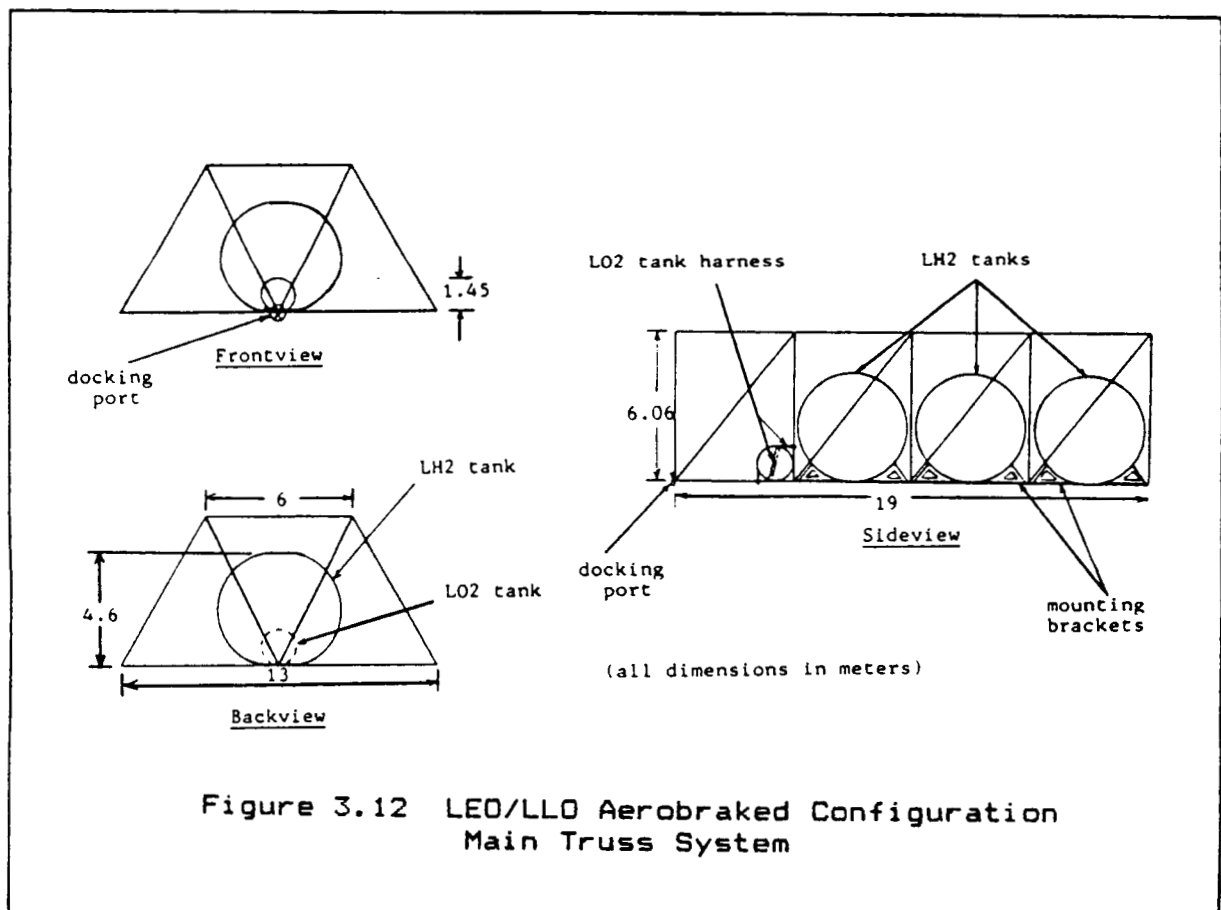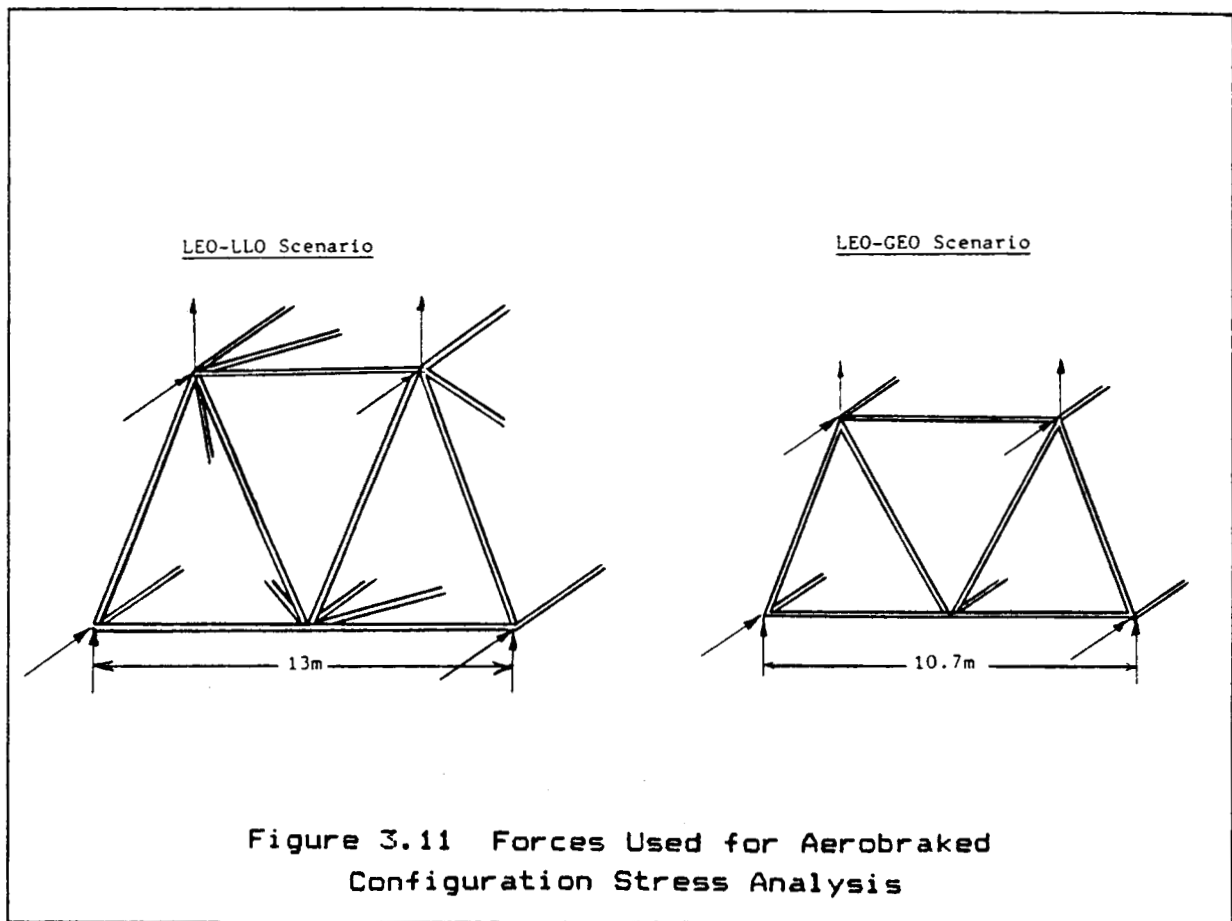
small errors that would tend to overestimate, they are adequate for our purposes. The maximum compressive load for this vehicle was found to be 132 kN. This occurs in the front upper diagonal of the truss, which has a critical load of 198 kN, thus giving a factor of safety of 1.5. (See reference 3.9)

3.4.2 LEO/LLO AEROBRAKED SCENARIO

3.4.2.1 Design Considerations

This configuration is an LOTV designed to travel from LEO to LLO carrying a detachable payload and returning to LEO carrying return payload within the ship. This ship will require a larger amount of fuel than either the aerobraked or non-aerobraked LEO to GEO configurations due to increased delta-V requirement and an extended travel distance. This vehicle employs a larger primary mirror than the LEO/GEO configurations because of the significantly greater distance between the LOTV and the LPS. In addition, it has a total ship length of 19 meters with a 13 meter equilateral triangular cross-section (see figure 3.12).

Upon return to LEO, a ballute aerobrake is deployed and used to slow the ship instead of burning extra fuel for that purpose. Three fuel tanks are located as shown in figure 3.12, and will be emptied from back to front during a mission, in order to achieve the most favorable center of gravity for aerobraking.

The mirror system consists of a 36 meter diameter primary mirror and three additional elliptical mirrors, situated so that the captured beam will be reflected to the engine. The primary mirror is connected by a jointed arm to a telescoping trapezoidal optical truss. This truss has the freedom to rotate 360 degrees, independent of the main structure, on a central turntable so that the beam can be captured from any direction. The turntable itself is made of two rectangular disks with holes in them to allow for the beam to pass through. During aerobraking, the primary mirror, called a wrapped rib mirror, wraps into a 4 meter diameter hub and is stored, along with the other mirrors within the structure. When the optical system is completely folded, the cross-section of the ship is an equilateral triangle with 13 meter sides. Figure 3.13 shows a detailed sideview of the ship, including the optical system and the stored ballute aerobrake.

The hull of the ship consists of a truss structure of trapezoidal cross-section with a bottom length of 13 meters and a top length of 6 meters. The members of this truss, along with those of the optical truss, are also to be fabricated of boron/aluminum. The members will be joined by titanium end fittings and pinned so that the side members can be easily detached for better replaceability and refueling of the fuel tanks. These fuel tanks were designed to be constructed of aluminum with insulation and a protective film over each.
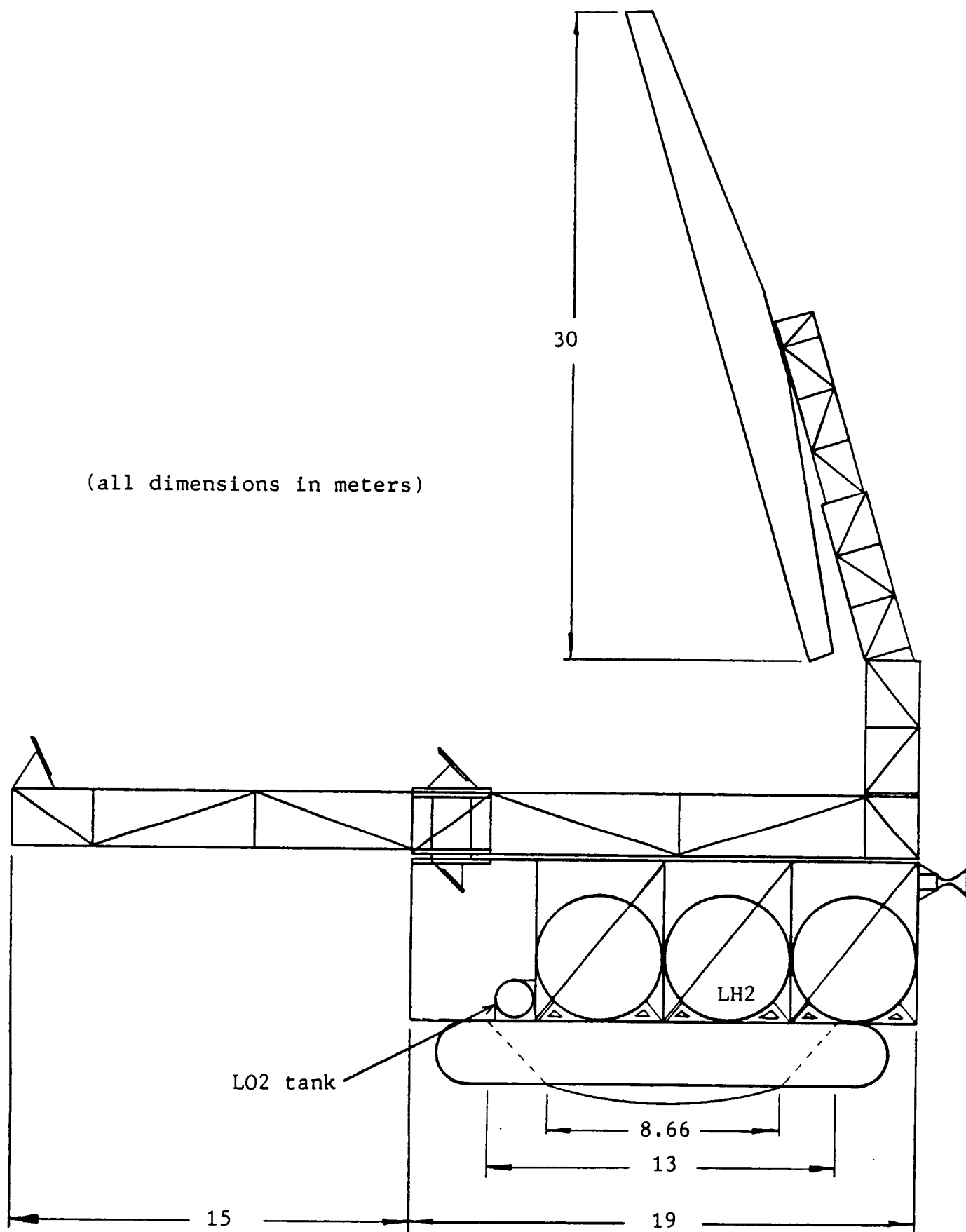
(all dimensions in meters)

30

LH2

LO2 tank

8.66

13

15

19

Figure 3.13   LEO/LLO Aerobraked Configuration
Side View Schematic

3.4.2.2 Mass Estimates

Mass estimates for this ship were obtained in the same way as for the LEO/GEO ship, i.e., density multiplied by volume of the material. Reasonable assumptions were made in the calculations of the moments of inertia for the LEO/LLO ship. First, the optical turntable was assumed to consist of two thin, rectangular plates. Also, all four mirrors were treated as thin disks and the engine as a sphere. The liquid hydrogen fuel tanks were designed to be cylindrical with spherical caps, but for the calculations were assumed to be right circular cylinders. The mountings were then added as small rectangles. Finally, the aerobrake was modelled as a short cone (see references 3.6, 3.7, and 3.8). Table 3.6 lists the mass estimates (in kilograms) for the LEO/LLO Scenario.

Table 3.6 Mass (kg) Estimates - LEO/LLO Scenario

LH2 and LOX Propellant Tanks	=	850
Main Hull Truss Structure, Engine and Tank Supports	=	1012
Optical Turntable Mechanism	=	250
Main Optical Truss Structure and Mirror Supports	=	600
Primary Mirror Arm	=	240
Primary Mirror	=	1400
Second Mirror	=	160
Third Mirror	=	160
Fourth Mirror (variable optics)	=	250
Primary Propulsive System	=	320 *
Pointing and Tracking	=	150
Electrical Power System	=	150
Guidance, Navigation and Control, Data Management and Communication System	=	250
CMG's and R.C.S.	=	470
Detachable Payload Module	=	550
Docking/Connecting Apparatus	=	50
Instrumentation/Additional	=	200
Aerobrake and Cap	=	1200

Structural Dry Mass = M_s	=	8300
Initial Propellant Mass = M_p	=	12000
Payload Mass = M_{pl}	=	16000

OVERALL INITIAL MASS = M_{tot}	=	36300
Overall Payload Ratio = $M_{pl}/(M_p+M_s)$	=	0.79
Overall Structural Coefficient = $M_s/(M_p+M_s)$	=	0.41

* including propellant feed system and nozzle gimbaling system

3.4.2.3 Center of Gravity and Moments of Inertia

The center of gravity locations were calculated for this ship with the mirror deployed and the aerobrake stored, and also in the aerobraking configuration (see reference 3.8). When the mirror is deployed, the center of gravity changes with the rotation of the mirror. This range may be seen as follows (all units in meters):

Beginning of mission:
$$5.51 < Xbar < 6.43$$
$$Ybar = 3.50$$
$$-0.98 < Zbar < 0.98$$

Before aerobraking:
$$4.96 < Xbar < 6.92$$
$$Ybar = 3.90$$
$$-2.082 < Zbar < 2.082$$

The center of gravity during aerobraking is as follows:

$$Xbar = 7.34$$
$$Ybar = 2.64$$
$$Zbar = 0.00$$

The corresponding moments of inertia are as follows (in kg*m):

$$I_x = 247,140$$
$$I_y = 451,590$$
$$I_z = 673,790$$

3.4.2.4 Stress Analysis

Stress analysis was performed on the main hull truss structure. The hull alone was analyzed since it is assumed to handle most of the stresses caused by aerobraking. Computer analysis was used due to the complex structure. The program used was a compilation of programs, outlined in section 3.4.1.4, called Structural Analysis for Micros (SASM), and was developed by B. J. Korites. It was modified and compiled for our uses. The results gave a maximum member force of 184 kN in the front upper diagonal of the truss. This is less than the critical load of 296 kN by a factor of safety of 1.6. (See reference 3.9).

3.4.3 FUEL TANK MOUNTING SYSTEMS

Design of mounting systems for the aerobraked configurations was based upon low mass considerations and ease of space construction and adaptability. Separate mounting systems for the liquid hydrogen and liquid oxygen tanks were employed due to their difference in mass, size, and location. Mass estimates for the systems total 55 kg for the LEO/GEO mission and 75 kg for the LEO/LLO mission, based on material density and volume.

The liquid hydrogen tank mountings for LEO/GEO and LEO/LLO are shown in figures 3.14 and 3.15, respectively. The two mounting brackets are very similar, differing only in certain dimensions.
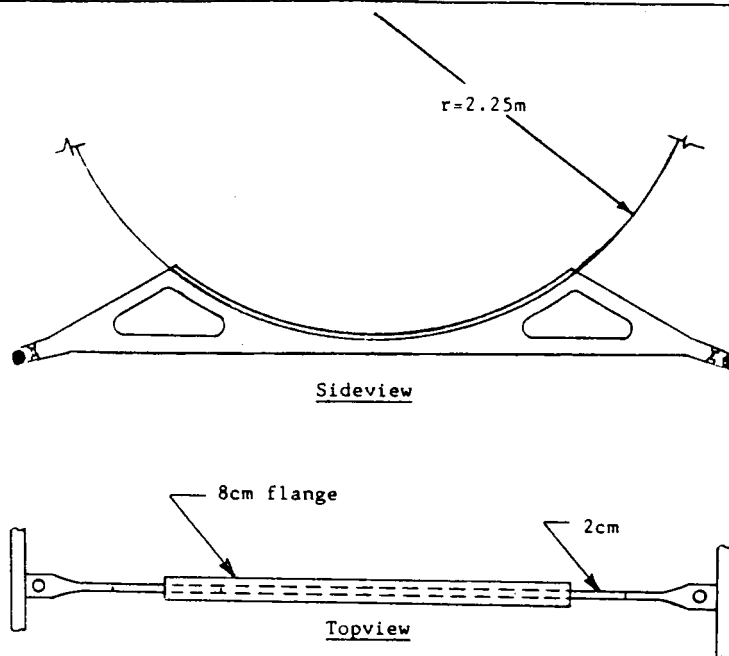
r=2.25m

Sideview

8cm flange

2cm

Topview

Figure 3.14   LEO/GEO Aerobraked Configuration
LH2 Tank Mounting

r=2.3m

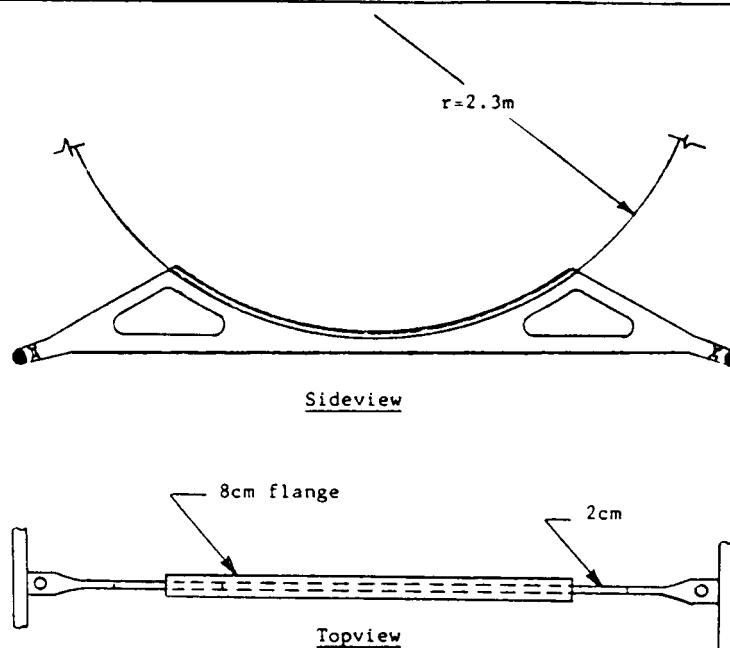Sideview

8cm flange

2cm

Topview

Figure 3.15   LEO/LLO Aerobraked Configuration
LH2 Tank Mounting

They are intended to be fastened around truss bar members on the base of the ship, and have the fuel tanks rest on top of them, with one bracket being at each end along the width of the tanks. An aluminum band attaches through the bracket and wraps around the tank. The band has an inner polymer coating to prevent slippage and scarring of the tank surface.

The liquid oxygen tank in each of the two missions is to be secured with a harness system shown in figure 3.16. Five titanium clamps with inner polymer coatings will attach the harness to the main truss structure, three on the base below the tank, and two on vertical members at the top of the tank. A titanium ring with a polymer under-coating fits on top of the spherical tank, to which the five harness straps are connected. The straps are made of a high-strength, high-modulus composite braided weave. By merely adjusting the strap length and location of the clamps, the liquid oxygen tank could be located anywhere convenient within the truss structure, and can be easily removed to further access the inner truss structure.

3.5 PAYLOAD AND DOCKING SYSTEMS

One advantage of the detachable payload scheme is the LOTV's flexibility in linking with and transporting various types and sizes of payload modules. For this mission we chose a cylindrical DPM 4 m in diameter and 15 m in length, made of a 1 millimeter thick boron/aluminum. This gives a DPM dry mass of 526 kg. Capable of carrying 16,000 kg (35,280 lbm) of cargo, the DPM will attach via male/female drogue connector on the front face of the main hull, which will also be used for docking during LOTV rendezvous operations.

The LOTV docking mechanism must perform two main functions: (i) connection of the LOTV with the detachable payload module, and (ii) attachment during rendezvous with the space station or refueling/service platforms. Both must be accomplished with a connection system which is structurally rigid, has a high degree of reliability, and is able to withstand repeated loadings throughout the vehicle's life.

The essential concept agreed upon for the docking system is a male/female or probe/drogue link which will lock securely upon insertion. After considering several schemes it was decided to utilize a single male probe apparatus, located at the center of the LOTV front face. Figure 3.17 shows the schematic of the docking latch mechanism with the featured axis of rotation and hydraulic pressure system.

The male probe member will be the active mechanism of the docking system, containing several latch members which will lock into place upon insertion into the drogue or receptacle. The detachable payload module will contain a passive drogue (recepticle) device. The drogue will contain a spring-loaded damping system to absorb most of the initial shock of engagement. The probe mechanism will be primarily titanium-aluminum with a

47

mass of 30 kg. The probe will be 40 cm in length with a diameter of 10 cm. Figure 3.18 shows a highly simplified sketch of the latch system on the probe, which will activate and retract via a hydraulic spring system.

A one-probe mechanism was selected due to the simplicity, mass savings, and diversity in docking capabilities. Several probe connectors would necessitate a similar drogue pattern on any structure with which the LOTV could rendezvous, whereas the single probe could link directly or with the aid of a single adaptor. Likewise, small deflections in any of the connectors in a multi-probe system at any time during the mission could offset the alignment and lead to complications in the docking procedure. Thus a single probe-receptacle connection was agreed upon. The use of an electromagnet at the head of the connecting surface was considered but was ruled out due to cost and power requirements outweighing its benefits. (See references 3.2 and 3.3).

3.6 CONCLUSIONS

The selected non-aerobraked configuration effectively meets a wide range of design criteria including mass savings (the dry mass of the present configuration has been reduced by some 40 percent from the original configuration), structural rigidity and stress limitations (no member in the truss has a load exceeding critical loading, with a 1.5 factor of safety), efficiency of docking procedures (see section 3.5 for a detailed discussion), and such life cycle considerations as accessibility for refueling and servicing, which are enabled by the movable x-member on the front face. Additionally, the modularity of the LOTV with regard to payload transportation will make it useful over a wide range of mission requirements.

The aerobraked versions of the LOTV have the advantage over the non-aerobraked version of smaller fuel requirements, making them quite versatile in uses for several types of missions. The reason for this is that there are many options available for the transport of payload, such as in a detachable module or contained within the main hull of the ship. The design also allows for the simple removal and refueling of fuel tanks, which contributes to the cost effectiveness of the ship. In conclusion, the LOTV should prove to be an extremely useful tool in future missions and will play an essential role in cost effective transport of payload and fuel in space.

They are intended to be fastened around truss bar members on the base of the ship, and have the fuel tanks rest on top of them, with one bracket being at each end along the width of the tanks. An aluminum band attaches through the bracket and wraps around the tank. The band has an inner polymer coating to prevent slippage and scarring of the tank surface.

The liquid oxygen tank in each of the two missions is to be secured with a harness system shown in figure 3.16. Five titanium clamps with inner polymer coatings will attach the harness to the main truss structure, three on the base below the tank, and two on vertical members at the top of the tank. A titanium ring with a polymer under-coating fits on top of the spherical tank, to which the five harness straps are connected. The straps are made of a high-strength, high-modulus composite braided weave. By merely adjusting the strap length and location of the clamps, the liquid oxygen tank could be located anywhere convenient within the truss structure, and can be easily removed to further access the inner truss structure.

3.5 PAYLOAD AND DOCKING SYSTEMS

One advantage of the detachable payload scheme is the LOTV's flexibility in linking with and transporting various types and sizes of payload modules. For this mission we chose a cylindrical DPM 4 m in diameter and 15 m in length, made of a 1 millimeter thick boron/aluminum. This gives a DPM dry mass of 526 kg. Capable of carrying 16,000 kg (35,280 lbm) of cargo, the DPM will attach via male/female drogue connector on the front face of the main hull, which will also be used for docking during LOTV rendezvous operations.

The LOTV docking mechanism must perform two main functions: (i) connection of the LOTV with the detachable payload module, and (ii) attachment during rendezvous with the space station or refueling/service platforms. Both must be accomplished with a connection system which is structurally rigid, has a high degree of reliability, and is able to withstand repeated loadings throughout the vehicle's life.

The essential concept agreed upon for the docking system is a male/female or probe/drogue link which will lock securely upon insertion. After considering several schemes it was decided to utilize a single male probe apparatus, located at the center of the LOTV front face. Figure 3.17 shows the schematic of the docking latch mechanism with the featured axis of rotation and hydraulic pressure system.

The male probe member will be the active mechanism of the docking system, containing several latch members which will lock into place upon insertion into the drogue or receptacle. The detachable payload module will contain a passive drogue (recepticle) device. The drogue will contain a spring-loaded damping system to absorb most of the initial shock of engagement. The probe mechanism will be primarily titanium-aluminum with a

47

mass of 30 kg. The probe will be 40 cm in length with a diameter of 10 cm. Figure 3.18 shows a highly simplified sketch of the latch system on the probe, which will activate and retract via a hydraulic spring system.

A one-probe mechanism was selected due to the simplicity, mass savings, and diversity in docking capabilities. Several probe connectors would necessitate a similar drogue pattern on any structure with which the LOTV could rendezvous, whereas the single probe could link directly or with the aid of a single adaptor. Likewise, small deflections in any of the connectors in a multi-probe system at any time during the mission could offset the alignment and lead to complications in the docking procedure. Thus a single probe-receptacle connection was agreed upon. The use of an electromagnet at the head of the connecting surface was considered but was ruled out due to cost and power requirements outweighing its benefits. (See references 3.2 and 3.3).

3.6 CONCLUSIONS

The selected non-aerobraked configuration effectively meets a wide range of design criteria including mass savings (the dry mass of the present configuration has been reduced by some 40 percent from the original configuration), structural rigidity and stress limitations (no member in the truss has a load exceeding critical loading, with a 1.5 factor of safety), efficiency of docking procedures (see section 3.5 for a detailed discussion), and such life cycle considerations as accessibility for refueling and servicing, which are enabled by the movable x-member on the front face. Additionally, the modularity of the LOTV with regard to payload transportation will make it useful over a wide range of mission requirements.

The aerobraked versions of the LOTV have the advantage over the non-aerobraked version of smaller fuel requirements, making them quite versatile in uses for several types of missions. The reason for this is that there are many options available for the transport of payload, such as in a detachable module or contained within the main hull of the ship. The design also allows for the simple removal and refueling of fuel tanks, which contributes to the cost effectiveness of the ship. In conclusion, the LOTV should prove to be an extremely useful tool in future missions and will play an essential role in cost effective transport of payload and fuel in space.

They are intended to be fastened around truss bar members on the base of the ship, and have the fuel tanks rest on top of them, with one bracket being at each end along the width of the tanks. An aluminum band attaches through the bracket and wraps around the tank. The band has an inner polymer coating to prevent slippage and scarring of the tank surface.

The liquid oxygen tank in each of the two missions is to be secured with a harness system shown in figure 3.16. Five titanium clamps with inner polymer coatings will attach the harness to the main truss structure, three on the base below the tank, and two on vertical members at the top of the tank. A titanium ring with a polymer under-coating fits on top of the spherical tank, to which the five harness straps are connected. The straps are made of a high-strength, high-modulus composite braided weave. By merely adjusting the strap length and location of the clamps, the liquid oxygen tank could be located anywhere convenient within the truss structure, and can be easily removed to further access the inner truss structure.

3.5 PAYLOAD AND DOCKING SYSTEMS

One advantage of the detachable payload scheme is the LOTV's flexibility in linking with and transporting various types and sizes of payload modules. For this mission we chose a cylindrical DPM 4 m in diameter and 15 m in length, made of a 1 millimeter thick boron/aluminum. This gives a DPM dry mass of 526 kg. Capable of carrying 16,000 kg (35,280 lbm) of cargo, the DPM will attach via male/female drogue connector on the front face of the main hull, which will also be used for docking during LOTV rendezvous operations.

The LOTV docking mechanism must perform two main functions: (i) connection of the LOTV with the detachable payload module, and (ii) attachment during rendezvous with the space station or refueling/service platforms. Both must be accomplished with a connection system which is structurally rigid, has a high degree of reliability, and is able to withstand repeated loadings throughout the vehicle's life.

The essential concept agreed upon for the docking system is a male/female or probe/drogue link which will lock securely upon insertion. After considering several schemes it was decided to utilize a single male probe apparatus, located at the center of the LOTV front face. Figure 3.17 shows the schematic of the docking latch mechanism with the featured axis of rotation and hydraulic pressure system.

The male probe member will be the active mechanism of the docking system, containing several latch members which will lock into place upon insertion into the drogue or receptacle. The detachable payload module will contain a passive drogue (recepticle) device. The drogue will contain a spring-loaded damping system to absorb most of the initial shock of engagement. The probe mechanism will be primarily titanium-aluminum with a
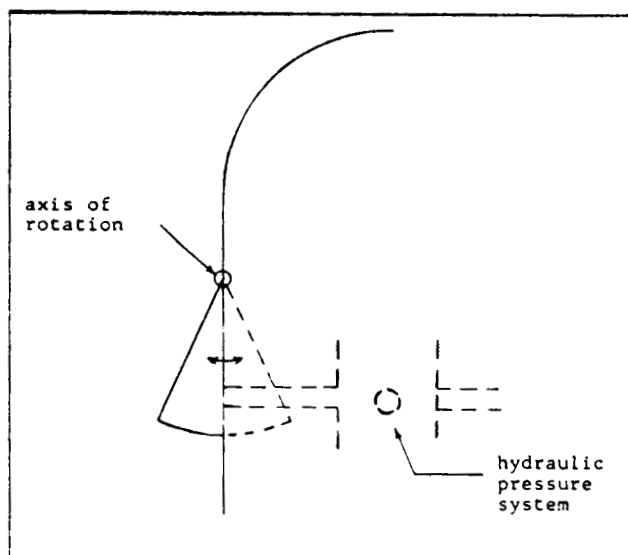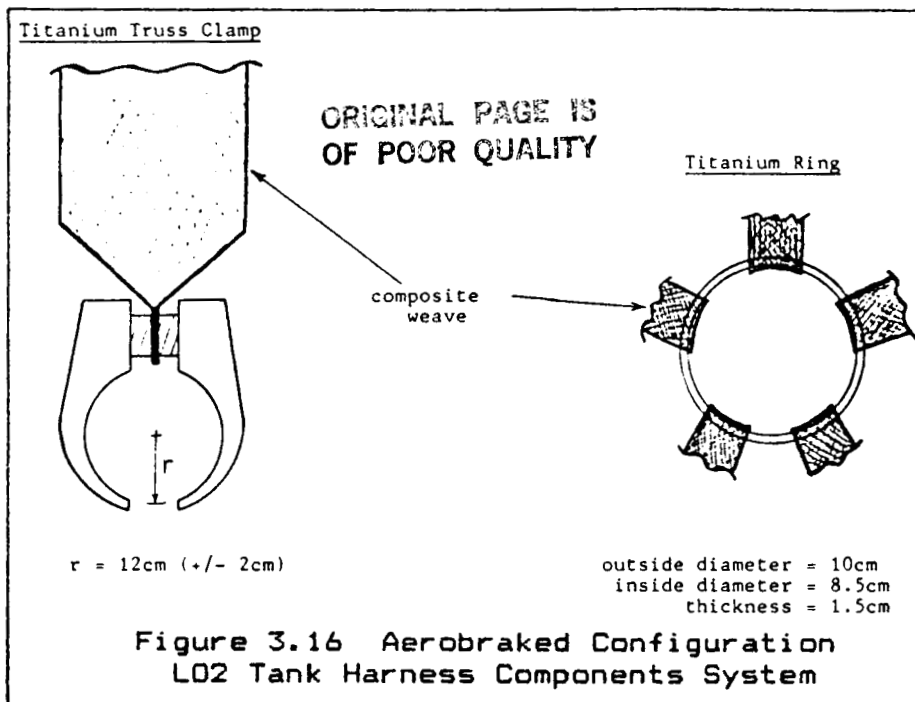
47

mass of 30 kg. The probe will be 40 cm in length with a diameter of 10 cm. Figure 3.18 shows a highly simplified sketch of the latch system on the probe, which will activate and retract via a hydraulic spring system.

A one-probe mechanism was selected due to the simplicity, mass savings, and diversity in docking capabilities. Several probe connectors would necessitate a similar drogue pattern on any structure with which the LOTV could rendezvous, whereas the single probe could link directly or with the aid of a single adaptor. Likewise, small deflections in any of the connectors in a multi-probe system at any time during the mission could offset the alignment and lead to complications in the docking procedure. Thus a single probe-receptacle connection was agreed upon. The use of an electromagnet at the head of the connecting surface was considered but was ruled out due to cost and power requirements outweighing its benefits. (See references 3.2 and 3.3).
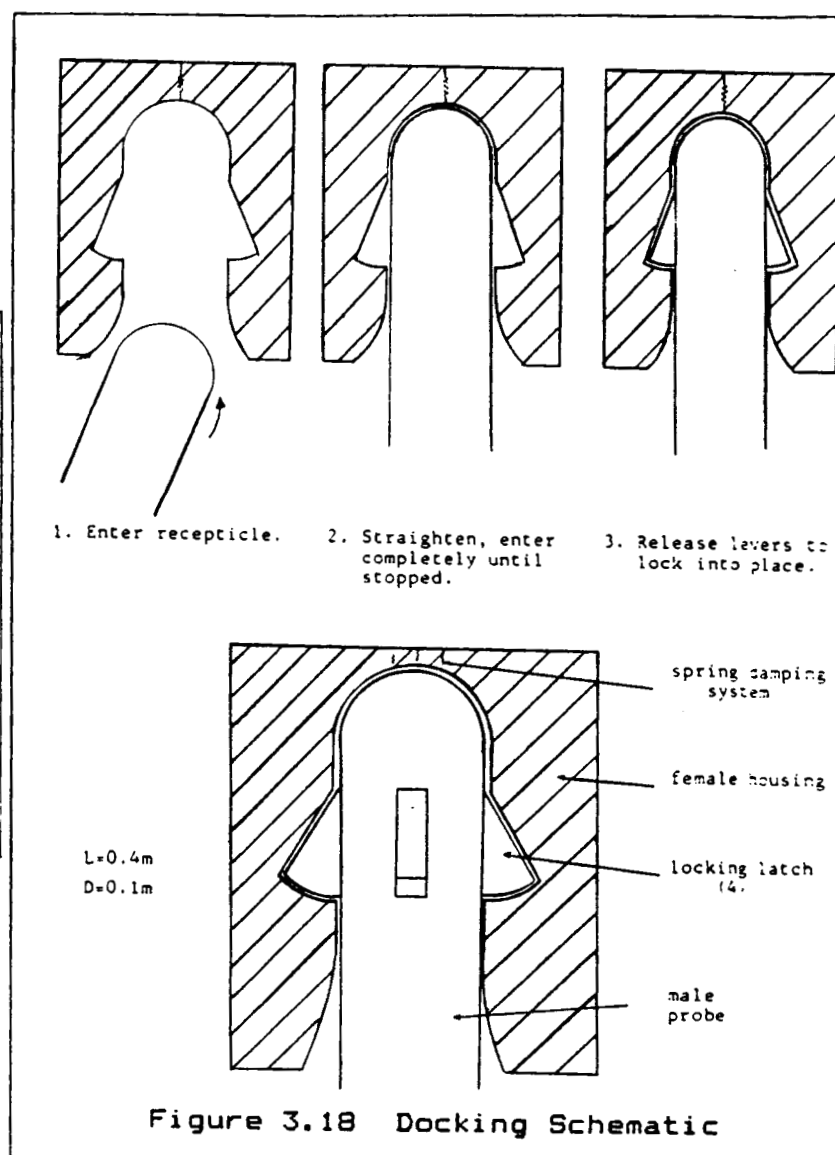
3.6 CONCLUSIONS

The selected non-aerobraked configuration effectively meets a wide range of design criteria including mass savings (the dry mass of the present configuration has been reduced by some 40 percent from the original configuration), structural rigidity and stress limitations (no member in the truss has a load exceeding critical loading, with a 1.5 factor of safety), efficiency of docking procedures (see section 3.5 for a detailed discussion), and such life cycle considerations as accessibility for refueling and servicing, which are enabled by the movable x-member on the front face. Additionally, the modularity of the LOTV with regard to payload transportation will make it useful over a wide range of mission requirements.

The aerobraked versions of the LOTV have the advantage over the non-aerobraked version of smaller fuel requirements, making them quite versatile in uses for several types of missions. The reason for this is that there are many options available for the transport of payload, such as in a detachable module or contained within the main hull of the ship. The design also allows for the simple removal and refueling of fuel tanks, which contributes to the cost effectiveness of the ship. In conclusion, the LOTV should prove to be an extremely useful tool in future missions and will play an essential role in cost effective transport of payload and fuel in space.

ORIGINAL PAGE IS
OF POOR QUALITY

Titanium Truss Clamp

Titanium Ring

composite
weave

r = 12cm (+/- 2cm)

outside diameter = 10cm
inside diameter = 8.5cm
thickness = 1.5cm

Figure 3.16 Aerobraked Configuration
LO2 Tank Harness Components System

1. Enter recepticle.

2. Straighten, enter
completely until
stopped.

3. Release levers to
lock into place.

axis of
rotation

hydraulic
pressure
system

Figure 3.17 Docking
Latch Mechanism

L=0.4m
D=0.1m

spring damping
system

female housing

locking latch
(4)

male
probe

Figure 3.18 Docking Schematic

49

3.7 REFERENCES

1. "OTV Mission Studies," General Dynamics Space Systems Division, Fort Worth, Texas, 1985.

2. Chandler, J.A., "Apparatus for Releasably Connecting First and Second Objects in Predetermined Space Relationship," NASA Report N82-28318, April 14, 1982.

3. "Aeroassisted Manned Transfer Vehicle (Taxi)," Department of Aerospace and Ocean Engineering, VPI&SU, June 1987.

4. "Structural Indices in Design Optimization With Metal-Matrix Composites," Schoutens, J.E. and Zarate, D.A., Composites, Volume 17, July 1986.

5. "Metal-Matrix Composites --- Overview," Kinna, M.A., D.O.D. Metal-Matrix Composites Information Analysis Center, Volume 253, January 1988.

6. Mechanics of Composite Materials, Jones, R.H., Hemisphere Publishing Corporation, New York, 1975.

7. Engineering Thermodynamics, Second Edition, Jones, J.B. and Hawkins, G.A., John Wiley & Sons, Inc., 1986.

8. Vector Mechanics for Engineers - Statics and Dynamics, Fourth Edition, Beer, F.P. and Johnston, R.E. Jr., McGraw- Hill, Inc., 1984.

9. "Structural Analysis Software for Microcomputers," Korites, B. J., Kern International, Inc., 1975.

4. OPTICS

4.1 EVOLUTION OF THE OPTICAL SYSTEM

The purpose of the optical system is to intercept a laser beam and focus it into the thrust chamber where its energy can be used to propel the vehicle. With this basic mission and the requirements of high efficiency, low mass, and the ability to collapse for stowage behind an aerobrake, deliberation of a satisfactory system started.

The first proposed design was a very simple one mirror system which intercepted the beam and focused it through a window in the top of the thrust chamber. The mirror was an inflatable semi-reflective envelope consisting of 20 preformed gores, surrounded by a higher pressure torus which served to shape the reflector circumferentially. The envelope was shaped to proper parabolic contour through pressurization of the individual gores.

In order for the mirror to be able to catch the beam from any angle, the mirror rotated about its focal point and the ship rotated on its axis.

The main advantages of this design were its very low mass and its simplicity of construction and deployment.

The design was dropped as a possibility because of two disadvantages. The efficiency of such a mirror is not very high compared to the other mirrors that were later proposed because in addition to losing some of the energy of the beam to imperfect reflection, the beam passes through the front surface twice. This surface has less than perfect transparency, subsequently causing the beam to lose more of its energy.

The second disadvantage is that this mirror would not retain a constant shape due to punctures from small particles. These punctures would release some of the pressure that holds the mirror in its proper shape and alignment, and the change in the geometry would throw the beam off its focus in the thrust chamber. This disadvantage can be partially overcome by continuous pressurization of the reflective envelope, but the additional equipment necessary for this solution reduces the advantages of this design by increasing the mass and the complexity.

For better efficiency, the design of the thrust chamber was changed so that the window was no longer in the top but moved to the front. Therefore, a different system that angled the beam into the new window with the addition of a second mirror was considered.

In order to turn the beam through an angle approaching ninety degrees, the primary mirror was required to be of much greater diameter than the incoming beam so that most of the beam was intercepted. It was determined that for maximum efficiency

51

inside the thrust chamber the focal point should be oval in shape. To achieve this, the mirror should have a large f number (defined as focal length over diameter). Since the diameter of the mirror was already determined to be large, this condition could only be achieved by lengthening the focal length of the mirror. With this configuration, the mirror would be positioned far above the rest of the vehicle, needing extra mass for the long supporting structure and causing large moments due to its rotation. These characteristics were unacceptable, so a new configuration·was sought. The need to direct the laser beam into the front of the thrust chamber meant that the beam had to be routed through the main vehicle structure. Therefore the beam had to be turned at least once more if it were to follow a path through the vehicle structure.

In order to protect the optical system from the heat of aerobraking, it was to be designed to collapse to fit behind the brake. A system of four mirrors was proposed that met both the condition that the beam path travel through part of the vehicle and the need for a longer focal distance without excessive truss lengths or masses. The beam is first intercepted by a main mirror that is almost perpendicular to the beam and is then focused down the length of the optical truss onto a second mirror, which again reflects the beam back along the truss. A third mirror sits atop the point of rotation of the optical truss and turns the beam into the structure of the vehicle where a forth mirror focuses it into the thrust chamber.

The first four mirror system considered placed the point of rotation of the optical truss along the axis of the center of mass of the system so that its rotation would not upset the center of mass of the whole vehicle. This system met all the constraints so far placed on the design. Unfortunately, the truss extended over the edge of the vehicle a distance of 16 meters, and when in the position to catch the beam coming from the rear of the vehicle, it extended into the plume of gas from the engine. Exposure to the excessive heat of the plume would cause damage to the optical equipment; therefore, a change had to be made.

The point of rotation was changed to the middle of the truss so that none of the optical equipment was exposed to the plume. This design slightly shortened the focal length of the system but now required that the control mechanisms of the vehicle compensate for the fact that the system rotates about a point some distance from the axis of the center of mass. However, all the system constraints are satisfied.

The truss structure for this system was designed to telescope and fold up so that the whole system could fit behind the aerobrake during the return trip from GEO. The main mirror design was required to also collapse for aerobraking, and this constraint restricted the possible designs.

The initial calculations of beam size indicated that the main
mirror would have to have a capture diameter of 36 meters to
intercept the beam at the average operating distance between the
laser and the vehicle. The design of the main mirror required a
minimal mass and an acceptable efficiency. As previously
discussed, an inflatable mirror was not acceptable. A solid
mirror would provide the best efficiency, but the mass would be
intolerable. Two possible designs were researched and proposed.
The first is termed a hoop-column mirror because its structure is
made up of hoops that give shape to the surface supported by
cables attached to a central column. This design allowed the
mirror to collapse for aerobraking, but the central column
interfered with the beam to a degree that was detrimental to the
efficiency. Thus, the second possible mirror design was chosen.
This design is called a wrap-rib mirror and is discussed later.

A reassesment of the calculations of the beam dispersion showed
that a mirror diameter of only 11.5 meters was necessary instead
of 36 meters. This smaller size allowed new possibilities for
the main mirror design because the mirror mass could be
significantly reduced and also because the lighter vehicle did
not necessarily need to aerobrake.

A semi-rigid mirror was considered because of increased
efficiency. The design adopted is sufficeintly low in mass to
meet constraints and provides greater utilization of the beam
energy than the collapsible mirrors. A 11.5 meter aerobraked
version was designed as an option because aerobraking was not
ruled out as an alternative.

The 36 meter mirror aerobraking version was not abandoned,
however. Instead, it was proposed for a lunar transfer vehicle.

4.2 DETERMINATION OF KEY SIZES OF OPTICAL SYSTEM

4.2.1 PRIMARY MIRROR SIZING - LASER SPOT CONSIDERATIONS

As mentioned previously, the primary mirror of the LOTV serves to
capture and direct the incoming laser energy toward the second
mirror located on the optical truss. Sizing of this first mirror
is one of the few design variables driven by factors outside of
the ship, namely the diffraction of the laser beam as it travels
through space. It was first assumed that the orbiting laser
utilized a high quality ($\lambda/20$) transmitting mirror and operated
in the TEM 00 mode. The spot size of the beam was found to be
11.66 m over the worst-case separation of the laser and LOTV in
LEO to GEO transfer. This quantity was calculated using the
following equations:

$$\text{Beam spread} \quad \acute{\imath} = ((\acute{\imath}_o)^2 + (\acute{\imath}_j)^2 + (\acute{\imath}_w)^2)^{.5}$$

$$\text{where:} \quad \acute{\imath}_o = .538\, \lambda/D \quad \text{(diffraction half-angle)}$$

$$\acute{\imath}_j = 0.05 \times 10^{-6}\, \text{RAD} \quad \text{(beam jitter)}$$

$$\acute{I}_W = \frac{\lambda/20}{D} \text{ (wave front error)}$$

$$D = 30 \text{ m (laser transmitting mirror aperture)}$$

Spot size $= 4 \acute{I} R$

where: $R = 52726 \text{ km}$

A reflector diameter was calculated by assuming the average angle of inclination of the reflector to be less than 20 degrees. This resulted in a mirror diameter of 12.4 m which was reduced to 11.5 m on the basis of an assumption that, by the period of 2000 – 2010, the beam jitter can be reduced below the 0.05 Ìrad value projected for the 1990's.

4.2.2 OPTICAL SYSTEM GEOMETRY

The proposed mirror system for the LOTV is similar to a true Cassegrain. The true Cassegrain incorporates a concave parabolic primary mirror and a convex hyperbolic secondary mirror, both aligned on a common axis with a common inertial reference point in order to focus an image to a specific point. The effective focal length is longer than the focal length of the primary parabolic mirror, but the total length of the Cassegrain system is shorter. The LOTV optical system, however, incorporates a convex parabolic secondary reflective surface, which shares the same focal point as the primary parabolic mirror (see figure 4.1). The effect achieved in this configuration is merely to reduce the diameter of the beam while keeping it parallel to the incident beam and the common axis. In the Cassegrain system, the beam reflected from the second mirror converges to a point, while in the LOTV optical system, the beam reflected from the second mirror can be thought of as converging to a point at an infinite distance from the system. In order to redirect the circular beam from the second mirror to the fourth mirror, a planar, elliptic third mirror is placed in the beam path at a 45 degree angle to the common axis. The fourth mirror, which is basically concave and parabolic, is divided into seven sections and acts to split the beam and focus it to seven separate sections in the thrust chamber.

In order to minimize the weight of both the primary mirror and the ptical truss, a primary reflective surface with a focal length of 14 meters (assuming an incident beam diameter of 11.5 meters) was employed in the LEO/GEO configurations, and a primary mirror with a focal length of 34 meters was employed in the LEO/LLO configuration. The equation used to generate points on the first, second, and fourth mirrors is as follows:

$$X^2 + Z^2 = 4PY$$

where p is the focal point. The position along the common axis of the 'vertex' of the secondary mirror (figure 4.1) was

FIGURE 4.1   VISUALIZATION OF MIRROR CONTOURS
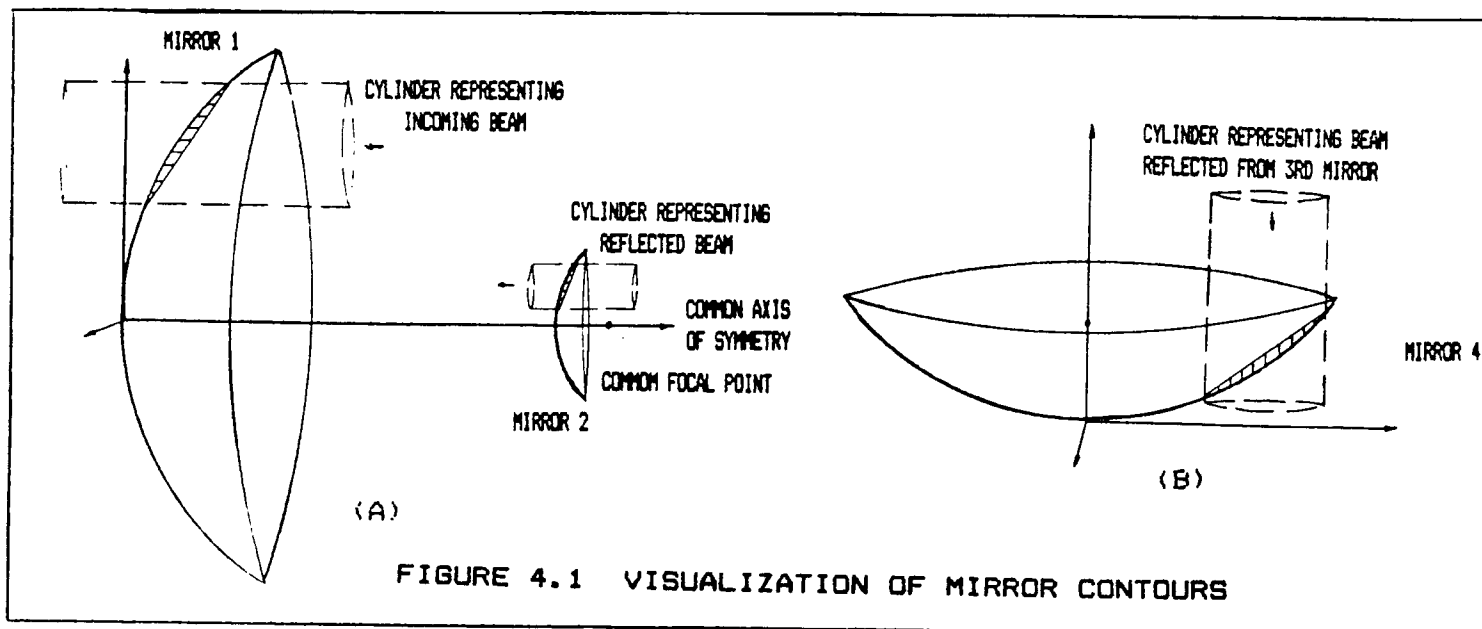
determined (and verified using 2-D CAD graphics) from the following relationship:

$$\frac{\text{BEAM DIAMETER (source to mirror 1)}}{\text{BEAM DIAMETER (mirror 2 to mirror 3)}} = \frac{\text{FOCUS MIRROR 1}}{\text{FOCUS MIRROR 2}}$$

The restriction on the basic shape of the fourth mirror is that it must focus the beam through the thrust chamber window to an imaginary point (actually seven points) beyond the chamber. The resulting reflective surface configurations are shown in figure 4.2.

4.3 OPTICAL SYSTEM DESIGN OVERVIEW

Of the many design parameters involved with the LOTV optical system, those of paramount importance are the system mass, system efficiency, and damage resistance. The rigid mirrors of the LOTV were thus designed around these criteria, and exhibit satisfactory mass and performance characteristics.

4.3.1 MIRROR 1 - MULTIFACETED REFLECTOR

The primary reflector (mirror 1) of the LOTV consists of a leightweight support frame upon which is fixed a number of reflective facets (figure 4.3). The local curvatures of the individual facets, taken together, approximate the off-axis parabolic contour necessary for the main mirror. Each facet is a low mass, dielectrically coated structure with a mass per unit area of approximately 2.92 kg. The entire mirror, once assembled, has a mass on the order of 500 kg. (Ref. 4.4).

55

INCIDENT BEAM DIAM.: 11.5M
BEAM DIAM. MIRROR 2-3: .8M

X-AXIS

Y-AXIS
COMMON AXIS FOR MIRRORS 1 & 2

.15M

.85M

.25M

FOCUS MIRROR 1: 14M
FOCUS MIRROR 2: .9739M
FOCUS MIRROR 4: 5.75077M

MAJOR AXIS MIRROR 3: 1.414M
MINOR AXIS MIRROR 3: 1M
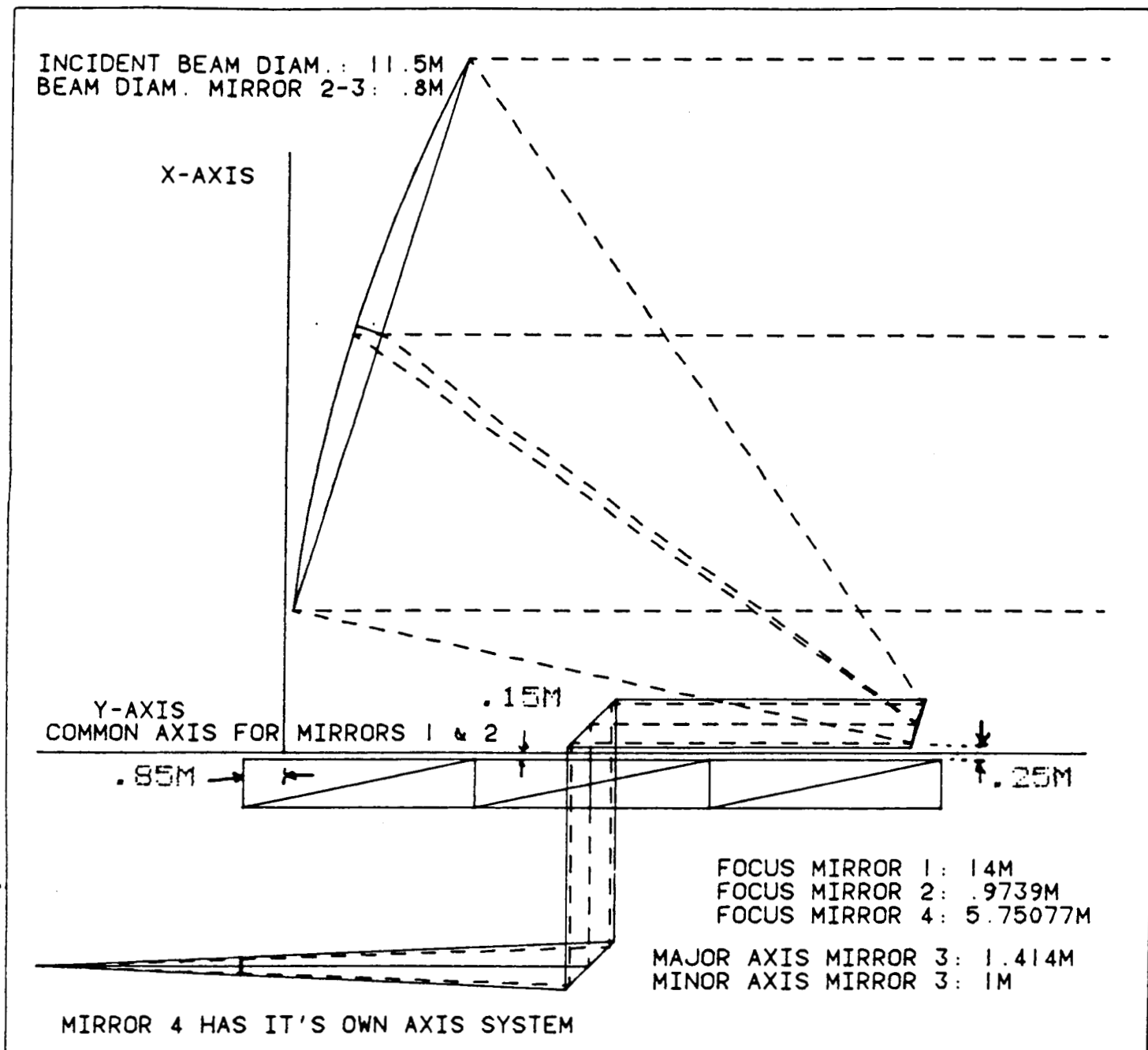
MIRROR 4 HAS IT'S OWN AXIS SYSTEM

FIGURE 4.2 OPTICAL SYSTEM GEOMETRY
(LEO/GEO SCENARIOS)

4.3.2 COMMON CHARACTERISTICS OF LOTV MIRRORS 2, 3, 4

To ease the design of mirrors 2 through 4, a generalized reflective surface was first constructed to perform within certain limits driven by the initial beam characteristics - i.e. 99%+ reflectivity required at a wavelength of 1.315 micrometers, adequate ability to withstand the high beam energy required, etc. In addition, mirror mass was to be minimized as much as possible.

This generalized reflective surface is illustrated in Figure 4.4. The surface consists of a multi-layer dielectric coating applied to a substrate of fused silica. This single facesheet is supported by a honeycomb backing, also of fused silica. SiO_2 (quartz) was chosen as the coating material since it is slightly more transmissive than magnesium fluoride for this particular application. The material for the facesheet and honeycomb was chosen primarily for its low coefficient of thermal expansion. Although the nature of this mission does not require high precision optics per se, the fused silica was nonetheless attractive. Mass considerations led to the choice of a lightweight backing such as the honeycomb (see figure 4.5), which yields up to 85% lightweighting over an equivalently rigid solid thickness.

With the generalized reflective surface thus developed, one need only specify the particular physical situation to which it is applied. What follows are functional descriptions of the individual mirrors.

4.3.3 MIRROR 2

The function of the second mirror is to produce an axi-symmetric circular beam which runs parallel to the optical truss. Thus this mirror's surface is a convex, off-axis parabola with a slightly elliptical circumference. After leaving the primary mirror, the beam converges toward mirror 2 and is reflected by the parabolic surface, which is a smaller scale duplicate of the primary mirror surface. Mirror 2 is mounted at the end of the optical truss opposite the primary reflector.

4.3.4 MIRROR 3

The third mirror is planar and serves to direct the now parallel beam along the optical truss' axis of rotation. This allows the truss to rotate a full 360 degrees without affecting the beam geometry. Note also that the optical thicknesses of the dielectric layers on this mirror are configured for 45 degree reflection.

4.3.5 MIRROR 4

The fourth and final mirror is the heaviest and most complex of the three smaller reflectors. This mirror transforms the parallel, circular, vertical beam into seven horizontal beams of finite focal length. This requires that the mirror have seven
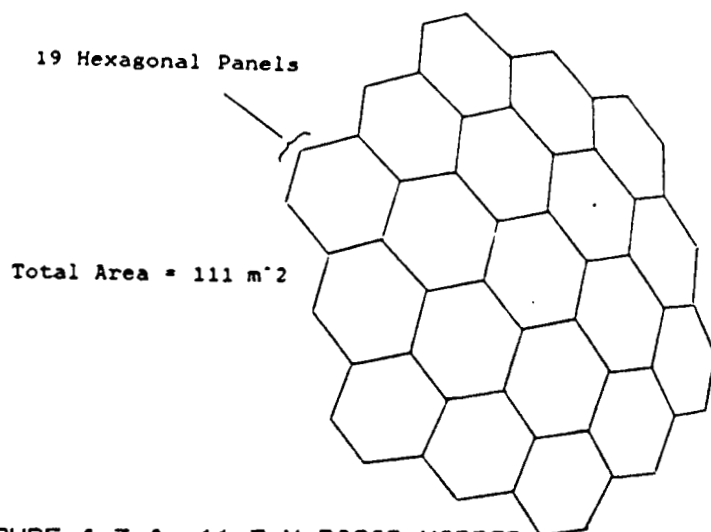
19 Hexagonal Panels

Total Area = 111 m^2

FIGURE 4.3 A 11.5 M RIGID MIRROR

reflective
surface

protective
surface

honeycomb
core

graphite epoxy
facesheets

FIGURE 4.3 B FACET CROSS-SECTION

HONEYCOMB   FACESHEET

MULTIPLE DIELECTRIC LAYERS
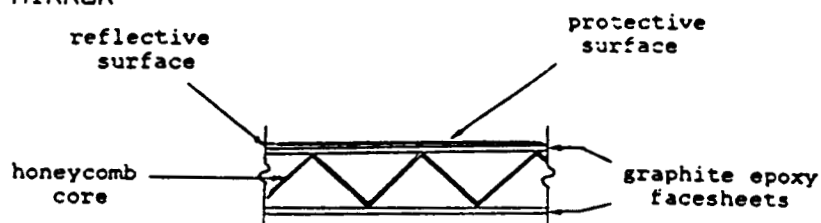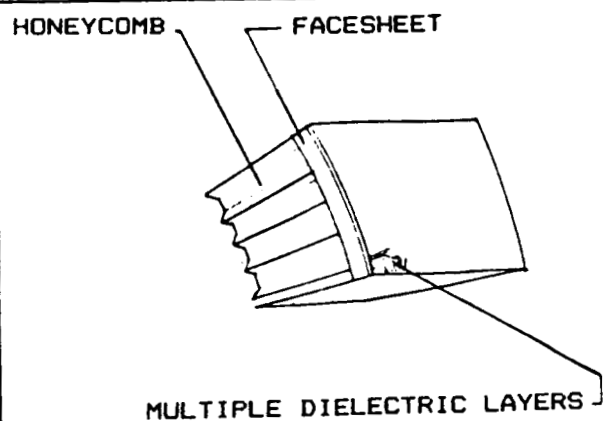
FIG. 4.4 GENERALIZED MIRROR SURFACE

- 99%+ REFLECTIVITY
- LIGHTWEIGHT
- LOW THERMAL EXPANSION
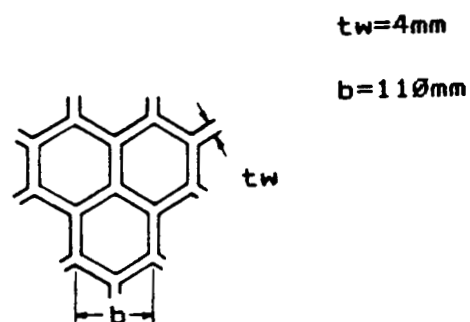- GOOD SURFACE QUALITY

tw=4mm

b=110mm

tw

b

FIG. 4.5   HONEYCOMB GEOMETRY

parabolic facets. Furthermore, it was decided to give these facets some measure of adaptability to correct beam deviations due to structural fluctuations. They are thus controlled by linear actuators which vary a facet's position by rotating it about a spherical mount. Feedback control is provided by a "template" of filtered and protected x-y detectors. Figure 4.6 depicts the adaptive optics system. The accompanying flowchart, figure 4.7, illustrates typical operative proceedure for this system. The system is first calibrated before high-power operation begins, most likely with a full scale low-intensity beam or a system of smaller lasers. Once the LOTV begins operation, the system cycles until an error is detected by the photodetectors located on the template. Within this idle cycling period, a number of self-tests are administered and if not successful, appropriate action is taken to alert the ship to any potentially hazardous situation. If a beam error is detected by the template, the corrective software first identifies the mirror facet(s) in question. Next, it is determined if those facets are moving, i.e. correcting a previous beam error. If so, the system cycles so as to prevent an overlap of corrective signals. Once the facet is free, a corrective command is sent to it in incremental form. The facet will thus move one increment per cycle in a direction calculated to alleviate the problem.

4.3.6 CONSTRUCTION OF LOTV MIRRORS 2, 3, 4

Mirrors 2 and 3 are quite similar in construction. Both consist of 0.381 cm thick fused silica facesheet bonded to a 7.62 cm thick honeycomb slab. Table 4.1 lists several properties of the selected fused silica. It should be understood that the facesheet thickness was chosen as a projection of the current 0.635 cm thick manufacturing limit.

Mirrors 2 and 3 are of open-back design. This not only results in a lighter mirror, but is conducive to radiative cooling as well. Figure 4.5 shows the honeycomb geometry used for these mirrors.

As would be expected, mirror 4 is somewhat more complicated structurally. The facesheet is once again 0.381 cm thick. The honeycomb, however, is now only 5.08 cm thick. Since the honeycomb is not attached to the mirror support legs, this reduction in thickness is tolerable. The surface of mirror 4 (which consists of the facesheet and honeycomb) is divided into 7

Table 4.1 Properties of Fused Silica

Density . . . . 2.20×10^3 kg/m^3
CTE . . . . 0.03×10^{-6}/K
Thermal Conductivity . 1.31 W/m K
Surface Smoothness . . 5 Angstroms (rms)
Maximum Service Temp. . 1070 K (continuous)

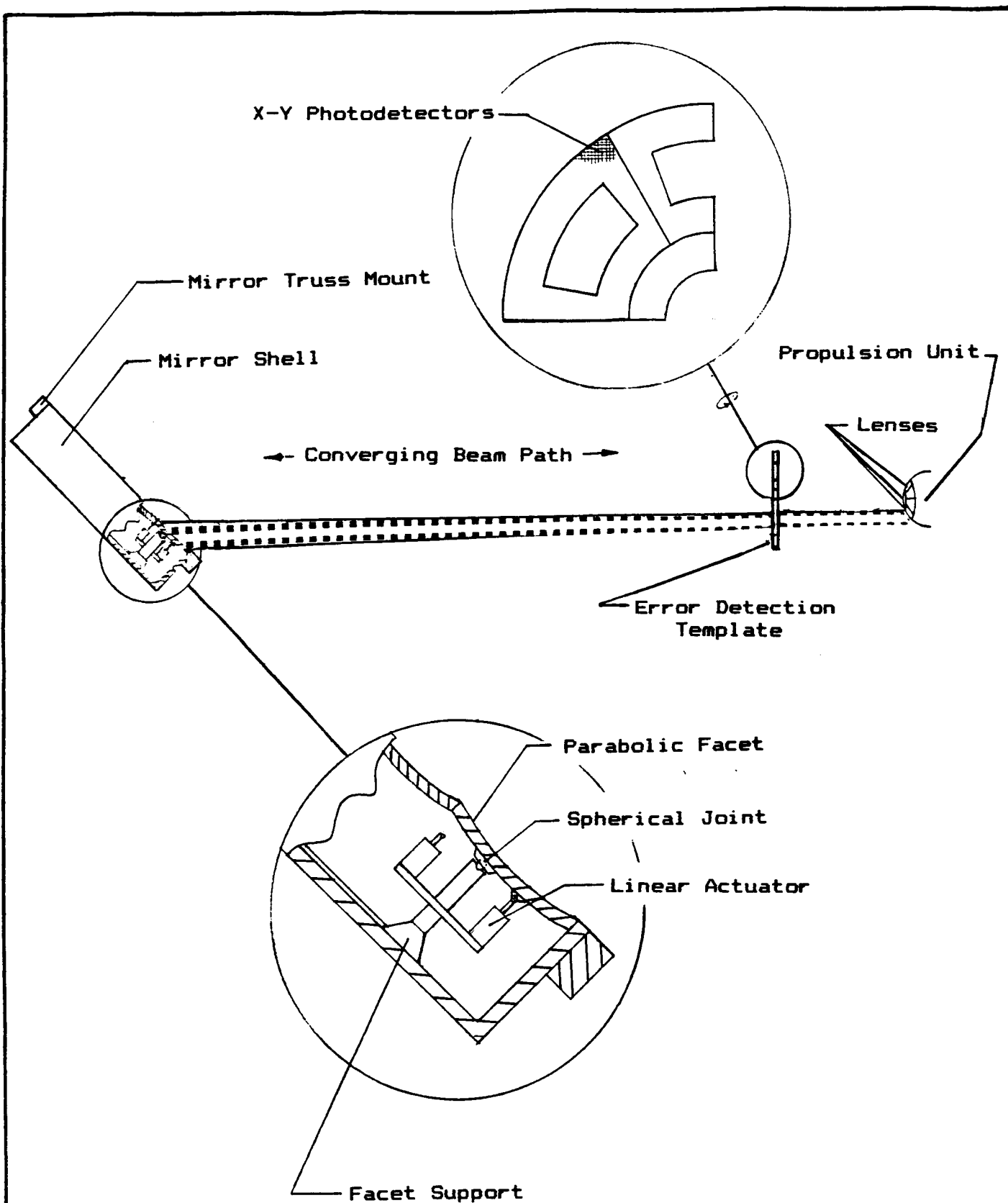X-Y Photodetectors

Mirror Truss Mount

Mirror Shell

Propulsion Unit

Lenses

Converging Beam Path

Error Detection
Template

Parabolic Facet

Spherical Joint

Linear Actuator

Facet Support

FIG. 4.6
ADAPTIVE OPTICS SYSTEM

Calibration → Go

Detection? —Y→ Identify Beam(s)/Facet(s)

Detection? N

System Check Req'd? —N→

System Check Req'd? Y

Ok? —Y→

Ok? N

Report Error

Shutdown Req'd? —N→

Shutdown Req'd? Y

Alert Laser

Stop

Facet(s) Moving? —Y→

Facet(s) Moving? N

Calculate Deviation

Calculate Rel. Actuator Displacements
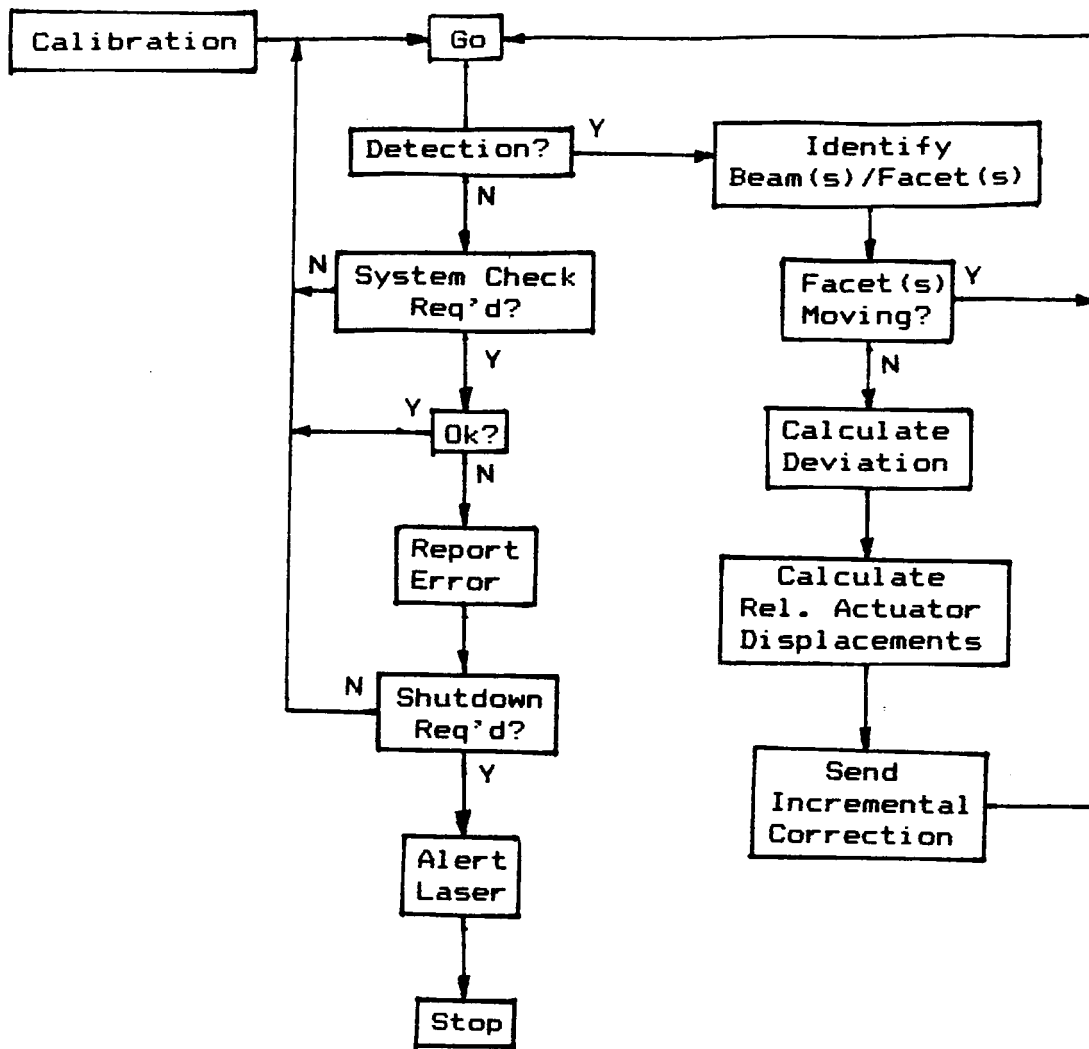
Send Incremental Correction

FIG. 4.7

INCREMENTAL FEEDBACK
ADAPTIVE OPTICS CONTROL LOOP

facets: a circular central facet surrounded by 6 pie-shaped facets. Each facet is supported by a set of 3 linear actuators and a central spherical mount. This configuration is depicted in Figure 4.6. This mounting scheme allows each facet to rotate through any small angle about its central support. The central support for each facet, to which each set of linear actuators is connected, is anchored at the rear of the mirror to a back surface cover.

The error correction template associated with mirror 4 is quite simple in construction. It consists of a circular sheet of boron/aluminum composite upon which is affixed a layer of x-y photodetectors. This apparatus is perforated in such a way as to allow each of the 7 converging beams leaving mirror 4 to pass through it to a prescribed tolerance. Thus, the holes in the template correspond to both the facets of mirror 4 and the lenses of the propulsion unit. Both the template and mirror 4 are interfaced with the LOTV main control computer system.

4.3.7 STRUCTURAL SUPPORT OF MIRRORS 2, 3, 4

Just as mirrors 2 and 3 are similar in construction, so, too, are they similarly supported. Figures 4.8A and 4.8B illustrate these mirror-to-optical truss support configurations. Note that at the back of each mirror is a rotational adjustor. This adjustor allows for "fine-tuning" of each mirror's angular position once initial placement is complete. Flush with the rear surface of each mirror is placed a diamond-shaped frame which serves to connect the mirror to its support legs. These legs, in turn, anchor the mirror to the optical truss. Figure 4.9 depicts a typical connector used to join a mirror leg to the optical truss. The connector consists of a housing which is first clamped on to the optical truss. The mirror support leg is then inserted and locked into place via a slip-ring connector. These slip-ring connectors, as shown in figure 4.10, permit the mirror systems to be assembled with relative ease and are quite secure as well.

Mirror 4 and its template are, by design, located and thus supported within the main body of the LOTV.

4.4 OPTICAL SYSTEM SUPPORT STRUCTURE

4.4.1 OPTICAL SUPPORT STRUCTURE DESIGN CRITERIA

After determination of the configuration and geometrical dimensions of the support truss, the two most important criteria that the design must take into consideration are rigidity and mass. The rigidity of the structure is very important since the performance of the entire vehicle depends upon the optical systems' performance.

The amount of laser energy that can be harnessed in the thrust chamber depends on the efficiency of the optical system in getting as much of the beam as possible focused into the chamber. The efficiencies of the mirrors are not the only factors in
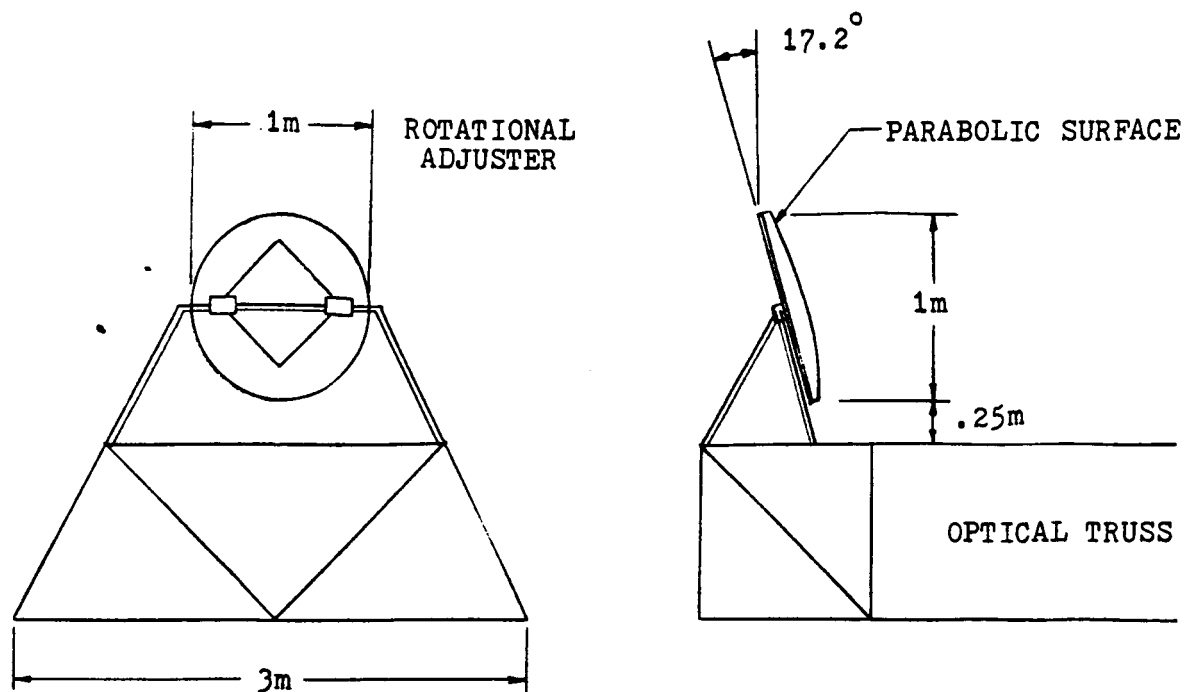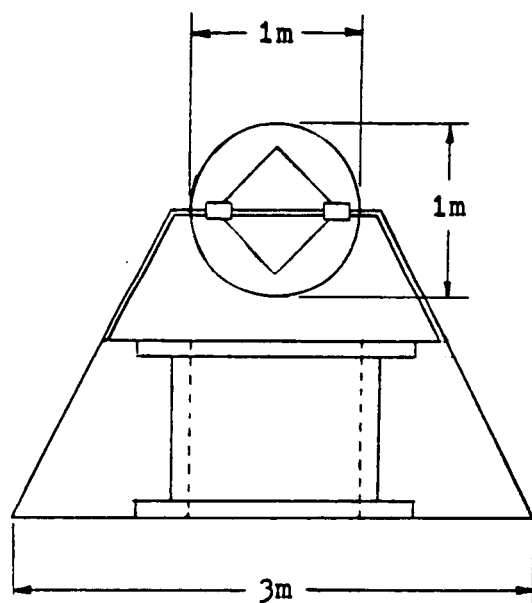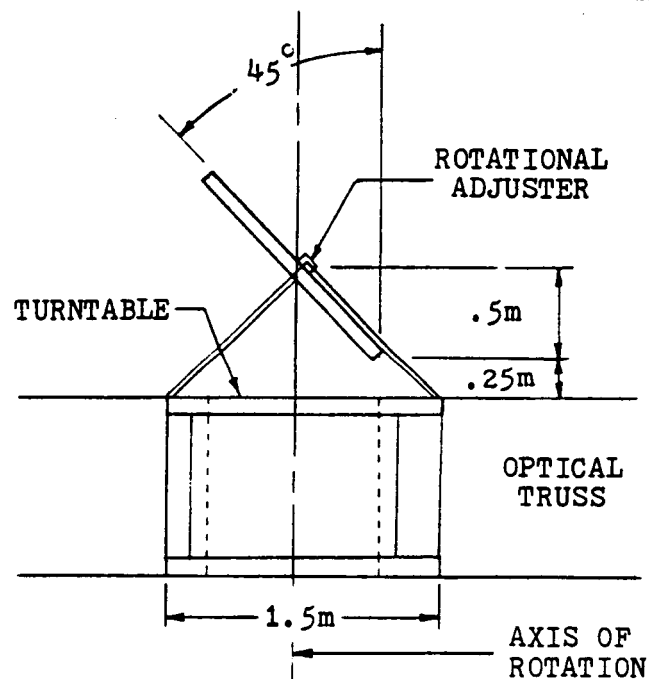
FIG. 4.8 A
MIRROR 2 STRUCTURAL SUPPORT

BACK FACE VIEW — SIDE VIEW

FIG. 4.8 B
MIRROR 3 STRUCTURAL SUPPORT

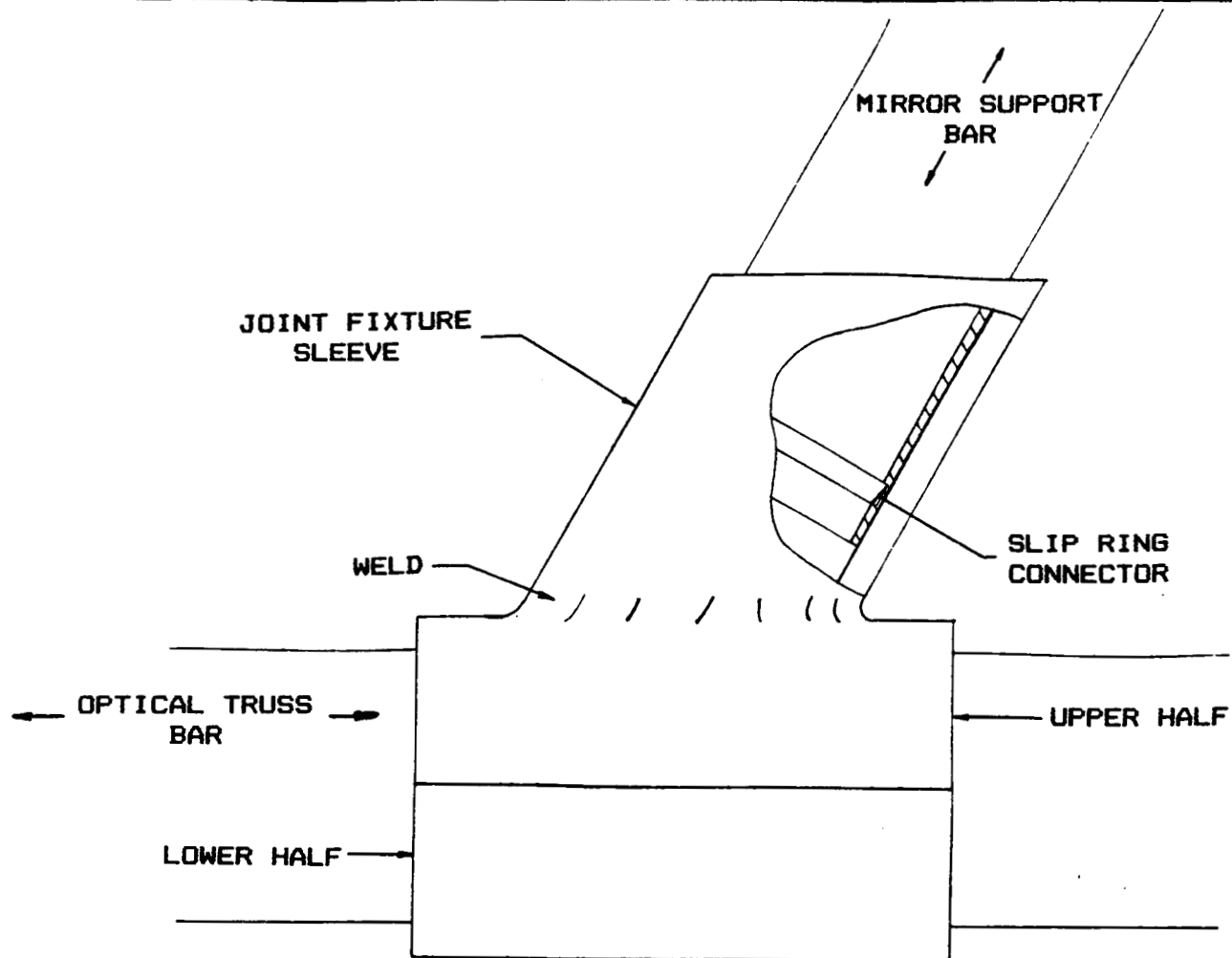BACK FACE VIEW — SIDE VIEW

63

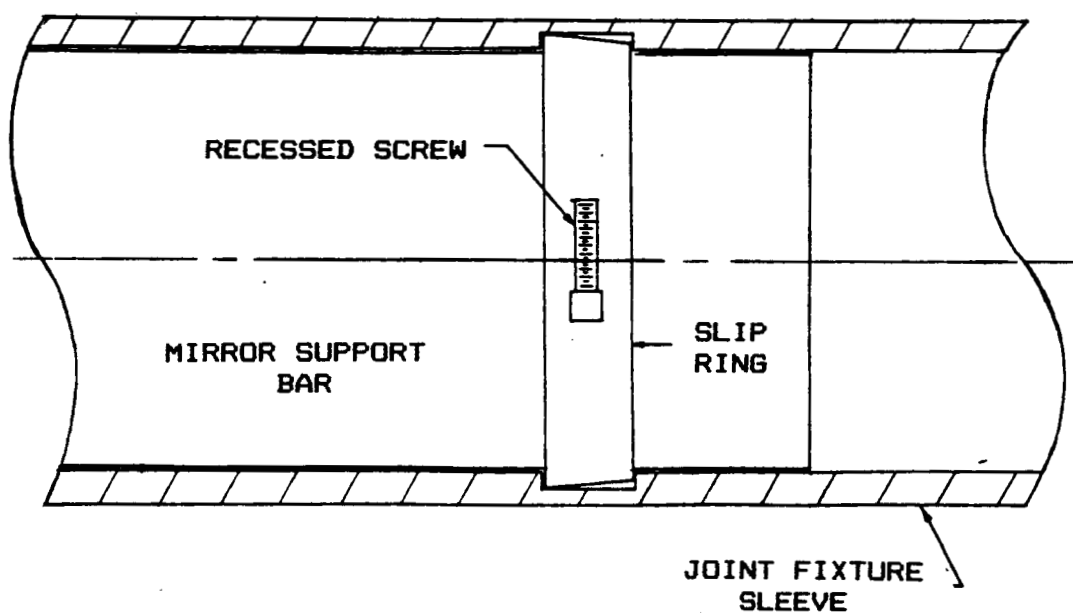FIG. 4.9
TYPICAL MIRROR-TO-TRUSS JOINT

FIG. 4.10
SLIP RING CONNECTOR

determining how much of the beam makes it into the thrust chamber, since any deflections in the beam path will cause some of the beam to miss the window of the chamber. Therefore it is very important that the structure that supports the mirrors be designed to provide sufficient rigidity.

The acceptable amount of energy that could be lost due to deflections of the mirror system was set at .1 % of the energy that reached the main mirror. The maximum deflection in the structure occurs when the truss is perpendicular to the direction of the acceleration since both ends of the truss will experience forces that cause lateral deflections of the beam path. The maximum allowable deflection was determined by computing how much of the area of the beam could fail to hit the proper part of the second mirror and the necessary angle of deflection to cause the loss of beam area. The structure was then iterated from an initial design until the deflections were not only acceptable but were kept to 90% of that allowable without changing the necessary mass of the structure. The calculations used to determine the maximum allowable deflections are listed in Appendix B.

The cross sections of the truss members were originally chosen for resistance to bending and normal stresses. By continuous examination of the structural analysis (discussed in Appendix B), those members that were of more than sufficient strength lost some of their size to members that needed extra resistance to stresses. Once the cross sectional areas had been determined, the inside and outside radius of each member was changed to provide optimum moments of inertia and thus reduce the deflections.

Since the mass of the design was to be kept to a minimum, the selection of a material for the construction of the truss was given a great deal of consideration. Graphite-epoxy composites were first considered because of their high strength and low mass characteristics. Because the whole optical system will probably be struck by the incoming laser beam at one time or another, though, the performance under thermal loads of the material selected must be good enough that no permanent damage would occur to any member. Graphite-epoxy composites (at least the ones that were considered for this truss) do not offer acceptable performance under thermal loads, so other materials were researched. The boron/aluminum composite that was selected seemed to offer one of the best blends of strength, performance, and density.

4.4.2   DESCRIPTION OF THE OPTICAL SUPPORT STRUCTURE

The rotating support structure for the mirror system of the LOTV is composed of 236 members with hollow circular cross sections. The whole structure is made up of three basic sections. Figure 4.11 shows the entire structure along with its dimensions.
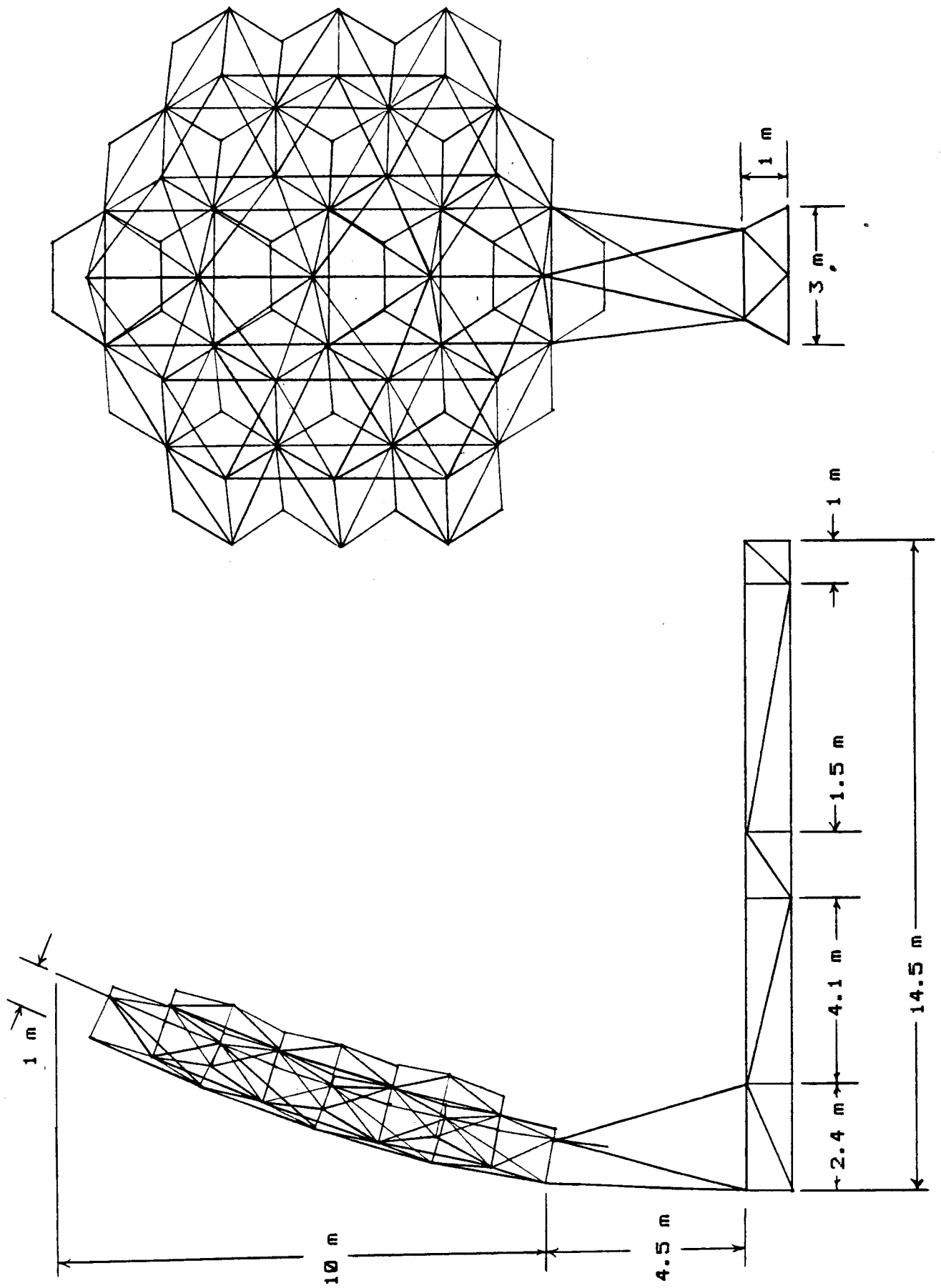
FIG. 4.11 OPTICAL SYSTEM SUPPORT TRUSS

The first of these sections is the network of members that attaches directly to the mirror panels themselves (see figure 4.12A). Each individual hexagon is connected to the truss at three of its corners. These points are connected by a triangular pyramid of truss members whose apex is one meter off of the back of the panel and whose base is parallel to the plane of the mirror. Each pyramid is connected to the adjacent pyramids at the vertices of the base and by another member that connects the apexes. The triangular pyramid design is the simplest way to achieve rigidity in three dimensions, and the mirror truss is merely a simple connection of one such support per mirror panel. The members in section 1 have the smallest cross-sectional area since this is where the forces and moments will be smallest. The diagonal members have slightly larger areas since they have to support higher stresses than the upper and lower layers of triangles. The structural analysis of this design shows that it has high rigidity and low translations and rotations.

The second section is an arm that extends from the turntable up behind the mirror and ends with a 'core' of members that is made up of the strongest of the members attached to the mirror (see figure 4.12B). This core is different in geometry from the rest of the mirror section and is basically a triangular column. Since section 2 of the truss deals with both the forces of the mirror under acceleration and also with the long moment arms between the turntable and the mirror, the maximum stresses and therefore the largest cross-sectional areas occur here.

The last section is the truss that extends from the turntable to the second mirror (see figure 4.12B). It is very similar in geometry to the horizontal part of section 2 except that its members cross- sectional areas are smaller. Table 4.2 lists the characteristics of these sections.

Table 4.2 Truss Section Characteristics

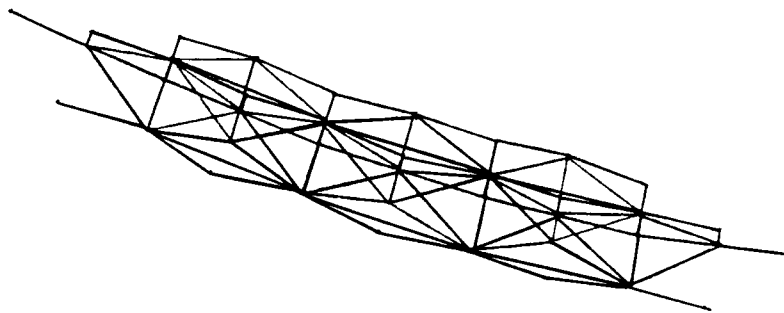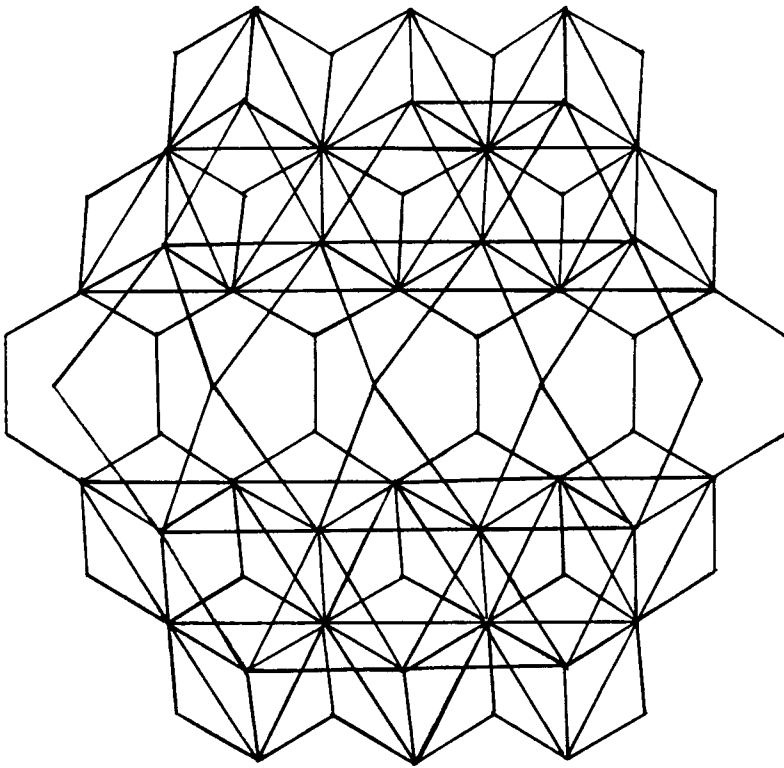|	Member Inside Radius	Member Outside Radius	Mass of All Such Members
Section 1: upper and lower			
layers of triangles-	.0591 m	.0594 m	42.16 kg
diagonals —	.0590 m	.0594 m	24.44 kg
Section 2: core members —	.0589 m	.0594 m	33.4 kg
all other members —	.0576 m	.0594 m	210 kg
Section 3: all members —	.0588 m	.0594 m	40 kg
Total mass —			350 kg

FIG. 4.12A OPTICAL SUPPORT TRUSS SECTION 1
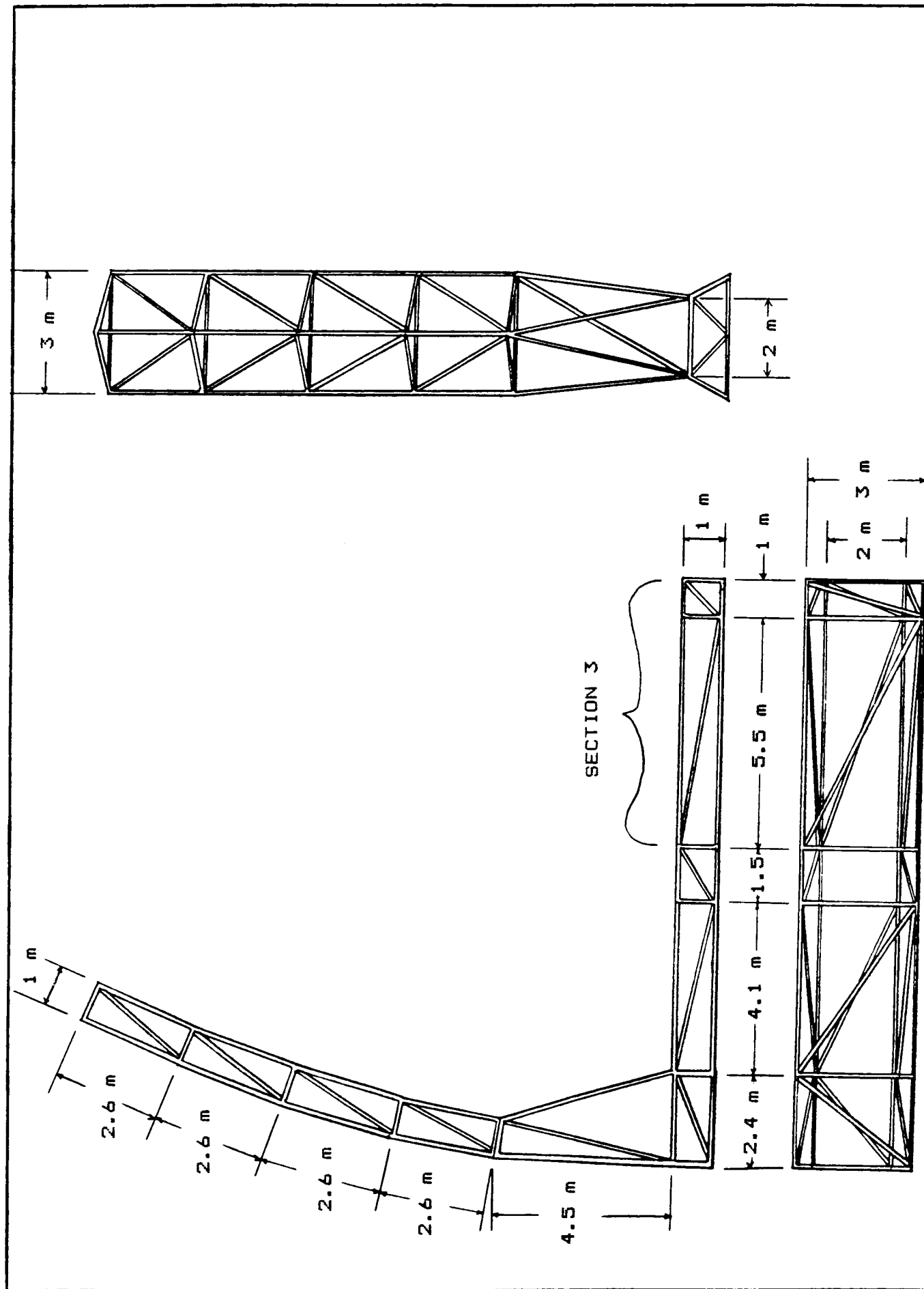(INCLUDES MIRROR PANELS)

FIG. 4.12B OPTICAL SUPPORT TRUSS SECTIONS 2 & 3

SECTION 3

69

4.5 OPTICAL TRUSS TURNTABLE

4.5.1 INTRODUCTION

A primary requirement for the optical system is to be able to accurately track and intercept the incoming laser beam. With a rotating optical system this requirement can be achieved throughout the ships orbit. If the orbit of both the ship and the laser are in the same plane, then tracking can be achieved by simply rotating the optical truss on the ship. If out of plane orbits are used, then rotation of the ship will also be needed to continuously track the laser. Since the later case would be much more complicated, in plane orbits are recommended whenever possible. In either case though, the optical truss needs to be able to rotate independently from the rest of the ship.

4.5.2 DRIVE SYSTEM

Although the design of the actual bearing is relatively simple, the system for driving it is rather unique. There were actually three different drive systems looked into for rotating the truss.

The first of these was simply a small reactionary control system placed on the ends of the truss structure. When the truss needed to turn, this system would fire in the appropriate direction. This is ideal as far as ease of operation is concerned, but it is lacking in simplicity of design. The reactionary control system would require its own fuel supply since linking it to the ship through the main bearing would be too complicated. This would require it to be continually refueled and serviced. Although these difficulties could be overcome, a better design seemed more appropriate.

The second way the truss could have been turned is by placing a gear on the main bearing with a motor on the ship. This would have been a rather simple design, but it would have caused other problems. For instance, turning the truss would also tend to rotate the ship in the opposite direction. In order to keep the ship oriented right in its orbit, its reactionary control system would need to be fired everytime the truss was rotated. This system would be simple to design but difficult to operate. Again a better design was needed.

The last design, which was the one chosen, is both simple in design and in operation. It consists of two momentum wheels attached to the optical truss structure. When the truss needs to be turned, the momentum wheels are spun in the opposite direction. Since the truss is in effect turning independent of the ship, no corrections need to be made to the ship's orientation while the truss is being turned. Without a reactionary control system, the problem of fuel storage and refueling is eliminated. Also, without meshing gears, there is less part wear and less servicing.

4.5.3 MOMENT OF INERTIA

In order to optimize the size of the momentum wheels needed to turn the optical truss, the moment of inertia of the whole optical system about the center of rotation needed to be calculated. Although an exact mathematical solution would be nearly impossible, a system of modeling several components separately and then superimposing their results gave an acceptable estimate for our purposes. In doing this, the whole optical system was broken up into six different components. These components were modeled using simplified shapes such as a rectangular prism, a slender rod, or a thin disk. The moment of inertia of each of these components was then solved about its own axis of symmetry. Each of these moments of inertia was then moved to the axis of rotation of the truss by using the parallel axis theorem. The approximate truss moment of inertia was calculated to be around 28,900 kgm^2.

4.5.4 DISK OPTIMIZATION

Along with the moment of inertia, the maximum angular velocity and acceleration of the truss during operation were also needed to size the momentum wheels. These were calculated by the Orbital Mechanics Group to be .014 rad/sec^2 for maximum acceleration, and .002 rad/sec for maximum velocity. These values would occur when both the ship and the laser were in a low orbit and relatively close to each other. Since burn at these times could be postponed till a more opportune time, our design need not be restricted by these maximum values. Reasoning that most of the time the ship and the laser would be at a great distance, the operating velocity and acceleration used for design purposes were .001 rad/sec and .007 rad/sec^2, respectively. These values are roughly half of the maximum values given.

To aid in optimizing the size of the wheels, a spreadsheet was set up. The inputted values are as follows: truss angular velocity and acceleration, truss moment of inertia, disk (momentum wheel) mass, and disk radius. With these values the following values were calculated: disk moment of inertia, disk angular velocity and acceleration, applied torque, and finally power required. The general aim of this optimization study was to keep the weight of the disks relatively low and also to keep the power requirement and applied torque low. By ranging through a set of values on one of the variables while keeping all the rest constant, the effect of each of these on power was found. By graphing power required versus each of the inputted variables, relationships could easily be seen and design values chosen.

For both angular velocity and acceleration a linear relationship with power is seen as would be expected. Variations in both disk mass and radius showed an inverse relationship with power. Graphs of these can be seen in figures 4.13 A, B, C, and D. While a larger disk mass would have cut down on the power required, it also added to the overall mass of the optical truss system. With this in mind, a disk mass of 75 kg was chosen.

71

TURNTABLE OPTIMIZATION

radius=.7m   mass=75kg   ang.vel=.001/sec

Truss Angular Acceleration (rad/sec^2)
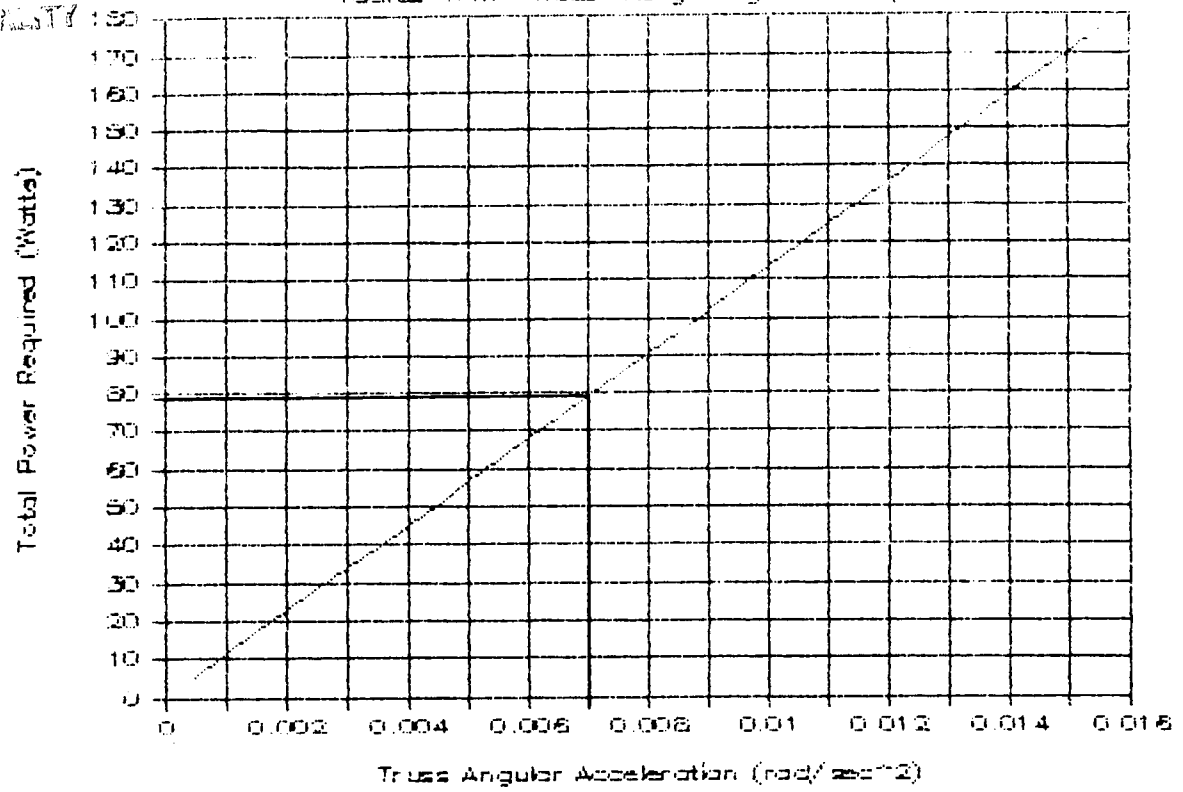
FIG. 4.13 A   POWER VS ANGULAR ACCELERATION

TURNTABLE OPTIMIZATION

radius=.7m   mass=75kg   ang.accel=.007

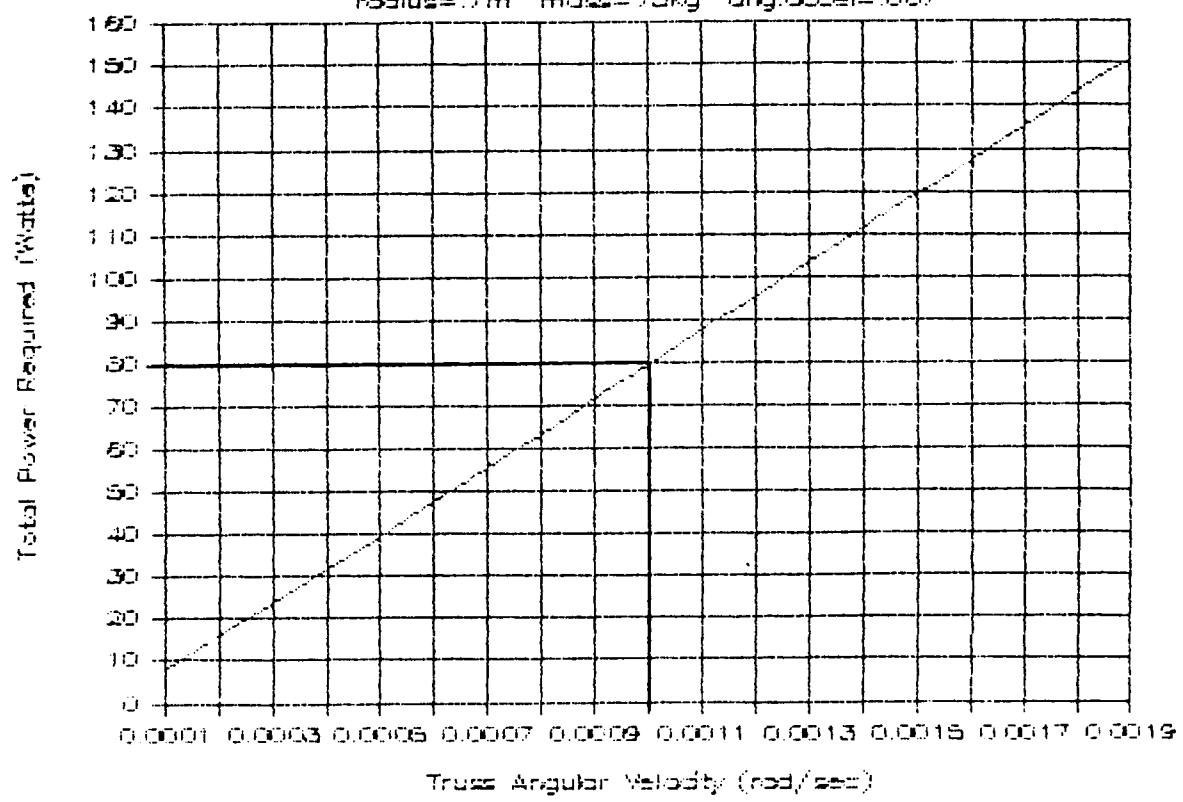Truss Angular Velocity (rad/sec)

FIG. 4.13 B   POWER VS ANGULAR VELOCITY

72

TURNTABLE OPTIMIZATION

radius=.7m   ang.vel=.001   ang.acd=.007
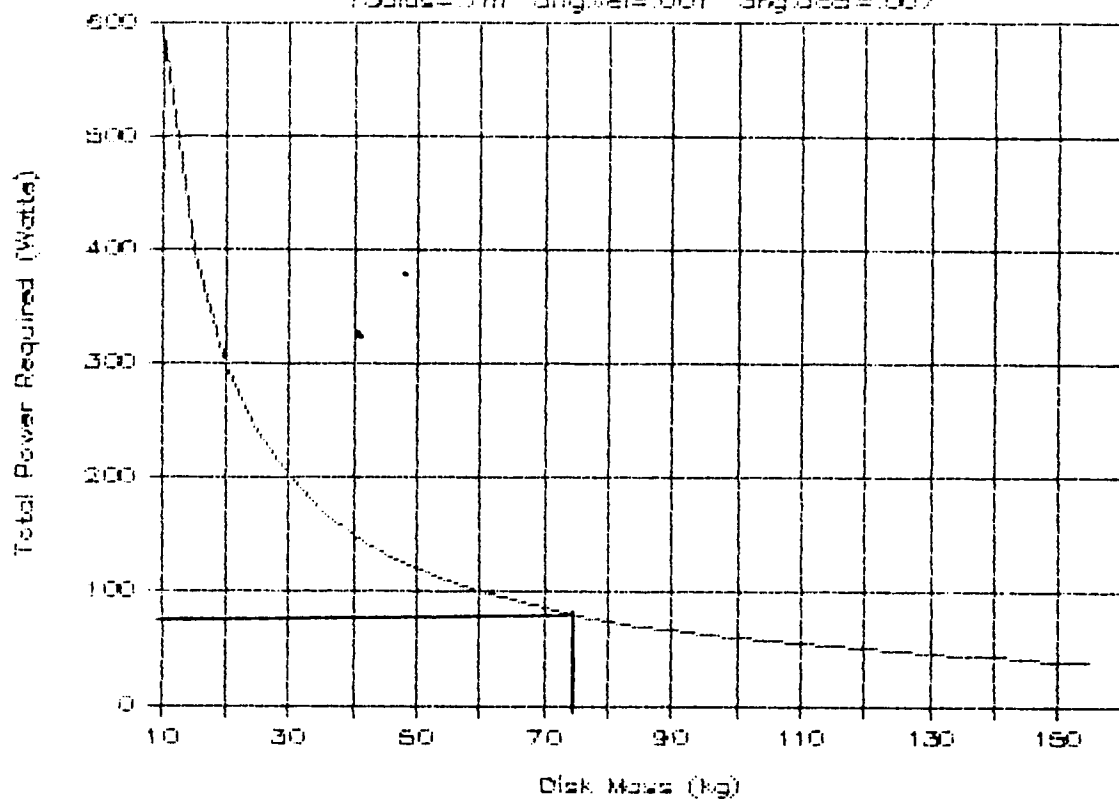

FIG. 4.13 C   POWER VS MASS

TURNTABLE OPTIMIZATION

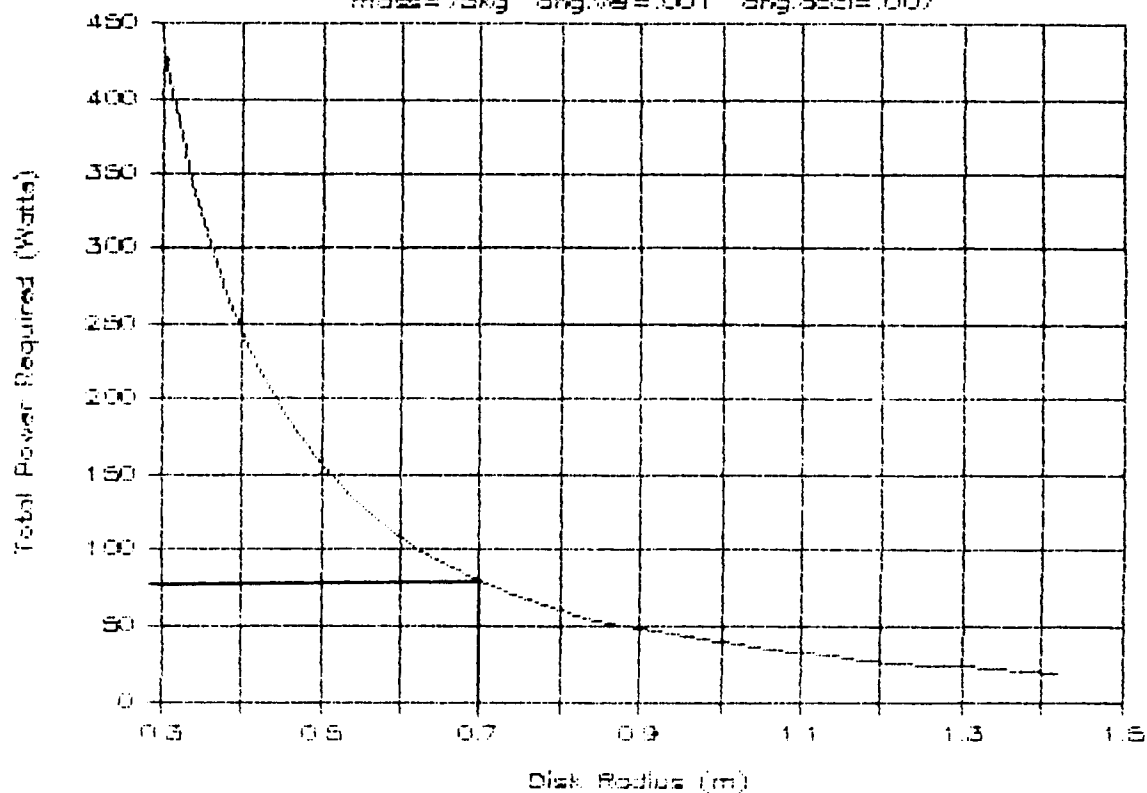mass=75kg   ang.vel=.001   ang.acd=.007

FIG. 4.13 D   POWER VS RADIUS

Increasing the disk radius also decreased the power, but it was limited in size by the truss structure within which it needed to fit. A final value of .7 meters was chosen for the radius. This size kept it well within the surrounding truss structure.

4.5.5 MOMENTUM WHEELS

The design of the momentum wheels or disks is rather simple. They consist of a weighted ring of radius .7 meters connected to a central rod by four spokes. By designing around a mass of 75 kg and a radius of .7 meters, the dimensions of the weighted ring are .04 meters thick by .05 meters wide. The material used is steel, which has a density of 7750 kg/m^3. This gives each disk a moment of inertia of 36.75 kgm^2. A picture of the disk is shown in figure 4.14.
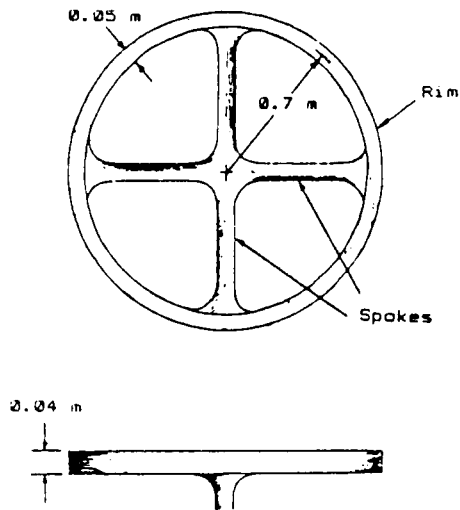
4.5.6 DRIVE MOTORS

From the spreadsheet used to optimize the momentum wheels, the power required for each wheel was found to be 40 Watts. The angular velocity and acceleration of the wheels during normal operation are .393 rad/sec and 2.752 rad/sec^2, respectively. This specifies an applied torque of 100 Nm. These values can be used to specify the motor best suited for the job. Ideally, the momentum wheel would be fixed directly to the motor, but if the torque is too high, reducing gears could be placed in between. Although the actual motor is not designed here, a picture of how it is attached to the truss is shown in figure 4.15. Since motors can be driven higher than their designed power rating for short periods of time, the higher truss angular velocities and accelerations seen in figures 4.13 A and B could be reached if necessary even if the motors were not power rated that high.

4.5.7 BEARING SYSTEM

The system for actually attaching the truss to the ship consists of two parts: plates which are fixed to the truss, and a hollow cylinder which is fixed to the ship.

The plates' dimensions are 1.31 m X 1.31 m. There are two plates: one attached to the upper two rods of the truss and one attached to the lower two rods. Each plate has a 1.15 meter diameter hole cut in the center. These plates are made of graphite-epoxy AS-4 because it is strong and lightweight. Also, to cut down on mass, the plates are tapered down to a thickness of .02 meters. The mass of these two plates is 42 kg. A picture of the plates is shown in figure 4.16.

The cylinder plays the part of a large main bearing. It is actually fixed to the ship and fits in the hole in the plates. The cylinder is made of graphite epoxy AS-4, too, because it is strong and lightweight. Although being lightweight is good for cutting down on the overall ship mass, it does not really affect the optical truss since it is not added in when calculating the moment of inertia of the truss. The cylinder has a lip on the

0.05 m

0.7 m

Rim

Spokes

0.04 m

Material: Steel
Density: 7750 kg/m^3
Mass: 75 kg

I = 36.8 kgm^2

FIG. 4.14   MOMENTUM WHEEL

Lower Portion
of Optical Truss   Motor

Motor
Support
Plate
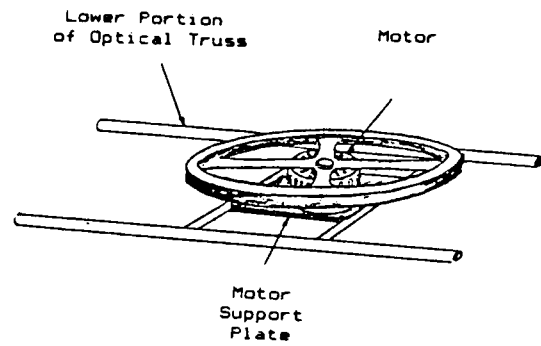
Mass: 25 kg
Power: 40 Watts
Torque: 100 Nm

FIG. 4.15   MOMENTUM
WHEEL DRIVE MOROR

Optical
Truss

Taper

0.575

1.31

0.02

1.31
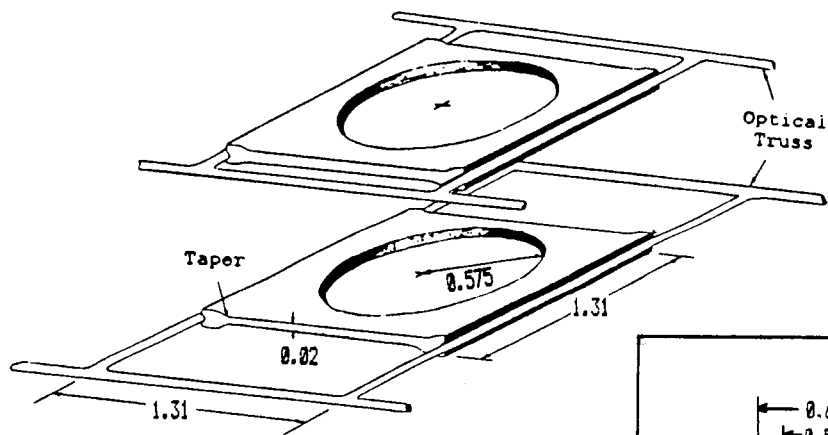
FIG. 4.16   TURNTABLE PLATES

(all dimensions in meters)

0.6
0.555
0.545

0.02

Roller
Bearings

Plates

1.0

0.05

Ship
Truss

FIG. 4.17   TURNTABLE CYLINDER

75

top and bottom to keep the two plates secured. Roller bearings are placed in the wall of the cylinder where the cylinder actually touches the plates. The inside radius of the cylinder is .5 meters, which allows the laser to pass through unobstructed. A picture of the bearing can be seen in figure 4.17.

4.5.8 TURNTABLE SYNOPSIS

The overall turntable system, consisting of the main bearing and the means of turning around it, is a feasible design and yet relatively simple. All the materials used are presently available and the system can be built with existing technology. One area where future improvements could be made deals with friction. Although the effect of friction between the bearing and the pla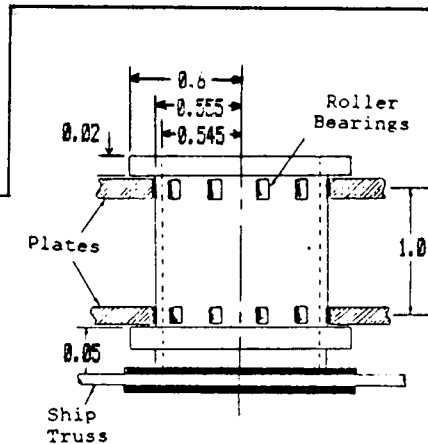tes would be small, it would have some effect on disorienting the ship from its orbit. Future improvements would reduce this friction, making its effect on the ship even less noticeable.

4.6 OPTICAL SYSTEM PERFORMANCE

4.6.1 DIELECTRIC BEHAVIOR

The performance of the LOTV optical train relies to the greatest extent on the combined reflectivity of its individual components. Initial designs of the mirrors incorporated metallic reflective media, namely silver. It was later realized that, for the wavelength with which we were dealing, dielectrics would yield better results. As mentioned earlier, vapor-deposited quartz was chosen as the thin film constituent best suited for this application. This choice was based mainly on the favorable transmissivity of this material at the laser wavelength. Figure 4.18 illustrates this property along with that of slightly less favorable magnesium fluoride (Ref. 4.1). It is likely that if the chosen dielectric layers were any less transmissive, the resulting thermal heating of the mirrors would adversely affect

Quartz (SiO$_2$)

Magnesium Fluoride (MgF$_2$)
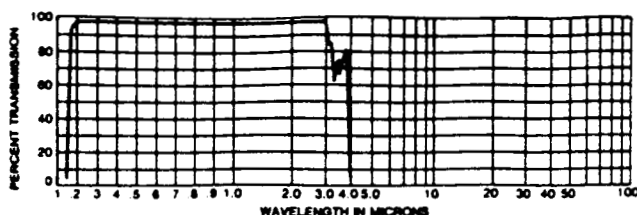
Quartz Refractive Index vs. Wavelength

$\lambda \mu m$	n_e	n_o	$\lambda \mu m$	n_e	n_o
0.20	1.66	1.65	0.31	1.59	1.58
0.21	1.65	1.64	0.33	1.58	1.57
0.22	1.64	1.63	0.38	1.57	1.56
0.23	1.63	1.62	0.49	1.56	1.55
0.24	1.62	1.61	0.77	1.55	1.54
0.25	1.61	1.60	1.30	1.54	1.53
0.27	1.60	1.59	2.05	1.53	1.52
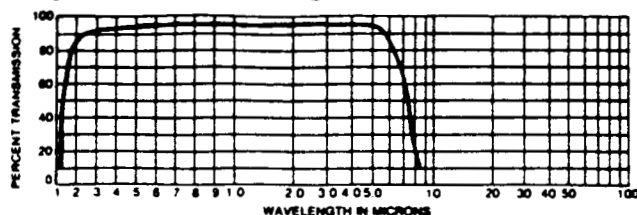
Magnesium Fluoride Refractive Index vs. Wavelength

$\lambda \mu m$	n_e	n_o	$\lambda \mu m$	n_e	n_o
0.20	1.43	1.42	0.34	1.40	1.39
0.23	1.42	1.41	0.56	1.39	1.38
0.27	1.41	1.40			

FIG. 4.18 TRANSMISSIVITY OF DIELECTRIC MATERIAL (REF. 4.1)

system performance. Additionally, thin film coatings can be "tailor-made" to suit a specific application, i.e. reflection at a specified angle of incidence, etc. Since thin film reflectivity is generally proportional to the number of dielectric layers, it was assumed that the coatings on the LOTV mirrors could yield up to 99.5% reflectivity.

4.6.2 OVERALL SYSTEM PERFORMANCE

The overall optical system efficiency is no more than the product of the individual mirror efficiencies. The reflectivity of each mirror is estimated as follows:

Mirror 1 - Assuming use of dieletrics, the surface reflectivity estimated to be 99.5%. A 0.5% loss is assumed due to panel joints as well as curvature inaccuracies. One final assumption is that this mirror captures only 95% of the incoming beam energy. The product of these reflectivities yields a total reflectivity for mirror 1 of 94.05%.

Mirror 2 - Also using dielectrics, this mirror reflects 99.5% of incoming energy.

Mirror 3 - This mirror is comparable to mirror 2 @ 99.5%   ˙ reflectivity.

Mirror 4 - An unbroken surface on this mirror would once again yield 99.5% refectivity, however cracks between the facets introduce small losses resulting in a final refectivity of 99.3%.

The overall efficiency for the entire optical train is now found to be 92.5%

Table 4.3 lists the mass estimates for the entire optical system for the non-aerobraked LEO/GEO version.

Table 4.3 Optical System Masses

	COMPONENT	MASS (kg)	
MIRRORS:	MIRROR 1	500	
	MIRROR 2	83	
	MIRROR 3	107	
	MIRROR 4	130	
TURNTABLE:	DISKS	150	(75 each)
	MOTORS	50	(25 each)
	PLATES	42	
TRUSS:	SECTION 1	66.6	
	SECTION 2	243.4	
	SECTION 3	40.0	
TOTAL:		1412	

4.6.3 THERMAL BEHAVIOR

The thermal gradients that arise in the mirrors due to the absorbed energy from the laser beam are an important consideration for the efficiency and the lifetime of each mirror. To simplify the calculations for the thermal gradients in the second mirror, it was assumed to be a flat, elliptical mirror with a semi-major axis of 1.0469 meters and a semi-minor axis of 1.0 meter. The impinging power upon the second mirror is 30.096 megawatts after the primary mirror reflects 94.05 percent of the original 32 megawatts. With a reflectivity of 99.5 percent, the second mirror absorbs through its front face 150480 joules per second. Multiplying this absorbed power by how long the beam is impingent upon the mirror gives the total amount of energy absorbed by the mirror. Dividing this energy by the mass of the mirror, derived from the density, surface area, and thickness of the mirror, gives the specific energy absorbed by the mirror. The properties of the mirror material, Fused Silica, were listed in table 4.1

Dividing the specific energy by the specific heat will give the temperature difference T at the front face of the mirror from its original state. Since it takes some time for the heat to conduct through the mirror, the temperature of the back of the mirror will remain roughly constant for some length of time. Assuming the entire mirror was at a constant temperature before the laser beam was fired, the temperature at the back of the mirror during this limited time period is the same as the original temperature at the front of the mirror. Thus, this temperature difference at the front of the mirror is also the temperature difference between the front of the mirror and a point x back from the front, where the temperature has not yet risen above the original temperature. Using the heat conduction equation:

$$x = k * A * T / q$$

where k is the thermal conductivity, A is the surface area of the mirror, and q is the absorbed power of 150480 watts. Assuming a linear distribution of the temperature through the mirror gives the thermal gradient in the mirror as a function of time. Figure 4.19 is a plot of the temperature difference versus distance from the front of the mirror for several burn times.

Figure 4.20 shows how the temperature at the front of the mirror decreases as a function of time after the completion of a two hour burn. This plot was calculated using the above equations and radiation cooling in an iterative procedure. The energy released by the mirror during radiation cooling is calculated using the following formula:

$$E = 5.669 * 10^{-8} * a * T^4$$

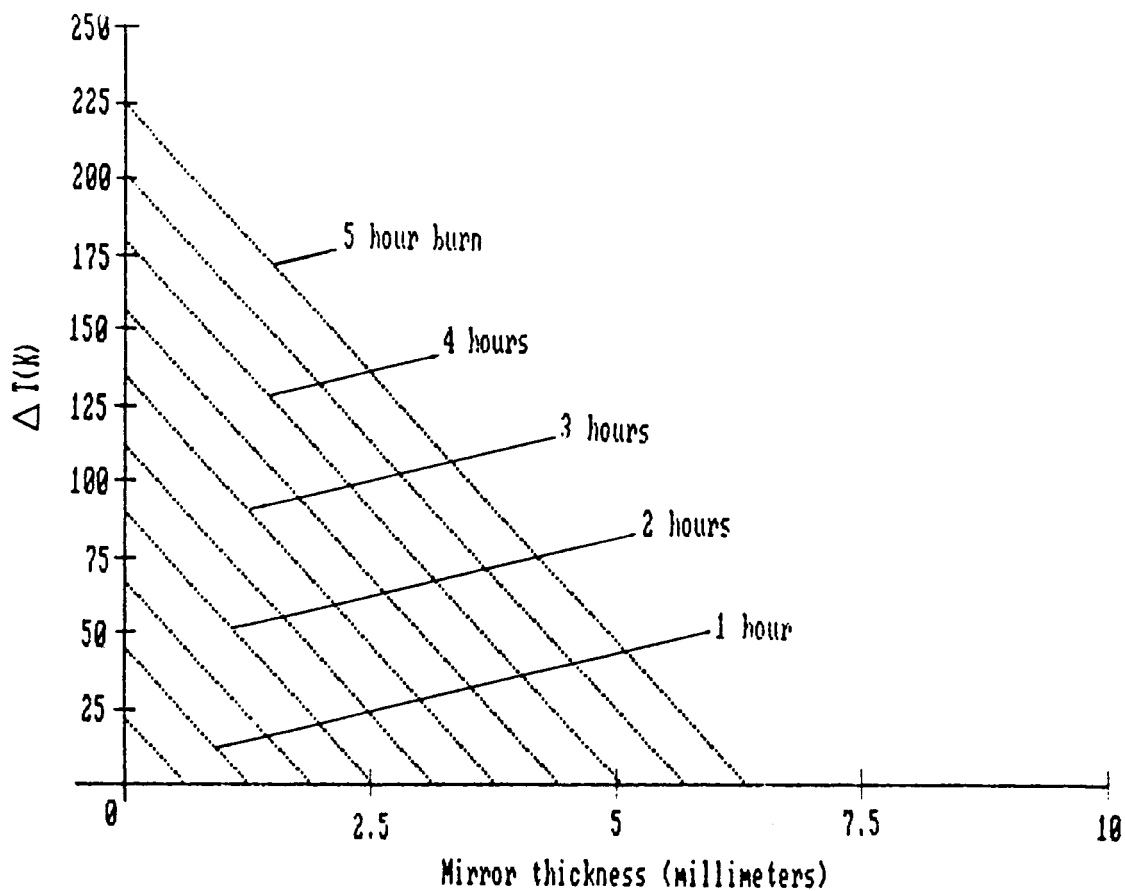where a is the absorptivity of the mirror and T is its temperature.

Figure 4.19 Temperature Gradients in Second Mirror
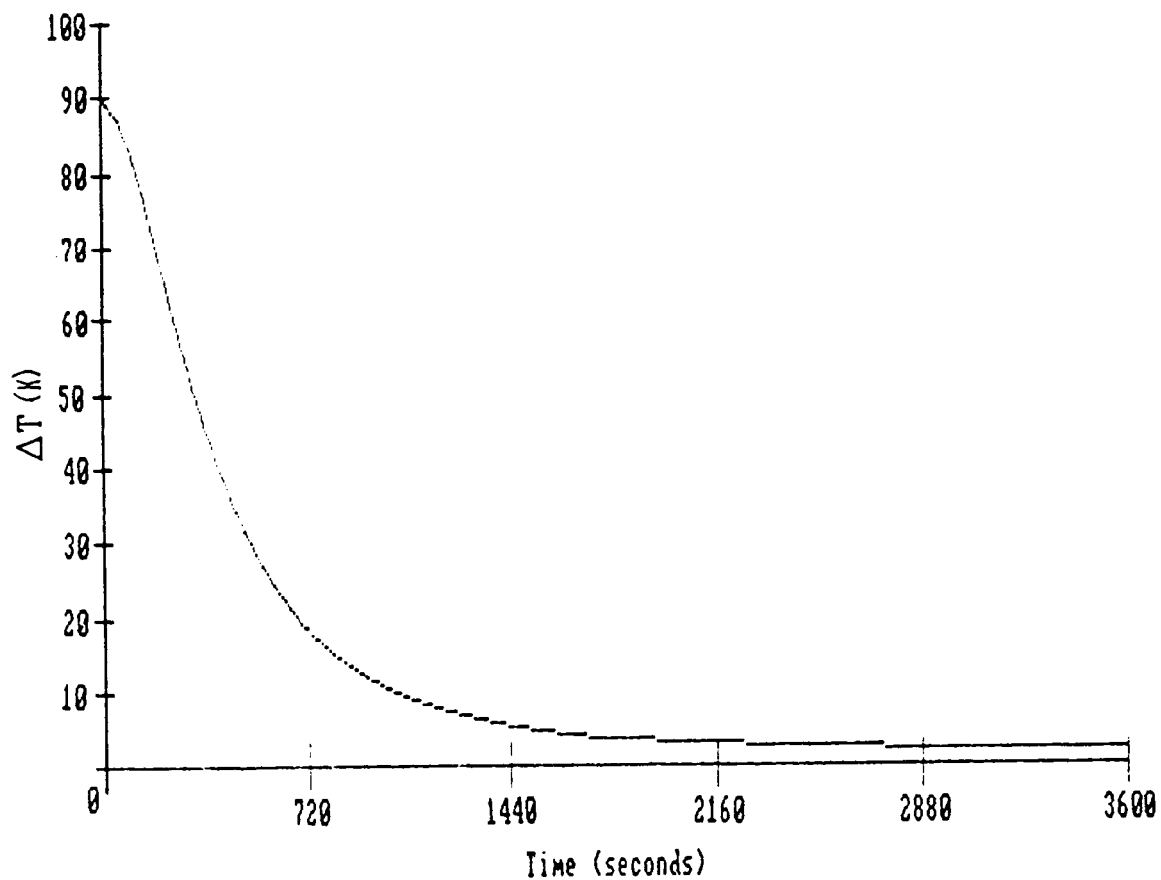
Figure 4.20 Temperature (after burn) of Second Mirror Front Face
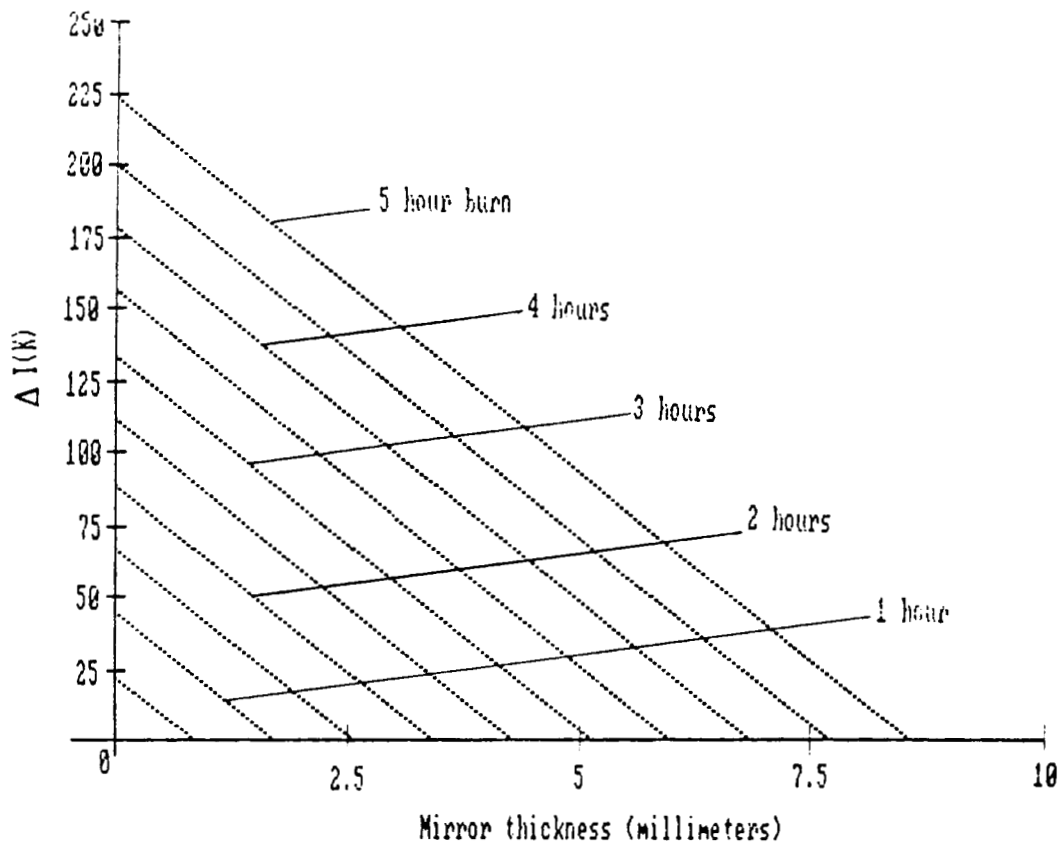
Figure 4.21 Temperature Gradients in Third Mirror

The mirror has a thermal expansion coefficient of $0.03 * 10^{-6}$ per Kelvin. Thus, according to Figures 4.19 and 4.20, the front surface of the mirror will go through a $2.7 * 10^{-4}$ percent expansion and then return to its orginial size during this three hour cycle.

The third mirror is actually a flat, elliptical mirror with a semi-major axis of 1.414 meters and a semi-minor axis of 1.0 meter. With a reflectivity of 99.5 percent, the absorbed energy per unit time is 149727.6 joules per second. With a larger surface area and a smaller impingent power, the third mirror's thermal gradient, as shown in Figure 4.21, is slightly smaller than the second mirror's.

The fourth mirror is roughly the same size as the third mirror but with a smaller reflectivity of 99.3 percent. However, this reflectivity is in reference to the effective amount of the beam that is reflected into the thrust chamber. This reduced reflectivity comes from the material between the facets of the variable optics; however, this material will also be reflective so that the mirror does not absorb any more energy than it would if it were a planar mirror. Thus, the thermal gradients in this mirror will be smaller than those of the third mirror since there is a smaller impingent power on the fourth mirror.

All of these calculations assume the honeycomb backing of the mirrors to be a solid backing. Future calculations on the thermal behavior will have to include the actual thickness and composition of the backing of the mirrors; however, these future

calculations will only improve the thermal gradients because radiation cooling will occur out the back much sooner with this composition. Taking into account heat radiated out the edges of the mirrors will also improve the thermal behavior of the mirrors.

One other thing that has to be taken into consideration for the thermal behavior is the effects of solar radiation. The Sun produces about 1395 watts per square meter over a wide range of wavelengths. Most of the radiation, however, comes from smaller wavelengths where the reflectivity of the mirror material is very small. However, even if all of it is absorbed, this power density is still very small in comparison to the impingent power of the laser beam. Thus, these effects can essentially be ignored.

Although these calculations were a very rough estimate of the thermal behavior, they do show that cooling of the mirrors will not have to be a future design consideration. These calculations show that the mirror temperatures will not approach the maximum service temperature of 1070 K unless they start out extremely close to that temperature. These calculations also show that the thermal stresses on the mirrors are minimal; however, a future consideration should be to calculate how much this thermal stress does degrade the mirrors during each mission.

4.7 AEROBRAKED VERSIONS OF THE LOTV

4.7.1 PRIMARY MIRRORS

Although the rigid mirror seems ideal for the non-aerobrake scenario, it cannot be used with an aerobrake, so an alternative system must be used. With the requirement that the mirror be able to both deploy and retract, the wrap rib mirror appears to be the best choice. While it is not rigid enough to be used as a permanent mirror, it is ideal as a temporary, foldable mirror.

Actual wrap rib technology is a concept from Lockheed Missile and Space Compny which is being developed at the Jet Propulsion Labora- tory (JPL). Although their use of the wrap rib was as an antenna, we have adapted it for our purposes by scaling it and selecting different materials.

For the LEO/GEO aerobraked version, the mirror sizing can be kept the same as the rigid mirror case. The shape is still parabolic but is approximated differently. The basic structure of the reflector is similar to an umbrella. It consists of a flexible material stretched taught between ribs which define the shape of the reflector. What makes the reflector unique though is in the way it is deployed. The ribs can be wrapped around a central hub making the stowed volume small enough to fit within the protection of the aerobrake. The ribs tested by Lockheed were graphite epoxy with either a lenticular or C shaped cross section. Since the C cross section is lighter and is good for rib lengths up to 20 meters, it was chosen. The polyester

film-Mylar was chosen as a mirror backing material because it is flexible and can be coated. The mechanism for deploying and retracting the mirror is shown in figures 4.22 and 4.23. The mass of this system is 200 kg.

For the LEO/LLO scenario, the size of the mirror chosen to supply the vehicle power requirement was 37.6 m in diameter with a 36 m capture diameter. Due to the increased size, the supporting truss structure and the secondary mirrors are scaled accordingly. Since this scenario also involves aerobraking at some point, a retractable mirror system was also needed. For this reason the wrap rib mirror was again chosen. Many problems appear since the mirror diameter has tripled. First, Mylar has a maximum unsupported width it can be used for. In order to avoid this problem, composite gores will be placed at various radii between the ribs for support. Secondly, since C shaped rib cross sections are only good up to 20m, the heavier lenticular cross section must be used. Although these changes need to be made, the basic design and deploying mechanism are essentially the same, as seen in figure 4.24. Mass estimates for this system are around 1400 kg.

4.7.2 SECONDARY MIRRORS

The secondary mirrors are the same in all details in the aerobraking versions except that mirrors 2 and 3 are mounted to allow them to fold into the truss for aerobraking. Figure 4.25 displays the different mounting designs, and table 4.4 compares the mirrors themselves with the mirrors in the rigid version.

Table 4.4 Mirror Parameters for Aerbraked Scenarios

		RIGID	LEO/GEO AEROBRAKING	LEO/LLO AEROBRAKING
MIRROR 2:	MOUNT ANGLE (degrees from vert.)	17.20	17.20	6.8
	SUPPORT	FIXED	COLLAPSIBLE	COLLAPSIB
	MAJOR AXIS (m)	1.414	1.414	2.818
	MINOR AXIS (m)	1	1	2
	MASS EST. (kg)	83	83	180
MIRROR 3:	MOUNT ANGLE	45	45	45
	SUPPORT	FIXED	COLLAPSIBLE	COLLAPSIBL
	MAJOR AXIS (m)	1.414	1.414	2.818
	MINOR AXIS (m)	1	1	2
	MASS EST. (kg)	107	107	220
MIRROR 4:	MOUNT ANGLE	45	45	45
	SUPPORT	INTERNAL	INTERAL	COLLAPSIBL
	MAJOR AXIS (m)	1.414	1.414	2.818
	MINOR AXIS	1	1	2
	MASS EST. (kg)	130	130	270

track

rollers

gear to move hub
along track

cut section
of track

TOP VIEW

hub

rib

FIG. 4.22 A   WRAP-RIB HUB

SIDE VIEW

mylar
cover

composite
shell
(fixed)

drive
arm
motor

rotating
arm

spring to keep
tension on ribs

track for
spool wheels

sprocket for
chain drive

rigid
mirror

Side Cut View
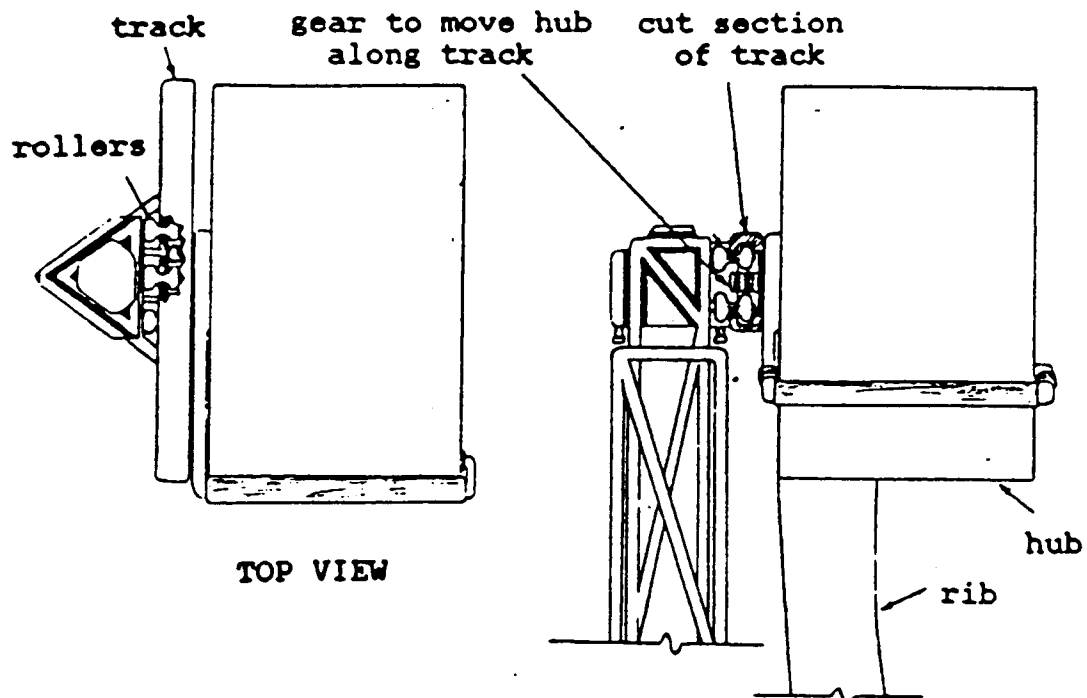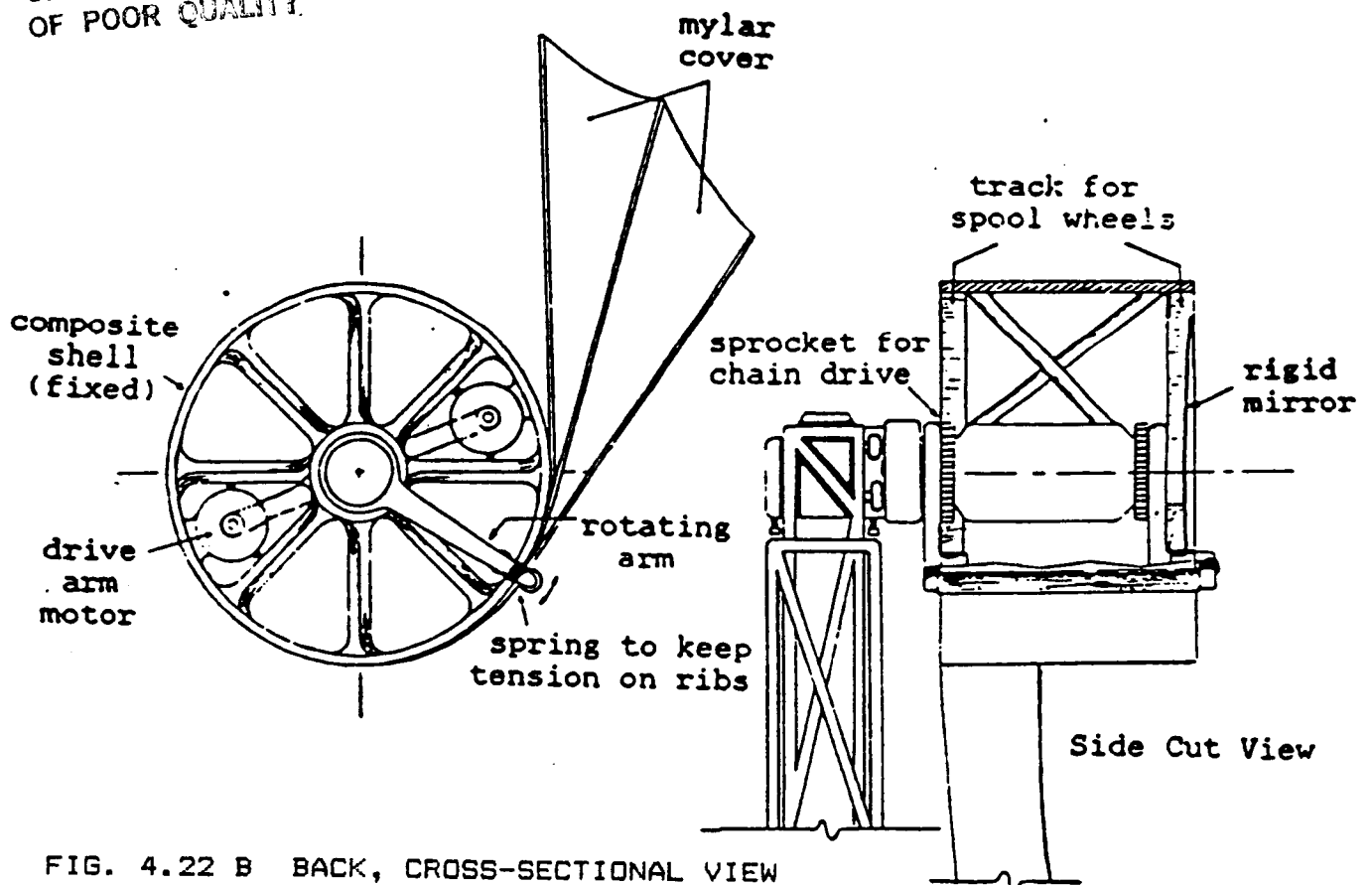
FIG. 4.22 B   BACK, CROSS-SECTIONAL VIEW

83

real diameter: 37.6 m
capture diameter: 36.0 m
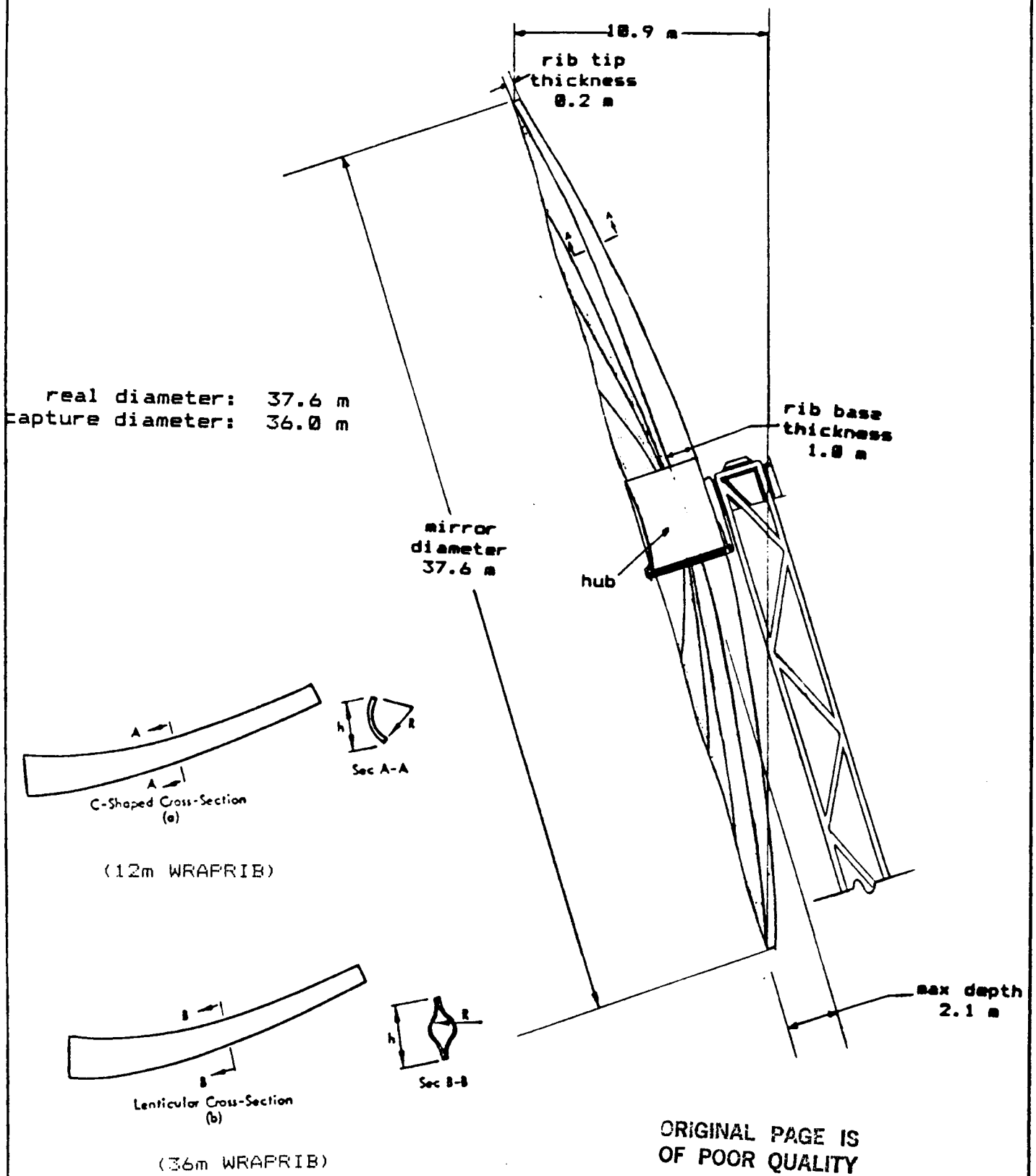
FIG. 4.23   WRAP-RIB SIDE SECTION VIEW

INCIDENT BEAM DIAM.: 36M
BEAM DIAM. MIRROR 2-3:.8M

FOCUS MIRROR 1: 34M
FOCUS MIRROR 2: .7556M

X-AXIS

Y-AXIS

.29M

.948M

FIGURE 4.24   OPTICAL SYSTEM GEOMETRY
(LEO/LLO SCENARIO)

FIG. 4.25 A LEO/GEO

MIRROR 2

MIRROR 3

MIRROR 4

FIG. 4.25 B LEO/LLO

SAME AS ABOVE
LARGER SCALE

SAME AS ABOVE
LARGER SCALE

MIRROR 2
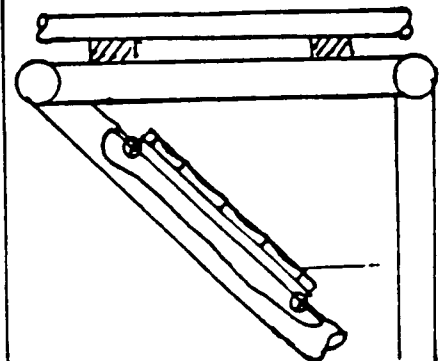
MIRROR 3

MIRROR 4

FIG. 4.25 MIRRORS 2, 3, 4 — MOUNTING CONFIGURATIONS

4.7.3 PRIMARY MIRROR SUPPORT ARM

The mirror for the aerobraking version of the vehicle requires a completely different design for the support arm. The arm is a tapering triangular frame that is perpendicular to the horizontal truss until it clears the edge of the main mirror when deployed. At this point there is a hinged joint which rotates the arm so that the primary mirror is at the necessary angle to direct the beam onto the second mirror (see figures 4.26 and 4.27). The arm/mirror configuration has to fold up to fit behind the deployed aerobrake during the return to LEO (see figure 4.28). To do this the arm is hinged at the base and at the joint which angles the second part of the arm. The tip of the arm which attaches to the hub of the mirror is able to rotate 120 degrees to allow the hub of the mirror to be slid alongside of the ship (see figure 4.29). These mechanisms enable the configuration to be rigidly deployed during the operation of the ship's engine and to fold to fit as ti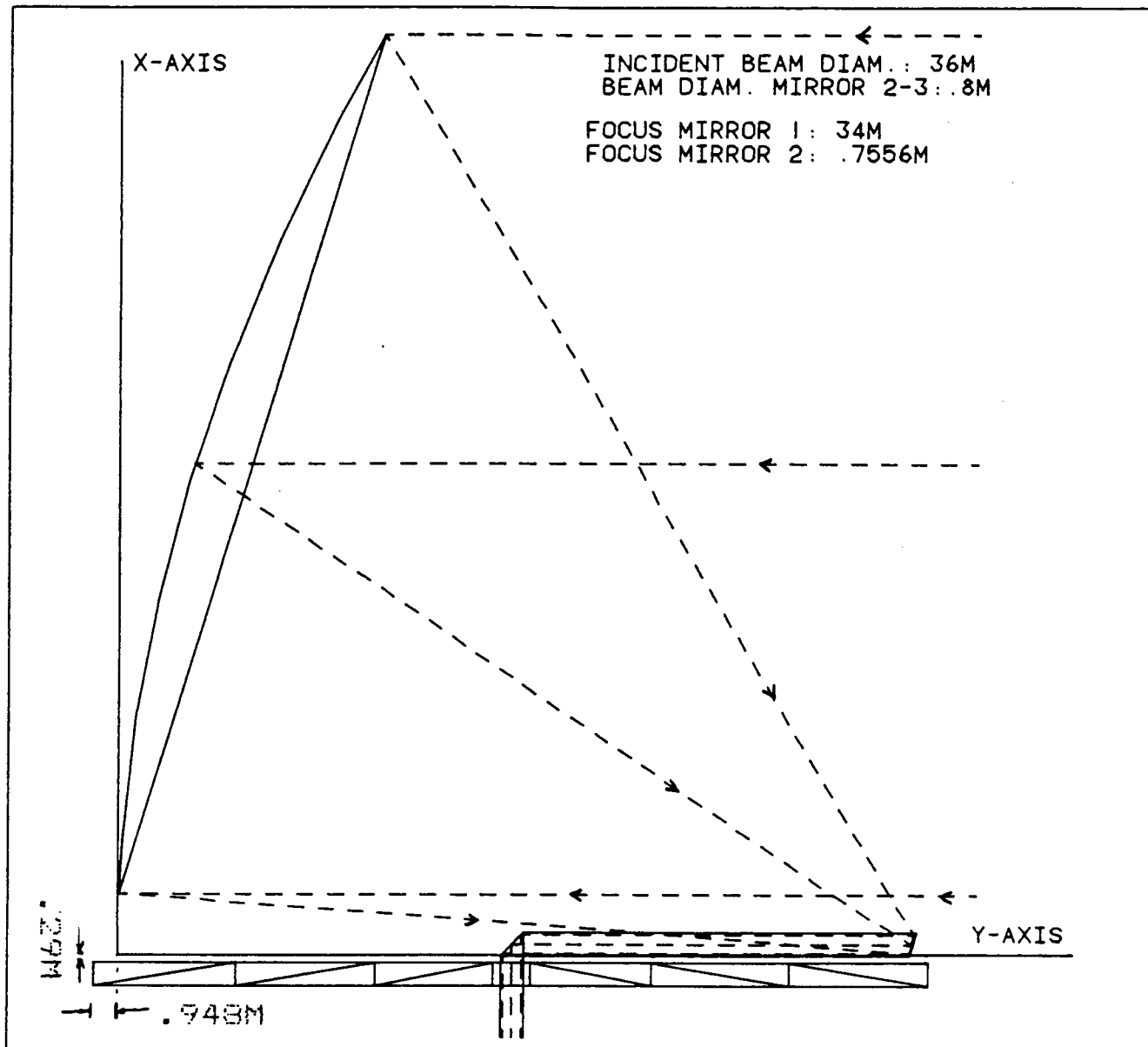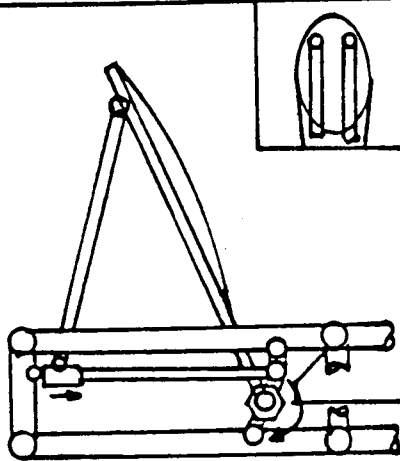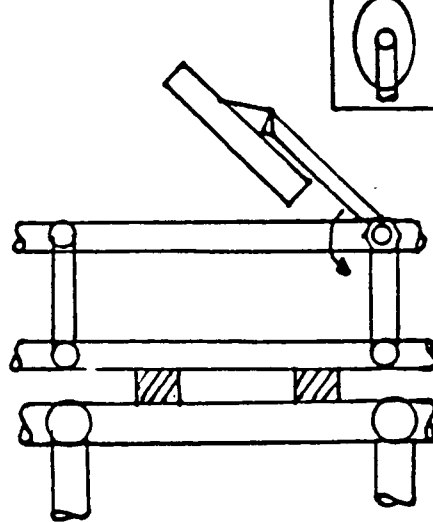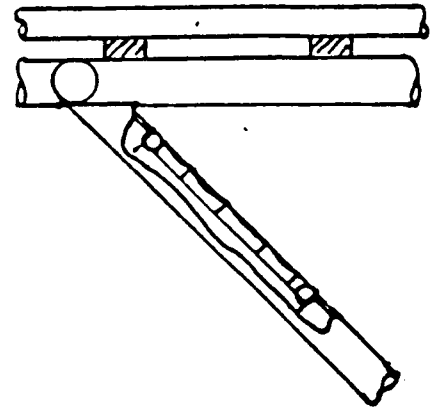ghtly as possible to the ship when stowed for aerobraking. The mechanisms are powered by small DC motors coupled to high precision, high reduction gearboxes which are similar to the servo mechanisms used to power the space shuttle manipulator arm (Ref. 4.5). The mass of this arm and the mechanisms is 110 kg.

A lunar version also has to fold up for aerobraking, but it differs from the previous version because of its size (see figure 4.30). The mirror is 36 m in diameter so the arm has to be longer and stronger. In order to fold this longer arm to fit snugly up against the ship, an 18.3 meter section telescopes in to a length of 9.15 meters (see figure 4.29). This arm also has hinges at the bottom and at the angled joint as well as being able to rotate the tip. Due to the additional size and strength and the additional mechanisms necessary to deploy this version, it has a mass of three times the smaller version, approximately 320 kg.

FIG. 4.27 PRIMARY MIRROR SUPPORT ARM (DEPLOYED)
LEO/GEO SCENARIO

FIG. 4.26 PRIMARY MIRROR SUPPORT ARM (DEPLOYED)
LEO/GEO SCENARIO
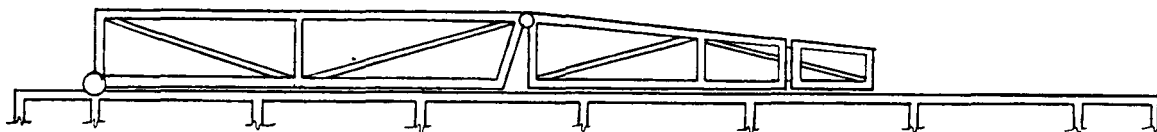
FIG. 4.28 PRIMARY MIRROR SUPPORT ARM (STORED)
LEO/GEO SCENARIO

1 m

9.45 m

5 m

4 m

16.95 m
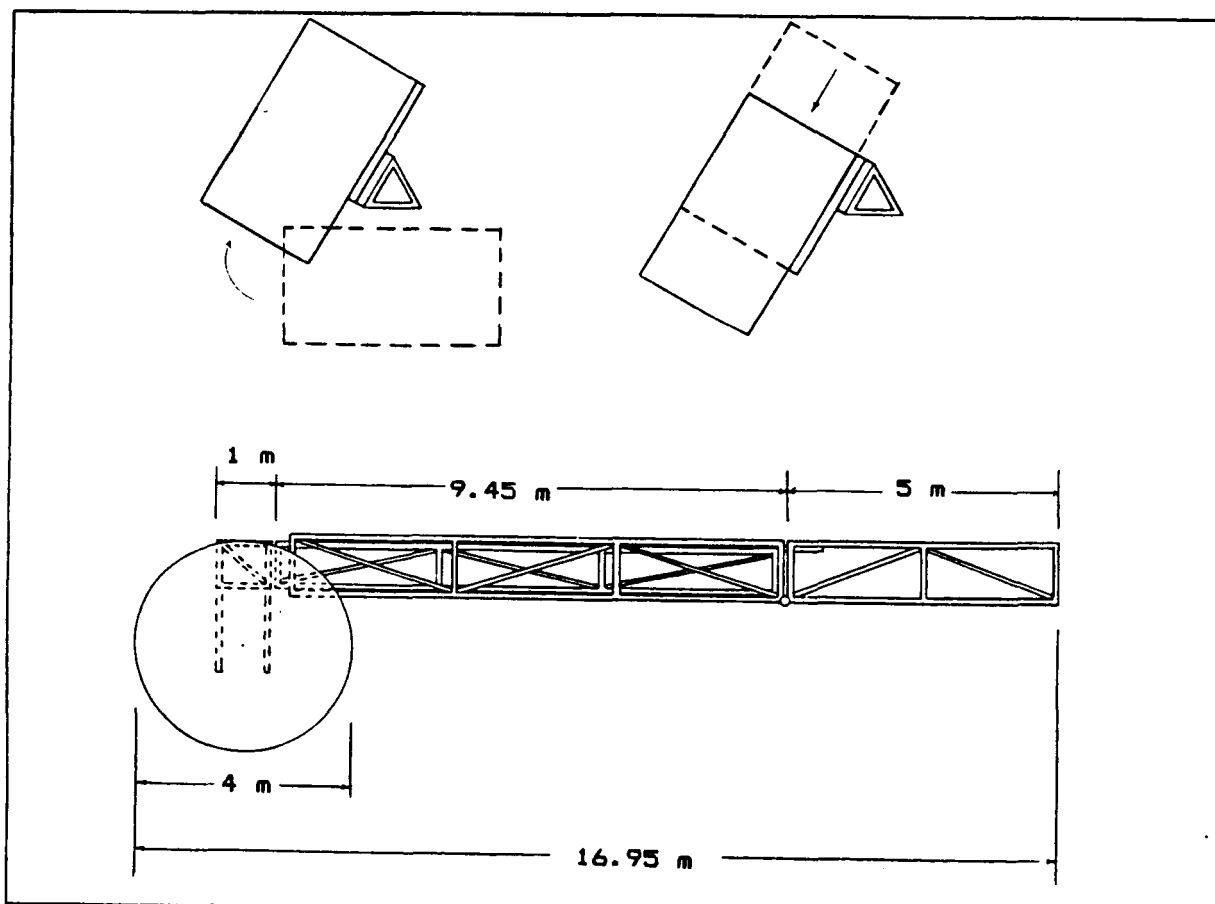
FIG. 4.29   PRIMARY MIRROR SUPPORT ARM (STORED)
LEO/LLO SCENARIO

16.48 deg

1 m

9.15 m

9.15 m

5 m

1.075 m

1.43 m
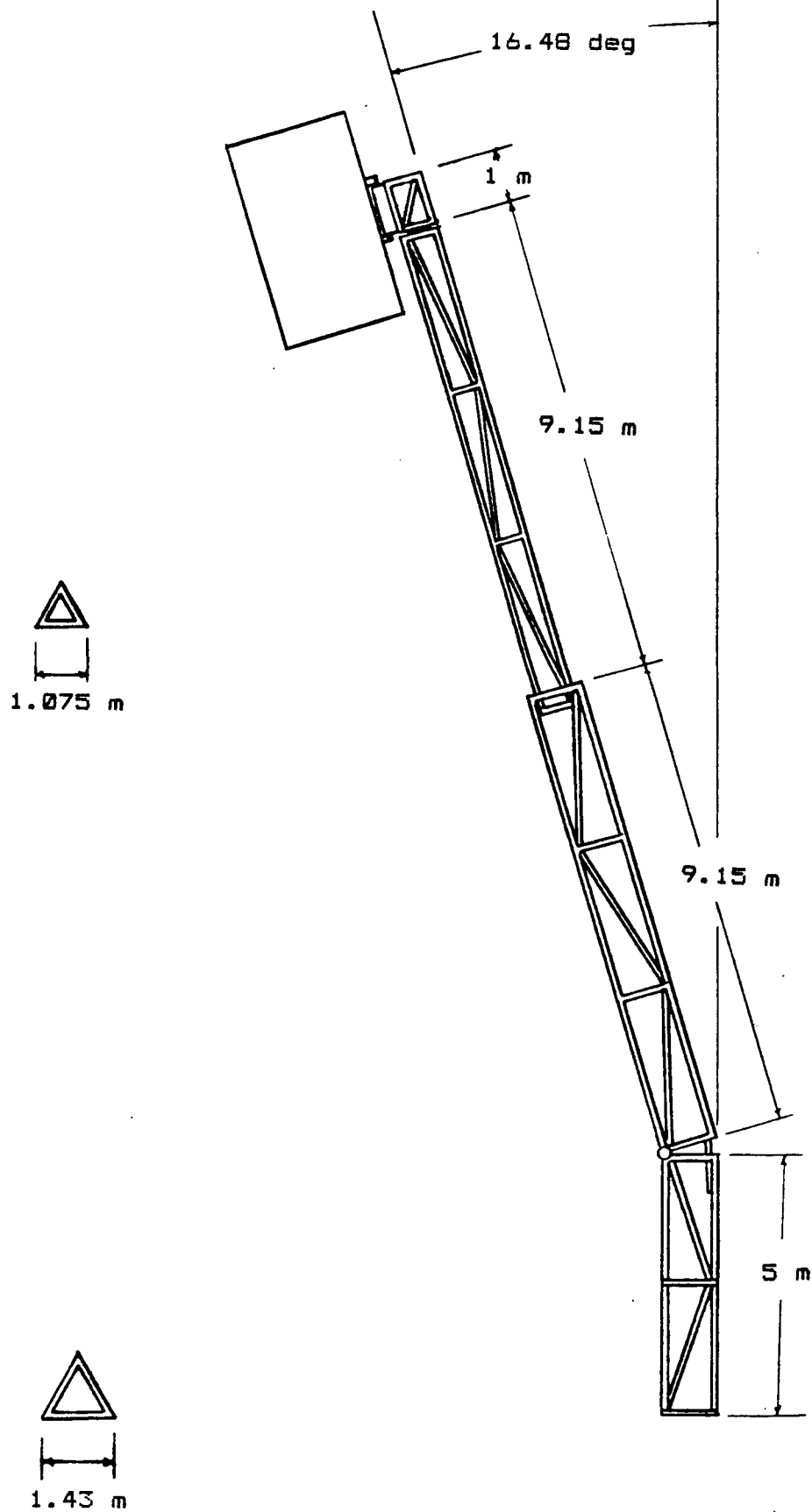
FIG. 4.30   PRIMARY MIRROR SUPPORT ARM (DEPLOYED)
LEO/LLO SCENARIO

4.8 REFERENCES

1. Clark, Robert S., ed. <u>The Photonics Design and Applications Handbook</u>. 33rd ed. Pittsfield, MA: Laurin Publishing, 1987.

2. Shannon, Robert R. and Wyant, James C., eds. <u>Applied Optics and Optical Engineering</u>. New York: Academic Press, 1979.

3. The International Society for Optical Engineering. "Reflective Optics." Proceedings of SPIE, volume 751 (Jan. 1987).

4. Irvine, Thomas B., Marsha M. nall, and Robert Seidel. "Solar Dynamic Power Systems for Space Stations." First NASA/DOD CSI Technology Conference, Norfolk, VA., Nov. 18-21, 1986.

5. Ussher, T.H., and K.H. Doetsch. "An Overview Of The Shuttle Remote Manipulator System." NASA Technical Report N85-16964.

6. The International Society For optical Engineering. "Structural Mechanics of Optical Systems II." Proceedings of SPIE, volume 748 (Jan. 1987).

C - 2

5. POINTING AND TRACKING

5.1 TRACKING SYSTEM

5.1.1 INTRODUCTION

The LOTV Tracking System is a complex system, involving components on both the LOTV and the LPS, since they have to act in concert. The system on the LOTV consists of a platform containing the optical tracking system and communications laser. The platform is mounted on the end of the optical truss behind the second mirror. It is able to move independently of the optical truss. The other part of the system is the computer control system necessary to communicate and translate information from the tracking system and laser into movements of the tracking platform, optical truss, and the main truss strucure. The main components of the optical tracking system are the tracking laser and optics, a telescope attached to an optical detector, an optical detector consisting of an avalanch photo diode array, the tracking platform, the thermocouples on the main mirror, the computer system, and the variable optics mirror alignment system. Each of these is discussed below in detail, followed by a discussion of the design considerations in developing this system. In addition, a block diagram of the· system is given, and flowcharts of a typical mission profile are discussed.

5.1.2 TRACKING LASER

The tracking laser on the LOTV is a pulsed, solid state, Yttrium-Aluminum-Garnet (YAG) Laser with an overall input of 50 watts, and an overall output of .2 watts. It operates at a wavelength of .532 micrometers, which is obtained through the use of optical doubling (see ref. 5.3). Normally, a YAG laser operates at 1.06 microns, but operating at this wavelength makes the tracking mirror on the LPS prohibitively large. The pulsed power of the laser is 200 watts at peak power for 1 microsecond, with a maximum of 1000 pulses per second. This allows the LPS to track without requiring large amounts of power for the laser. The laser itself is located on the tracking platform on top of the telescope tracking system. It is independently movable from the tracking sensors. This allows the laser to "lead" the target for long distances where the LPS will have moved significantly from its last location. The divergence of the laser beam is controlled by a simple variable lens system. At long distances, the spread is about 0.1 degrees. At short distances, the lenses are moved, and the beam spread is much greater to account for larger relative velocities.

5.1.3 TELESCOPE TRACKING SYSTEM

The telescope tracking system consists of a Schmidt-Cassegrain Telescope with a dielectric filter. The dielectric optical filter is tuned to a wavelength of 532 nanometers, which allows only tracking laser light to trigger the optical detector. The telescope itself is 38 centimeters in diameter and about 60

centimeters long, with a small central obstruction (see ref. 5.7). The field of view is 0.3 degrees wide. This is a compromise, since the optics on this telescope are non-variable. The optical paths for the telescope tracking system and tracking laser are shown in figure 5.3.

5.1.4 OPTICAL DETECTOR

The optical detector consists of nine photoelectric cells, arranged as in figure 5.4. Since shorter wavelengths are used, the cells can operate at 20 degrees Celsius, and cooling is generally not needed. The photocell array is about 2.5 centimeters in diameter, and consumes very little power.

The optical detector works by moving the tracking platform in response to signals from the photocells. If any of the non-central photocells are triggered, the tracking platform is moved right or left until a boundary between two photocells is reached. At this point, two photocells are triggered, causing the platform to move right, left, up, or down towards the center, depending on which two cells were triggered (ref. 5.4). The center photocell is the exact size needed for the accuracy desired. When the center cell is reached, the tracking system is aligned so that only the center cell is illuminated. If other cells are illuminated, the tracking system is adjusted again.

5.1.5 TRACKING PLATFORM

The tracking platform is located at the end of the truss behind the second mirror, as shown in figure 5.1, with dimensions as shown in figure 5.2. It consists of the tracking laser and laser optics assembly, mounted on top of the 38 cm Schmidt-Cassegrain telescope. Because of the large relative velocities and long distances, the laser is independently movable in order to account for the difference in position. The whole system of tracking laser, laser optics, Schmidt-Cassegrain telescope, and optical detector are mounted on an altazimuth mount, capable of rotating about two axes.

Six struts attach the tracking platform to 2.5 meter long extension/retraction rails on the optical truss. For the aerobraked version, the tracking system is fully retractable. For the non-aerobraked version, the tracking platform can only be deployed once.

5.1.6 THERMOCOUPLES ON THE PRIMARY MIRROR

The thermocouples on the main mirror are located at the ends of each rib for the wrap-rib mirror, and every 10 degrees for the rigid mirror. Any variety of small thermocouples can be used. When the laser hitting the primary mirror gets off focus, the thermosensors fire. Corrections are then sent to the LPS via the tracking laser, based on the location and number of thermosensors which are hit by the off focus beam. The windows to the thermocouples have dielectric filters which transmit only light

93

Figure 5.1 LOTV Tracking System

Optical Truss

Extension/Retraction Rails

17.5 cm Laser Optics System

38 cm Scmidt-Cassegrain Telescope

Tracking Laser

Optical Detector

Scale: 1:32

All Dimensions in Centimeters
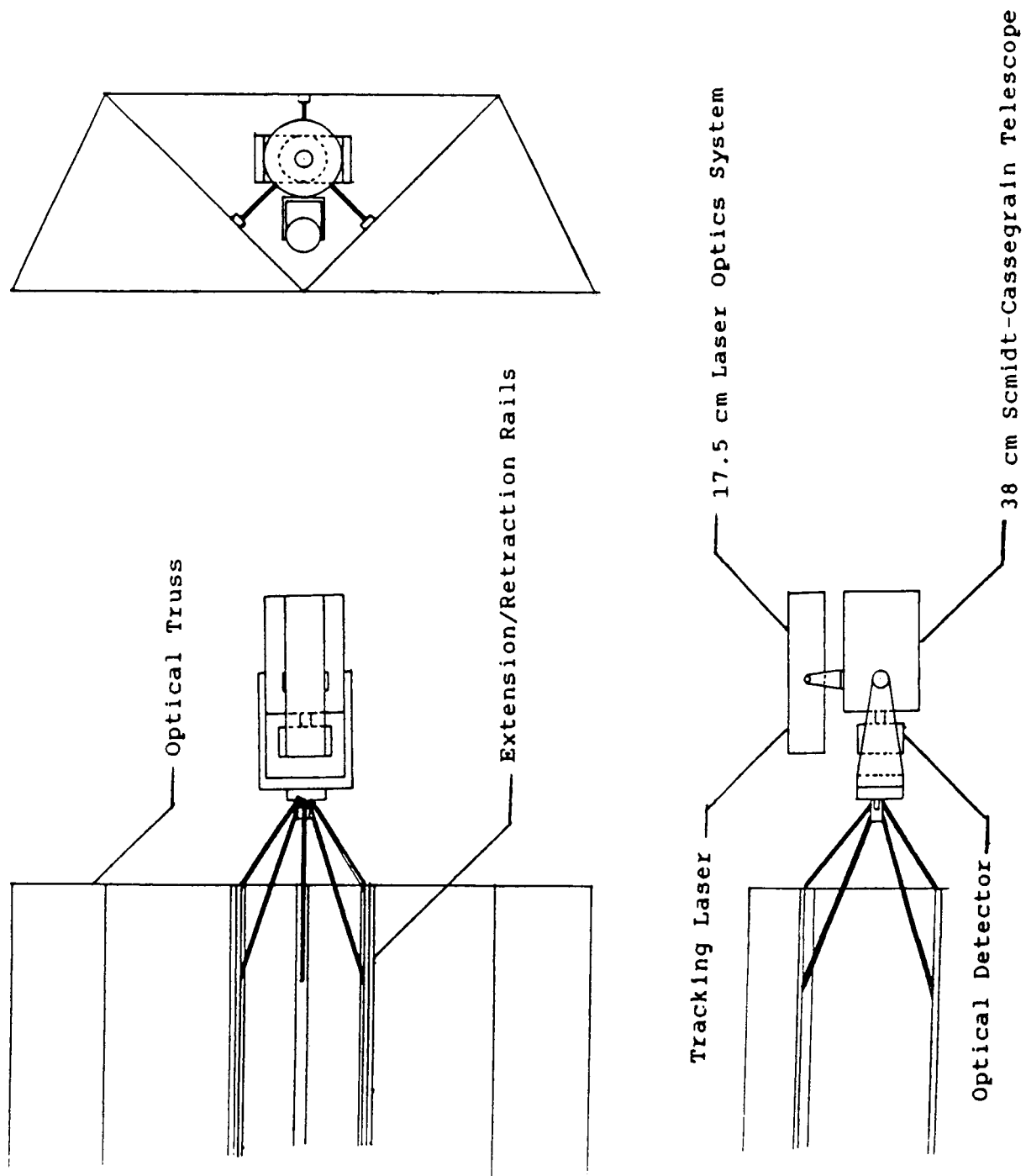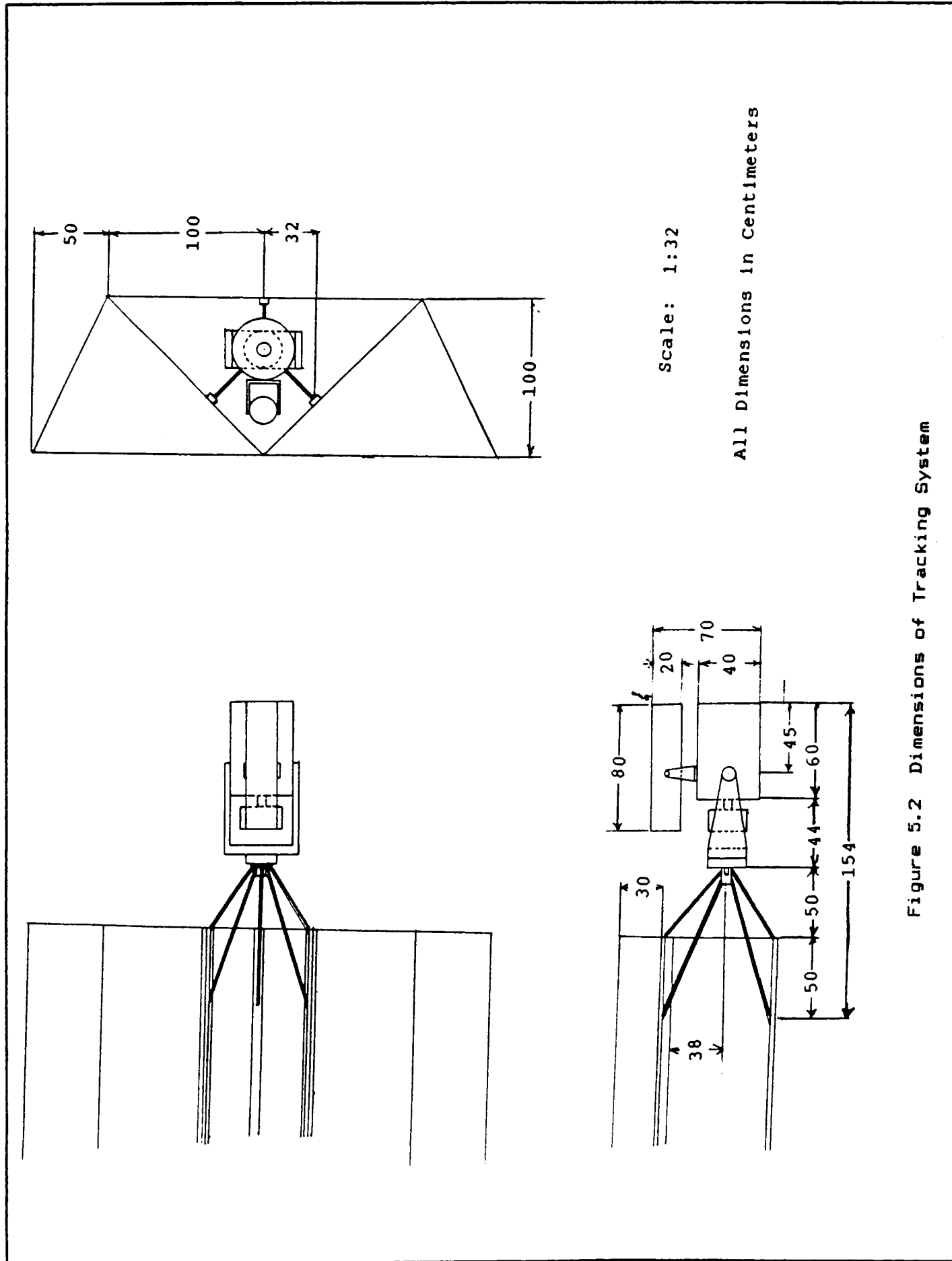
Figure 5.2 Dimensions of Tracking System

Tracking Laser

17.5 cm Laser Optics System

Optical Detector

38 cm Scmidt-Cassegrain Telescope

Figure 5.3 Optical Paths for Tracking Laser and
Schmidt-Cassegrain Telescope

Quadrant Photocells

Scale: 5:1

Central Photocell

Figure 5.4 Optical Detector Photocells

96
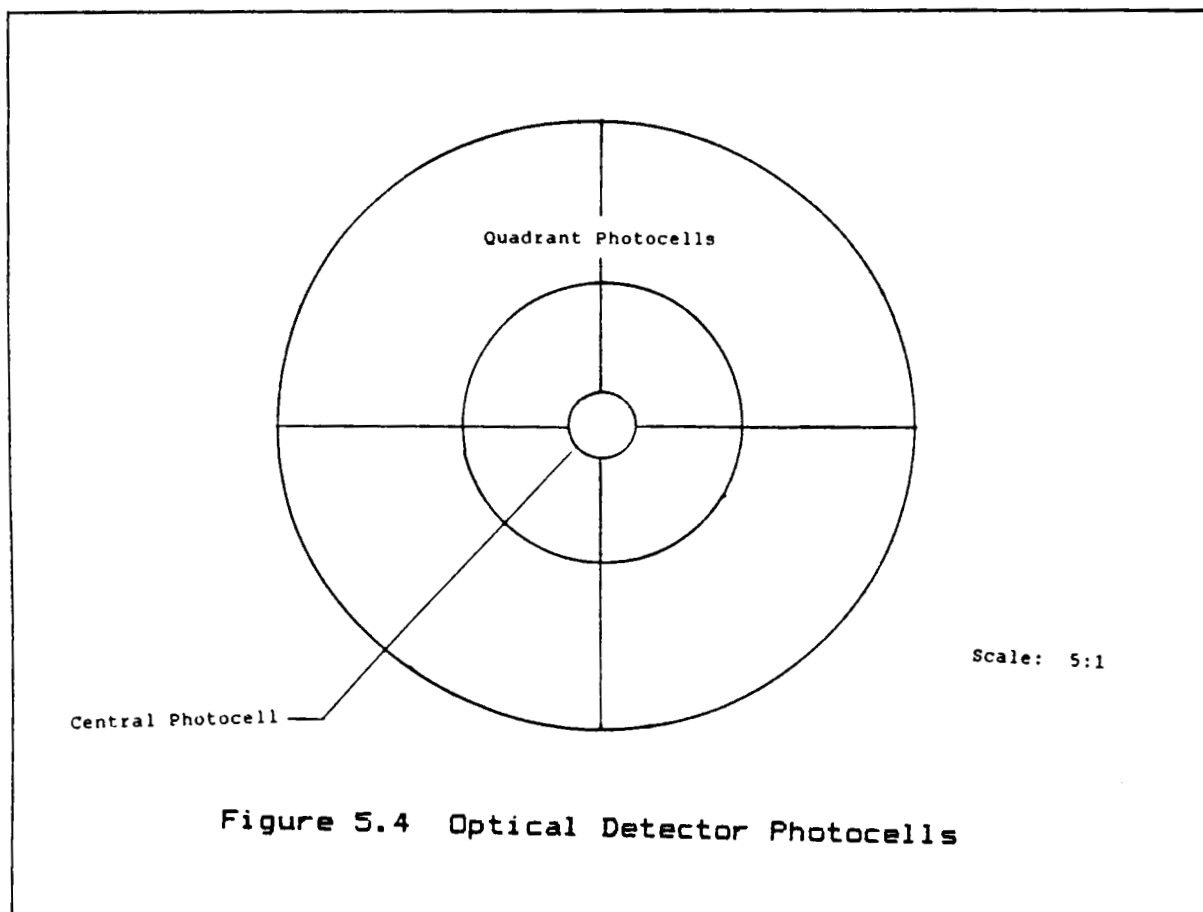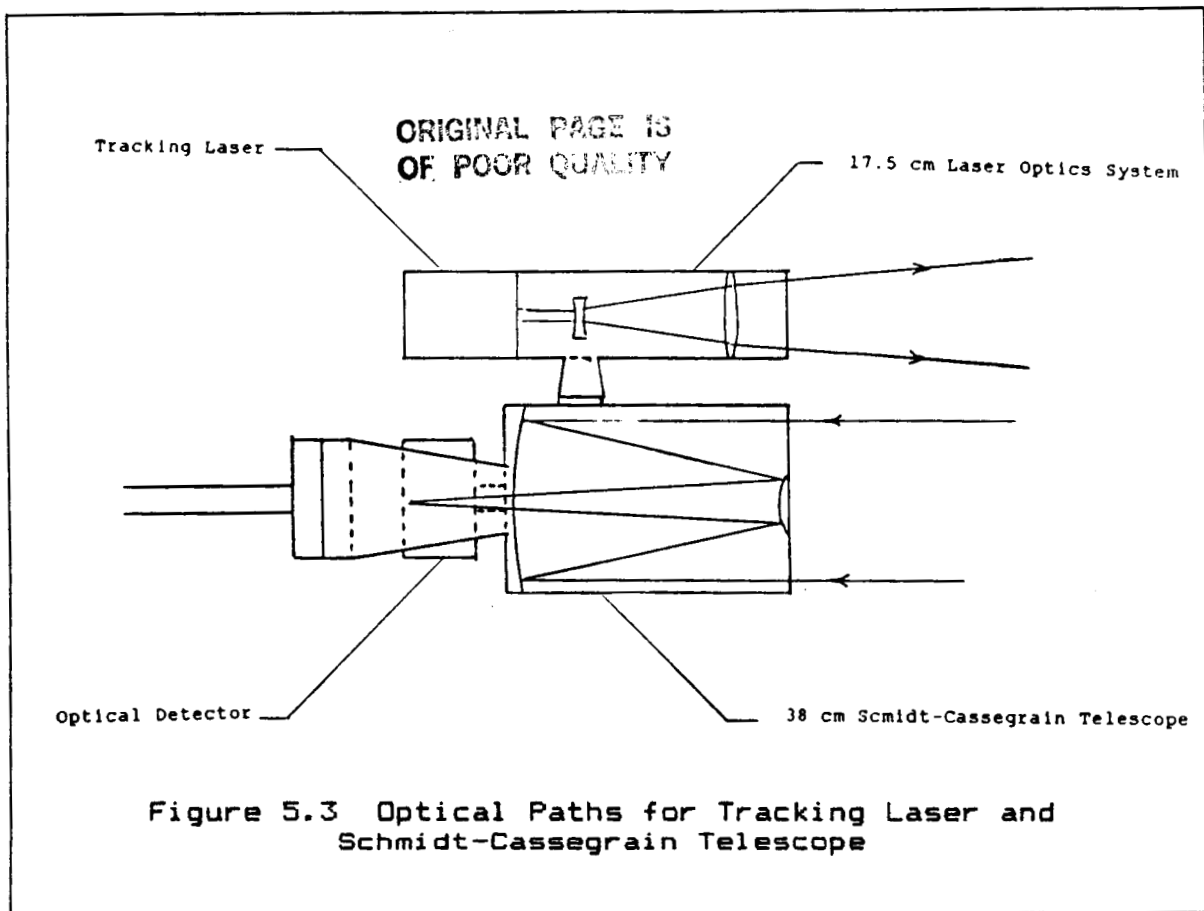
at the main laser wavelength of 1.315 micrometers. External
radiation from the sun will not trigger the thermocouples, since
the main laser delivers much more energy than the sun at this
wavelength.

5.1.7 COMPUTER SYSTEM

The computer system consists of a number of processors working
simultaneously, with a main processor controlling communications
between all the elements. This allows a variety of activities to
be undertaken at the same time, such as receiving data from the
LPS, sending correction information to the LPS, moving the truss
and tracking system, and calculating new LOTV and LPS orbits.

5.1.8 VARIABLE OPTICS MIRROR ALIGNMENT SYSTEM

The variable optics mirror alignment system consists of three
thermosensors on each facet of the variable optics mirror. When
the mirror is misaligned, the thermosensors detect this and
correct the mirror alignment.

5.2 DESIGN CONSIDERATIONS

The design of the tracking system has to take into account
several factors: accuracy, radiation intensity, and mass. Each
of these is addressed below.

5.2.1 ACCURACY CONSIDERATIONS

The accuracy of the LOTV system must be considered at both the
LPS and the LOTV, since they both have different requirements for
accuracy. For the LPS, the main consideration is the diffraction
limit for resolution. The diffraction limit is the distance in
radians that two objects can still be resolved as separate
objects. The equation governing this is:

$$d = 1.22 \times (lambda) / D$$

where d is the diffraction limit, lambda the wavelength of light,
and D the diameter of the primary mirror or lens (ref. 5.6). For
this system an arbitrary error of no more than 20% of the
diameter of the primary mirror on the LOTV was set. This
corresponds to an approximate error of 2.3 meters. The maximum
conceivable distance between LOTV and LPS is about 60000
kilometers. This corresponds to a diffraction limit of .04
microradians. The wavelength of light was chosen based on the
smallest wavelength solid-state laser. A solid-state laser was
chosen because it has a very high reliability. This turns out to
be a Yttrium-Aluminum-Garnet laser with a doubled wavelength of
.532 microns (see ref. 5.3). Plugging in the diffraction limit
and the wavelength and solving for the primary mirror diameter on
the LPS tracking system gives a diameter of 16.23 meters. Since
this diameter is near the diameter of the main laser beam, the
same optics system could be used for both tracking and firing.

97

The LOTV pointing accuracy is much less. The limiting factor for this is the accuracy of the beam at the propulsion system window. The maximum error the laser can have at the window is about 0.5 cm. Based on a distance of 40 meters from the window, the accuracy needed is about 125 microradians. Based on the same wavelength of light, the minimum diameter of the tracking system on the LOTV is 5.173 mm. Therefore, pointing accuracy is not a consideration for the design of the LOTV optics system.

5.2.2 RADIATION INTENSITY CONSIDERATIONS

The limiting factor in the design of the tracking system on the LOTV is the intensity of the incident radiation from the LPS tracking laser. A large number of factors go into the calculation of the system.

Since most of the factors in the system are based on distance losses, a db-log scale can be used to greatly simplify equations. By using a log scale, factors can be added and subtracted instead of multiplied. To convert from linear to db, the following formula can be used:

$$db=10 * log10 \text{ (linear value)}$$

The factors that govern intensity considerations are:

    Tracking Laser Power
    Antenna Gain (divergence of laser beam)
    Antenna Optics Error
    Wavefront Error
    Pointing Loss
    Propagation Loss (distance losses)
    Receiver Gain (based on collection diameter)
    Receiver Optics Error
    Required Signal (minimum signal detectable)
    Margin (margin for error)

The tracking laser power is what needs to be solved for. In these calculations the antenna and receiver optics errors, as well as the wavefront error and pointing loss error are all very small losses, so these factors are essentially ignorable.

The antenna gain of both systems is based on a beam divergence of .1 degree. This divergence is large enough so that the acquisition of a return signal is relatively easy, yet small enough to keep the laser power down. The antenna gain is defined by the formula:

$$Ga=10* log10 \text{ (32/Õt»)}$$

where Õt is the full width beam divergence angle (ref. 5.4).

Propagation losses are losses due to distance and can be defined as follows:

$$Ld=10* log10 (lambda/4*D*R)»$$

where R is the distance between the LOTV and LPS (ref. 5.4).

Receiver gain follows a formula that is nearly the exact inverse of the propagation loss:

$$Gr=10 * log10 (2*D*a/lambda)»$$

where a is the radius of the receiver (ref. 5.4). The receiver diameter size of 35.56 cm on the LOTV was based on the largest commercially available catadioptic telescope (ref. 5.7).

The smallest required signal, based on present optical detectors, is about -75 db (ref. 5.4).

A margin of around 3 db is a generally acceptable margin for error, and roughly corresponds to a safety factor of 2. A larger margin was used in the calculations to take into account problems with noise sources.

The results of the calculations using the above equations are listed in table 5.1. Based on these calculations, the pulsed power necessary on the LOTV is 200 watt-seconds, and for the LPS tracking laser is 100 kilowatt-seconds.

The tracking system uses pulsed lasers, using large amounts of power of short periods of time. In addition to keeping power consumption low, the pulsed lasers are much easier to detect, since they are the only light sources which pulse in a regular fashion. This allows them to be detected even when the sun is interfering, since it is necessary to only detect the difference in intensity rather than the absolute intensity.

5.2.3 MASS AND POWER BREAKUP

The mass and power breakup of the system, based on rather conservative estimates, is given in table 5.2.

5.3 LOTV TRACKING SYSTEM DESCRIPTION AND TRACKING FLOWCHART

The LOTV tracking system description refers to figure 5.5. It shows the interaction between the system hardware and the various computer modules. Each of the different modules is described below, and some of the operations are explained. The variable optics mirror alignment system is also described, and refers to figure 5.6. The tracking flowcharts detail the steps in acquisition, tracking, and communincation between the LPS and LOTV. There are two tracking flowcharts: one for the LOTV (fig. 5.7), and one for the LPS (fig. 5.8). A detailed description of each of the steps in the tracking flowcharts is given.

Table 5.1. Tracking Laser Power Calculations

LPS-LOTV:

	(db)
LPS Laser Power (per pulse):	50.0
Antenna Gain:	70.23
Antenna Optics Efficiency:	-3.0
Wavefront Error:	-1.0
Pointing Loss:	0.0
Propagation Loss:	-303.0
Receiver Gain:	129.0
Receiver Optics Efficiency:	-3.0
Required Signal:	-75.0
Margin:	14.23

LOTV-Laser:

	(db)
LOTV Laser Power (per pulse):	23.0
Antenna Gain:	70.23
Antenna Optics Efficiency:	-3.0
Wavefront Error:	-1.0
Pointing Loss:	0.0
Propagation Loss:	-303.0
Receiver Gain:	159.6
Receiver Optics Efficiency:	-10.0
Required Signal:	-75.0
Margin:	10.43

Table 5.2. System Mass and Power

Component	Mass	Power Required
Tracking Laser	15 kg	50 watts
Telescope and Sensors	40 kg	---
Computer System	45 kg	140 watts
Tracking Platform	15 kg	10 watts
Totals:	115 kg	200 watts

5.3.1 SYSTEM DESCRIPTION

A. Laser: About .2 watts output to cover a diameter of .1
    degrees. May be defocused more at short ranges to allow for
    shorter acquisition times and larger relative angular
    velocities between the two vehicles. Also used for
    communication between the two vehicles if a radio or
    microwave communications source is not used.

B. Communications Module: Handles all communications
    processing. There are several functions:

    1. Processes communications signal inputs from
        Tracking/Acquisition Sensor. (Laser lock-on signal,
        orbital data, Laser acquisition signal)

    2. Signals Tracking/Acquisition Module when LPS has locked
        on to LOTV signal and is ready to fire.

    3. Receives signal from Tracking/Acquisition Module when
        lock-on has been achieved by LOTV and truss is in
        position.

    4. Receives updated orbital data from Orbital Data Module.

    5. Receives Laser error correction data from Laser Error
        Correction Module.

    6. Process all signals to be sent and output signals to
        Laser

C. Tracking/Acquisition Module: handles all tracking and
    positioning processing, and activates hardware to move truss
    and pointing hardware.

    1. Receives pointing vector from Pointing Vector/Lead
        Computation Module. Also sends actual pointing vector to
        this module to compute new orbit parameters.

    2. Receives confirmation of lock-on from Communications
        Module. Also sends lock-on confirmation signal to that
        module for the LOTV.

    3. Receives location/error position of LPS tracking laser
        from Tracking/Acquisition Sensor Module.

    4. Controls truss pointing hardware and laser
        tracking/sensor pointing hardware, which are cross
        linked.

D. Tracking/Acquisition Sensor Module: Tracks laser from LPS
    and also receives communication signal input. It sends this
    data to the Tracking/Acquisition and the Communications
    Modules, respectively. Tracking sensors consist of a

photocell grid with an optical filter to capture only laser light wavelength and a lens to focus the light. The communications signal receiver consists of a single high-accuracy photocell with an optical filter and lens to process signals in a digital fashion.

E. Laser Tracking/Sensor Pointing Hardware: Various motors and gimbals to point the Tracking/Acquisition Sensor and Laser. One large set of controls moves both modules in tandem, while a smaller module adjusts the laser for beam lead. The movements of this system are coupled to those of the truss system.

F. Truss Pointing Hardware: Various motors and gimbals to point the truss in the direction of the beam. Coupled to movement of Laser Tracking/Sensor Pointing Hardware.

G. Pointing Vector/Lead Computation Module: Calculates the pointing vector and laser lead using orbital and tracking data. Also figures out if Earth is in the way of firing.

   1. Receives orbital data from Orbital Data Module. Sends pointing vector and processed tracking data to Orbital Data Module.

   2. Sends pointing vector and lead to Tracking/Acquisition Module. Receives updated pointing vector and lead from same module after aquisition has been established.

H. Orbital Data Module: Calculates and saves orbits of LOTV and LPS. Continually updates LOTV and LPS orbits when LOTV is changing orbits.

   1. Receives Pointing vector data and Lead from Pointing Vector/Lead Module. Sends orbital data to same module

   2. Receives orbital data of LPS from Communications Module. Sends orbital data to Communications Module for LOTV.

I. Thermosensors on Main Mirror: Senses when main laser from LPS is slightly off target. Signals Laser Error Computation Module.

J. Laser Error Computation Module: Computes target error of main laser based on data from Thermosensors on Main Mirror. Sends target error to Communications Module, which sends it to the LPS for correction.

5.3.2 VARIABLE OPTICS MIRROR ALIGNMENT SYSTEM DESCRIPTION

A. Sensor Assembily Hardware: Consists of three or four individual banks of photosensors. The output from these banks goes to the Error Computation Module.
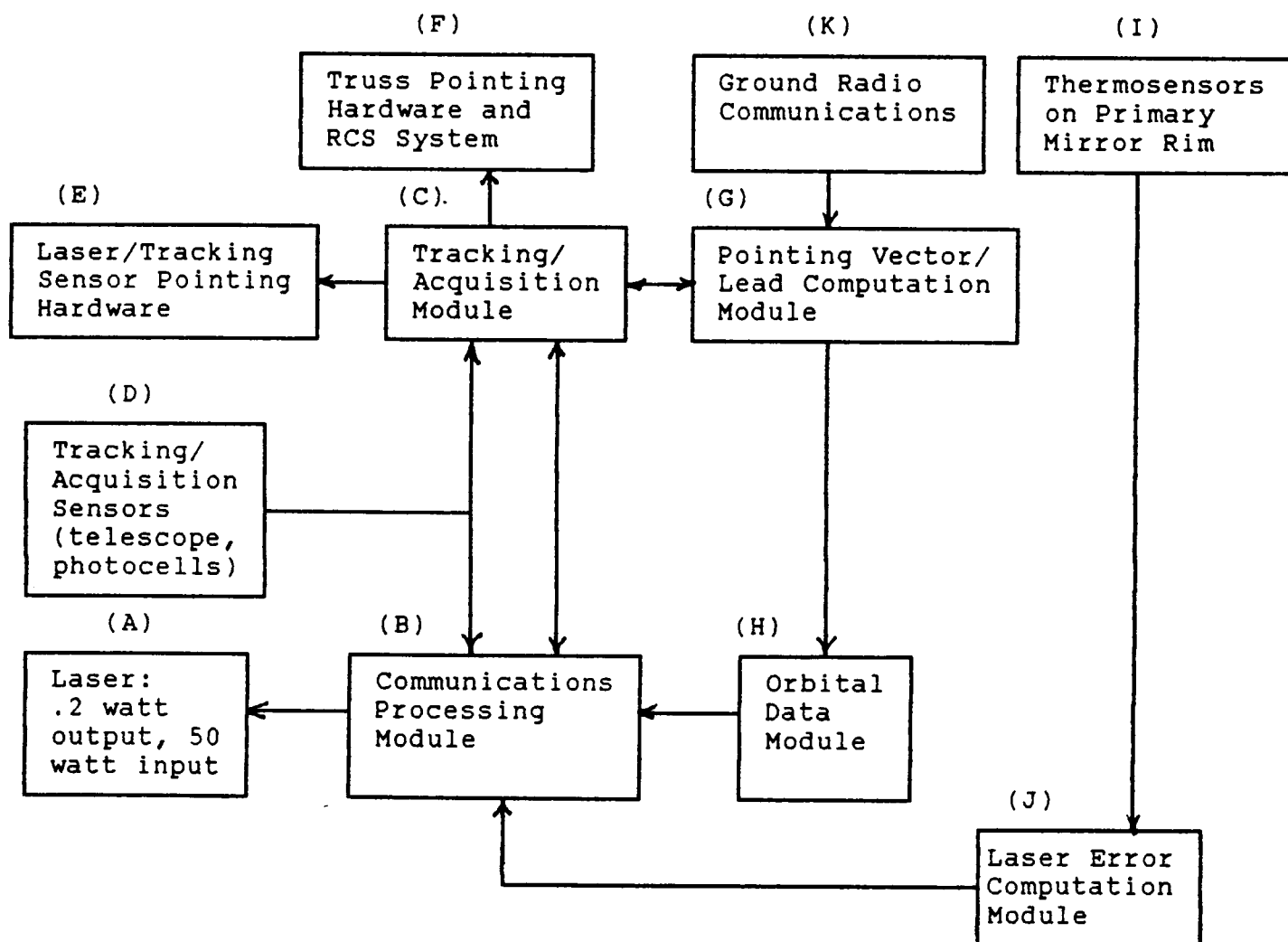
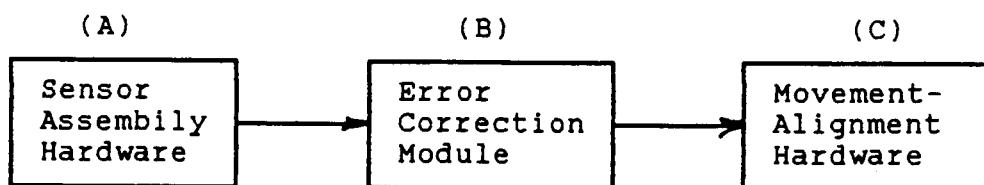Figure 5.5: LOTV Tracking System Schematic

Figure 5.6: Variable Optics Mirror Alignment System

B. Error Computation Module: computes adjustments necessary to minimize error of optical surface and sends output to Movement/Alignment Hardware.

C. Movement/Alignment Hardware: Corrects mirror surface in response to commands from Error Computation Module.

5.3.3 OPERATIONS DESCRIPTION

1) Start of Spacecraft mission: Initiated by external radio signal from Earth or other source.

2) Orbits of LOTV and LPS known or input from external source. Pointing vector for LOTV tracking and acquisition system calculated, and tracking system is aligned in that direction.

3) If the Earth is in the way or for some reason the tracking laser and sensors are not ready, continue adjusting pointing vector as in step 2) and wait until both LOTV and LPS are visible to each other.

4) Point telescope, tracking laser, sensors, and optical truss in general direction of LPS (within .1 degree). Account for laser lead if large distances and/or large velocities in tracking laser only. For close distances, laser beam can be spread out more.

5) Scan the error volume for signal from LPS. Fire the tracking laser in a pattern within error volume.

6) If signal not acquired from LPS, recompute pointing vector and repeat steps 2)-5).

7) If signal from LPS is acquired, signal lock-on to LPS by varying number of pulses per second out of tracking laser. Initiate pointing adjustments to tracking system and laser. Align truss with signal from LPS. Continue accounting for laser lead.

8) When Truss is aligned, signal the LPS that the LOTV is ready to begin laser firing. Wait for acquisition by LPS if this has not already been done.

9) Laser firing begins.

10) If there are errors in the LPS pointing, these are sensed by thermosensors on main mirror. The error is then computed, and corrections are sent via laser communicator.

11) The main laser is then corrected. Tracking is continued during this step.

12) If signal from LPS is lost, go to step 14)

13) If the mission is not over, repeat steps 10-12.

14) Determine reason for communications loss. (Is the Earth in
    the way or are there other causes?) Use new orbit
    information to reaquire tracking. Repeat steps 2-13.

15) End mission. Halt tracking and firing of lasers. Save
    orbital data.

All steps:
    -Calculate new orbit, velocity, and location based on
     tracking information.
    -Receive updated tracking information from LPS
    -If communications signal lost, determine causes and try
     to reaquire lock-on.
    -Continually refine LPS and LOTV orbits.
    -Continue Tracking.

5.3.4 OPERATIONS DESCRIPTION-LASER POWER STATION

1) Start of Spacecraft mission: Initiated by external radio
   signal from Earth or other source.

2) Orbits of LOTV and LPS known or input from external source.
   Pointing vector for LPS tracking and acquisition system
   calculated, and tracking system is aligned in that
   direction.

3) If the Earth is in the way or for some reason the tracking
   laser and sensors are not ready, continue adjusting pointing
   vector as in step 2) and wait until both LOTV and LPS are
   visible to each other.

4) Point telescope, tracking laser, and sensors in general
   direction of LOTV (within .1 degree). Account for laser
   lead if large distances and/or large velocities in
   tracking laser only. For close distances, laser beam
   can be spread out more.

5) Scan the error volume for signal from LOTV. Fire the
   tracking laser in a pattern within error volume.

6) If signal not acquired from LOTV, recompute pointing
   vector and repeat steps 2)-5).

7) If signal from LOTV is acquired, signal lock-on to LOTV
   by varying number of pulses per second out of tracking
   laser. Initiate pointing adjustments to tracking system
   and laser. Align main laser with signal from LOTV.
   Continue accounting for laser lead.

8) When main laser is aligned, signal the LOTV that the LPS is
   ready to begin laser firing. Wait for acquisition by LOTV
   if this has not already been done.

9)   Laser firing begins.

10) If there are errors in the LPS pointing, these are sensed by
     thermosensors on main mirror. The error is then computed,
     and corrections are sent via laser communicator to the LPS.

11) The main laser is then corrected. Tracking is continued
     during this step.

12) If signal from LOTV is lost, go to step 14)

13) If the mission is not over, repeat steps 10-12.

14) Determine reason for communications loss. (Is the
     Earth in the way or are there other causes?) Use new
     orbit information to reaquire tracking. Repeat steps
     2-13.

15) End mission. Halt tracking and firing of lasers. Save
     orbital data.

All steps:
   -Calculate new orbit, velocity, and location based on
    tracking information.
   -Receive updated tracking information from LOTV.
   -If communications signal lost, determine causes and try
    to reaquire lock-on.
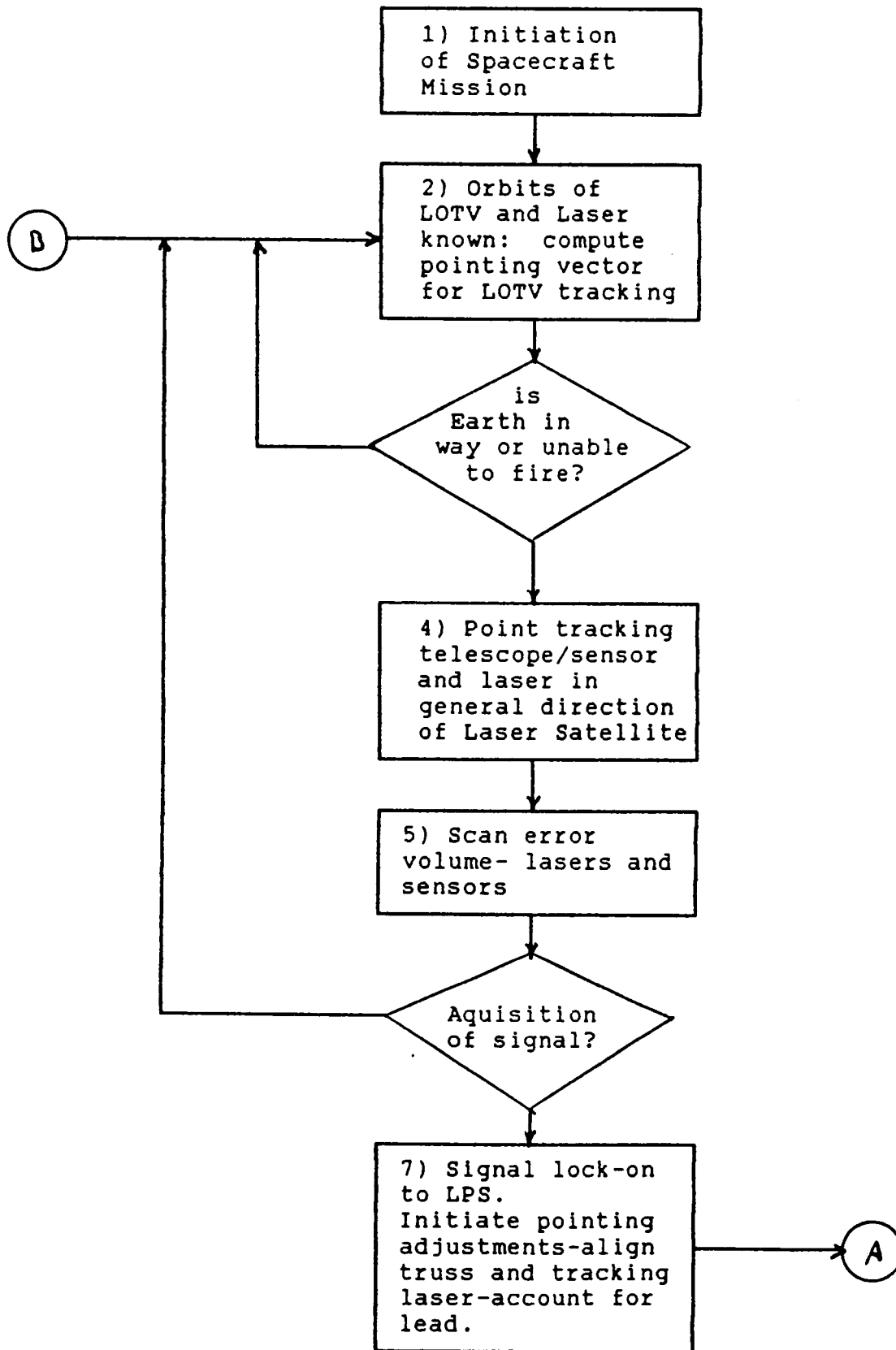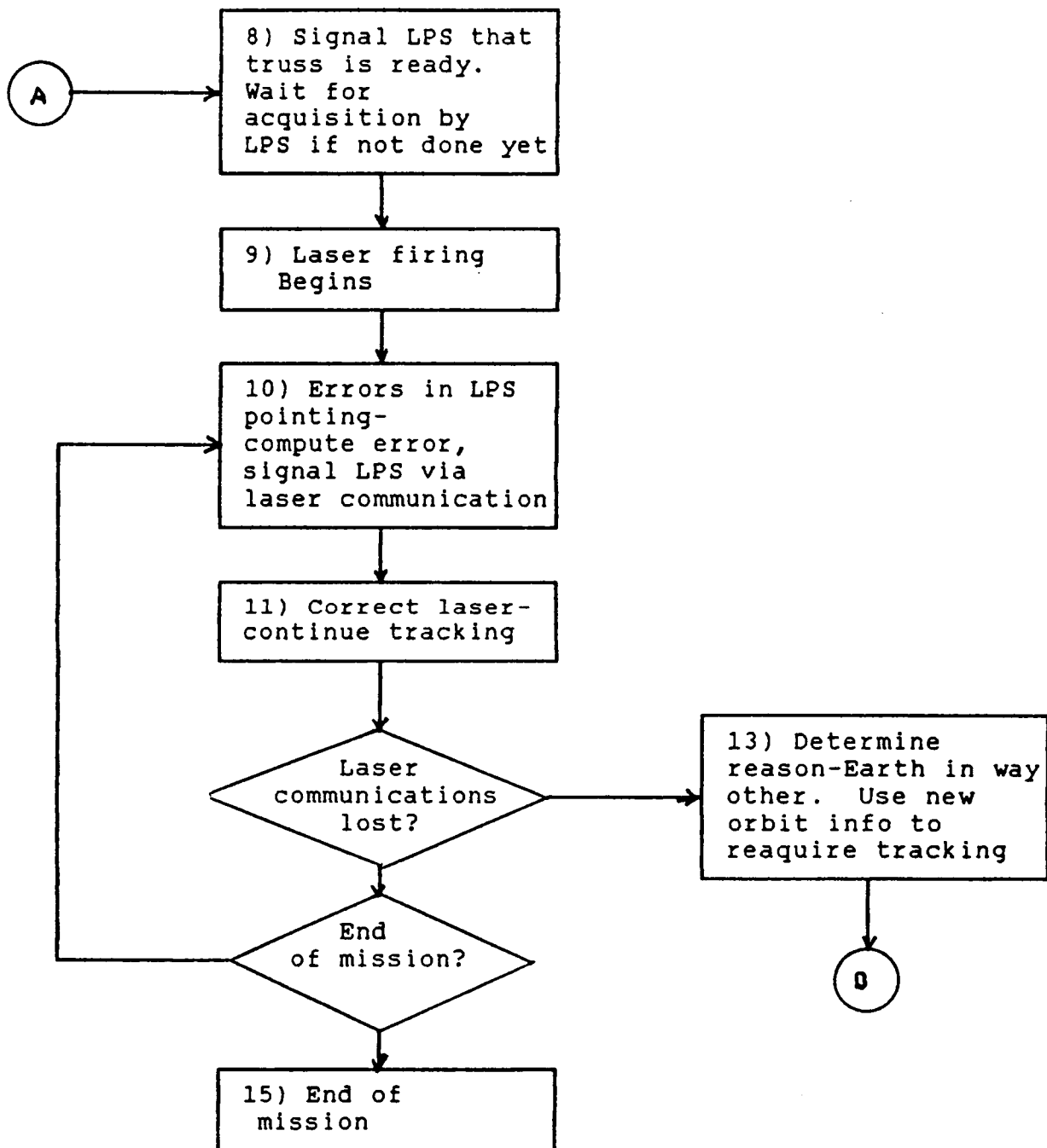   -Continually refine LPS and LOTV orbits.
   -Continue Tracking.

Figure 5.7: LOTV Flowchart of Operation

107

```
        ┌─────────────────────┐
  ┌───┐ │ 8) Signal LPS that  │
  │ A │→│ truss is ready.     │
  └───┘ │ Wait for            │
        │ acquisition by      │
        │ LPS if not done yet │
        └─────────────────────┘
                  │
                  ▼
        ┌─────────────────────┐
        │ 9) Laser firing     │
        │    Begins           │
        └─────────────────────┘
                  │
                  ▼
        ┌─────────────────────┐
        │ 10) Errors in LPS   │
        │ pointing-           │
        │ compute error,      │
        │ signal LPS via      │
        │ laser communication │
        └─────────────────────┘
                  │
                  ▼
        ┌─────────────────────┐
        │ 11) Correct laser-  │
        │ continue tracking   │
        └─────────────────────┘
                  │
                  ▼
             ╱─────────╲                    ┌──────────────────────┐
            ╱   Laser    ╲                  │ 13) Determine        │
           ╱ communications╲───────────────▶│ reason-Earth in way  │
            ╲   lost?     ╱                  │ other.  Use new      │
             ╲─────────╱                     │ orbit info to        │
                  │                          │ reaquire tracking    │
                  ▼                          └──────────────────────┘
             ╱─────────╲                                │
            ╱   End      ╲                               ▼
           ╱  of mission? ╲                            ┌───┐
            ╲           ╱                              │ D │
             ╲─────────╱                               └───┘
                  │
                  ▼
        ┌─────────────────────┐
        │ 15) End of          │
        │    mission          │
        └─────────────────────┘
```

All stages:
- calculate new orbit, velocity, location
- Signal new orbital data to LPS
- If communications lost, determine reason
- Continually refine Laser Sattelite location
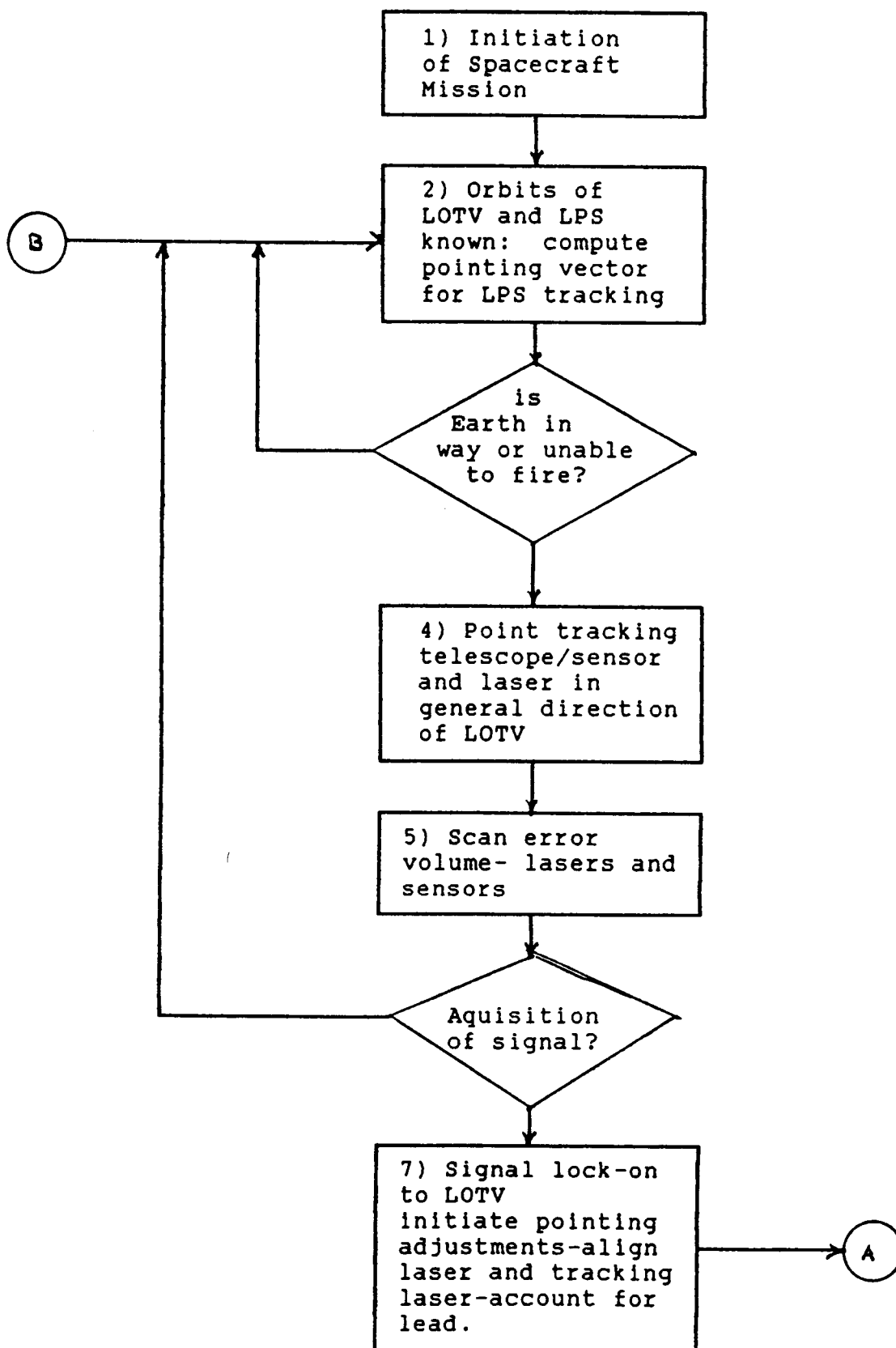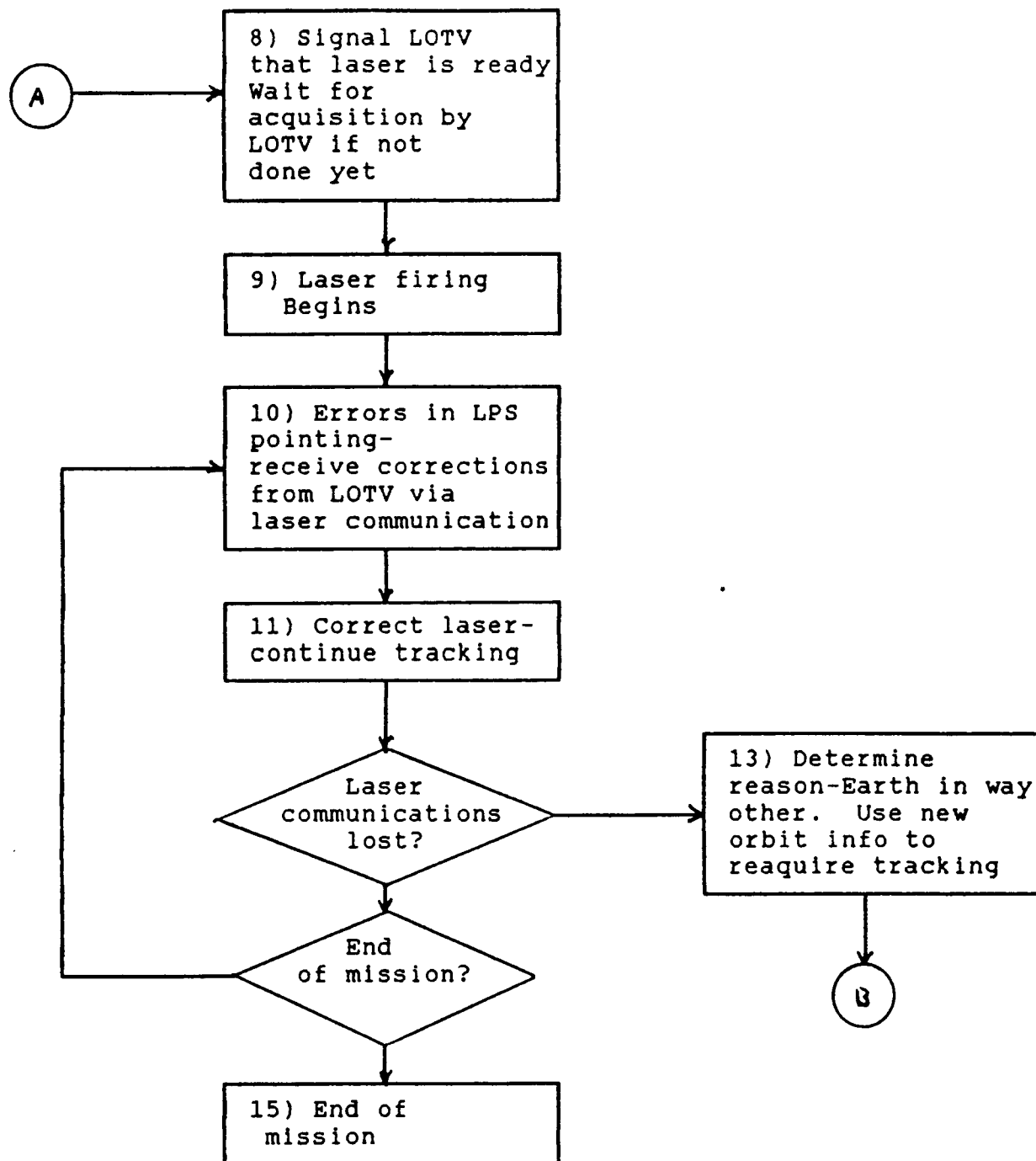- Continue tracking

Figure 5.7 (continued)

Figure 5.8: LPS Flowchart of Operation

```
  (A) ──────────►  ┌─────────────────────┐
                   │ 8) Signal LOTV      │
                   │ that laser is ready │
                   │ Wait for            │
                   │ acquisition by      │
                   │ LOTV if not         │
                   │ done yet            │
                   └─────────────────────┘
                             │
                             ▼
                   ┌─────────────────────┐
                   │ 9) Laser firing     │
                   │    Begins           │
                   └─────────────────────┘
                             │
                             ▼
                   ┌─────────────────────┐
                   │ 10) Errors in LPS   │
                   │ pointing-           │
                   │ receive corrections │
                   │ from LOTV via       │
                   │ laser communication │
                   └─────────────────────┘
                             │
                             ▼
                   ┌─────────────────────┐
                   │ 11) Correct laser-  │
                   │ continue tracking   │
                   └─────────────────────┘
```

Laser communications lost?

13) Determine reason-Earth in way other. Use new orbit info to reaquire tracking

(B)

End of mission?

15) End of mission

All stages:
- calculate new orbit, velocity, location
- Receive signals from LOTV
- If communications lost, determine reason
- Continually refine LOTV location
- Continue tracking

Figure 5.8 (continued)

5.4 REFERENCES

1. Beer, Ferdinand P. and E. Russell Johnston, Jr. 1984. <u>Vector Mechanics for Engineers: Statics and Dynamics</u>. New York: McGraw-Hill Book Company.

2. Beer, Ferdinand P. and E. Russell Jonhston, Jr. 1981. <u>Mechanics of Materials</u>. New York: McGraw-Hill Book Company.

3. Harry, John E. 1974. <u>Industrial Lasers and Their Applications</u>. London: McGraw-Hill Book Company.

4. Katzman, Morris. 1987. <u>Laser Satellite Communications</u>. New Jersey: Prentice-Hall Inc.

5. Lockheed Missles and Space Co. 1978. <u>Laser Rocket Systems Analysis</u>. NASA-CR-159521.

6. Menzel, Donald H. 1964. <u>A Field Guide to the Stars and Planets</u>. Boston: Houghton Mifflin Co.

7. 1987 telescope buyer's guide. October, 1987. <u>Astronomy</u>. Milwaukee: Kalmbach Publishing Co.

6. PROPULSION SYSTEM

6.1 INTRODUCTION

6.1.1 LASER PROPULSION

The propulsion unit for the LOTV is a multi-plasma hydrogen engine powered by a 32 MW laser. This system produces a relatively large thrust per unit mass of fuel consumed due to the low atomic weight and high energy content of hydrogen. An Advanced Propulsion Concept Study, performed by Boeing, comparing specific impulse, vehicle specific mass, and thrust to weight ratio of several advanced propulsion systems showed that laser propulsion concepts represent a compromise between high thrust to weight systems with short trip times and low thrust to weight systems with long trip times (Reference 6.1; see Figure 6.1)

6.1.2 BASIC ASSUMPTIONS AND REQURIEMENTS

The goal of this study was to perform a preliminary study of a laser propulsion system using liquid hydrogen as the propellant. This is to be driven by a direct solar pumped iodide laser of wavelength 1.315 microns, orbiting the Earth at an altitude of one Earth radius. A peak power density at the window of 25 kW/cm^2 limited the minimum window radius. From the initial orbital mechanics calculations it was determined that the thrust of the laser engine should be 2000 N in order to satisfy trip time requirements.

Assuming a specific impulse for laser propulsion systems of 1500 seconds and a thermal conversion efficiency of 50%, the required power from the laser coming into the thrust chamber is

$$P = I_{sp}*T*g/(2*n) = 29.43 \text{ MW}$$

where

I_{sp} = specific impulse
T = thrust
g = gravity at earth's surface = 9.81 m/s^2
n = efficiency

However, there is a 7.5% power loss through the optical train system. Therefore, the total power from the laser must be 32 MW. The mass flow for this thrust and specific impulse is

$$m = T/(I_{sp}*g) = 0.136 \text{ kg/sec}$$

6.1.3 LOTV MAIN ENGINE

The minimum diameter of the window, allowing a maximum power density of 25 kW/cm^2, is 40 cm. Thus, the inner diameter of the cylindrical thrust chamber was also defined to be 40 cm. In the plasma section of this report, it will be shown that this diameter is large enough to meet design criteria.
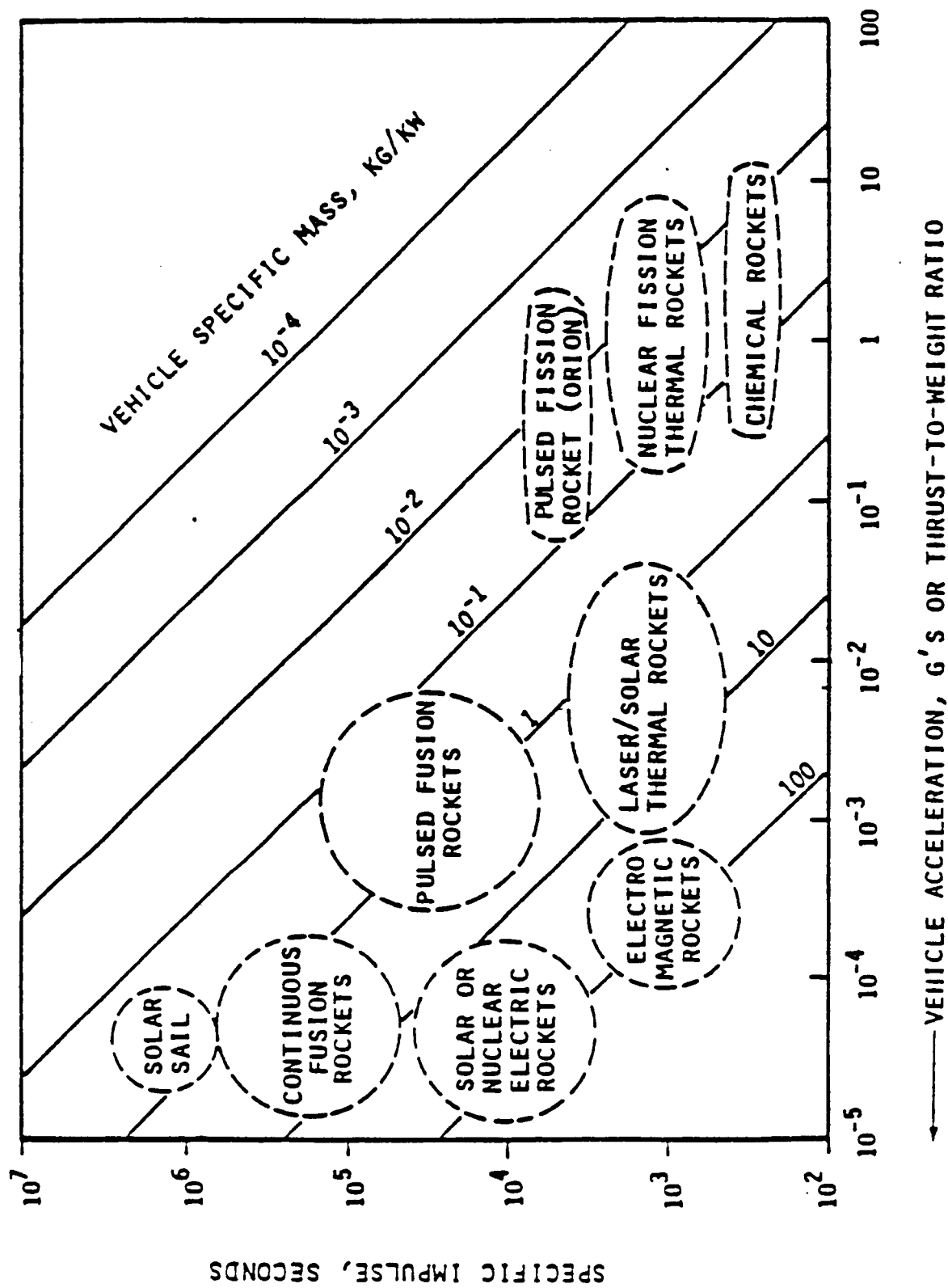
FIGURE 6.1 Propulsion System Performance (from Reference 1)

113

A multi-plasma arrangement is used to take advantage of the shadow effect. The shadow effect is when one plasma intercepts radiation from another plasma. Since the plasma receiving the radiation is at approximately 17,000 K, it will absorb the radiation striking it, making use of the radiation which would normally be lost. In addition, using several plasmas yields a higher cross-sectional area of absorptive hydrogen per volume of plasma, thereby intercepting more of the hydrogen flow in the thrust chamber. The actual plasma arrangement will consist of one central plasma and six surrounding plasmas (see Figure 6.4). The six surrounding plasmas have focal arcs instead of focal points such that they surround the central plasma, maximizing the shadow effect. Accordingly, the window is divided into seven lenses (see Figure 6.3--Window Configuration).

In order to withstand the high chamber temperatures encountered, a combination of two schemes is utilized (see Figure 6.2). First, a regenerative cooling system is used. Liquid hydrogen is circulated within the chamber walls and through tubes in the lens lattice support structure. One-fourth of the total mass flow goes through the lattice. The rest of the mass flow travels through tubes along the side of the chamber. The second method of protection is a layer of reflective material coating the inner walls of the thrust chamber. Since most of the heat transfer is radiative in nature, this layer will aid in shielding the walls.

Liquid hydrogen is injected into the chamber through six window injectors which vector the liquid hydrogen directly toward the plasma. Gaseous hydrogen is injected along the perimeter of the chamber wall just beneath the window. This provides cooling for the window and a mixing of the hydrogen. Figure 6.2 shows a schematic of the engine, and table 6.1 contains the engine parameters of the LOTV main engine.

Table 6.1 Main Engine Parameters

specific impulse	1500 sec
chamber pressure	5 - 7 atm
chamber temperature	5000 K
estimated engine efficiency	50%
thrust	2000 N
chamber diameter	0.40 m
chamber length	0.45 m
focal length of lenses	0.35 m
diameter of throat	6 cm
diameter of exit	52.5 cm
nozzle length	0.80 m
mass flow of hydrogen	0.136 kg/s
engine length	1.25 m
window diameter	0.40 m
MASSES:	
engine	120 kg
window	16 kg
total	136 kg

MOVEABLE NOZZLE

LASER – SUSTAINED PLASMA

COOLING JACKET

ACTUATOR

SEAL

WINDOW LENS
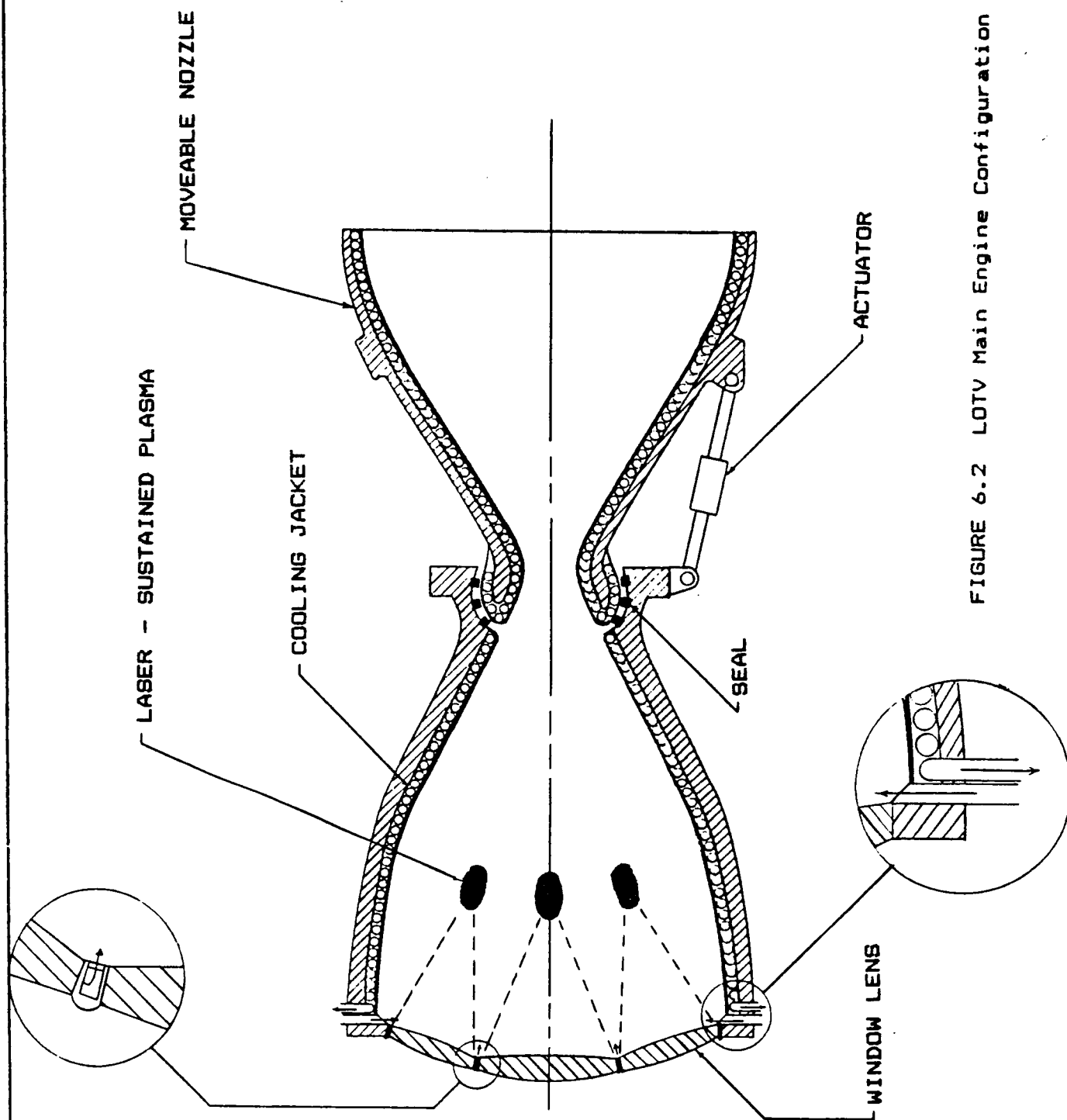
FIGURE 6.2 LOTV Main Engine Configuration

12000 K   Plasmas at 17000 K   140000 K
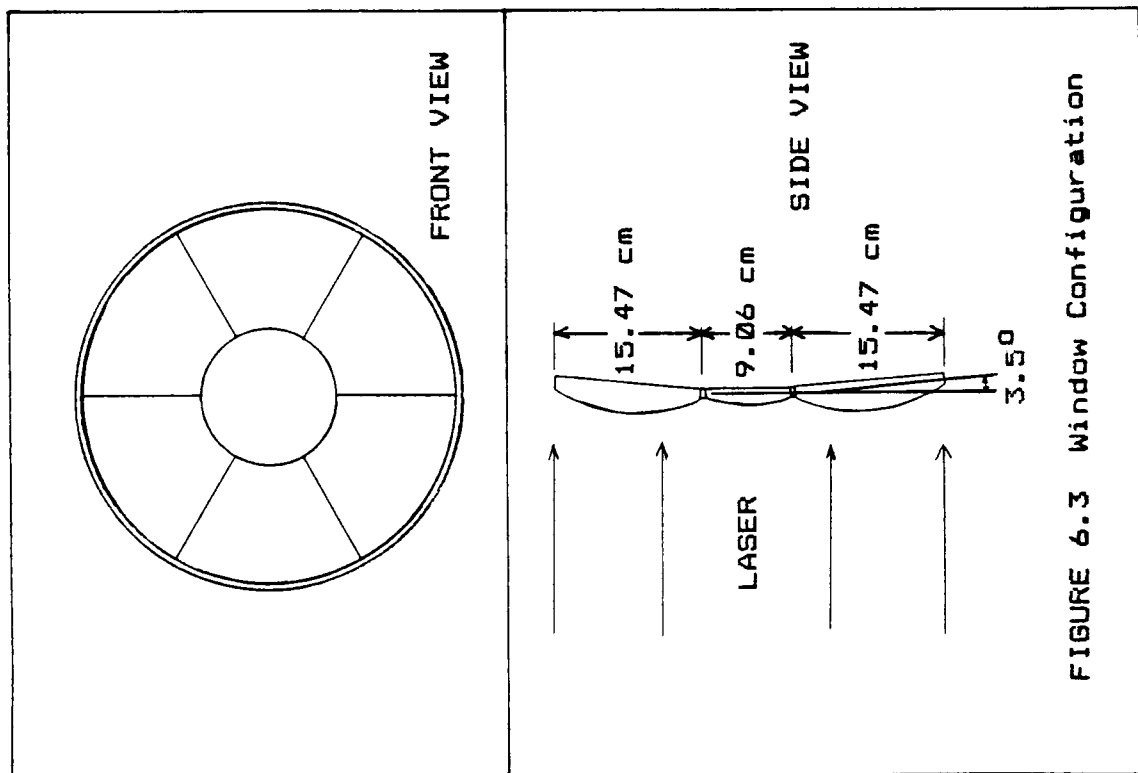
FIGURE 6.4 Plasma Temperature Distribution

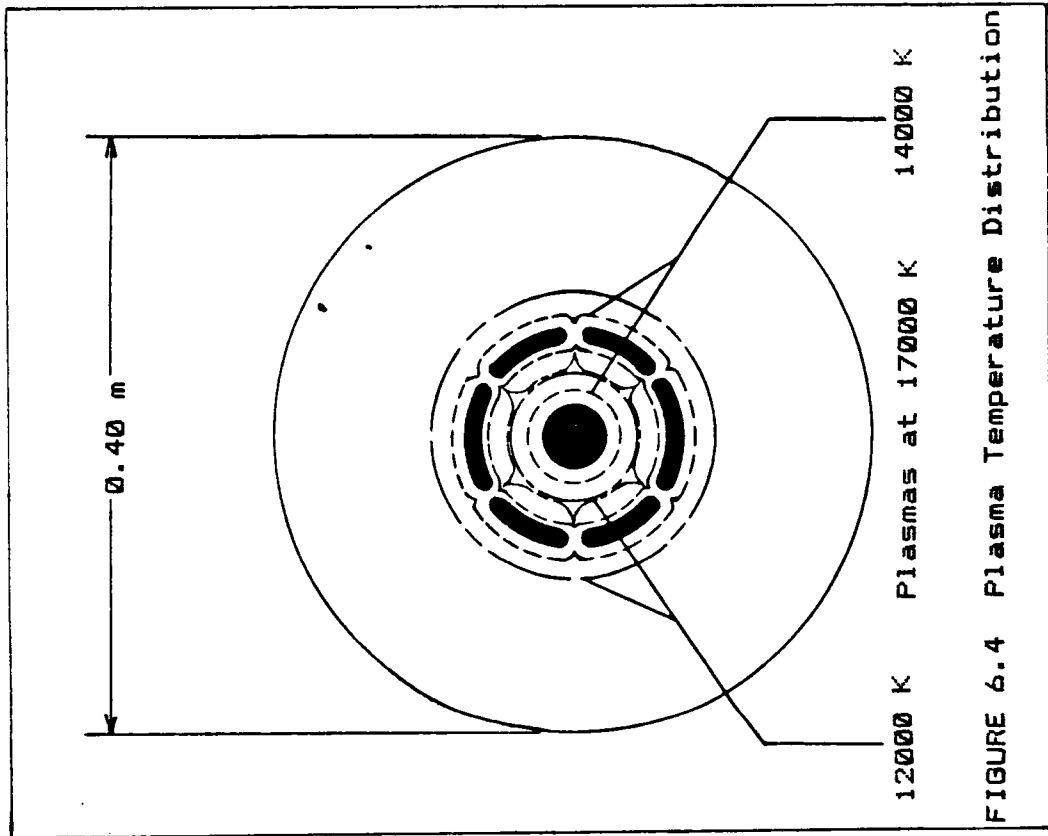FRONT VIEW

SIDE VIEW

15.47 cm   9.06 cm   15.47 cm

3.5°

LASER

FIGURE 6.3 Window Configuration

6.2 LASER WINDOW

Initially, three configurations were considered for the LOTV laser window. These included:

1. a flat window with an inner shell and an outer shell through which liquid hydrogen (LH$_2$) flowed for cooling purposes;

2. a concave window also with inner and outer shells for LH$_2$ cooling;

3. a concave window again with inner and outer shells for LH$_2$ cooling; however, the inner shell would have a hole in the center to inject the hydrogen into the plasma chamber.

A preliminary design of the third configuration was in progress when the decision to use multi-plasmas, and thus a multi-lens window was made.

A window design with an overall convex, circular shape was initiated. The window will consist of seven lenses: a circular center lens surrounded by six outer lenses, each lens corresponding to one plasma (see Figure 6.3). The lenses were originally to be made of calcium fluoride because of its high transmissivity of about 98 % in the infrared region. An improved material, such as a synthetic sapphire, will have to be developed to increase the transmissivity of the secondary lenses because of the reduced laser power density incident on them. A calcium fluoride lens cannot withstand thermal fracture from the 25 KW/cm^2 laser beam, and so the material selection was changed to strontium fluoride, which has a similar transmissivity in the infrared region. Upon further research, it was discovered that this material cannot withstand thermal fracture failure from the peak power density of the laser either, and for this reason the new material mentioned above will have to have a much higher rupture stress than either calcium fluoride or strontium fluoride.

For a laser power of 29.5 MW, and a window peak power density of 25 kW/cm^2, the area of the window is 1180 cm^2. A window radius of 20 cm was used. In order to determine the area of the center lens, the thermal fracture figures of merit had to be considered. According to reference 6.4, for a window whose edge (outer diameter) temperature is fixed, and which is subjected to a CW laser with a Gaussian profile, thermal fracture failure occurs when the maximum tensile stress (an azimuthal stress at the edge of the window) reaches the rupture strength. This critical total laser power is (Reference 6.4):

$$P = 4*D*K*Sc*[GEOMETRICAL\ FACTOR]/B*Á*E$$

where

        K = thermal conductivity
        Á = thermal expansion coefficient

```
B  = bulk absorption coefficient
E  = Young's modulus
Sc = rupture stress
```

The geometrical factor is a function of the relative sizes of the beam and the window, varying from one for a Gaussian beam radius small in comparison with the window radius, to two for a beam radius equal to the window radius. In the case of the LOTV window, the geometrical factor is two.

Analysis of these figures of merit, using strontium fluoride as the lens material, yields a critical total laser power of 1.6 MW, and thus a center lens area of 64.4 square centimeters to withstand a 25 KW/cm^2 laser intensity. Again, this critical laser power is much less than the 29.5 MW specified, and thus a material with a rupture stress of 76,800 N/cm^2 will have to be developed. Each of the lenses is plano-convex, with the outer (convex) side having a radius of curvature of 15.4 cm. This was determined using the "lens maker's formula:"

$$1/f = (n - 1)[1/r_1 - 1/r_2 + (n-1)t/r_1r_2]$$

where

```
f  = focal length
n  = index of refraction
r1 = outer surface radius of curvature
r2 = inner surface radius of curvature
t  = lense thickness
```

For the LOTV laser window, the focal length is 35 cm, and the radius of curvature of the inner surfaces of the lenses is infinite, those being the planar sides. These parameters yield a radius of curvature of the convex sides of 15.4 cm, as stated before.

Finally, the lengths of each of the secondary lenses is 15.47 cm, and the radius of curvature of the entire window is taken to be 35 cm. This yields a minimum thickness of 0.42 cm to withstand a pressure of 10 atm in the chamber, which is much less than the center thickness of 1.68 cm for the center lens, and 3.084 cm for the secondary lenses. See detailed drawing in Figure 6.3, as well as the window material properties and dimensions in Tables 6.2 and 6.3, respectively.

Table 6.2 Window Material Properties

material	STRONTIUM FLUORIDE
density	4.24 g/cm^3
index of refraction	1.44
thermal conductivity	0.1 W/cm-K
thermal expansion coefficient	15.8E-06 $^\circ$C^{-1}
bulk absorption coefficient	4.1E-05 cm^{-1}
Young's modulus	10.1E+06 N/cm^2
rupture stress	4206 N/cm^2

Table 6.3 Window Dimensions

1.	Center lens		
	radius of curvature	15.4	cm
	diameter	9.06	cm
	center thickness	1.68	cm
	edge thickness	1.0	cm
	mass	0.47	kg
2.	Secondary lenses		
	radius of curvature	15.4	cm
	length	15.47	cm
	center thickness	3.084	cm
	edge thickness	1.0	cm
	mass	2.66	kg
3.	Total window mass	16.0	kg

6.3 PLASMA

6.3.1 PLASMA CHARACTERISTICS

In gases at high temperatures, electrons escape from the neutral atom due to their high energy content; thus, the gas consists of ions and free electrons with large amounts of kinetic energy. When a fast moving electron collides with an ion, which has a much larger mass, it releases energy known as inverse Bremsstrahlung radiation (collision heating). Note that Bremsstrahlung literally translated from German means "braking radiation" and is the radiation due to a deceleration of the electron. (Sometimes the radiation itself is referred to as Bremsstrahlung).

The peak temperature for the plasmas will be the temperature corresponding to the maximum absorption coefficient for the hydrogen. This value is approximately 17,000 K (obtained from Dennis Keefer at the University of Tennessee Space Institute, where the most recent and comprehensive testing is being done on hydrogen plasmas; Reference 6.7). However, all calculations for plasma and chamber size were based on a peak temperature of 20,000 K due to a lack of data for hydrogen at 17,000 K (Reference 6.7).

At low temperatures, hydrogen is virtually transparent. In fact, the absorptivity of hydrogen doesn't become significant until the temperature reaches approximately 12,000 K. For this reason, the seven plasmas will be arranged such that their temperature profiles touch at 12,000 K (see Figure 6.4). This will provide the largest possible cross-sectional area of absorptive, high temperature hydrogen at the center of the thrust chamber for the given amount of plasma.

The plasma size (overall volume of all seven plasmas) was determined by setting the power needed to heat hydrogen at a

given mass flow rate to 2,000 K equal to the power radiated by the 20,000 K absorption region (Reference 6.8):

$$mq_r = VQ$$

where

> m = mass flow through cooling jacket
> q_r = energy/mass needed to raise hydrogen to 2,000 K
> V = volume of the absorption region
> Q = power radiated/volume by 20,000 K hydrogen.

Note that for simplicity, this model assumes that only the 20,000 K plasma region radiates energy. This will result in a liberal estimate of the cooling system. Since the pressure in the chamber is so high (6.804 atm), the plasmas will be roughly spherical in shape. Therefore, the radius of the plasma, R_p (assuming one large plasma with the radiating volume equivalent to that of the seven plasmas) can be solved for as follows:

$$R_p = \left[\frac{3mq_r}{4DQ} \right]^{(1/3)} = .901 \text{ cm}$$

6.3.2 PLASMA INITIATION

Initiation of the plasma at engine startup is an important and difficult process to coordinate with an engine design. Since hydrogen itself is transparent to the icident laser wavelength below 5,000 K, a scheme must be developed to heat the hydrogen to 12,000 K, at which temperature hydrogen becomes absorptive. Once the hydrogen reaches 12,000 K its temperature will continue to increase until the stable temperature of 17,000 K is reached. At this temperature hydrogen is at its most absorptive.

In order to increase the temperature of hydrogen to the desired levels it is necessary to develop some sort of heating mechanism. The easiest is simply to have a plasma of a different material, one that develops at relatively low temperatures, to heat the hydrogen. This plasma, called the initiation plasma (IP), will induce heating of the surrounding gas. It will cause radial flow ahead of and within the plasma itself. This will reduce the amount of gas that must be heated. Heating of the gas in front of the IP aids in the transition of the hydrogen from it's initially transparent condition to a strongly absorbing condition at a wavelength of 1.315 microns. The temperature profile of the gas heated radially and axially can be seen in Figure 6.5a. This figure was obtained from Byran (Reference 6.9) and represents a laser initiated plasma profile with air at 1 atm as the medium, a 10.6 micron wavelength, with titanium (Ti) as the target material. It is assumed that at the LOTV's engine conditions the temperature profile of the surrounding hydrogen will be similar. As can be seen from the figure, the gas in front of the IP

reaches very high temperatures and enters the plasma state itself. This occurs very quickly after IP formation. Since the hydrogen plasma (HP) is absorptive, it absorbs energy that would otherwise go to the IP, so the IP diminishes and the HP increases.

The target material most favorable in forming the IP appears to be Ti (Reference 6.9). In order to incorporate the solid target with the liquid fuel engine, the titanium is used in slurry form. To decrease the effects a slurry would have on tubes and injection slots, the slurry will be polyaphronated (Reference 6.10). Two possible schemes for this exist (see Figures 6.5b and 6.5c).

The first method is to surround the micron sized titanium particles with an aqueous film. This method is still in the experimental stage (Reference 6.10). The second method is to have powdered titanium suspended in an aphron medium. Both of these methods would substantially decrease the effects of settling, and if an aqueous film of 60% by volume of methanol is used, the aphrons would be stable to temperatures as low as 227 K. A polyaphronated slurry also has the advantage of significant decrease in friction and wear in the tubes and injection slots. During IP formation the film would evaporate first, resulting in a trace amount of water vapor and methanol. The effect of these on IP formation is not presently understood.

In order to simplify the process, a series of steps were developed called the Plasma Initiation Sequence or PINS.
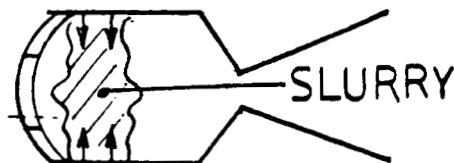
Plasma Initiation Sequence (PINS)

A.) Hydrogen Injection.
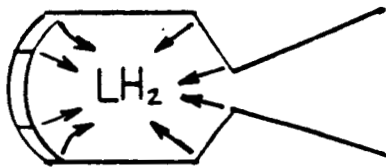
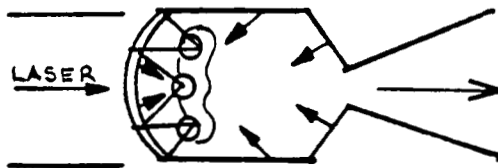1.) Provides medium upon which the I.P. can act.

B.) Slurry Injection.

1.) Slurry injection through select radial tubes near the focus points.

C.) Laser Startup.

1.) Aphron film evaporation occurs.

2.) The initial hydrogen mass flow will only be a
   fraction of the final mass flow.

D.) HP replacement of IP.

1.) Gradual increase of hydrogen injection. This
   will aid in the replacement of IP with HP.

2.) At HP formation the slurry flow will be stopped.

3.) The final step is to increase all flows to
   normal flow rates.

It should be noted that the sequence described is only an
estimate of the steps needed. The actual steps and interactions
can only be obtained through extensive analysis and
experimentation.

6.3.3 REGENERATIVE COOLING JACKET

The regenerative cooling system will be divided into two parts--
window cooling and chamber cooling. Because the tubes carrying
the hydrogen through the windows must be small so as not to
intercept much of the incoming laser power, the hydrogen through
the tubes will be injected at high velocity (45.72 m/s) as
liquid. The high velocity not only helps to keep the hydrogen
liquid, but also increases the temperature gradient of the
plasmas. Therefore, the temperature will decrease from the
maximum temperature much more quickly. This will result in lower
hydrogen temperatures near the chamber wall. The hydrogen used
for chamber cooling (75% of the total hydrogen mass flow) will be
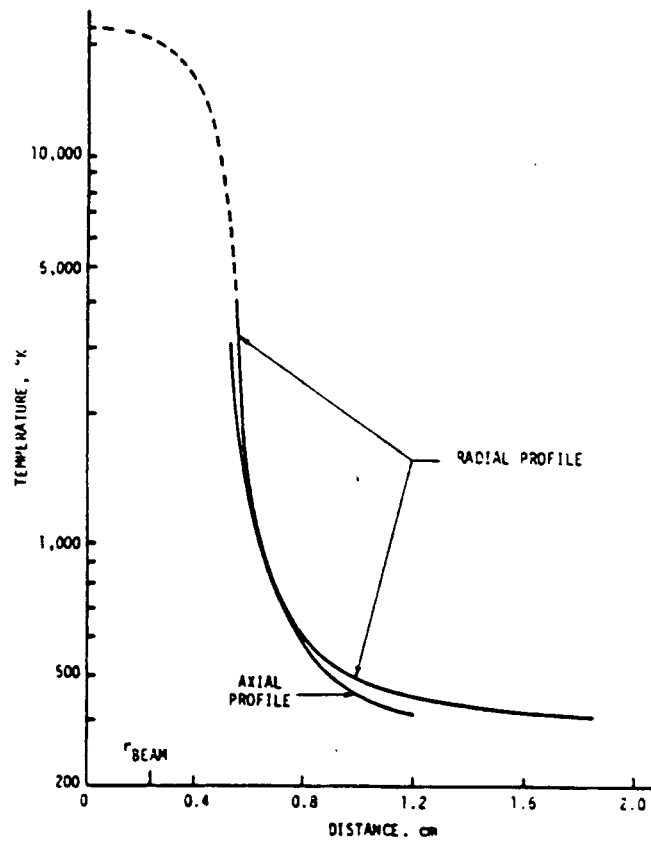heated to 2,000 K in order to obtain the appropriate cooling
capacity.

FIGURE 6.5 A   Temperature Profile
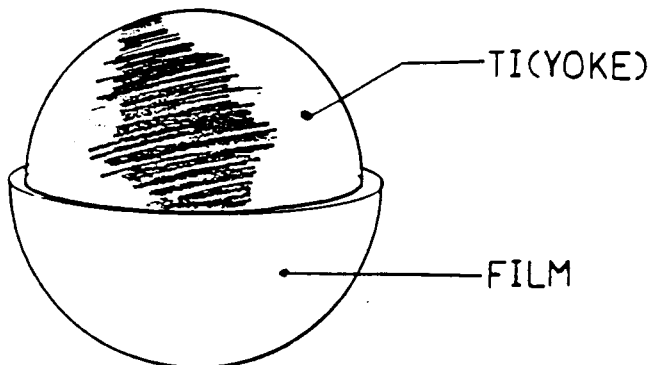of a Gas Heated Radially and Axially
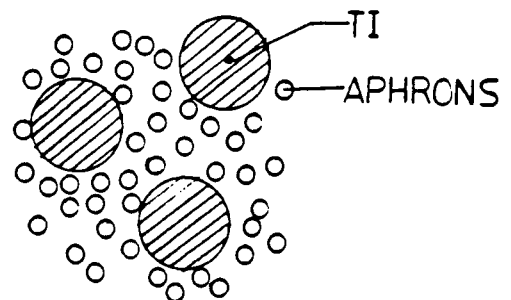
FIGURE 6.5 B   Slurry Aphron

FIGURE 6.5 C   Slurry Suspension

The tubes will be made of a carbon/carbon composite selected for its high melting point ($\sim$3870 K) and low density. The coating on the inside of the thrust chamber must also have a high melting point and must be selected/treated such that it is highly reflective to 1.315 micron wavelength radiation. Presently, Rhenium seems to be the best candidate assuming it can be properly treated.

The tubes were arranged such that they will touch on the outer surface of the cylindrical part of the chamber. A reiterative technique was used to determine the diameter of the tubes based on having the diameters touch and having the appropriate mass flow through the tubes (velocity was set at 45.72 m/s):

$$d = \left[\frac{4(m_C/N)}{D(rho)u} \right]^{(1/2)}$$

where

d = inner diameter of a tube
m_C = total mass flow in the cooling jacket
N = number of tubes
rho = density of hydrogen
u = velocity of hydrogen in tube

$N = D[D + 0.8(d + 2t)]/(d + 2t)$

where

t = thickness
D = diameter of the chamber.

The factor 0.8 accounts for the fact that the tube centers lie on a circle, rather than on a straight line.

As a result, the cooling jacket will have 73 tubes surrounding the thrust chamber, each with an inner diameter of 1.08 cm.

At the throat of the nozzle, the cooling jacket will consist of concentric circles with vanes to direct the flow as well as support the outer shell. Solving the continuity equation for the outer diameter gives:

$$D_O = \left[\frac{4m_C}{D(rho)u} + D_i^2 \right]^{(1/2)} = 10.4 \text{ cm}$$

where

D_O = outer diameter
D_i = inner diameter

Thus, the distance between the circles is:

$$\frac{D_o - D_i}{2} = 2.8 \text{ cm}$$

6.3.4 WINDOW COOLING

One quarter of the hydrogen mass flow entering the thrust chamber will be injected through the window as liquid. Since there are · six support tubes for hydrogen injection, each of these will carry one twenty-fourth of the total mass flow (.005667 kg/s). With an injection velocity of 45.72 m/s (150 ft/s), the cross sectional area of the tube is:

$$A = \frac{m}{(rho)u} = 0.0159 \text{ cm}^2$$

where

     m   = mass flow through one lattice support tube
     rho = density of hydrogen at 20 K
     u   = injection velocity of hydrogen

Determination of the tube wall thickness is a complex problem since the thermal expansion coefficient must complement the thermal expansion coefficient of the window material to reduce the risk of stress fracture in the window. In addition, the material must be able to withstand the internal pressures and hold the lenses in place. Therefore, design of the tubes has been left for further research. However, in designing the tubes, two important factors should be considered. First, the tube walls adjacent to the window should be parallel to the incoming radiation (see Figure 6.2 inset). If they are not, the radiation reflecting off of the tube walls will reflect into the window, thereby increasing the amount of heat absorbed by the window. Second, the top of the tube (facing the incoming radiation) should be convex to ensure that the reflected radiation does not focus on a point on the external structure (see Figure 6.2).

6.4 PROPELLANT FEED SYSTEM

6.4.1 TURBOPUMPS

The feed system for the LOTV uses a turbopump system with an electric motor to initiate the rotation of the pump until the operation speed is achieved. An electric motor was chosen due to the low amount of power required by the pump. The gaseous hydrogen from the regenerative cooling system is used to drive the turbine.

The propellant feed system, shown in Figure 6.6, is initiated by an electric motor which drives the pump shaft using three identically sized bevel gears: one on each of the motor and pump
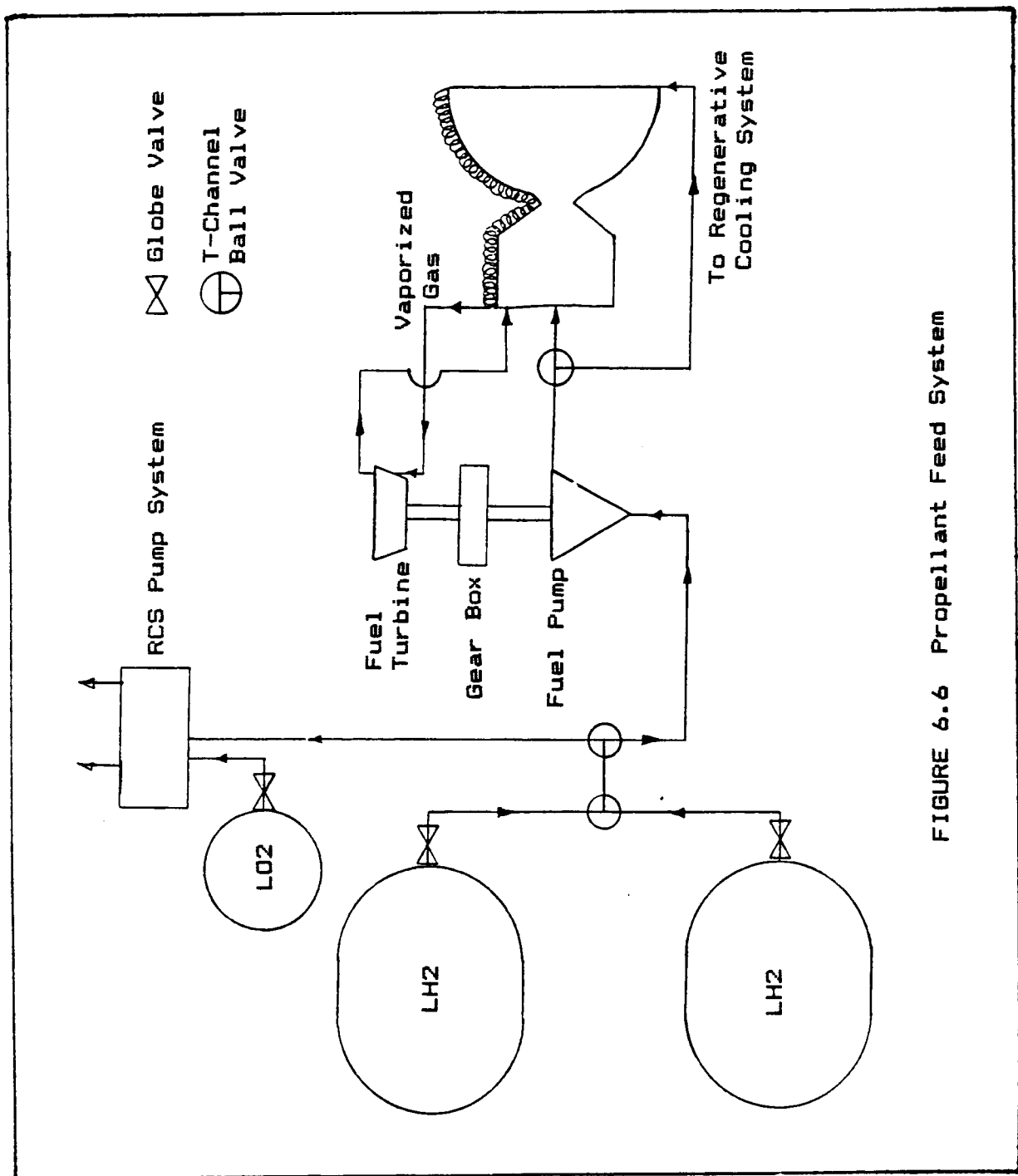
125

FIGURE 6.6 Propellant Feed System

126

drive shafts, and one between the two. The middle gear can be
released from the system by an electronically switched hydraulic
system when operation speed has been achieved. The hydraulic
system would pull this middle bevel gear away from the bevel
gears on the drive shafts separating the motor from the pump
drive shaft. The electric motor can then be turned off and would
not be driven by the turbopump. This would prolong the service
life of the motor.

The turbopump consists of a centrifugal pump driven by a single-
stage turbine with a gear box to relate the operation speeds
together. The pump is between the storage tanks and the engine.
The LH_2 pressure is increased by 1100 kPa across the centrifugal
pump. The LH_2 is heated as it passes through the regenerative
cooling system to a temperature of about 2,000 K. The gaseous
hydrogen then flows through the turbine and transfers the energy
from the hydrogen into power to drive the pump. The power
required by the pump is 2.7 kilowatts and was calculated from
(References 6.12 and 6.13):

$$Power = rho*Q*H*g/n$$

where

> rho = density
> Q   = volume flow rate
> H   = head
> g   = gravity
> n   = efficiency

Assuming that axial velocity would be constant through the
turbine, and using the configuration in Figure 6.6, the power
output of the turbine was calculated by:

$$Power = m*U*(V_x*(\tan(Á)+\tan(Ã))-U)$$

where

> m   = mass flow rate
> U   = blade speed
> V_x = velocity in the axial direction
> Á   = absolute flow angle upstream of rotor
> Ã   = relative flow angle downstream of rotor

The power output from the turbine is 3.23 kilowatts at a
rotational speed of 52,500 RPM to drive the pump, as indicated in
Table 6.4.

The inlet and exit pressures were calculated from:

$$\frac{P_{t2}}{P_{t1}} = [1 + W/(n_t c_p T_{t1})]^{k/(k-1)}$$

127

Table 6.4 Turbopump Parameters

Pump:
Power required   2.7 kW
Inlet density   71 kg/m^3
Inlet pressure   69.9 kPa
Discharge pressure   1.17 MPa
Pump developed head   1580 m
Volume flow rate   1.92 x 10^{-3} m^3/s
Mass flow rate   0.136 kg/sec
Shaft speed   24,500 RPM
Turbine:
Inlet pressure   1.17 MPa
Exit pressure   703 kPa
Inlet temperature   2000 K
Shaft speed   52,500 RPM
Power output   3.23 kW
Gearbox:
Reduction speed ratio   1/2.143

where

p_t = stagnation pressure
T_t = stagnation temperature
c_p = specific heat
k = ratio of specific heats
n_t = turbine efficiency
W = work of the turbine

The work of the turbine was calculated from:

$$W = \frac{P}{m}$$

where

P = power out of turbine
m = mass flow

The pump developed head was calculated from:

$$H_{il} = U^2/g$$

where

H_{il} = ideal head
U = blade speed
g = gravity

A mass breakdown of the propellant feed system appears in Table 6.5.

Table 6.5 Mass Breakdown of Propellant Feed System

Turbine	25 kg
Pump	40 kg
Shafts and Gears	10 kg
Electric Motor and Hydraulic System	25 kg
Total	100 kg

6.4.2 FLUID TRANSFER

There will be globe valves on the fuel storage tanks. These valves will require actuators in the case of one tank being closed due to a leak. One tank will also be shut when the engine is not in use. Fixed T-channel ball valves will be used to join the pipes from the tanks into a pipe that will go through the main engine only or to the main engine and the RCS system. This valve will also require an actuator. A pipe will then go to another fixed T-channel valve which will send part of the fuel to the regenerative cooling system and the rest of the fuel to the engine for direct injection. There will be globe valves on both of the pipes (see Figure 6.6). The valve on the pipe entering the regenerative cooling jacket will be set to allow three-fourths of the total mass flow to pass while the valve on the pipe to the engine will only allow one-fourth of the total mass flow to pass. Actuators will be required on both so that they keep this ratio exact. The valves, depending on the specific series, will have a mass between 3.5 and 10 kg. The actuators, depending on the pressure requirement, will have a mass of 45 to 90 kg. The valves and actuators will be stainless steel, and the valves will be cryogenically adapted for the LH2. The pipes will be crafted from an aluminum alloy and will have an inner diameter of 1.5 cm, a wall thickness of 0.25 cm, and a total length of around 3.5 m. The pipes will be adapted for cryogenic use (Reference 6.13).

6.5 FUEL STORAGE TANK INSULATION

The fuel tanks for the LOTV are designed with a multi-layered insulation (MLI) scheme to contain the liquid hydrogen (LH_2) at the temperature required to prevent it from returning to the gaseous state (20 K). Double aluminized Mylar (DAM) will be used as the insulating material (see Figure 6.6) due to the extremely low thermal conductivity of Mylar (8.903E-06 W/cm-$^{\circ}$C) at vaccuum pressure. This DAM will consist of 2 sheets of 0.25 mil (6.36E-06 m) aluminum on either side of a 0.25 mil sheet of Mylar. Between the sheets of DAM there will be a silk net spacer to allow radiation heat transfer between layers. This spacer will be vented to outer space to prevent convection heat transfer.

There will be 21 layers of DAM in each wall of the tanks. This number was obtained by assuming 10,500 kg of fuel in each tank,

and allowing 1% total boiloff. This corresponds to a boiloff flow rate of 8 kg/day (assuming a 12 day trip) or 1.87E-04 kg/s. Using the heat of vaporization of LH_2 (499,500 J/kg) this results in a maximum allowable heat flux of 46.7 W:

$$q_{all} = m * \text{ŠHv} = 46.7 \text{ W}$$

Given the density of LH_2, the required volume of the tanks to hold the 10,500 kg of fuel is 123.323 m^3. The tanks will be 10.46 m long with spherical end caps of radius 2.08 m. This gives a projected area of each tank of 39.8 m^2. The heat flux incident on the tank due to solar radiation is 1924.24 W:

$$q = \text{Á} * q'' * A = 1924.24 \text{ W}$$

where

        Á = emissivity of aluminum (0.035)
        q'' = solar radiation constant (1395 W/m^2)
        A = projected area of tank (39.8 m^2).

Radiation shield theory was used to determine the number of layers of DAM required to reduce the heat transfer flux to 46.7 W:

$$q_{all} = 1/(n+1) * q$$

where

        n = the number of shields.

This equation yields 42 shields to reduce the heat flux. Because each sheet of DAM has two layers of aluminum, only 21 layers of DAM are required.

The layup density for 21 sheets of DAM is 0.7176 kg/m^2. This is given by:

$$D_{LU} = D_M * t_M + D_{Al} * t_{Al}$$

where

        D_M = density of Mylar (27 kg/m^3);
        t_M = thickness of Mylar;
        D_{Al} = density of aluminum (2707 kg/m^3);
        t_{Al} = thickness of aluminum;
        D_{LU} = layup density

6.6 GIMBALLING OF THE ENGINE NOZZLE

There are two factors which have an adverse effect on the stability of the ship. One is that the optical truss system rotates. The other is that the center of mass of the ship moves significantly.

The optical truss structure has a large moment of inertia. As
the motor that drives the truss structure tries to turn it, the
main ship will also be turned in the opposite direction. To
solve this problem the two "momentum wheels" will be placed in
the turntalbe itself, as discussed in section 4.5.

However, the large mass of the optical system also adds to the
second problem of the stability of the ship: that the center of
mass moves. If the line of thrust of the main engine does not go
through the center of mass of the ship, then a moment will be
created that will tend to turn the ship. Since alignment is so
important to the ship this, is a bad effect.

One possibility to counter this effect is to gimbal the nozzle of
the main engine (see figure 6.2). This way the line of thrust
can be lined up to pass through the center of mass. The nozzle
will have to gimbal about 8° off center of the main axis in all
directions to line up with the center of mass. Due to the very
high temperatures of the engine this gimballing of the nozzle may
be very difficult. It requires some advancement in high
temperature materials.

6.7 CONCLUSIONS

There are many advances that need to be made before a laser
system is technically feasible. Probably the most difficult
problem to solve is the choice of lens material due to the high
power density of the laser. Other difficulties include detailed
thermal analyses of the lenses, selection of chamber materials,
plasma stability, and chamber flow characteristics.

Note that if the laser wavelength were increased, then the
temperature corresponding to the maximum absorptivity of hydrogen
decreases. This would help to alleviate the problem of cooling
the thrust chamber. The disadvantage of increasing the laser
wavelength is that the laser beam increases more as it travels to
the LOTV, and a larger mirror would be needed to receive the
required 32 MW of power from the laser. This, of course, would
increase the mass of the ship significantly, as well. Thus, a
compromise between the two must be met before a larger wavelength
laser can be used.

6.8 REFERENCES

1. Boeing; <u>Advanced Propulsion Concept Study</u>; APCS-094.

2. <u>Catalog of U. S. Valves</u>; Valve Manufacturers Association of America; Washington, D. C.; 1986.

3. Chandra, Suresh; <u>Photoelectrochemical Solar Cells</u>; Vol. 5; Gordon and Breach Science Publishers; New York; 1985.

4. Deutsch, Thomas F.; "Laser Window Materials -- An Overview;" <u>Journal of Electronic Materials</u>; Vol. 4; No. 4; 1975.

5. Fox, Robert W. and McDonald, Ala T.; <u>Introduction to Fluid Mechanics</u>; John Wiley & Sons; New York; 1978.

6. Keady, J. P.; "Production of Aphrons Through the Breakup of a Coumpound Jet;" AIAA Student Paper, Midatlantic AIAA Conference; April 22, 1988.

7. Keefer, Dennis R.; University of Tennessee Space Institute; phone conversations.

8. Keefer, Dennis R., Elkins, Rush, and Peters, Carroll; <u>Laser Thermal Propulsion</u>; The University of Tennessee Space Institute (working copy).

9. Klosterman, E. L. and Byron, S. R.; "Measurements of Subsonic Laser Absorption Wave Propagation Characteristics;" <u>Journal of Applied Physics</u>; Vol. 45; p. 4751; 1974.

10. Sebba, Felix; <u>Foams and Biliquid Foams-Polyaphrons</u>; John Wiley and Sons; U. K.; 1987, 1st ed.

11. Stewart, John W.; <u>How to Make Your Own Solar Electricity</u>; Tab Books; Blue Ridge Summit, PA; 1979.

12. Warring, R.H.; <u>Pumps: Selection, Systems and Applications</u>; Gulf Publishing Company; Houston, TX; 1984.

13. Warring, R.H.; <u>Handbook of Valves, Piping and Pipelines</u>; Gulf Publishing Company; Houston, TX; 1982.

7. DYNAMICS CONTROL

The LOTV has a special need for dynamics control. The ability to keep the main mirror fixed on the incoming laser beam is essential, and this requires the ability to precisely and accurately control the attitude of the LOTV. The attitude of the LOTV is actively and continuously controlled by the Attitude and Pointing Control System (APCS), which assures that the vehicle, most importantly the main mirror, is pointed in the desired direction for reception of the laser beam. Futhermore, the APCS is utilized in docking manuevers with space stations. The APCS consists of the following operational control systems:

1. Control Moment Gyros

2. Reaction Control System.

The Control Moment Gyro (CMG) System represents the prime method for attitude control of the LOTV. While the CMG has only the ability to rotate the ship, the RCS has the ability to rotate and translate it.

7.1 CONTROL MOMENT GYROS

The CMG system consists of three large double gimbaled gyroscopes with mutually perpendicular axes (see Fig. 7.1). Table 7.1 lists the specifications for these CMGs. The double gimbaling assures 100% redundancy. Each of the three CMGs has an inner and an outer gimbal ring. The outer gimbal ring allows the LOTV to rotate around the gimbal axis of each CMG. In addition, an electric torque motor attached to the LOTV acts upon the outer gimbal ring to produce a torque between the LOTV and the CMG, which results in a tilting motion, referred to as precession, of the CMG rotor axis around the inner gimbal ring axis. This result is the characteristic property of a spinning gyroscope to respond to torques around one axis along with a tilting motion (precession) around the other axis. Correspondingly, the reactive force of the torque motor then causes the LOTV to change its angular position while the rotor axis moves or precesses. The overall operation of the torque motor is controlled by commands received from the LOTV digital control computer.

The driving factor in the design of the CMG system is the output torque. This torque must be large enough to perform the necessary maneuvers. The output torque determines the size and power consumption of the CMG. The magnitude of the torque is determined by two factors:

1. Controlling the roll rate of the ship

2. Counteracting the slew rate of the optical truss system.

Table 7.1 CMG Specifications

Output torque	2250 N-m
Angular momentum	1290 N-m-sec
Speed	4,500 RPM
Weight	100 kg
Size	
Length	1.22 m
Width	1.17 m
Height	0.56 m
Gimbal rotation	unlimited
Total power	
Standby	16 watts
Quiescent	70 watts
Torquing (peak)	750 watts

FIGURE 7.1   CONTROL MOMENT GYRO SYSTEM (REF. 7.1)
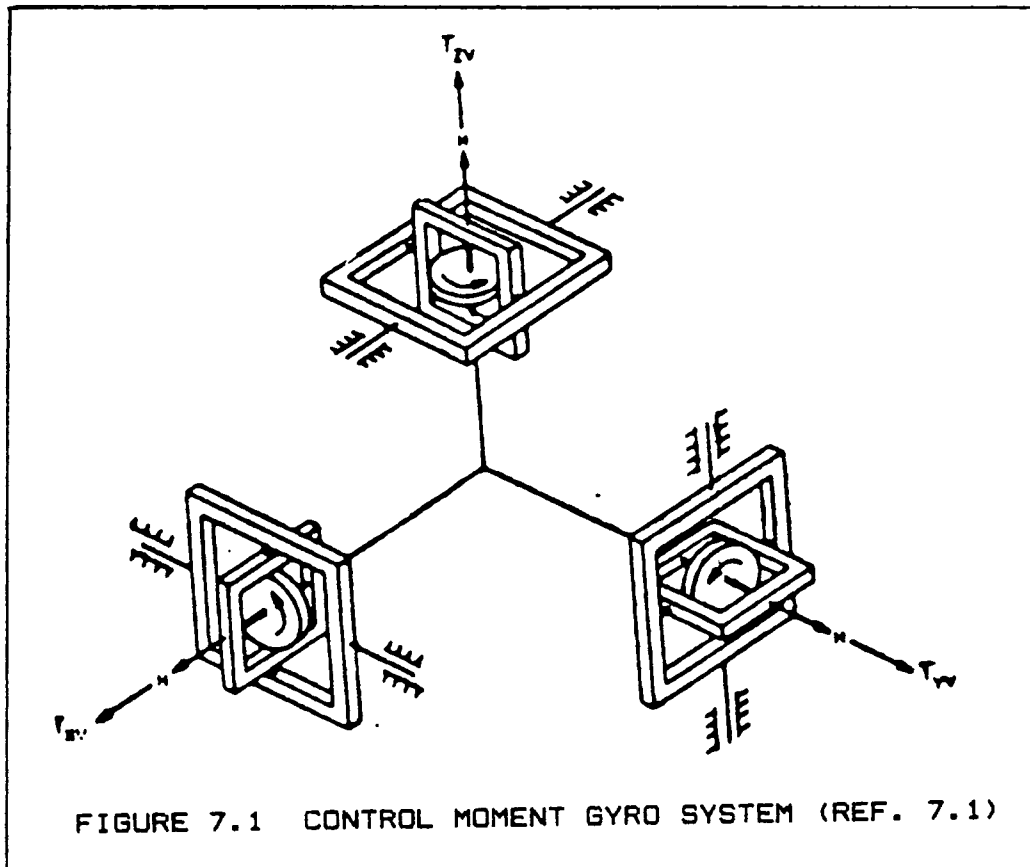
These are the main functions that the CMGs must perform. The computer code that was written by the orbital mechanics group was used to determine the roll and slew rates. This data was examined to determine the largest change in angular rate over the smallest amount of time. This gave the following angular accelerations (the corresponding moments of inertia are also listed):

$$\text{slew rate acceleration} = .1415 \times 10^{-1} \text{ rad/sec}^2$$
$$I_x = 282,896 \text{ kg-m}^2$$

$$\text{roll rate acceleration} = .6612 \times 10^{-5} \text{ rad/sec}^2$$
$$I_y = 1,992,147 \text{ kg-m}^2$$

By multiplying the angular acceleration times the moment of inertia, the moment needed to accelerate the moment of inertia to the required angular velocity was calculated.

During an attitude control procedure, the rotor axis of each CMG will slowly tilt. If the control torque persists long enough, each CMG will continue the tilting motions until the rotor axis of each CMG becomes parallel with the axis of the control torque. As a result, none of the CMGs would then be able to react to the control torque by further precession. Most importantly, if all three CMG rotor axes should be parallel with their torque axes, the CMG system is said to be "saturated", which means that the CMGs would be incapable of controlling the attitude of the LOTV. In order to prevent saturation of the CMG system, the CMGs will have to be occasionally desaturized, which will be performed by the Reaction Control System. This desaturization process will be performed after each burn of the main engine. The CMGs can not be desaturized during a burn of the main engine because the process would interfere with the reception of the laser beam. If the CMS were not desaturized after each burn then it is possible that during a burn they would saturate. The desaturization process will be controlled by the LOTV digital control computer.

7.2 REACTION CONTROL SYSTEM

The CMG system was chosen to assist in attitude control, roll, pitch and yaw. Steady attitude adjustments are needed to keep the primary mirror aligned with the laser throughout the mission. As stated earlier in order to desaturize the LOTV and for translational maneuvers, such as docking, a Reaction Control System (RCS) is needed.

The RCS is composed of two parts. The primary part consists of four clusters of five primary RCS engines each (P-RCS). Each P-RCS engine delivers 500 N thrust. The secondary part of the RCS system consists of 14 vernier or low thrust magnetoplasma thrust units. Each secondary unit delivers 5 N thrust. The secondary units provide low acceleration maneuvers such as docking. The P-RCS provide the necessary thrust for orbit change, when needed, as well as desaturization.

7.2.1 RCS-SECONDARY SYSTEM

The secondary RCS system consists of a low thrust magnetoplasma system. There has been much experience in the use of similar systems for attitude control of satellites. A simple pulsed system is shown in Figure 7.2. The system consists of a rail accelerator which accelerates a current carrying plasma through a conical nozzle. When the capacitor is discharged, an arc is struck at the left side of the rails. The high current plasma arc induces a magnetic field. The action of the current and magnetic field causes the plasma to be accelerated at right angles to both the current and magnetic field, namely in the direction along the nozzle. With each pulse of thrust, a small amount of the solid propellant (Teflon) is vaporized and converted to a plasma cloud. The actual characteristics of the secondary units are given in table 7.2. Each unit is radiatively cooled.
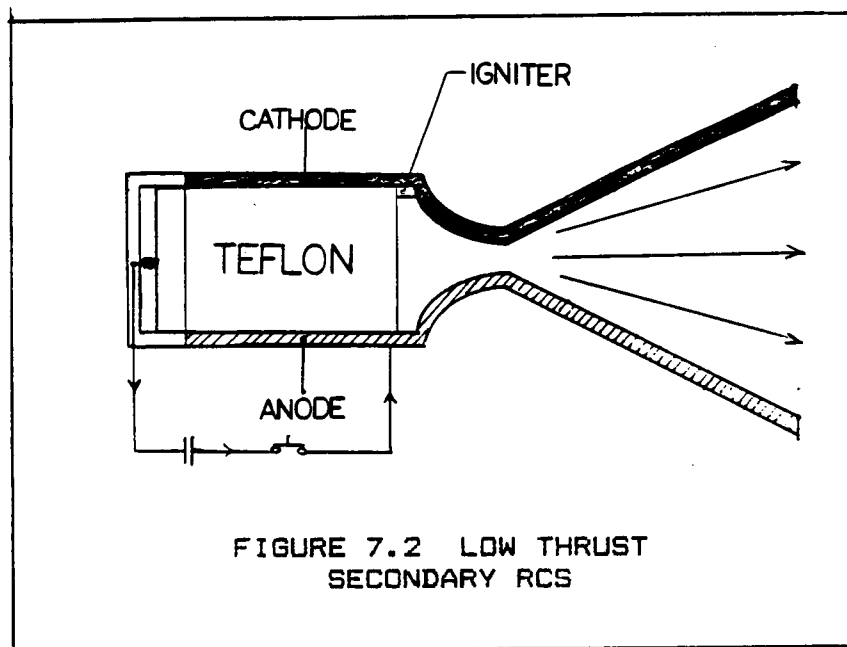
FIGURE 7.2   LOW THRUST
SECONDARY RCS

Table 7.2 Secondary RCS

Thrust	5 Newtons
Type	Pulsed
Fuel	Teflon
Specific Power (kw/kg sec)	1x10^-3
Pulse Time	.08-.32 seconds
Life Time (# pulses)	10,000
Approx. Specific Imp.	3000 sec

7.2.2 RCS-PRIMARY SYSTEM

The P-RCS consists of four modules containing five thrust units each (see figures 7.3). The P-RCS utilizes Liquid Hydrogen from the main LOTV fuel tanks. Since the P-RCS is a bi-propellant system it needs an oxidizer. Since, in future scenarios, liquid oxygen can be obtained from the Lunar base, it was decided to utilize Oxygen as the oxidizer. The Oxygen tank for the P-RCS is contained within the main truss system.

Since the P-RCS operates for longer increments of time than the secondary system and is also radiatively cooled, a design chamber temperature must be chosen. The maximum chamber temperature is dependent upon maximum operation time and material properties. A major contribution to the chamber temperature is the type of propellants and their respective mass ratios in the mixture. The equivalence ratio (ER) is the fuel to oxidizer ratio of the mixture divided by the stoichiometric ratio (EQN #1).

$$\text{EQN \#1} \qquad ER=(\text{Mass Fuel/Mass Oxidizer})Have/(Mf/Mox)stoic.$$

Three factors were chosen as design criteria. First it was decided that in case of emergencies the summation of the P-RCS thrust should equal the thrust of the main engine, 2000 N. Therefore each unit was designed to deliver 500 N. This enables redundancy and enables maneuvers even when the LOTV is out of sight of the laser. Since the thrusters are radiatively cooled to decrease complexity and added mass, a design chamber temperature of 2000 K was chosen. Although a transient heat analysis was not performed upon the P-RCS it was assumed that a steady state maximum operation time of 60 seconds would be possible if needed.

Utilizing Figure 7.3 it can be seen that an ER ratio of 4.4 or higher is necessary to maintain the limit on the chamber temperature. An ER ratio of 4.4 was chosen. For this case thermochemical analyses were computed utilizing the NOTS computer program. These analyses can be seen in tables 7.3 and 7.4. Table 7.3 lists the theoretical properties in the chamber of the P-RCS. Table 7.4 lists the theoretical properties at an area ratio of 80. An area ratio of 80 was chosen because, as can be seen in figure 7.4, the performance characteristics vary little beyond this area ratio. Table 7.3 lists the characteristics of the P-RCS system.

As stated earlier the P-RCS consists of four modules of five engines each. As shown in figure 7.3, a single thrust chamber has five injection ports. A central oxidizer port and four fuel injection ports. These ports are fed by a circular oxidizer feed pipe as shown. Also shown is the fuel feed pipe consisting of five circular pipes with four injector port feeds on each circular section. Various cut off valves not shown in the figure provide redundancy and channeling of the flows to specific thrust chambers. The P-RCS, being a chemical engine, produces exhaust plumes that could damage the truss structure. In order to
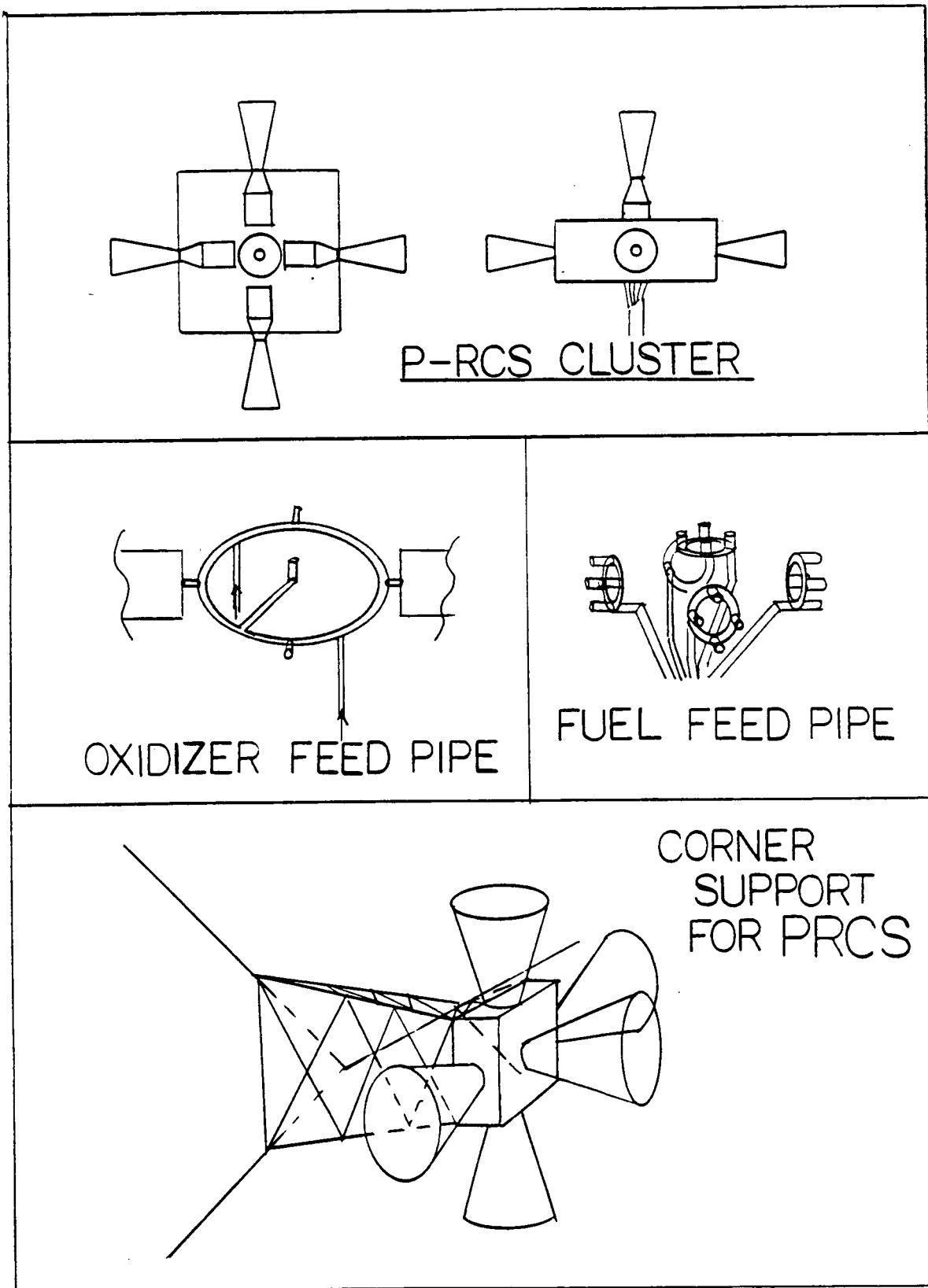
P-RCS CLUSTER

OXIDIZER FEED PIPE
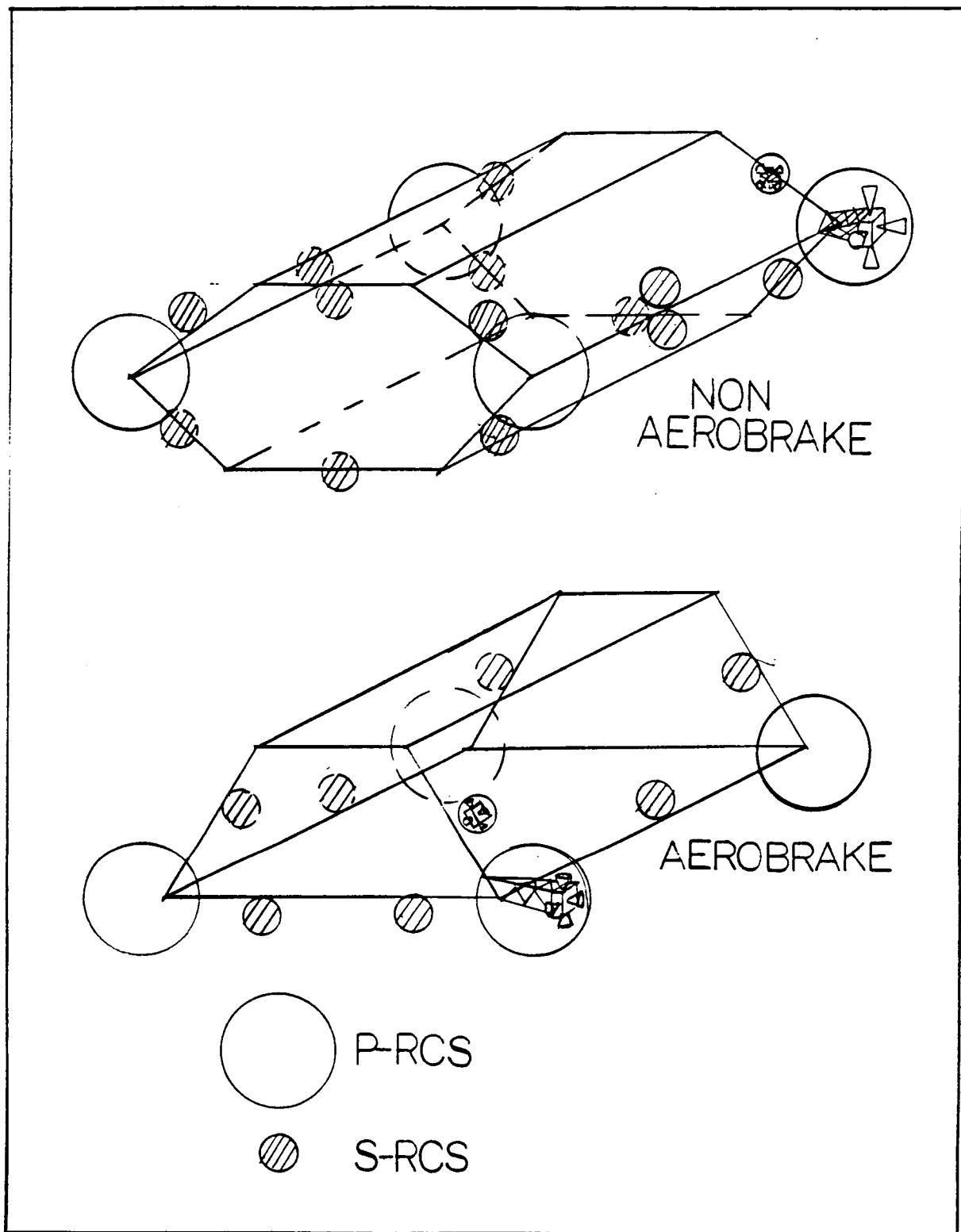
FUEL FEED PIPE

CORNER SUPPORT FOR PRCS

FIGURE 7.3   REACTION CONTROL SYSTEM

FIGURE 7.4   LOCATION OF RCS ON MAIN HULL

Table 7.3 P-RCS System Characteristics

Thrust	500 N
Mass flow (kg/sec)	.136
Exhaust velocity	4300 m/sec (4563 theoretical)
Mass ox. / Mass fuel	1.8038
Specific Impulse	375 sec (475 theoretical)
Cstar	206637.8 m/sec
Chamber Temperature	2000 K
Chamber Pressure	1034 kPa (150 psia)
A/A*	80
A*	3.08 cm^2
Ae	246.40 cm^2
Nozzle cone half angle	30 degrees
Nozzle length	15.34 cm
Molecular mass mixture	5.654 kg/kg-mole

decrease this problem and to increase the size of the effective moment the P-RCS can provide, a support truss structure for the module was studied (Figure 7.3). The support truss can vary in length depending upon mission needs and is connected at the mid angles of the main truss system. ·

There are two schemes to the LOTV concept. An aerobraked scheme and a non-aerobraked scheme. On the aerobraked scheme there are four P-RCS and eight secondary systems. On the non-aerobraked scheme since it might be necessary to make more maneuvers there are fourteen secondary systems and four P-RCS. The locations of these systems with respect to the main truss structure can be seen in figure 7.4.

In order to analyze fuel consumption of the P-RCS system three mission scenarios were considered. Since the modules are made up of five thrust units the variation between mission scenarios is the variation of the number of the five engines that are firing per orbit. A total of twenty one spirals is predicted for a round trip by Orbital Mechanics calculations. For mission 1 it is assumed that only one of the five engines per module fire at any one time during the orbit. Mission 2 assumes two fire and mission 3 assumes 3 fire. The first consideration is course correction during the orbit. It is assumed that during an entire orbit an engine needs only to fire for two seconds. For docking maneuvers that require thrust from the P-RCS it is assumed that each engine needs to fire a total of four seconds. For orbit changing maneuvers each engine needs to fire for four seconds. The summation of the total operation times and fuel consumption can be seen in table 7.4.

Table 7.4 Mission Scenarios

	MS1	MS2	MS3
Total burn time (sec) for course correction and desaturization.	216	432	648
Docking maneuver total burn time (sec)	20	40	60
Total burn time for orbit changing maneuvers	16	32	48
Total Burn Time (seconds)	252	504	756
Total mass of Oxidizer (kg)	22.848	45.696	68.544
Total mass of Fuel (kg)	11.424	22.848	34.272

7.3 REFERENCES

1. B. J. O'Connor and L. A. Morime, "A Description of the CMG and Its Application to Space Vehicles," AIAA Paper No. 67-589, AIAA Guidance, Control, abd Flight Dynamics Conference, Huntsville, Alabama, August 14-16, 1967.

2. "Control Moent Gyros," Sperry Flight Systems, May 1982.

3. Leland F. Bellew and Ernst Stuhlinger, Skylab, A Guidebook (U. S. Government Printing Office, 1973).

8. AEROBRAKE

Aerobraking is incorporated in both scenarios investigated for LOTV missions, the LEO/GEO and the LEO/LLO missions. The aerobrake provides the needed delta-V for return to LEO in both missions.

An inflatable ballute type aerobrake was chosen for use in both scenarios (see figure 8.1). This type of aerobrake was chosen instead of a rigid type aerobrake for many reasons. First, an inflatable ballute is considerably lighter than a rigid one. Second, the uniqueness of the LOTV required an aerobrake that could be stored out of the way of the RCS and the deployed mirror system. The ballute is jettisoned out of the way of the optical system and RCS after aerobraking. Because the ballute is jettisoned and designed to be easily replaced, it eliminates the upkeep that is required for a rigid aerobrake. The fact that the ballute can be stored away allows the LOTV to be much smaller than it would be if a rigid aerobrake was used. A final reason for the choice of the ballute over the rigid brake is that it allows for better LOTV control during aerobraking (ref. 8.1).

The unusual shape and requirements of the ship made the design of the aerobrake very difficult. The configuration used was determined by the fact that the aerobrake had to be kept out of the way of the mirror system and also had to be attached to a triangular ship. The ballute sizes and shapes were determined by aerodynamic and heating considerations. The thermal protection system was designed to protect the ship from high temperatures and to minimize failure.

8.1 OVERALL CONFIGURATION

There are two configurations of the aerobrake, one for each scenario. They are similar except in size (see figures 8.2 - 8.6). There are three major components of the aerobrake: the ballute, the cap and support structure, and the storage and deployment components.

8.1.1 BALLUTE

The ballute is composed of three Nextel bags which surround the ship. The bags are carefully attached together in order to maintain continuity and eliminate the possibility of crevice heating. One disadvantage in choosing a ballute over a rigid lifting brake was that the rigid brake has better lifting characteristics; however, by using three bags, this disadvantage is minimized. Varying the pressure in the bags will change the lifting characteristics of the aerobrake during flight.

The ballute has 240 meridian straps running from the ballute attachment at the cap to the base of the structure. These straps carry tension during aerobraking to the attachments at the structure. The ballute protects itself and the ship from heating with a flexible surface insulation (FSI). As part of the FSI,
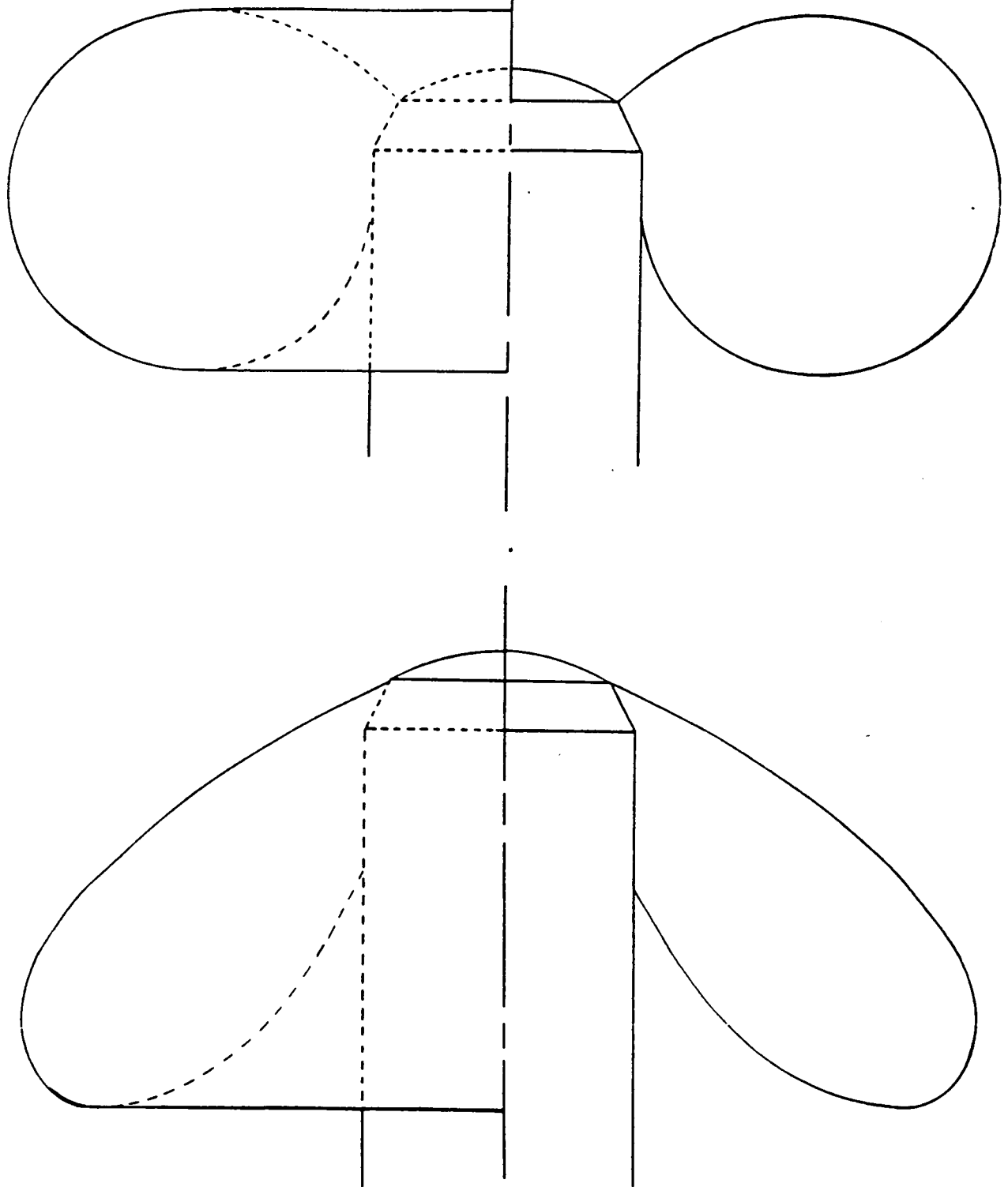
FIGURE 8.1 - INFLATED BALLUTE BEFORE AND DURING AEROBRAKING

143

Nextel was chosen for the bag because it can withstand high temperatures. Surrounding the Nextel bags is a quartz-felt (Q-felt) surface insulation. Attached to the Q-felt on the windward side is Nicalon fabric, which can withstand the high temperatures during the aerobrake pass and helps to reduce the temperatures which reach the Nextel bag. Another FSI that was considered was the Tailorable Advanced Blanket Insulation (TABI).

During the course of the design there were few changes made in the design of the ballute. The diameter of the ballute for both missions changed as changes in the center of gravity and mass of the ship were made. Final diameters of 20 meters for the LEO/GEO mission (see figures 8.2 and 8.3) and 33 meters for the LEO/LLO mission (see figures 8.4 - 8.6) were calculated.

8.1.2 CAP AND SUPPORT STRUCTURE

It was necessary to design a cap and support structure to hold the ballute in place, to carry the forces placed on the aerobrake during braking and to provide a rigid heat shield capable of withstanding the stagnation temperatures. The cap was designed to be hyperbolic in shape in order to have a smooth transition from the cap to the ballute during aerobraking. The diameter of the cap for the LEO/GEO mission is 7.13 meters (see figures 8.2 and 8.3) and the diameter of the cap for the LEO/LLO mission is 8.66 meters (see figures 8.4 - 8.6)

The structure of the aerobrake was designed to make the transition from the triangular shape of the ship to a hexagonal shape which approximates a hyperbola. Boron/aluminum, hollow, circular cylinders are used in the structure. Boron/aluminum was chosen over the original design of graphite/epoxy because of its higher strength to weight ratio. Also, since the ship structure is made of boron/aluminum, replacements and repairs are made easier. A two part structure was originally considered. The upper structure, which included the structure under the cap, was jettisoned along with the ballute after the aerobrake pass was completed. However, a structure which will jettison only a small part was chosen instead because the less structure that must be replaced each time, the more economical the brake is (ref. 8.8).

The cap structure is to be attached at the front of the ship to the connections which are used for the detachable payload. The cap structure is moved from its stored position on the base of the ship into male-female locks before aerobraking. Stored within the structure are the components necessary for inflation of the ballute. There are three spherical liquid nitrogen tanks and a system of two-way pumps and valves which send the nitrogen into the ballute for inflation.

The cap is covered with an aluminum shield which has a rigid surface insulation (RSI) of fibrous refractory composite insulation (FRCI), which protects the ship from high heating near the stagnation region. The FRCI consists of small tiles to eliminate the possiblity of failure of the entire system. The
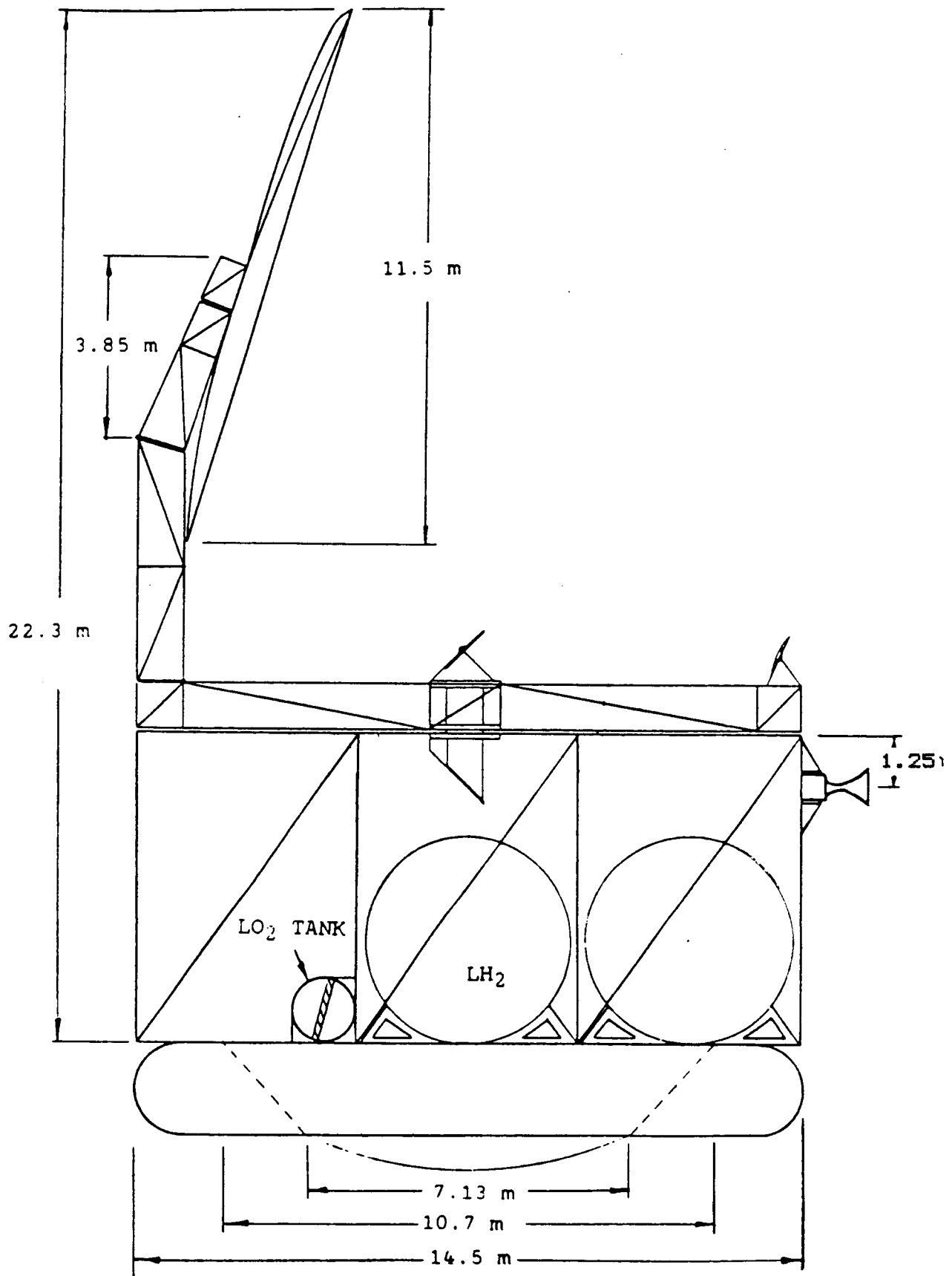
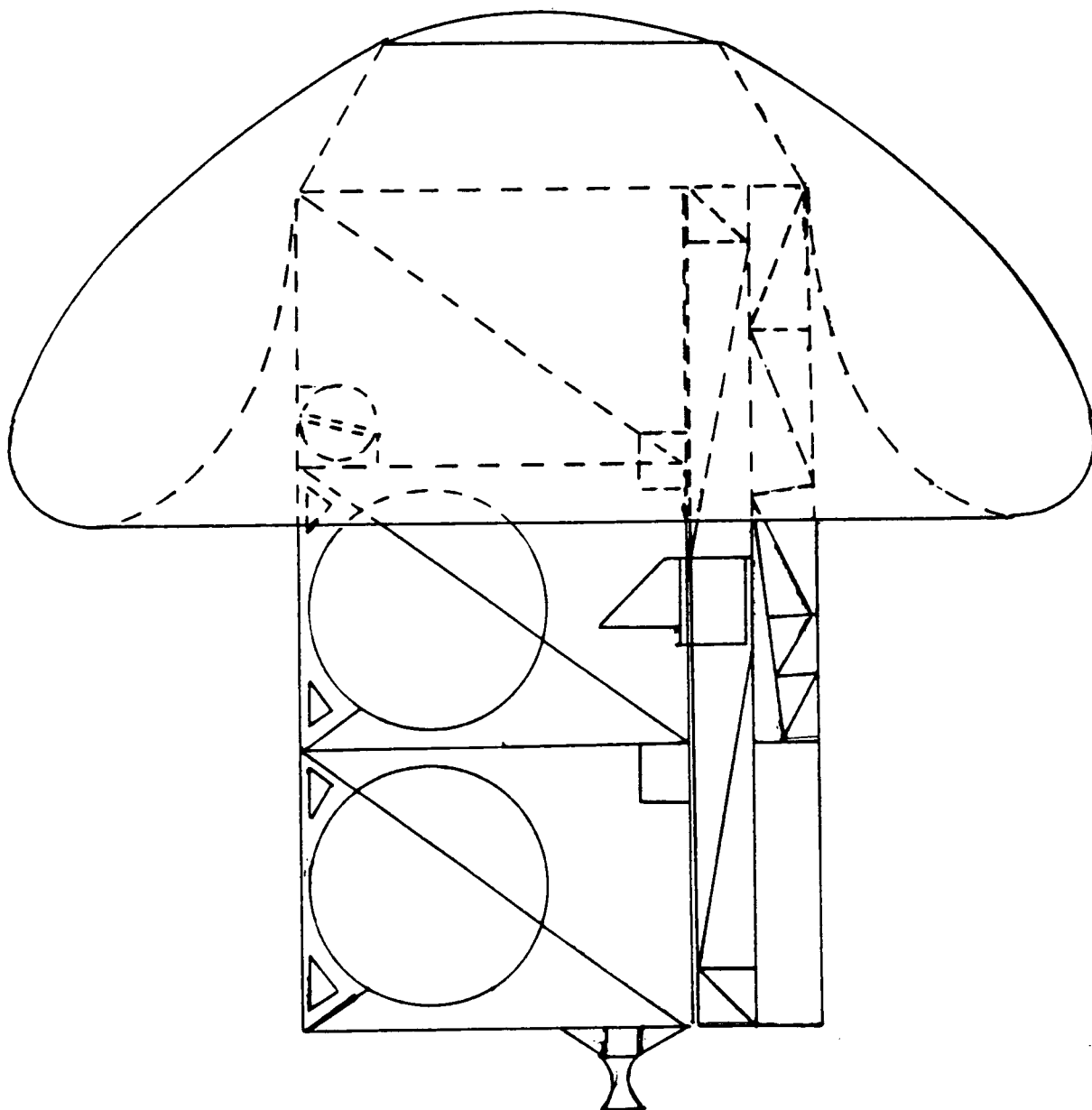FIGURE 8.2 LEO/GEO VEHICLE CONFIGURATION
WITH AEROBRAKE STORED

145

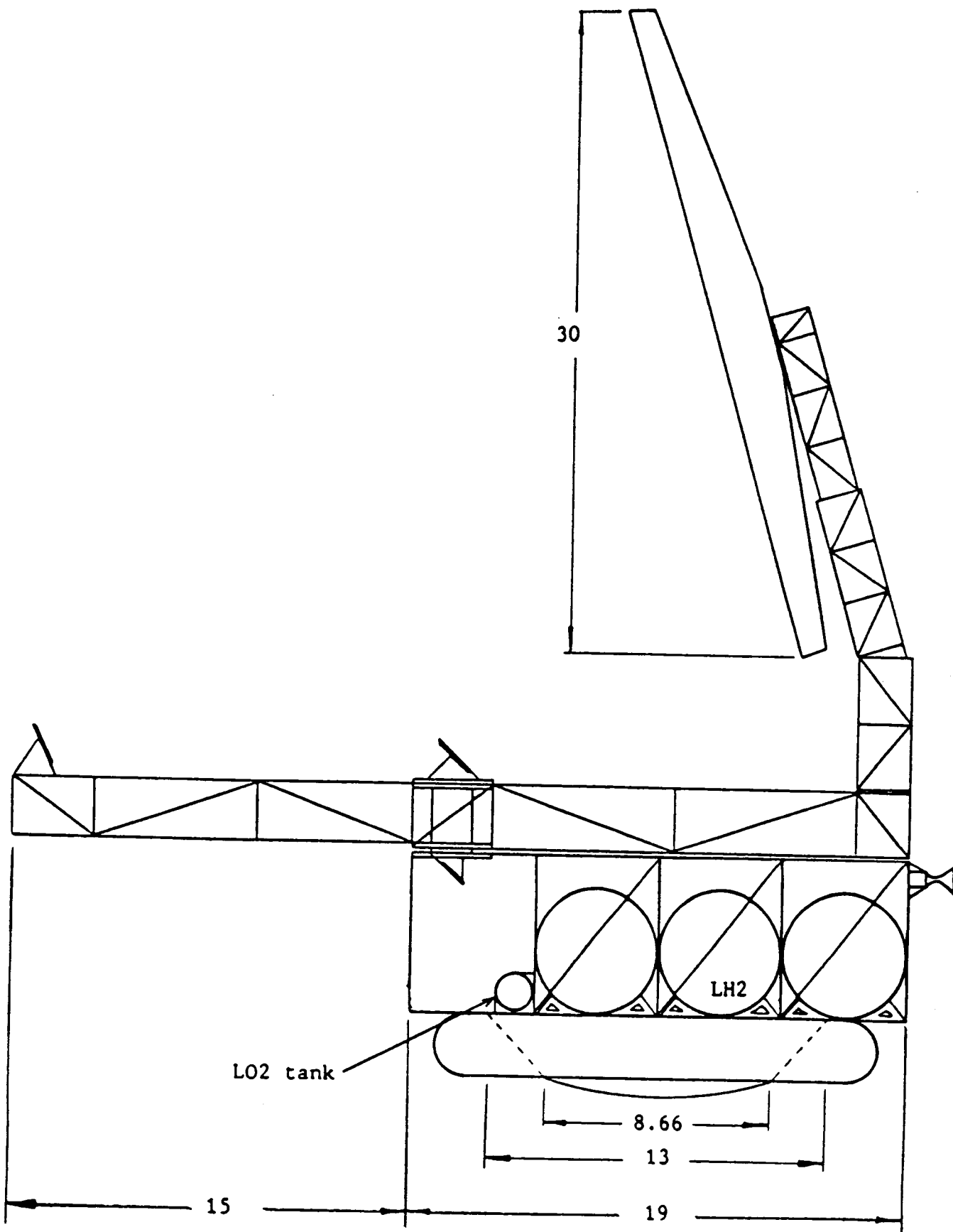FIGURE 8.3   LEO/GEO VEHICLE CONFIGURATION DURING AEROBRAKING

FIGURE 8.4   LEO/LLO VEHICLE CONFIGURATION
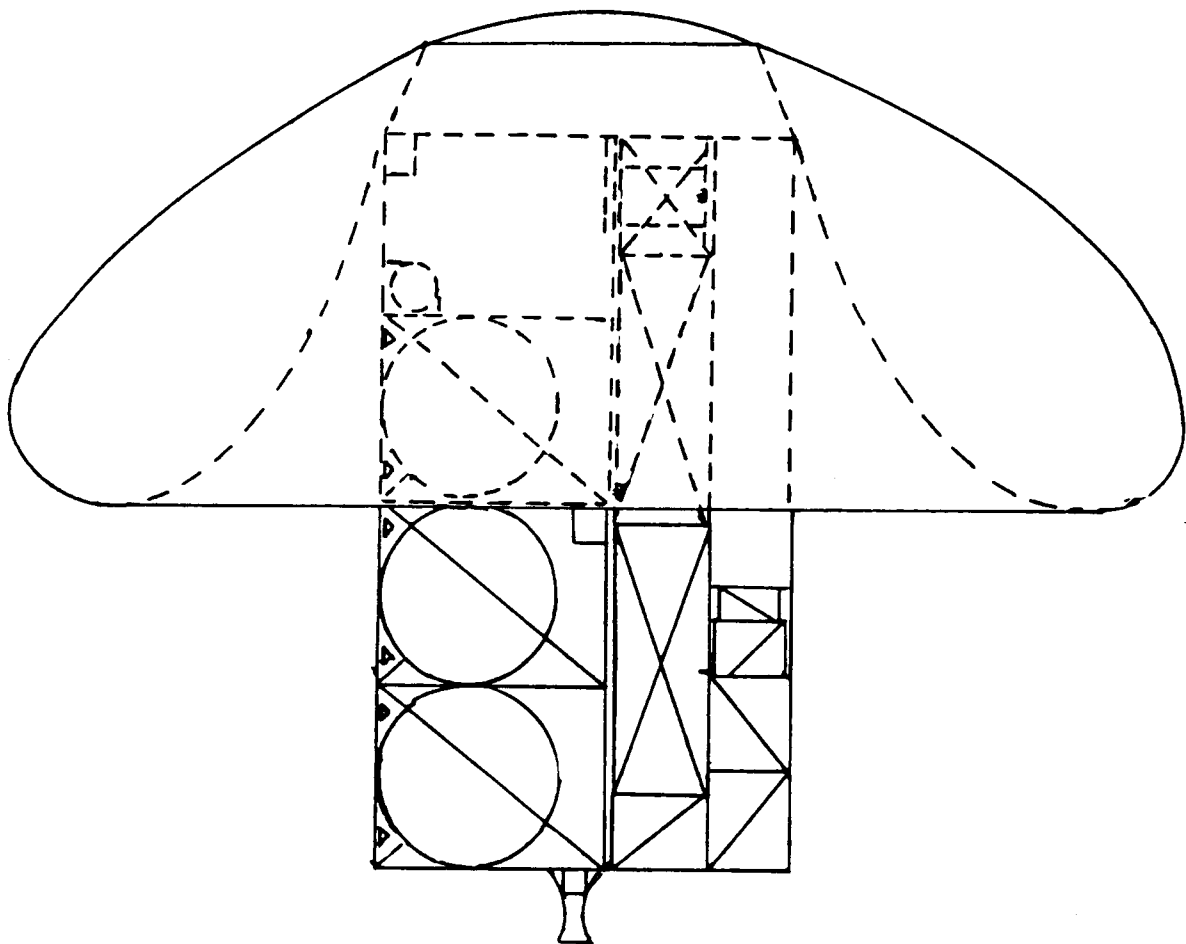WITH AEROBRAKE STORED

147

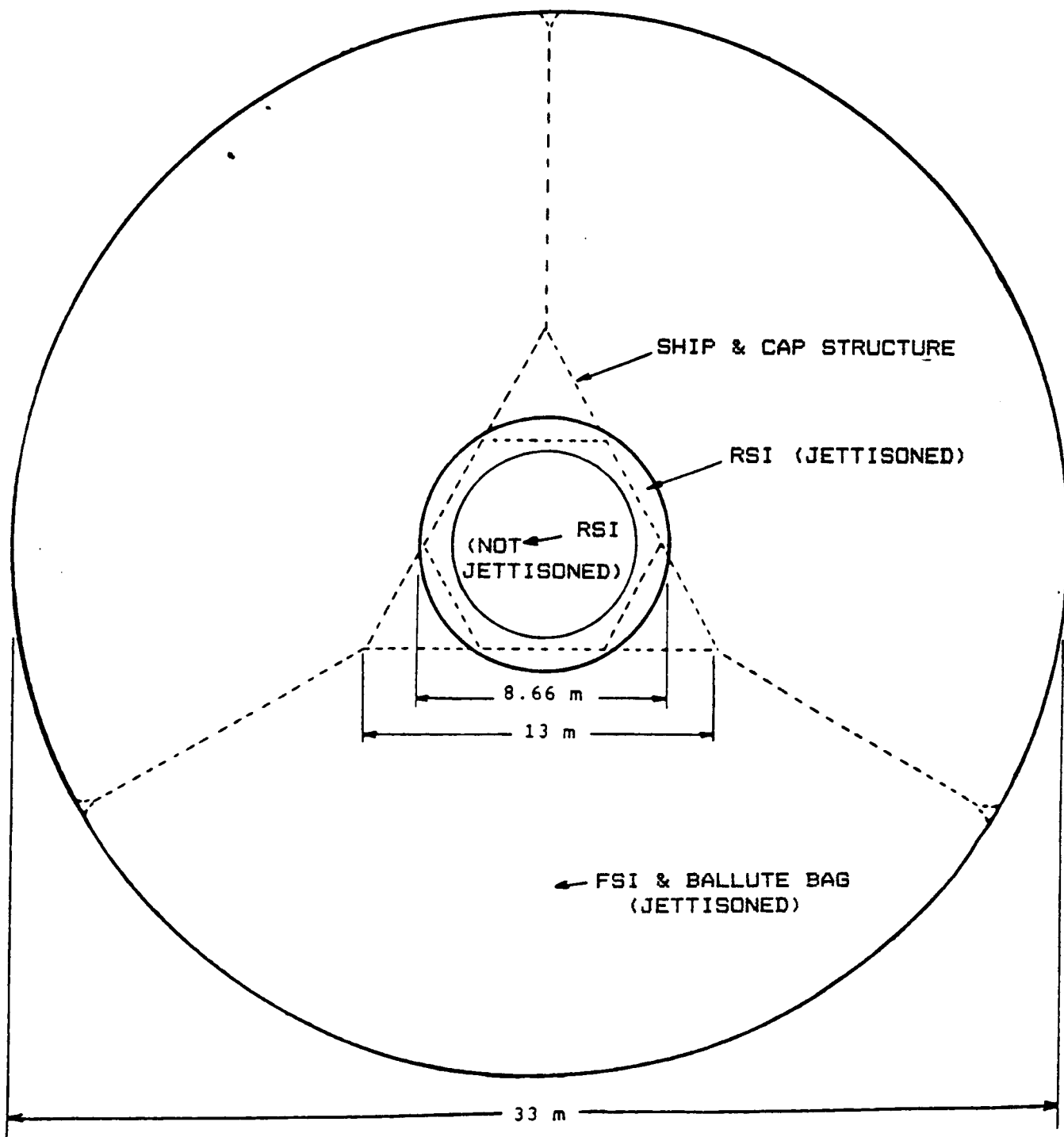FIGURE 8.5 LEO/LLO VEHICLE CONFIGURATION DURING AEROBRAKING

FIGURE 8.6   LEO/LLO INFLATED AEROBRAKE AND CAP STRUCTURE

tiles are attached to the ship with strain isolation pads which allow the tiles more movement without brittle failure. The tiles are hexagonal in order to accomodate the hyperbolic shape of the cap.

8.1.3 STORAGE AND DEPLOYMENT COMPONENTS

Due to the detachable payload and mirror system, the aerobrake, which includes the ballute, cap and cap structure, had to be stored along the base of the ship. In order to move the aerobrake to the front of the ship for reentry, a system was designed to do the transfer. Tracks are layed along the base of the ship with a guidance roller between them. The aerobrake is moved into position with a cable/pulley system and N_2 jacks. After the aerobrake is positioned the ballute bags are inflated and the ship is prepared for reentry.

8.2 AERODYNAMICS

The shape of the ballute aerobrake was modeled with an axisymetric hybrid blending of a hyperbola and an ellipse (see figure 8.7). The turn-down angle (δ) is defined as the angle between the ballute and the horizontal, measured where the ballute is attached to the rigid cap (see figure 8.7). The aerodynamic characteristics of the ballute were analyzed using three- dimensional Modified Newtonian Impact Theory. The derivation of the force and moment equations is given in appendix C. Cp_{max} was taken to be the stagnation pressure coefficient. For design purposes, the value of the stagnation pressure was found using the normal shock isentropic relations. As the air dissociates, the value of the ratio of specific heats (k) approaches 1.667. As can be seen in Table 8.1, the value of Cp_0 is not strongly influenced by k. For a free stream velocity of 10.3 km/sec, the value of Cp_0 is approximately 1.8 over the entire range of k's investigated.

The possibility of using the turn-down angle to control the lift and drag was investigated. The results are presented in figures 8.8a and 8.8b. As can be inferred from the results, the

Table 8.1 Cp_0 as a Function of k

k	Cp_0 *
1.4	1.84
1.45	1.82
1.5	1.81
1.55	1.79
1.6	1.78
1.667	1.76

* Values of Cp_0 were evaluated with a free stream velocity of 10.3 km/sec
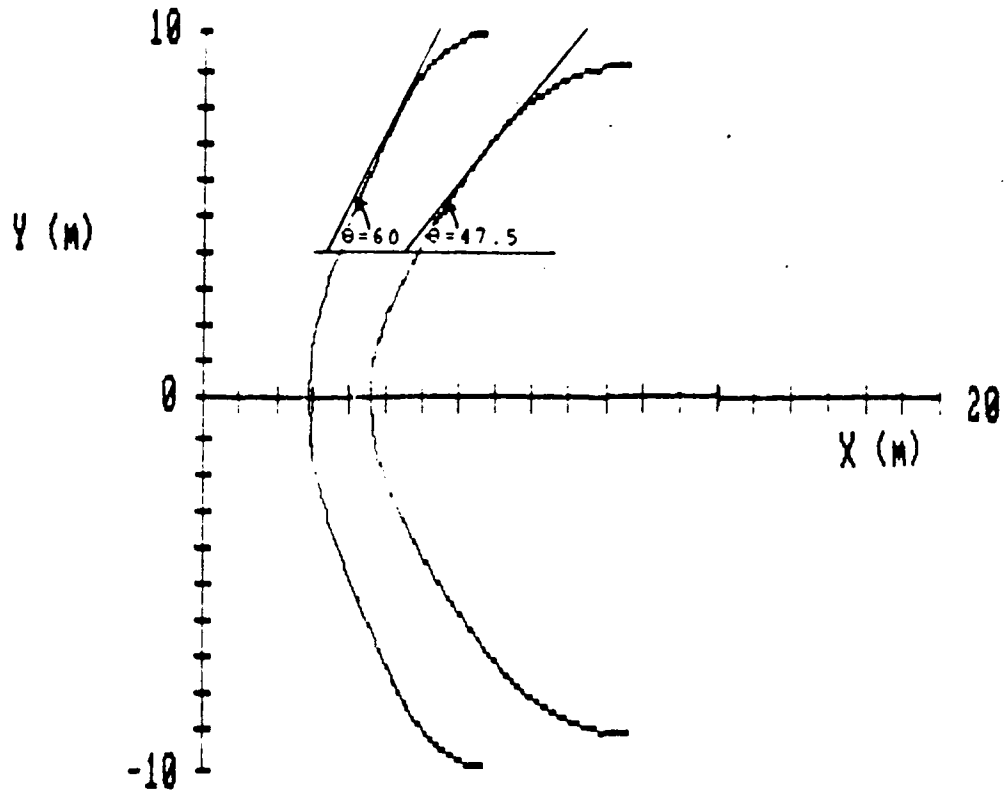
Ballute Shape (D = 20 m)

FIGURE 8.7 Cross-sectional view of the axisymetric hybrid blending of the hyperbola and ellipse used in the aerodynamic analysis. θ equal to 60° is the nominal turn-down angle, and θ equal to 47.5° is the maximum turn-down angle.

turn-down angle can be a powerful method of controlling the lift and drag. The angle of attack and sideslip effects were also investigated. The desired L/D ratio, based on preliminary trajectory considerations, is 0.15. Referring to figure 8.9a, the desired L/D ratio occurs at an angle of attack of -10°. At this angle of attack CL, CD, and CM are 0.149, 1.067, and -0.678, respectively. The sideslip results were also computed at an angle of attack of -10°. As can be seen in figure 8.10a the sideforce is of the same order of magnitude as the lift. This result, in conjunction with the ships RCS, can be used to perform plane change manuevers during aerobraking. As the sideslip angle increases, the magnitude of the sideforce can be on the order of ten times the lift. The positive slope of the yaw moment verses sideslip angle, as can be seen in figure 8.10b, is an important result for stability considerations.
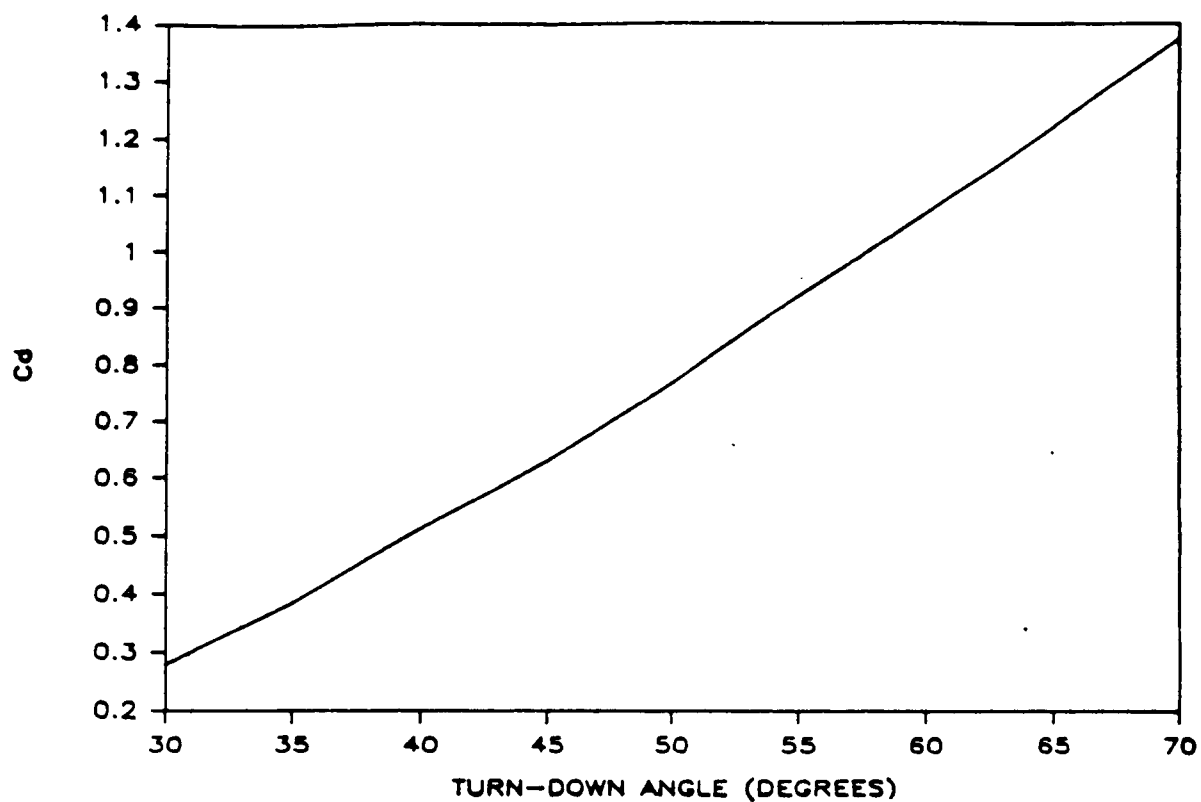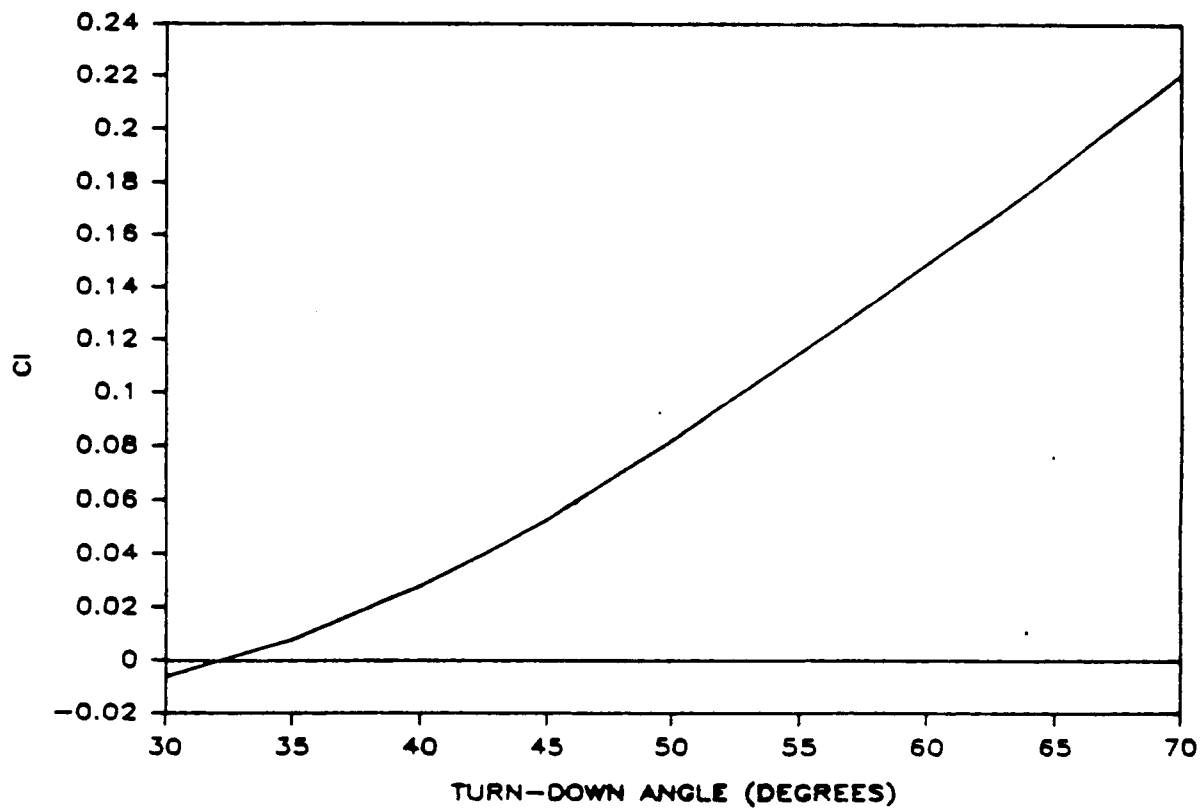
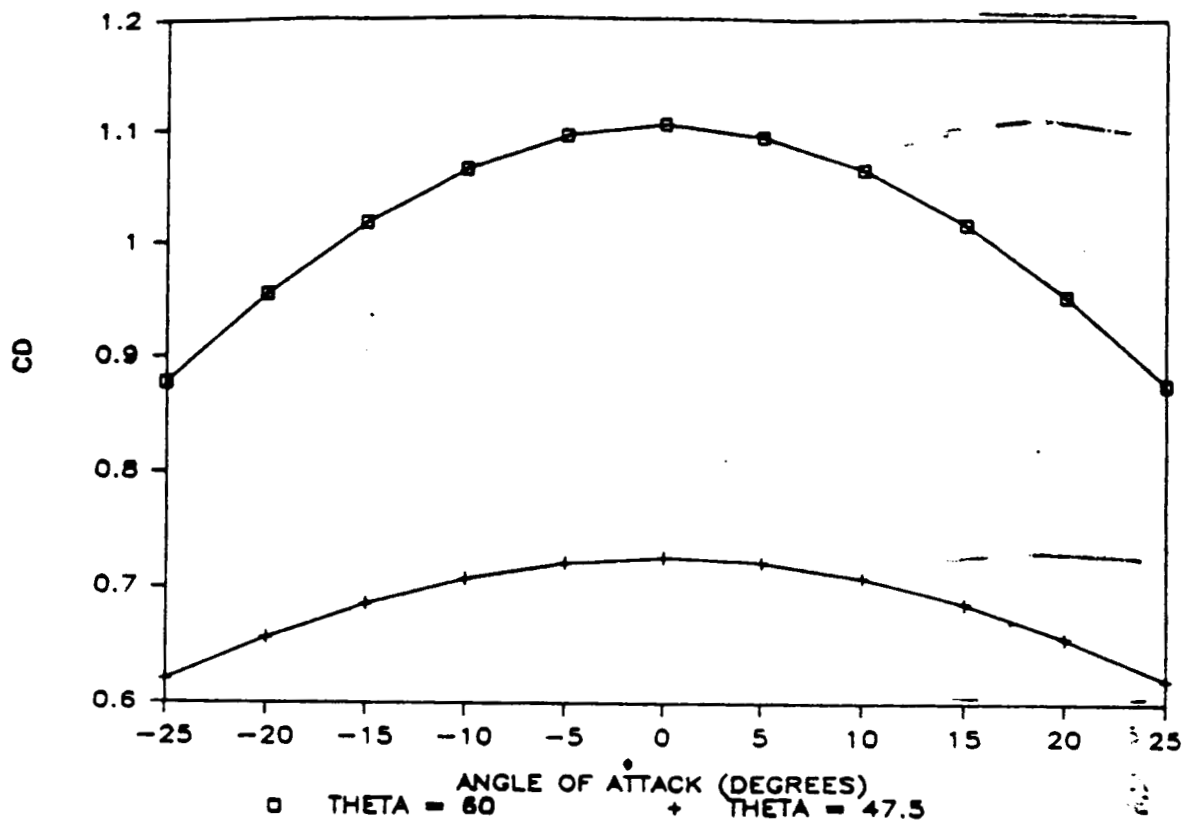FIGURE 8.8a - Cd vs. TURN DOWN ANGLE

FIGURE 8.8b - Cl vs. TURN DOWN ANGLE

152

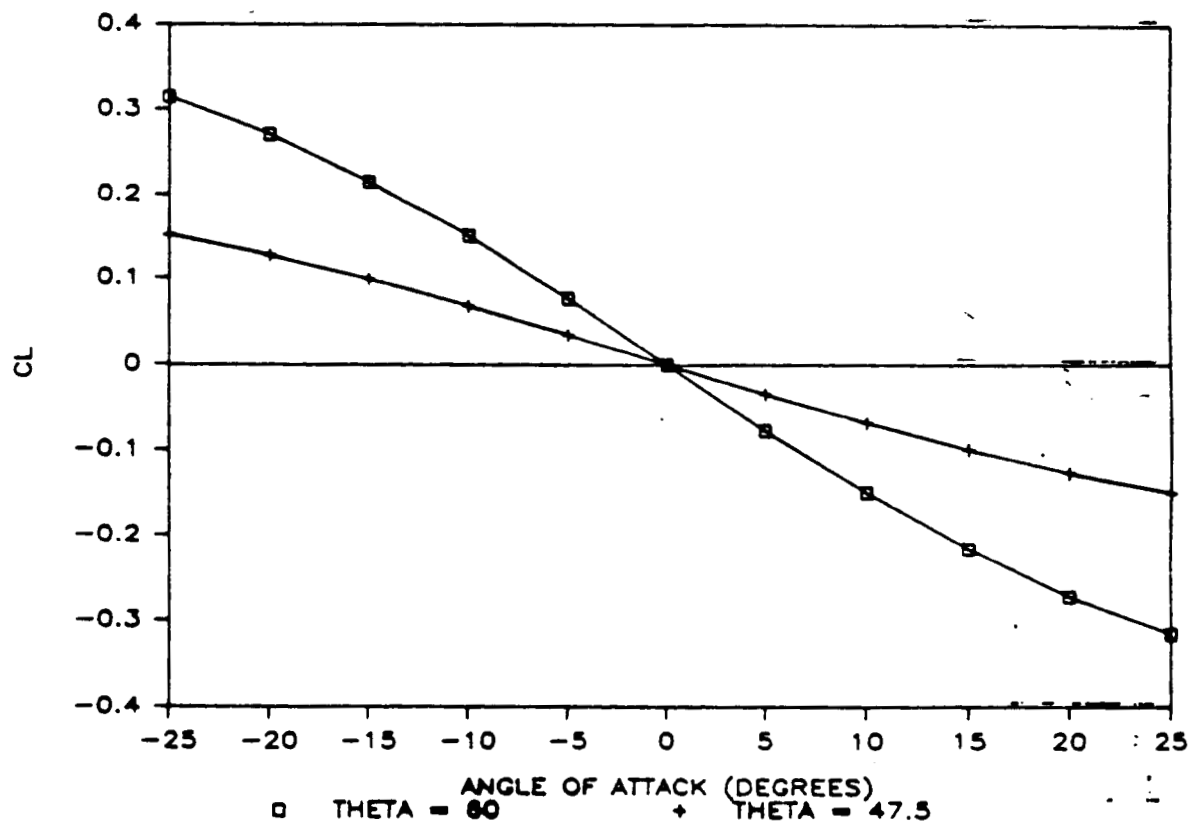FIGURE 8.8c - Cd vs. ANGLE OF ATTACK

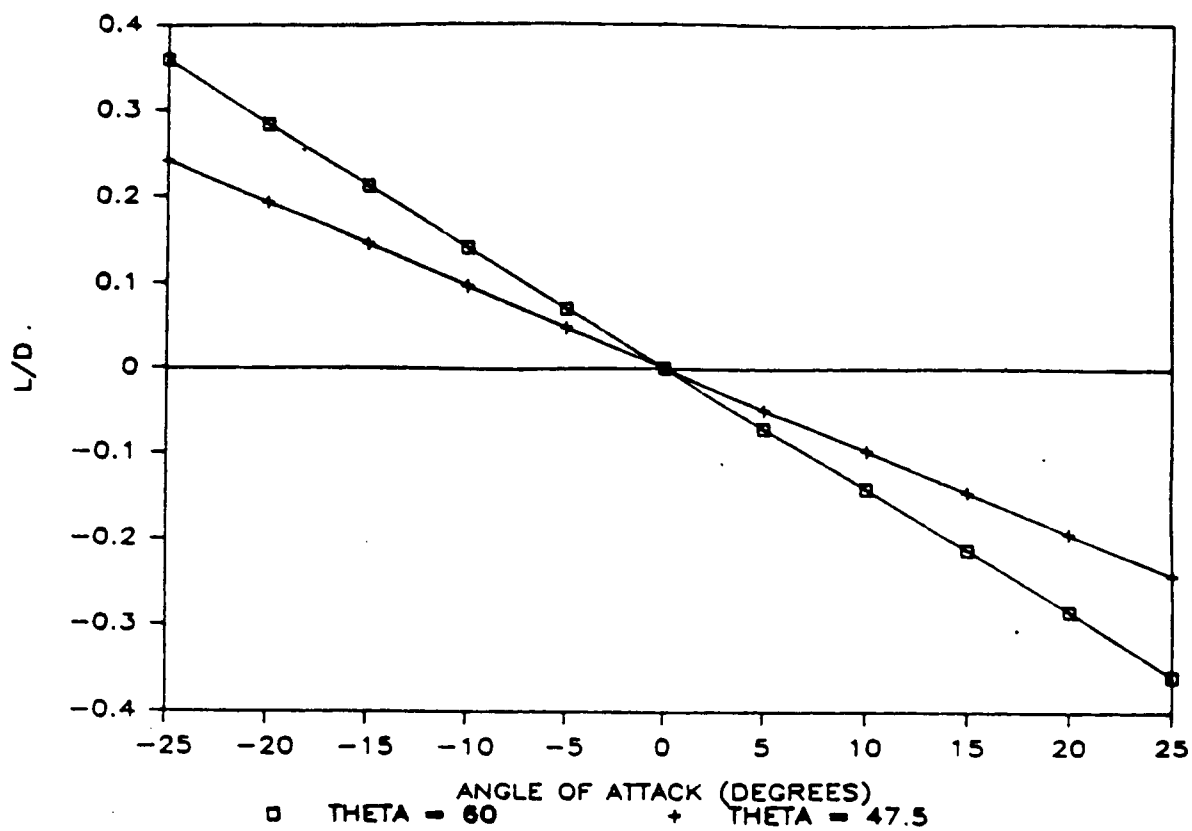FIGURE 8.8d - Cl vs. ANGLE OF ATTACK
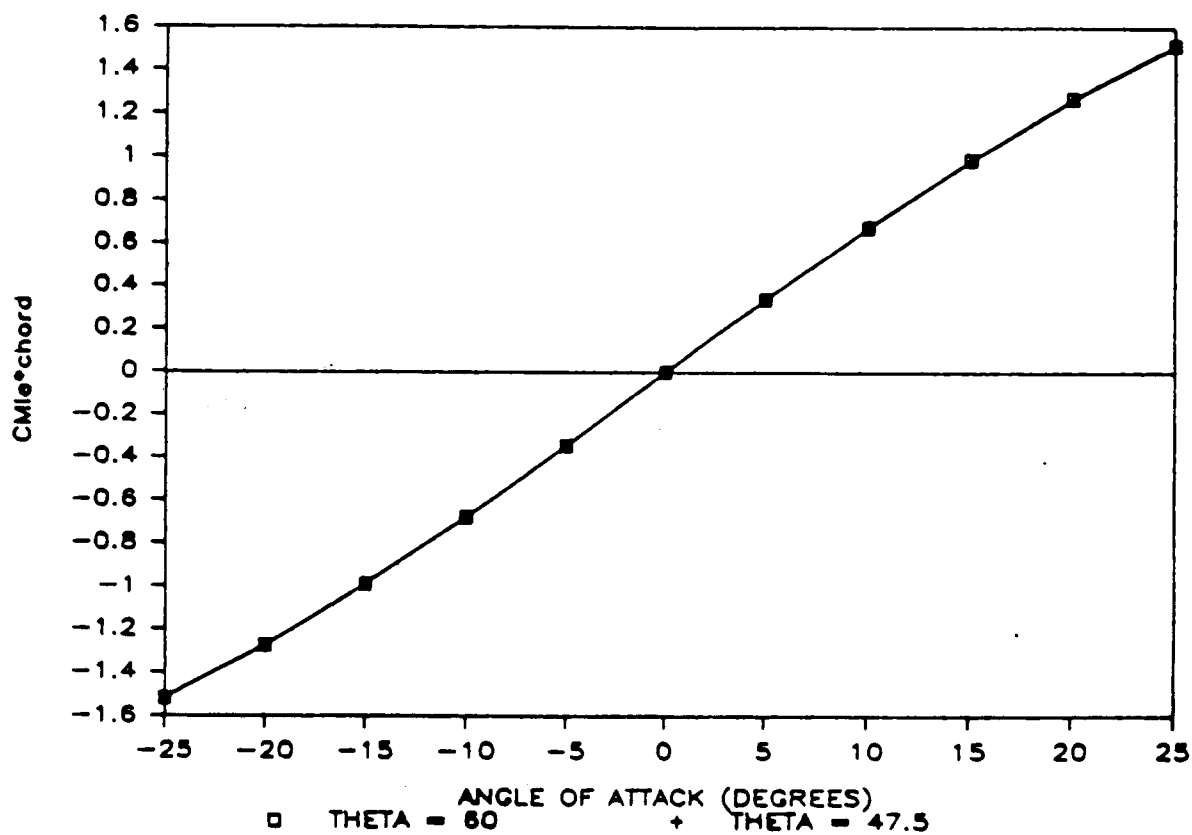
153

FIGURE 8.9a - L/D vs. ANGLE OF ATTACK

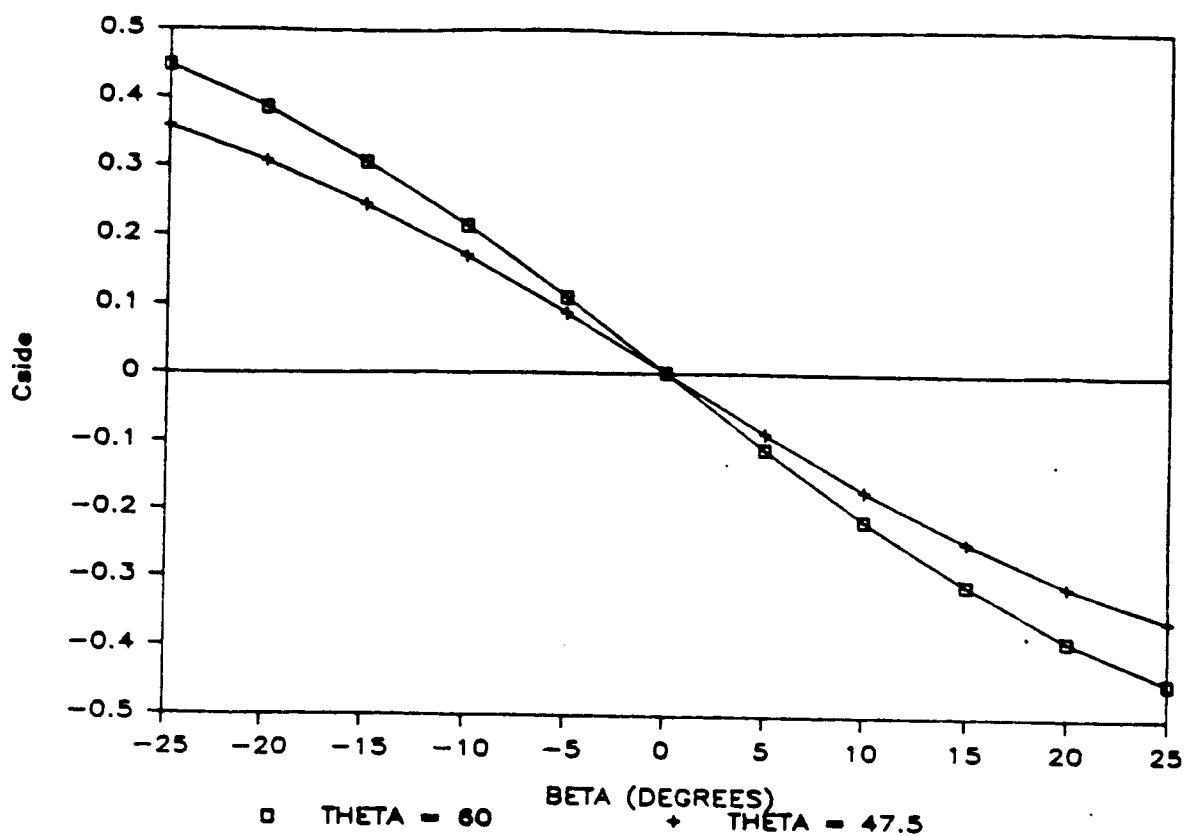FIGURE 8.9b - CMle*CHORD vs. ANGLE OF ATTACK

154

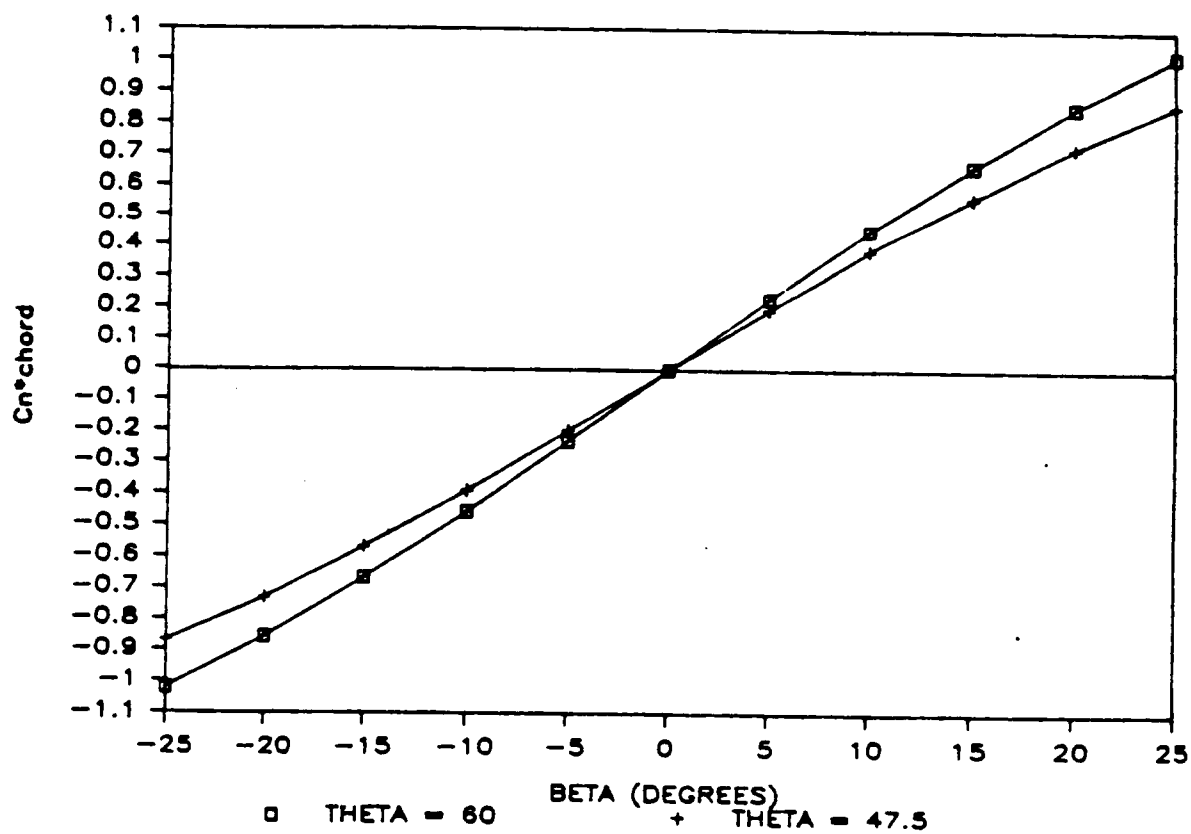FIGURE 8.10a - SIDE FORCE vs. SIDESLIP ANGLE

FIGURE 8.10b - YAW MOMENT vs. SIDESLIP ANGLE

155

8.2.1 SIZING

The four criteria for selecting an optimum ballute size were: (1) static stability margin, (2) maximum turn-down ratio, (3) the wake heating, and (4) the ballistic coefficient (related to heating). For the vehicle to be statically stable, the static margin (Xcp-Xcg margin) must remain positive. The maximum turn-down ratio is defined as [(CDA)nominal/(CDA)min]. A commonly used criteria is that the maximum turn-down ratio should be greater than or equal to 1.5 (i.e. 50% reduction in CD). The wake heating was investigated by the following equation:

$$Dmin = hs + 2(ls-lb)\tan(\bar{o}w)$$

where Dmin is the minimum diameter, hs is the ship height, ls is the ship length, lb is the portion of the ship covered by the ballute, and $\bar{o}$w is the wake angle. A commonly used wake angle is on the order of 15°. After comparing the ballute diameters of 15, 20, 25, 30, 35, 40, and 45 meters, the diameters of 20 and 33 meters were decided upon for the LEO/GEO and LEO/LLO scenarios, respectively (see figure 8.11). The ballistic coefficient is defined as W/CdA. The ballistic coefficients for the LEO/GEO and LEO/LLO scenarios are 22.39 and 18.85 (kg/m^2), respectively. The ballute diameters for both scenarios maintain a positive static margin for turn-down angles as low as 47.5^o. The maximum turn-down ratio is 1.5 for both cases. This property allows for the CD to be varied over a large enough range to allow for the required drag and delta-V control throughout the aeromaneuver. Each of these diameters provides a ballistic coefficient within the design heating limit of the ballute fabric, the necessary aerodynamic stability, and an acceptable turn-down ratio.

8.2.2 STABILITY AND CONTROL

As previously mentioned the ballute was designed to be pitch stable. This was accomplished by requiring that the static margin be positive. The static stability about the Yg axis (the vertical axis through the center of the gravity), sometimes referred to as "weathercock" stability, requires that Cn_{β} be positive, since the ship is a symmetric body, therefore it should be inherently roll stable. This presumption was shown to be true by the results of the trajectory analysis. There is an initial bank angle fluctuation (d$\grave{o}$/dt=0.1^o/sec, where $\grave{o}$ is the bank angle), but this damps out after about 35% of the total aerobraking time.

As mentioned earlier the velocity and pitch is controlled by changing the turn-down angle. The sideforce, yaw moment, and roll, however, must be controlled by forces other than aerodynamic forces. For this reason, the ship includes a Reaction Control System which may be used to correct any undesirable situations.
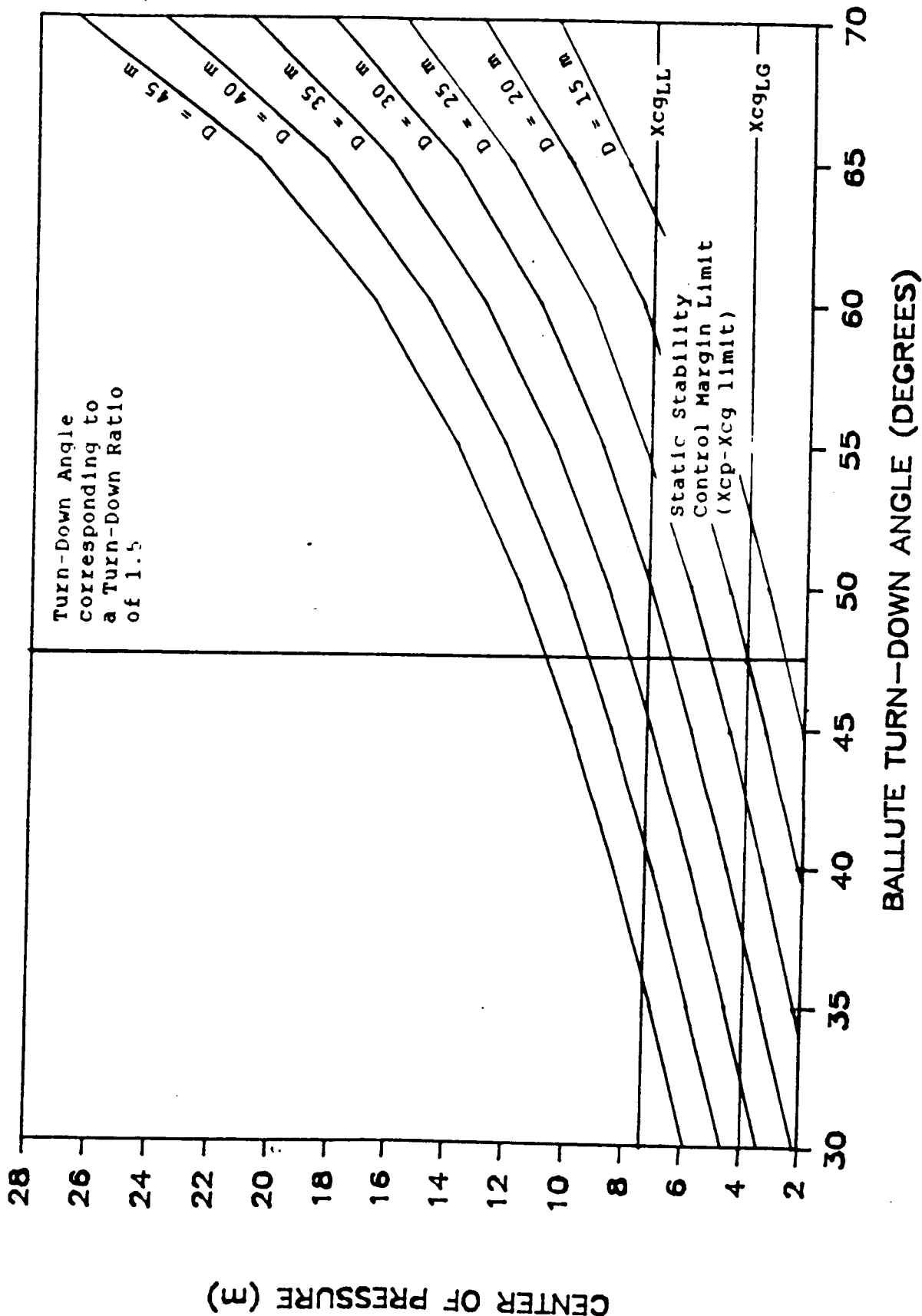
BALLUTE TURN-DOWN ANGLE VS. Xcp

CENTER OF PRESSURE (m)

Turn-Down Angle
corresponding to
a Turn-Down Ratio
of 1.5

D = 45 m
D = 40 m
D = 35 m
D = 30 m
D = 25 m
D = 20 m
D = 15 m

Xcg$_{LL}$

Static Stability
Control Margin Limit
(Xcp-Xcg limit)

Xcg$_{LG}$

BALLUTE TURN-DOWN ANGLE (DEGREES)

FIGURE 8.11

157

8.3 THERMAL PROTECTION SYSTEM (TPS)

8.3.1 THERMAL PROTECTION REQUIREMENTS

There were several criteria used in the selection of the TPS. The primary concern was that the rigid surface insulation (RSI) needed to be able to withstand a heating rate of 122 kw/m^2 returning from LLO and 96 kw/m^2 returning from GEO. At the same time, the flexible surface insulation (FSI) needed to be able to withstand a heating rate of 70 kw/m^2 returning from LLO and 90 kw/m^2 returning from GEO. Another concern was that the TPS must be able to minimize the temperature that the LOTV structure will encounter due to the effects of the aerothermal enviornment. The final criteria was that FSI thicknesses of .25 cm would not effect its continuity or performance as a thermal protection system.

8.3.2 TPS MATERIALS

The TPS consists of both an RSI and an FSI (see fig. 8.12). The RSI is a Fibrous Refractory Composite Insulation (FRCI-12) hexagonal tile system (see fig. 8.13). A tile system was chosen in order to handle the aerodynamic pressure, vibrations, and temperature gradients experienced during the aerobrake pass. An RSI consisting of large panels was rejected because they would be more susceptible to cracking, which could lead to structural damage of the ship. The FRCI-12 was chosen due to its low weight (193 kg/m^3) and its ability to withstand temperatures of up to 1500 K. Heating analysis indicated that the RSI would not encounter temperatures greater than 1300 K. Other options considered for the RSI were Alumina Enhanced Thermal Barrier (AETB), LI-2200 and a High temperature Reusable Surface Insulation (HRSI). FRCI was chosen because it has a higher tensile stress than AETB, and HRSI won't withstand as much heat as FRCI. LI-2200 is a 100% silica insulation while FRCI contains 20-80% aluminoborosilicate fibers. Because of this, FRCI has a higher thermal conductivity and is better suited for our mission (ref. 8.2, ref. 8.9 and ref. 8.12).

The ballute system is composed of three bags which are made from a Nextel AB-312 fabric sealed with CS-105 which is a glass frits coating. Attached to the ballute bags is an Advanced Flexible Reuseable Surface Insulation (AFRSI). The original choice for the FSI was a Tailorable Advanced Blanket Insulation (TABI) because of its ability to withstand larger heating rates than the AFRSI. However, the AFRSI was chosen after the heating analysis indicated that a thickness of .25 cm for the FSI was acceptable. The TABI manufactures (Woven Structures, Inc.), indicated that thicknesses of less than one centimeter would result in fabrication problems. It was felt that the increase in heating capabilities did not offset the added mass associated with a thicker FSI. The AFRSI utilizes a Quartz felt insulation (Q-felt) with Nicalon on the outer (windward) surface and Nextel on the inner surface (see fig. 8.14; ref. 8.2 and ref. 8.7).
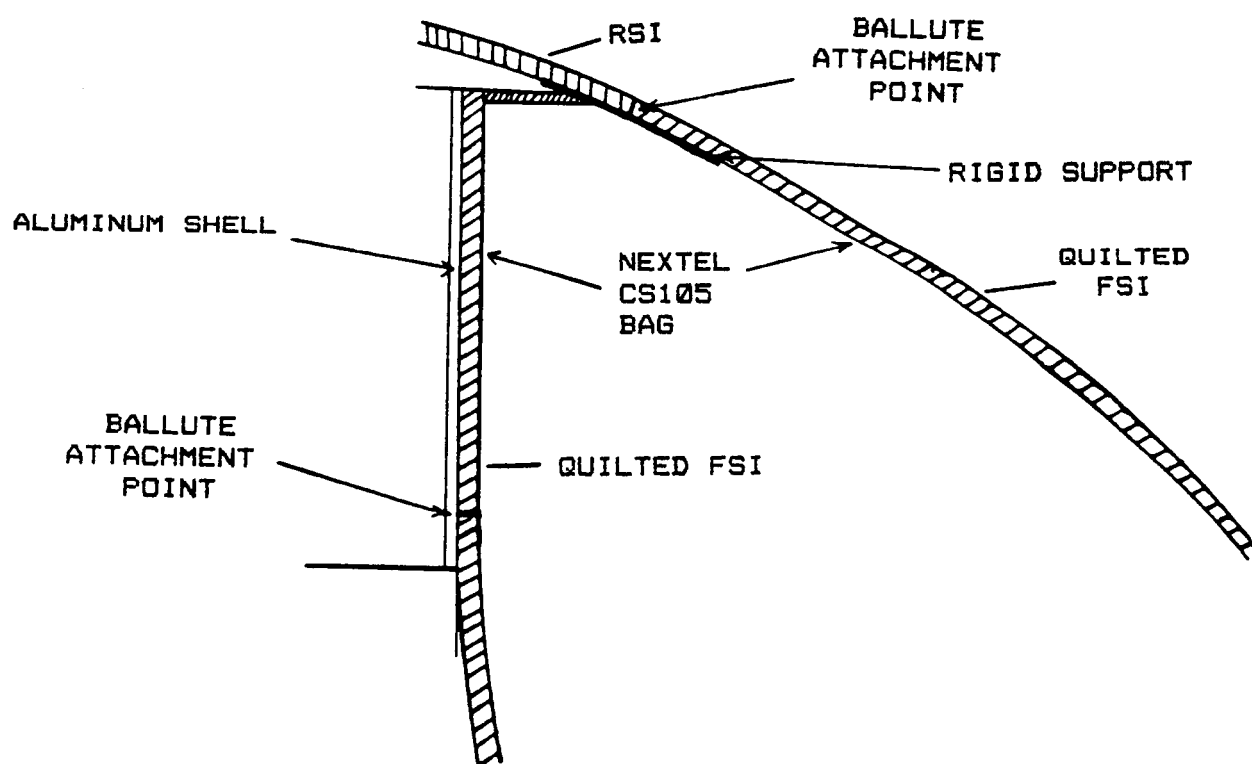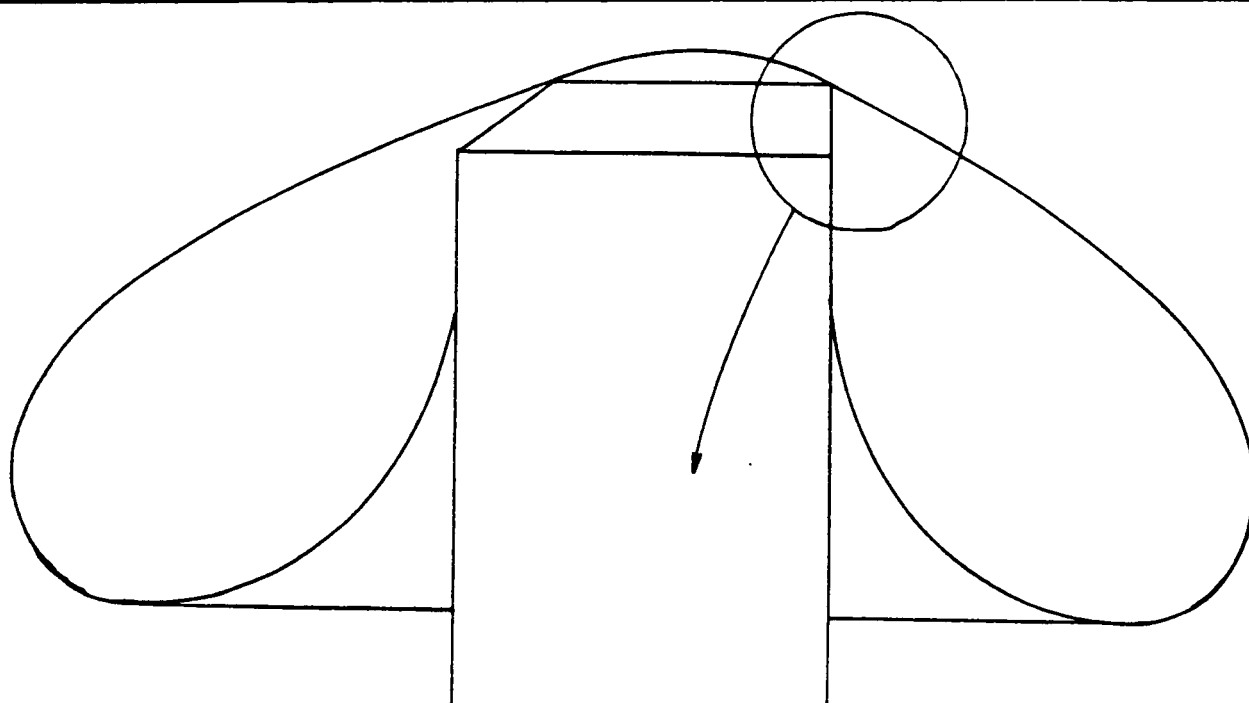
FIGURE 8.12   TPS CONFIGURATION

159

SECTION X-X

RSI TILES

NICALON

GAP FILLER

STRAIN ISOLATION PADS

RSI TILES

FILLER BARS

STRAIN
ISOLATION PADS

FIGURE 8.13   RSI CONCEPT

NICALON FABRIC

NICALON FABRIC

NICALON FABRIC

NEXTEL
FABRIC

Q-FELT

NEXTEL FABRIC

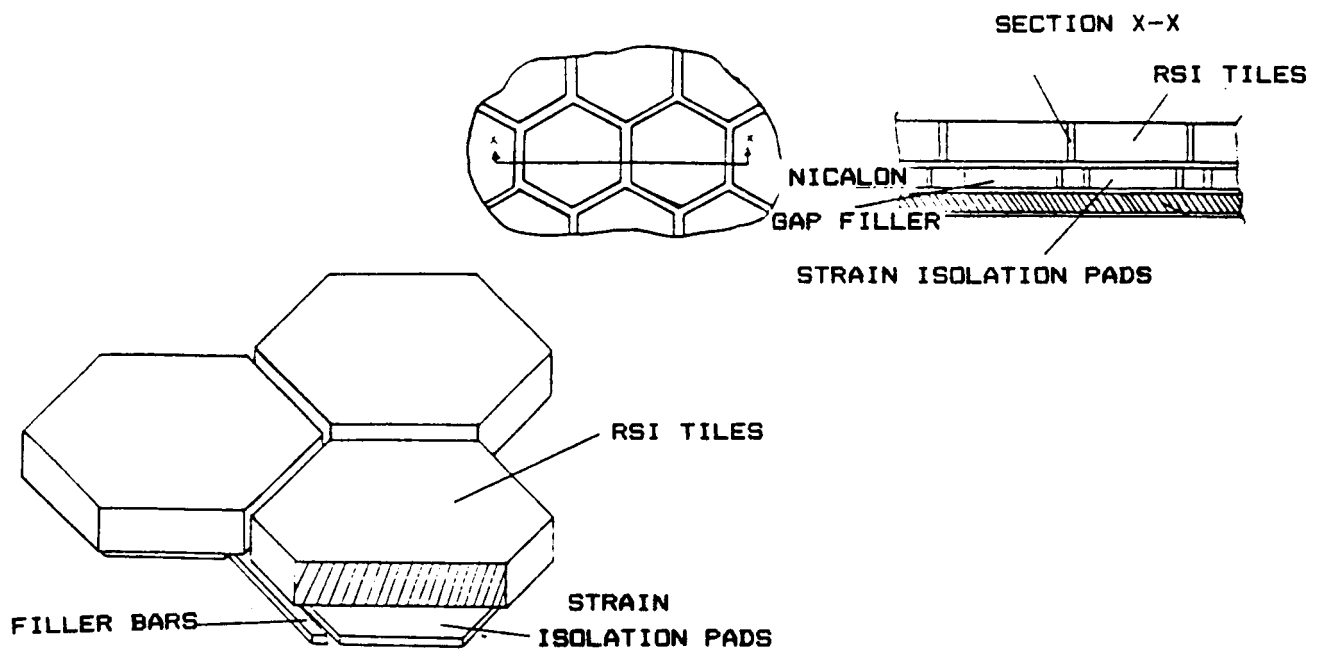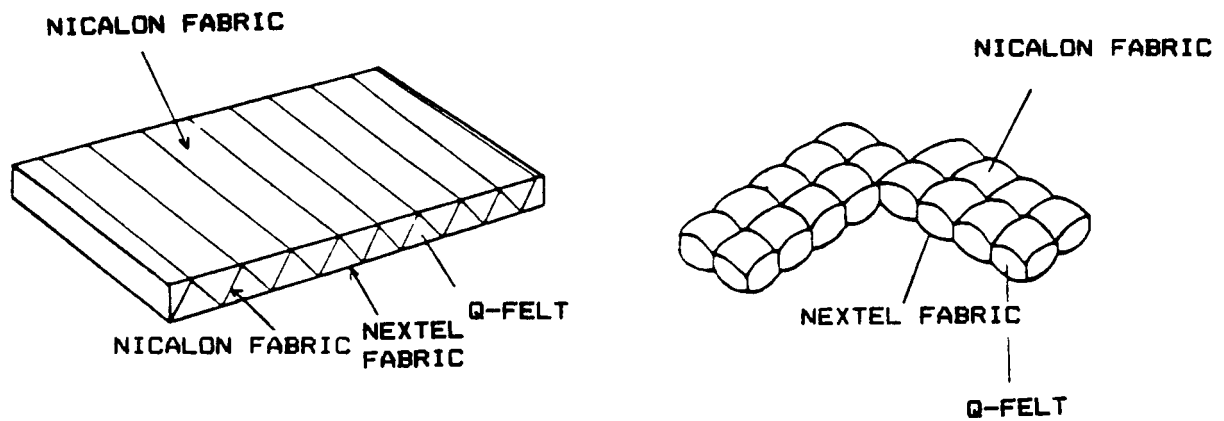Q-FELT

FIGURE 8.14   FSI CONCEPTS

8.3.3 ATTACHMENT OF TPS

The attachment of the RSI to the cap structure is accomplished by attaching the tiles to a Strain Isolation Pad (SIP), which is epoxied to the cap (an aluminum sheet). The purpose of the SIP is to give the tile support during the aerobrake procedure when it will experience some flexing due to the dynamic loads. It will also assist in absorbing the internal cold soak thermal differential strain. Placed in between the tiles is a filler bar which alleviates any problems in continuity (see figure 8.13). Two possible ways for attaching the FSI to the Nextel are presented in figure 8.15. The major concern is to minimize the amount of radiation which would become trapped in the crevices between the lobes since this would increase the heat transfer through the ballute. Two hundred forty meridian straps span the ballute with the Q-felt either attached to the Nextel through a high temperature velcro, or by fixing it to one of the meridian straps with Nextel loops. At the junction of two bags the same system is employed; however, there is more reinforcement to insure that there is continuity (ref. 8.2).

8.3.4 TEMPERATURE ANALYSIS

The heat transfer rate at the stagnation point was determined by NASA using the POST (Brauer) program. The program assumes a generalized point mass and a one meter sphere and calculates the heat transfer rate using the Chapman Equation. The heat transfer rate along the surface of the ballute was calculated using a program written by Samir Deshpande while doing graduate work at Virginia Polytechnic Institute and State University. The program uses the conventional boundary layer equations to calculate the convective heat transfer. The analysis of the heat transfer rate along the surface of the ballute was performed at the altitude and Mach number which corresponded to the maximum heating rate generated by the POST program. For the return trip from GEO, the analysis was conducted at an altitude of 95 km with a Mach number of 36.2. The return from LLO was calculated at an altitude of 95 km and a Mach number of 37.5. Note that the heat transfer rates are based upon a perfect gas assumption which does not allow for real gas effects at high temperatures. For a graph of the heat transfer rate along the surface of the ballute for the return from LLO and from GEO, see figures 8.16 and 8.17, respectively. Allowing for real gas effects will reduce the heat transfer rate. The effective thermal conductivity of the multilayered AFRSI was determined by (ref. 8.6):

$$1/k_{eff} = \text{d } 1/k_i$$

and was found to be .13 W/m K at 1200 K. Its thickness was chosen to be .25 cm in order to maintain backwall temperatures below 800 K. See figure 8.18 for the heating rate versus time at the stagnation point for the return from GEO. Figure 8.19 shows the heating rate versus time at the stagnation point for the return from LLO. The thermal conductivity of the FRCI-12 was found to be .14 W/m K at 1200 K (ref. 8.1 and 8.2). Heat
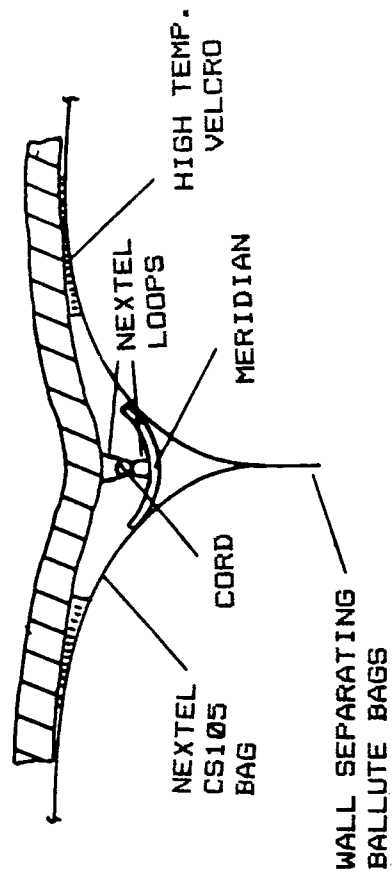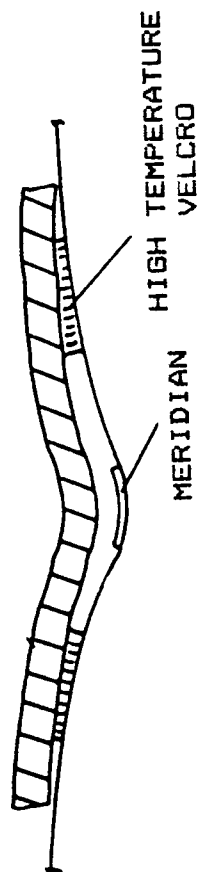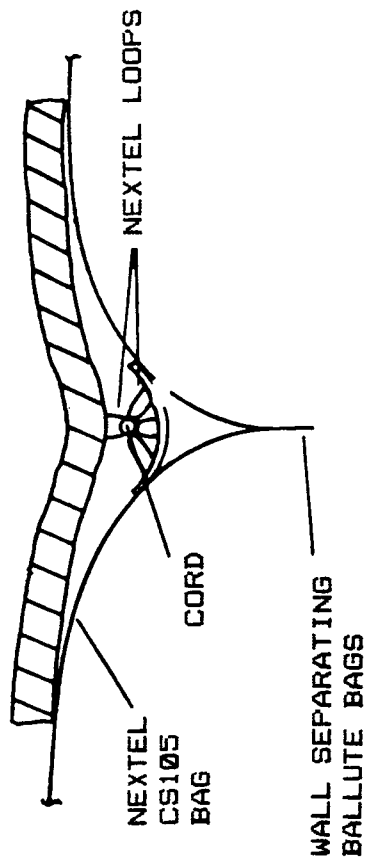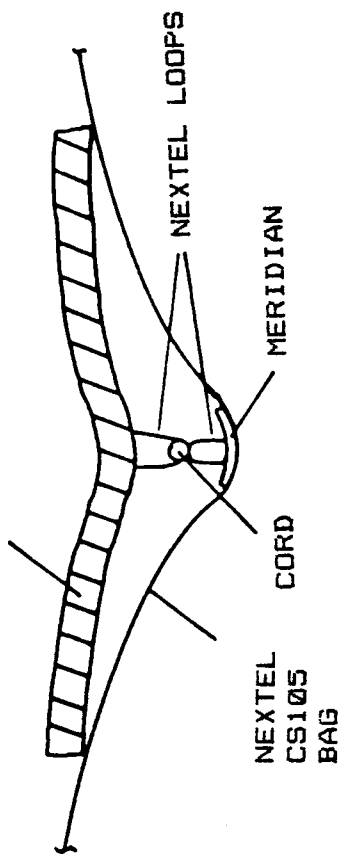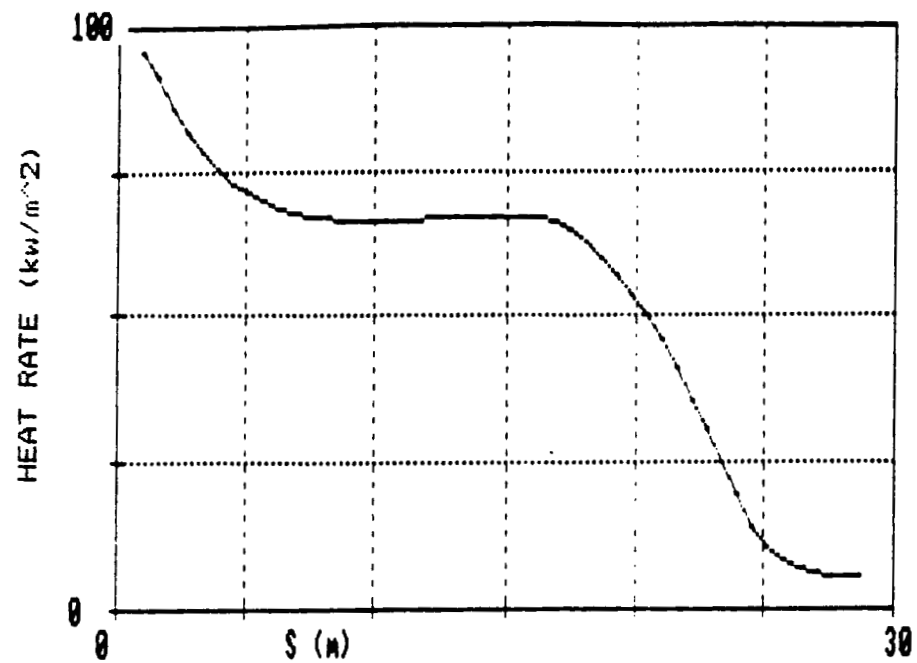
FIGURE 8.15 - FSI/BALLUTE ATTACHMENTS
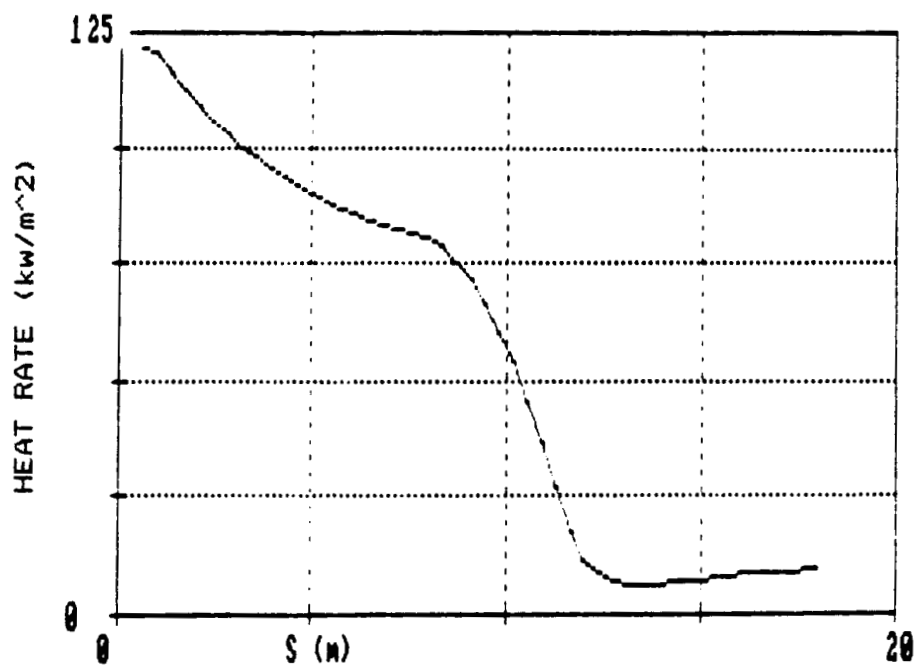
FIGURE 8.16 - HEATING RATE (33 m BALLUTE)

FIGURE 8.17 - HEATING RATE (20 m BALLUTE)
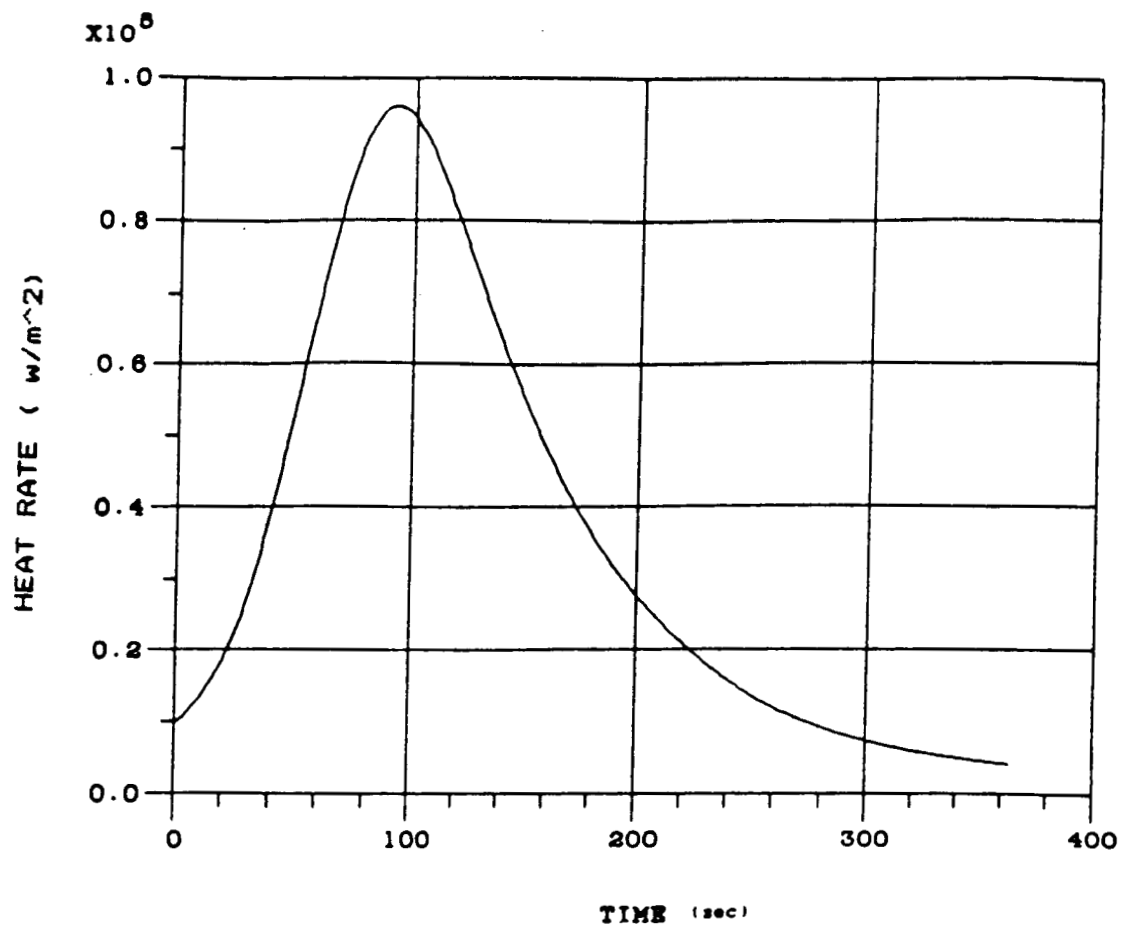
163

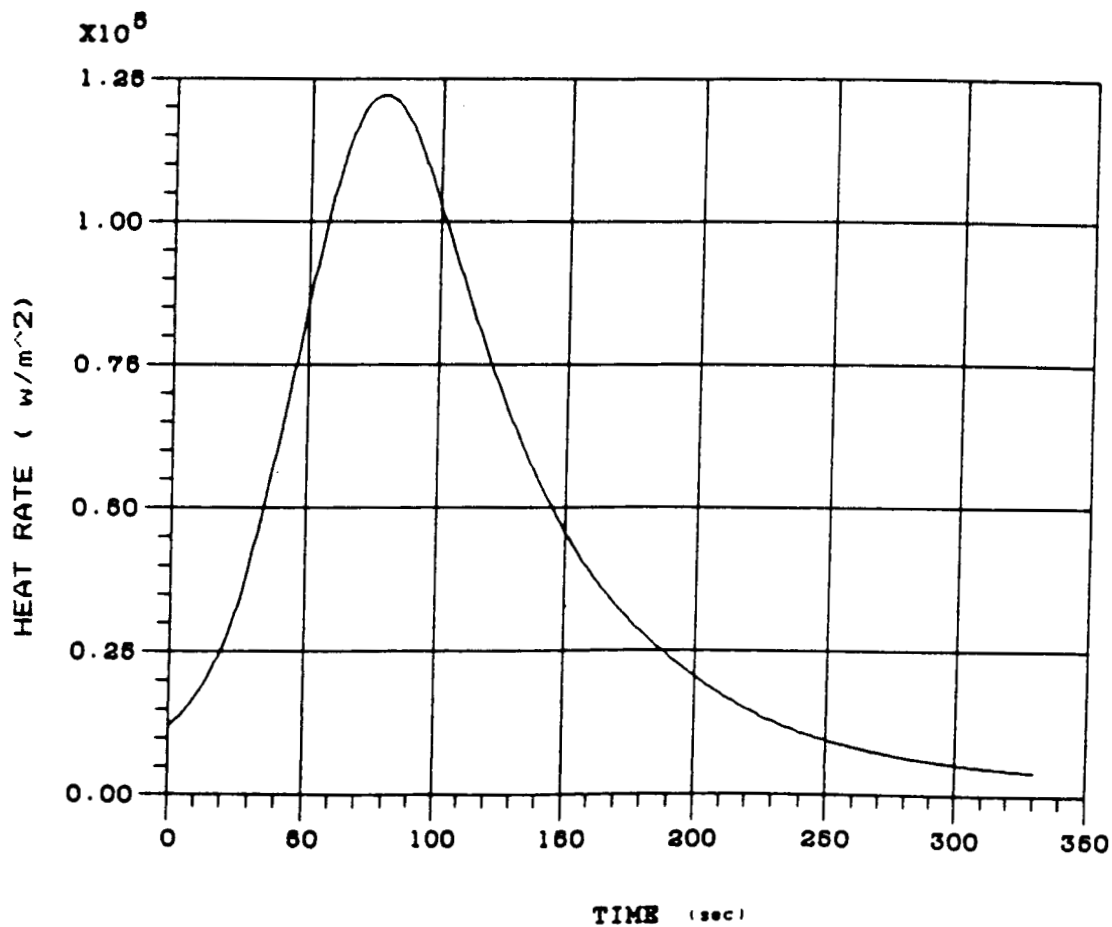FIGURE 8.18 - GEO-LEO AEROBRAKING

FIGURE 8.19 - LLO-LEO AEROBRAKING

transfer analysis indicated a tile thickness below what would be considered acceptable for fabrication. Therefore, a thickness of 1.78 cm was chosen for the RSI thickness for both scenarios (ref. 8.10).

8.4 TRAJECTORY

The trajectory analyses for both the GEO-to-LEO and LLO-to-LEO scenarios were performed by NASA using the Program to Optimize Simulated Trajectories (POST) (ref. 8.3). POST assumed a generalized point mass, in this case a one meter sphere, to target and optimize a point mass trajectory for an unpowered vehicle operating near the Earth. The analyses were done using the basic equations of motion based on the 1976 Standard Atmosphere.

8.4.1 GEO-to-LEO (20 m Ballute)

Due to the fact that the LOTV project was separated into a non-aerobraked versus an aerobraked scenario, it was necessary to have a standard in order to compare the two. The standard which was chosen was based upon returning from GEO with 5000 kg of payload. For this reason the POST analysis was performed using an LOTV mass of 9745 kg. The LOTV will enter the atmosphere at 130 km with a velocity of 10.3 km/s and an angle of attack of -10 degrees. The angle of attack was chosen in order to obtain a L/D of .15. The trajectory analysis indicated that only one pass would be required to obtain the delta-V necessary to place the LOTV into LEO, and the total time in the atmosphere would be approximately six minutes. For a detailed summary of the governing conditions, the initial versus the final conditions and the characteristics of the reentry into LEO, see Table 8.2.

Table 8.2 GEO-to-LEO Aerobrake (20 m Ballute)

GOVERNING CONDITIONS

Ballistic Coefficient (kg/m^3)	22.39
L/D	.15
Angle of Attack (degrees)	-10.00
Mass (kg)	9745.00
Delta-V (km/s)	2.40

TRAJECTORY CONDITIONS	INITIAL	FINAL
Velocity (km/s)	10.3	7.9
Altitude (km)	130.0	130.0
Flight Path Angle (degrees)	-3.8	1.3

LEO CHARACTERISTICS

Orbit (km)	60 x 465.3
Inclination (degrees)	2.24

Figures 8.20 and 8.21 show altitude versus time and velocity versus time, respectively.

8.4.2 LLO-to-LEO (33 m Ballute)

The analysis for the LLO-to-LEO trajectory was based upon returning from LLO with 5000 kg of payload and 10000 kg of liquid oxygen which gave an LOTV mass of 22500 kg. The LOTV will enter the atmosphere at 130 km with a velocity of 11 km/s at an angle of attack of -10 degrees which corresponds to an L/D of .15. As was the case with the GEO-to-LEO trajectory, only one pass will be required to obtain the delta-V necessary to place the LOTV into LEO. The total time in the atmosphere is approximately 5.5 minutes. Table 8.3 gives a detailed summary of the governing conditions, the initial versus the final conditions and the characteristics of LEO. For a summary of altitude versus time and velocity versus time see figures 8.22 and 8.23, respectively.

8.4.3 PLANE CHANGE

For both scenarios the necessary plane change will be performed during the aeromaneuver. The necessary side force is generated by using the RCS to change the side slip angle. Future projections are to vary the pressure inside the ballute bags in order to create an asymmetric cross-section.

8.5 STRUCTURES

The support structure of the aerobrake cap is designed to insure proper coupling of the ballute to the ship. It allows the ballute to be stored, deployed, and operated without obstructing the ship's functions. It is also designed to support the dynamic loads associated with the aeromaneuver.

Table 8.3 LLO-to-LEO Aerobrake (33 m Ballute)

GOVERNING CONDITIONS

Ballistic Coefficient (kg/m^3)	18.85
L/D	.15
Angle of Attack (degrees)	-10.00
Mass (kg)	22 500.00
Delta-V (km/s)	3.10

TRAJECTORY CONDITIONS	INITIAL	FINAL
Velocity (km/s)	11.0	7.9
Altitude (km)	130.0	130.0
Flight Path Angle (degrees)	-4.2	1.2

LEO CHARACTERISTICS

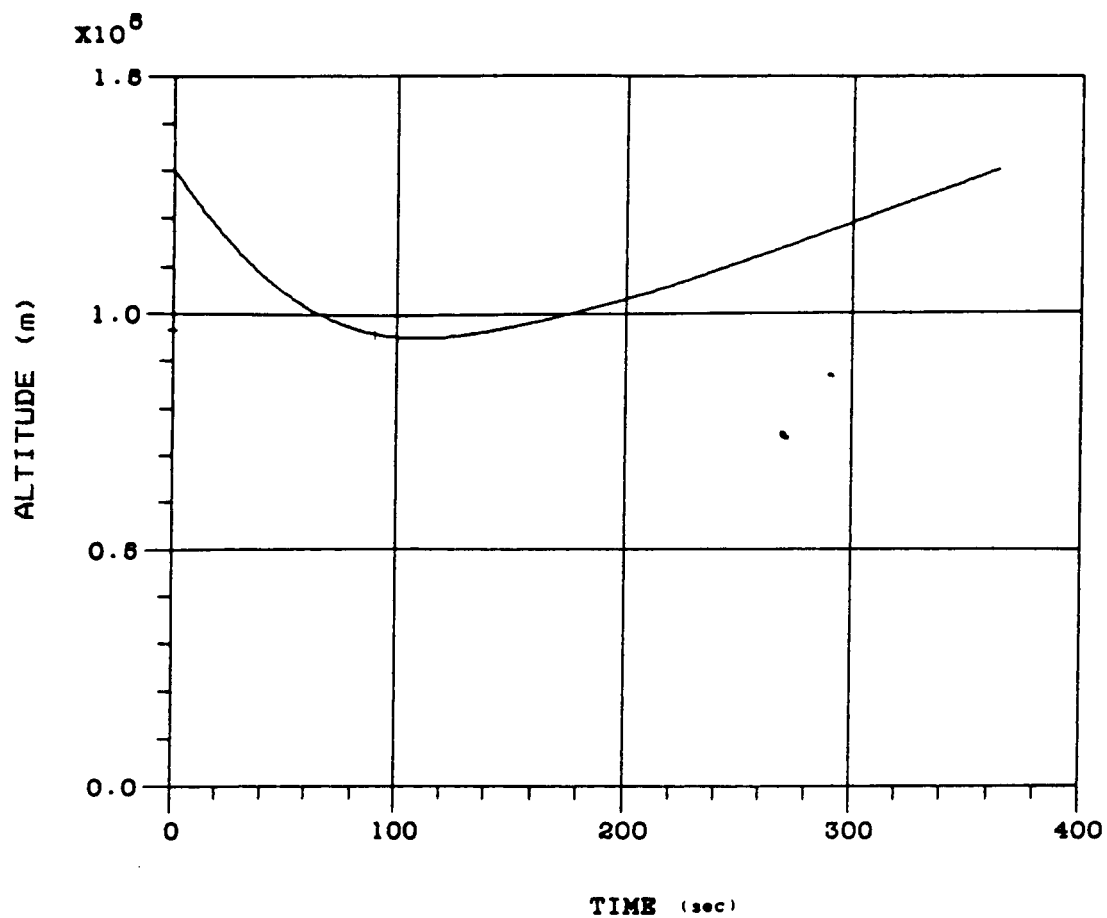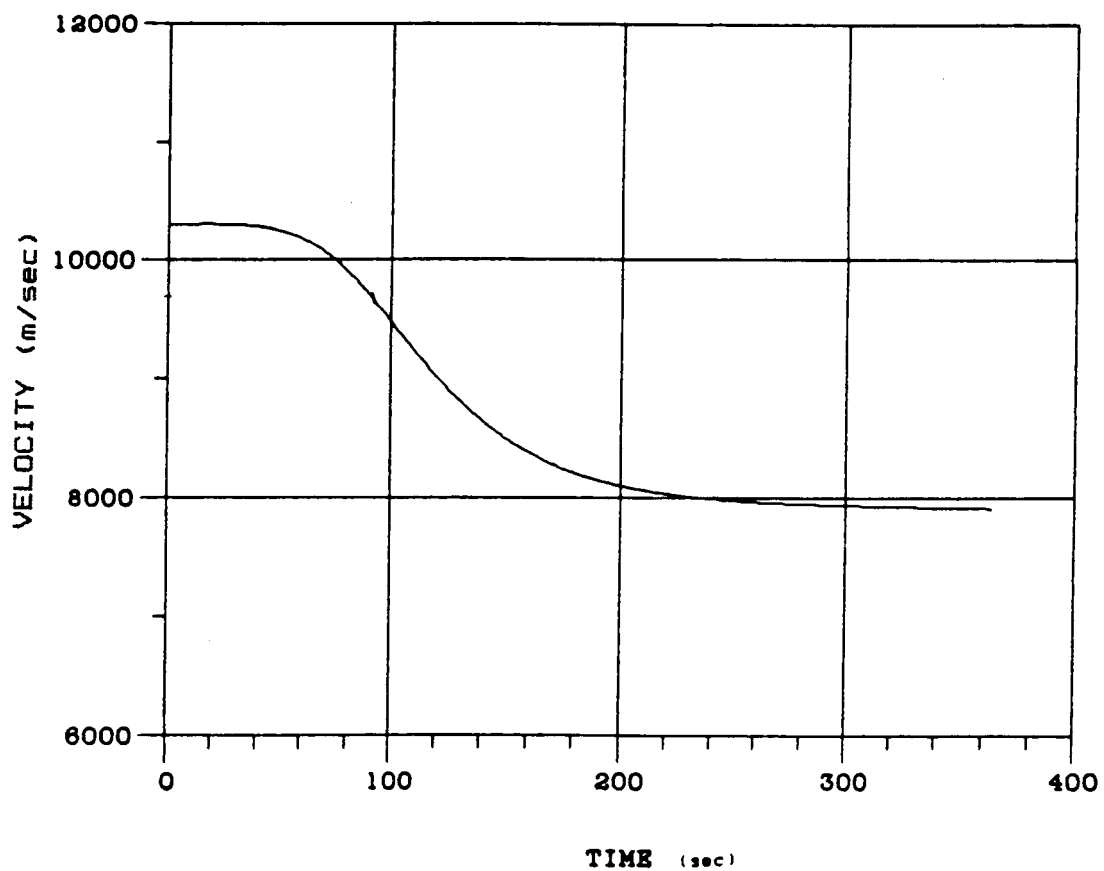|	
Orbit (km)	49.7 x 466
Inclination (degrees)	7.82

FIGURE 8.20 - GEO-LEO AEROBRAKING
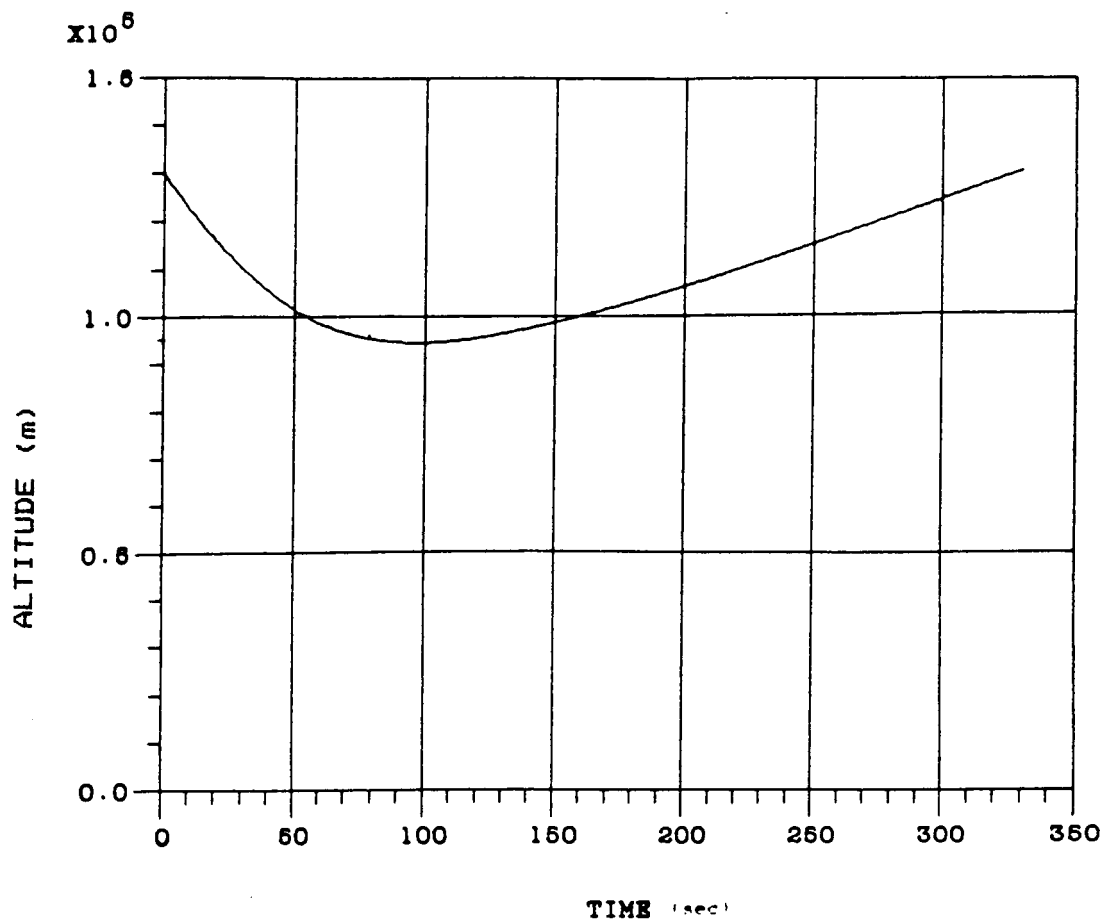

FIGURE 8.21 - GEO-LEO AEROBRAKING

167

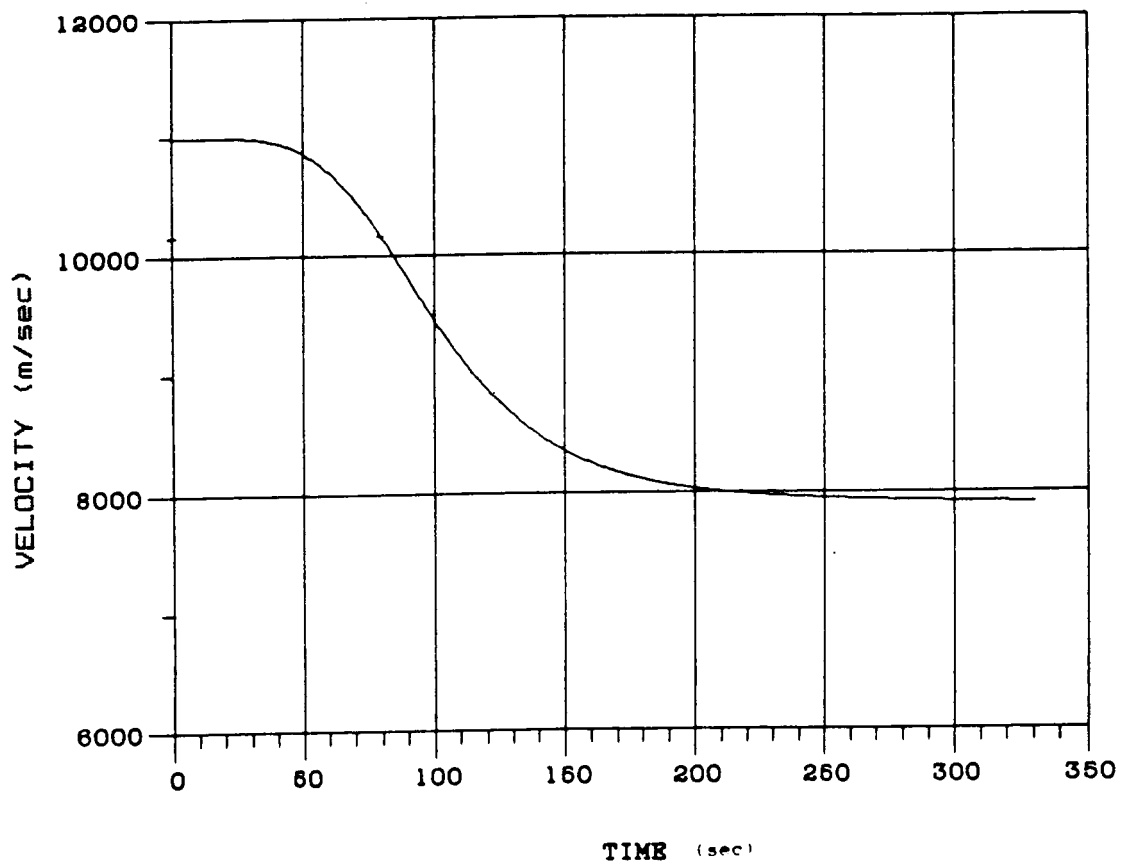FIGURE 8.22 - LLO-LEO AEROBRAKING

FIGURE 8.23 - LLO-LEO AEROBRAKING

168

The primary purpose of the lower truss structure is to provide support for the cap. It houses the liquid nitrogen (LN$_2$) tanks, and the mechanism to position and lock the cap into place. The interior structure and the position of the LN$_2$ tanks can be seen in fig. 8.24. Figure 8.25 shows how the LN$_2$ tanks are attached to the truss structure.
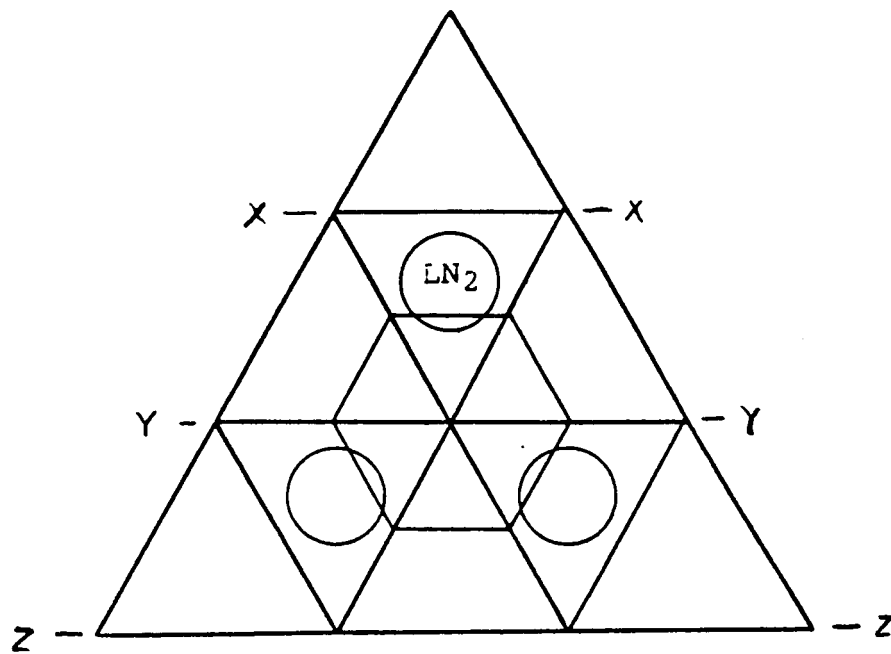
Since the rigid cap is circular and the ship has a triangular cross section, it is necessary for the truss structure to provide a smooth transition between the two. For this reason, the lower truss structure tapers into a hexagon which is rounded at the top. The rigid heat shield consists of an RSI which is bonded to boron/aluminum sheets. The truss is fabricated from hollow circular tubes. Because of the high tensile strength of boron aluminum, relatively small members can be used.

The jettisonable part of the structure consists of the outer ring of the RSI .5 m wide, the FSI and ballute bags, and the aluminum skirt around the cap. This configuration was chosen in order to minimize the amount of material lost due to jettisoning. The point where the outer ring of the RSI connects with the inner part of the RSI is shown in fig. 8.26.

Reducing discontinuities in the insulation is a major design criteria. Stagnation points can produce high heating rates which could damage the insulation or the LOTV. The two points of concern are where the inner and outer ring of the RSI are joined, and where the rigid and flexible insulations meet. Within the RSI, boron/aluminum sheets overlap one another to prevent discontinuties. At the point where the RSI and FSI meet, a rigid support is placed under the insulation so that the transition from the RSI to the FSI will be smooth when the ballute is turned down.

The lower edge of the ballute bag is attached to an aluminum skirt which surrounds the lower truss structure. The skirt is attached to the outer ring of the RSI for jettisoning purposes. By attaching the ballute to the skirt, the ballute will remain in a stable position against the ship during aerobraking and the ballute will be prevented from becoming entangled on the ship structure when jettisoned (see fig. 8.4). The attachments between the truss structure and the jettisonable stucture are shown in fig. 8.27. When the ballute is jettisoned, the nitrogen pipes will separate and the expelled nitrogen will help push the ballute away from the ship.

The forces on the ship were determined by Modified Newtonian Theory. They were modelled in Structural Analysis Software for Microcomputers (ref. 8.4) by a concentrated centric force on the cap, a distributed force over the ballute and a distributed force due to dynamic pressure. The software used the Direct Stiffness Method to determine the stresses and deflections in the material. The deflections were negligable and the stresses were well below the ultimate stress of boron/aluminum, which has a stiffness of 230 GPa.

169
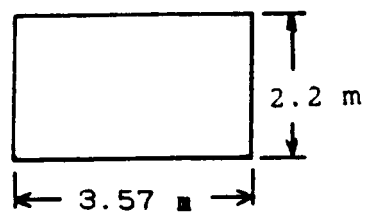
SECTION X-X

SECTION Y-Y
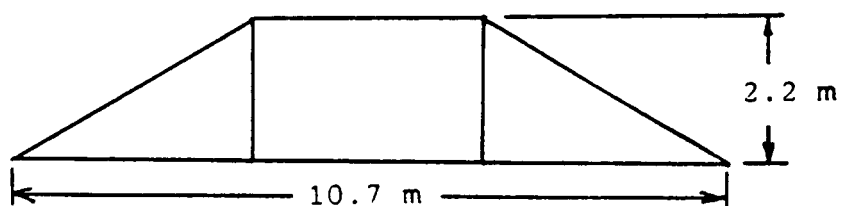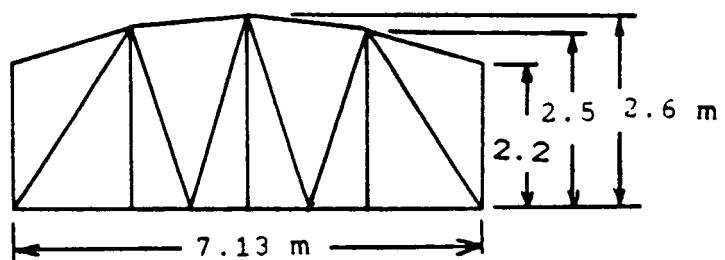
FIGURE 8.24 - CAP STRUCTURE
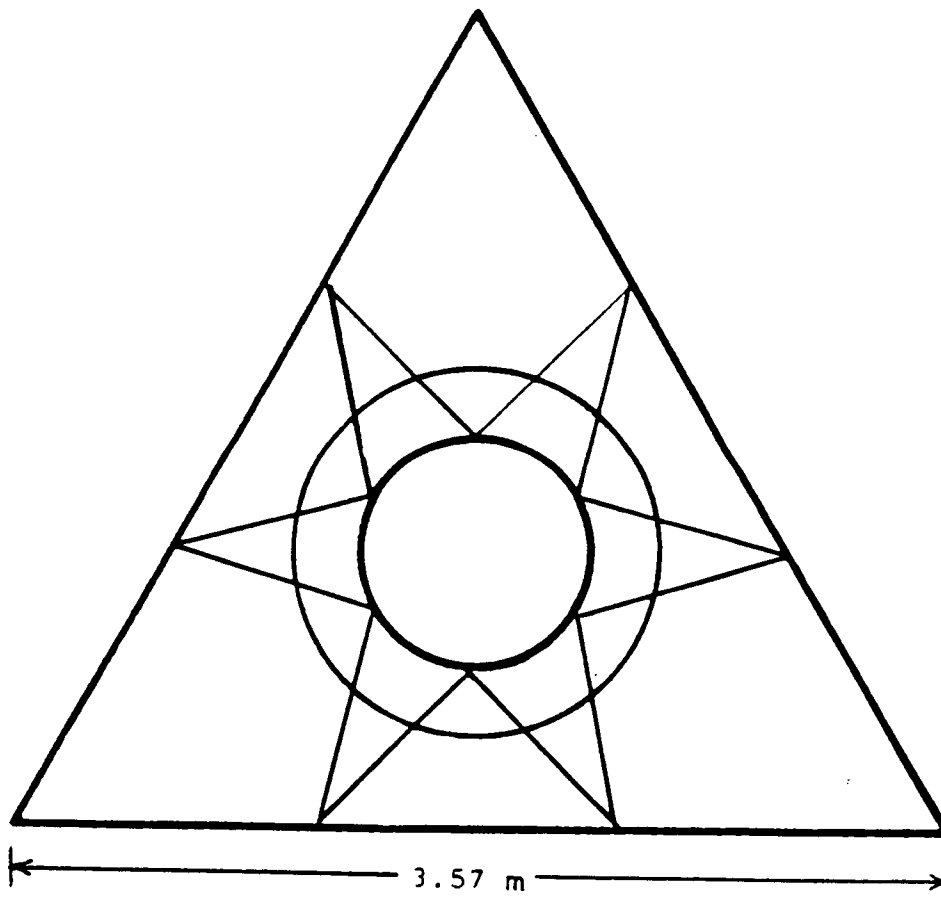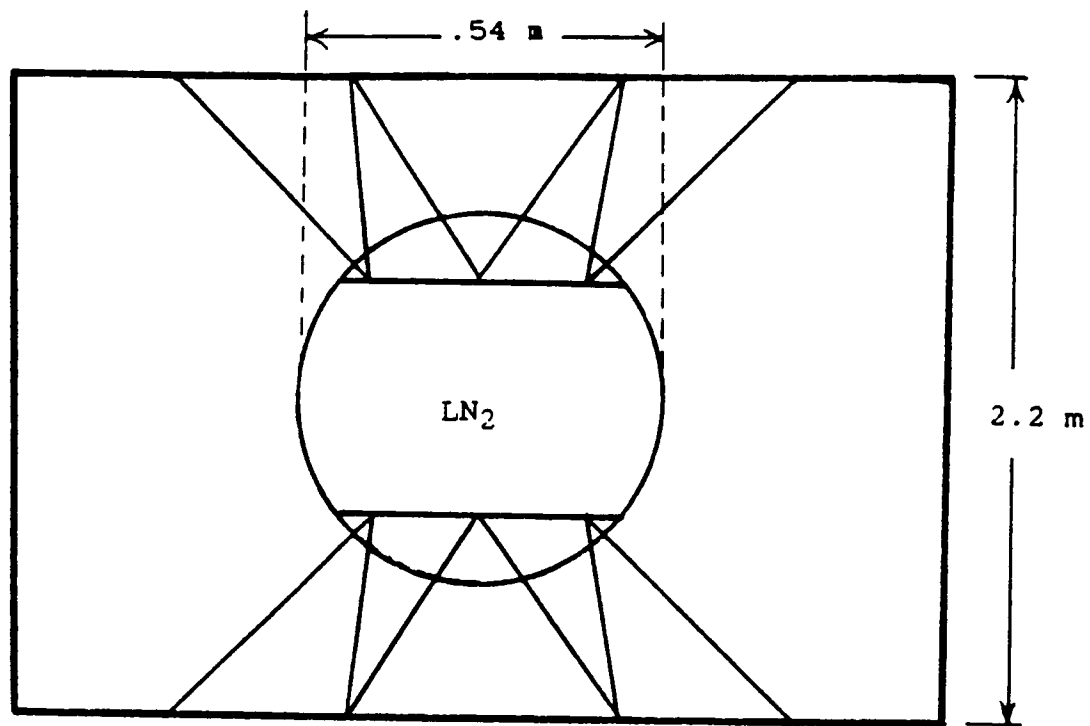
FIGURE 8.25 - TANK SUPPORT STRUCTURE

JETTISONED AFTER
AEROBRAKE PASS

JETTISONING
SEPARATION POINT

RSI TILES
(NOT JETTISONED)

RSI TILES (JETTISONED)

BALLUTE ATTACHMENT POINT

RIGID SUPPORT

ALUMINUM SHELL
(JETTISONED)

NEXTEL
CS105 BAG

QUILTED FSI

BALLUTE ATTACHMENT POINT
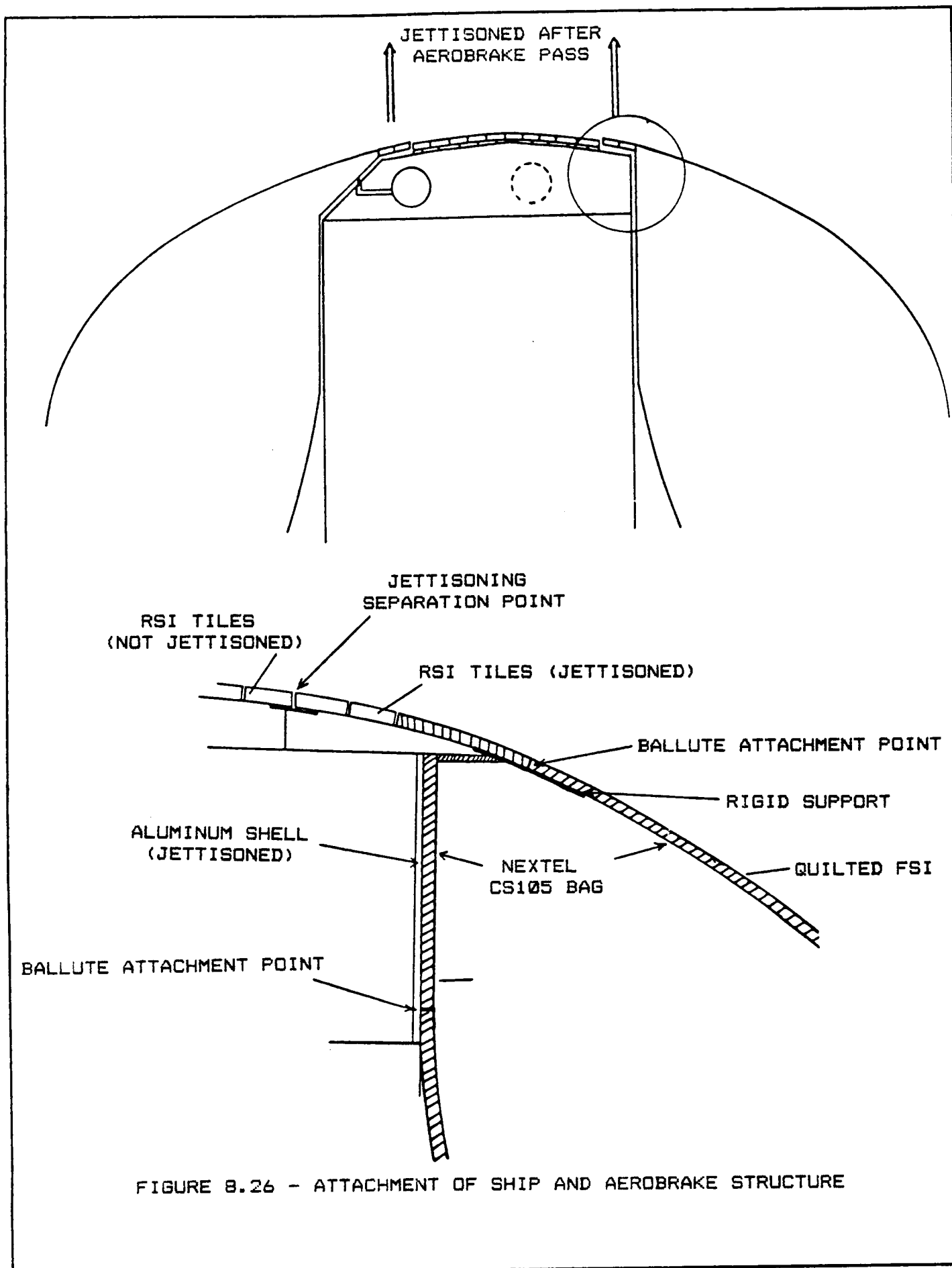
FIGURE 8.26 - ATTACHMENT OF SHIP AND AEROBRAKE STRUCTURE

SHIP

SHELL

MALE-FEMALE
LOCK

SHIP STRUCTURE

GASKET

EXTENDED CONNECTOR

TO N$_2$ TANK
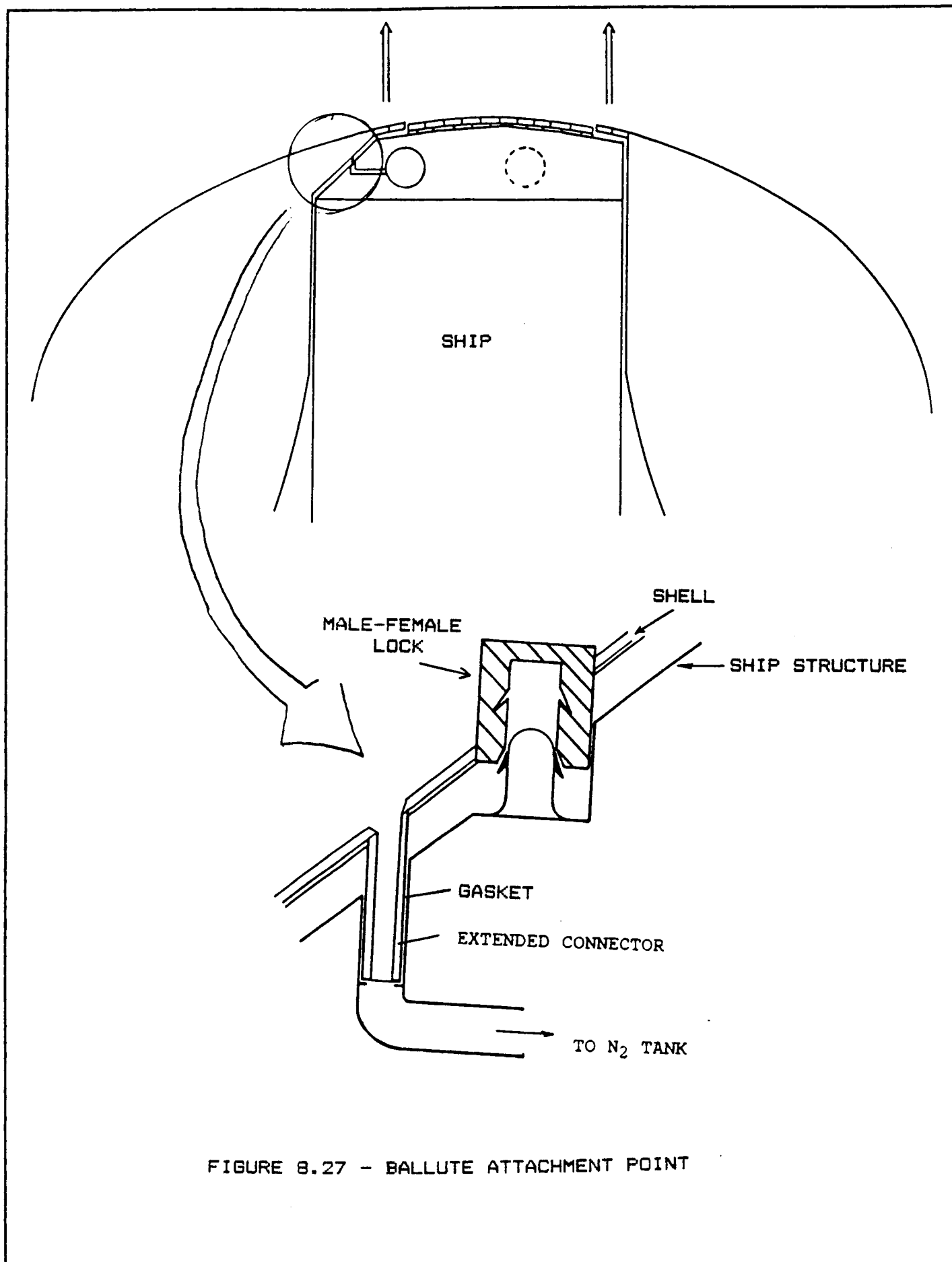
FIGURE 8.27 - BALLUTE ATTACHMENT POINT

Thus, buckling is the most likely mode of failure. The cross sectional members were chosen so that they will not buckle under the highest loads with a safety factor of 1.5. The method used to determine the buckling failure was the Euler Equation for buckling of a circular cylinder. The most reasonable and cost efficient choice was to make all the members of the same cross section. For the LEO/GEO ship, the structural members have an outside diameter of .05 m, and an inside diameter of .038 m. For the LEO/LLO ship the structural members have and outside diameter of .05 m and an inside diameter of .048 m.

The LN_2 tanks are spherical and made of kevlar wrapped aluminum. Each is .54 m in diameter for the LEO/LLO mission and .45 m in diameter for the LEO/GEO mission. The sizing of the tanks was determined by assuming an internal pressure of .01 atmospheres for the ballute.

8.6 STORAGE AND DEPLOYMENT

The aerobraking system is stored on the bottom of the ship so that it will not obstruct the RCS, the position of the payload, or the movement of the mirror system (see figures 8.2 and 8.4). When the ship is in the proper orientation for aerobraking, the aerobrake system is moved to the front of the ship (see figure 8.30).

The mechanism for moving the cap is shown in figure 8.31. The aerobrake is first moved toward the front of the ship along the teflon coated tracks (see figure 8.28). When the cap reaches the
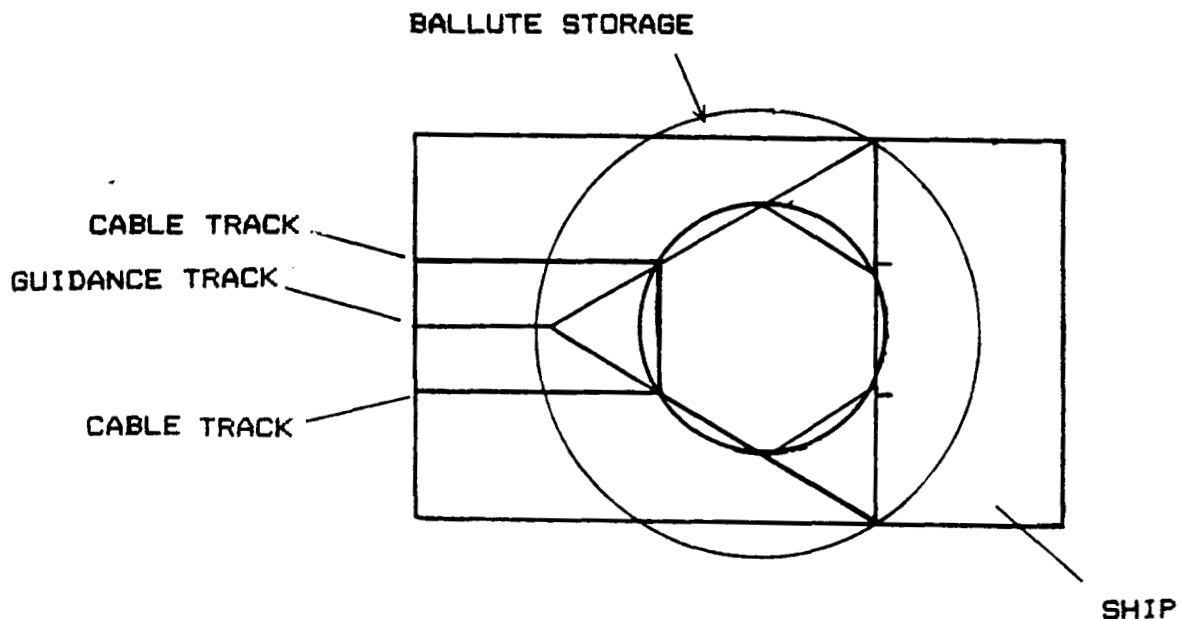
FIGURE 8.28 - POSITION OF CAP WHILE ON SURFACE OF SHIP

174

front of the ship, nitrogen is injected into the jack. This creates a moment which rotates the cap onto the front of the ship. The cap is locked into place using the attachment points for the payload.

The ballute is folded and stored underneath a lightweight tarp which encircles the cap. When the cap is in position, the tarp is released and the ballute is inflated (see figure 8.29). Each ballute section is connected to two of the three LN_2 tanks. Each section also has a bleed valve to remove excess nitrogen (see figure 8.32). Because each ballute can get nitrogen from two different tanks, failure of one tank will not result in complete failure of the system. Liquid nitrogen can also be pumped between tanks. After aerobraking the ballute is jettisoned.

8.7 MASS ESTIMATES

The masses were determined by multiplying the density of the material by its volume. The densities of the FSI and RSI were found in reference 8.2. The densities of boron/aluminum, aluminum, and nitrogen were found in standard material properties tables. The mass of the two structures were relatively low for the size of each ship.

Table 8.4 Mass Estimates (kg)

	LEO/GEO	LEO/LLO
Structure	70	110
N_2 and N_2 tanks	120	200
RSI	170	240
FSI	160	660
Aluminum Shield	230	330
Piping and Pumps	20	20
Total	770	1560

COVERING TARP

TARP LOCKED IN PLACE

TARP BEING RELEASED
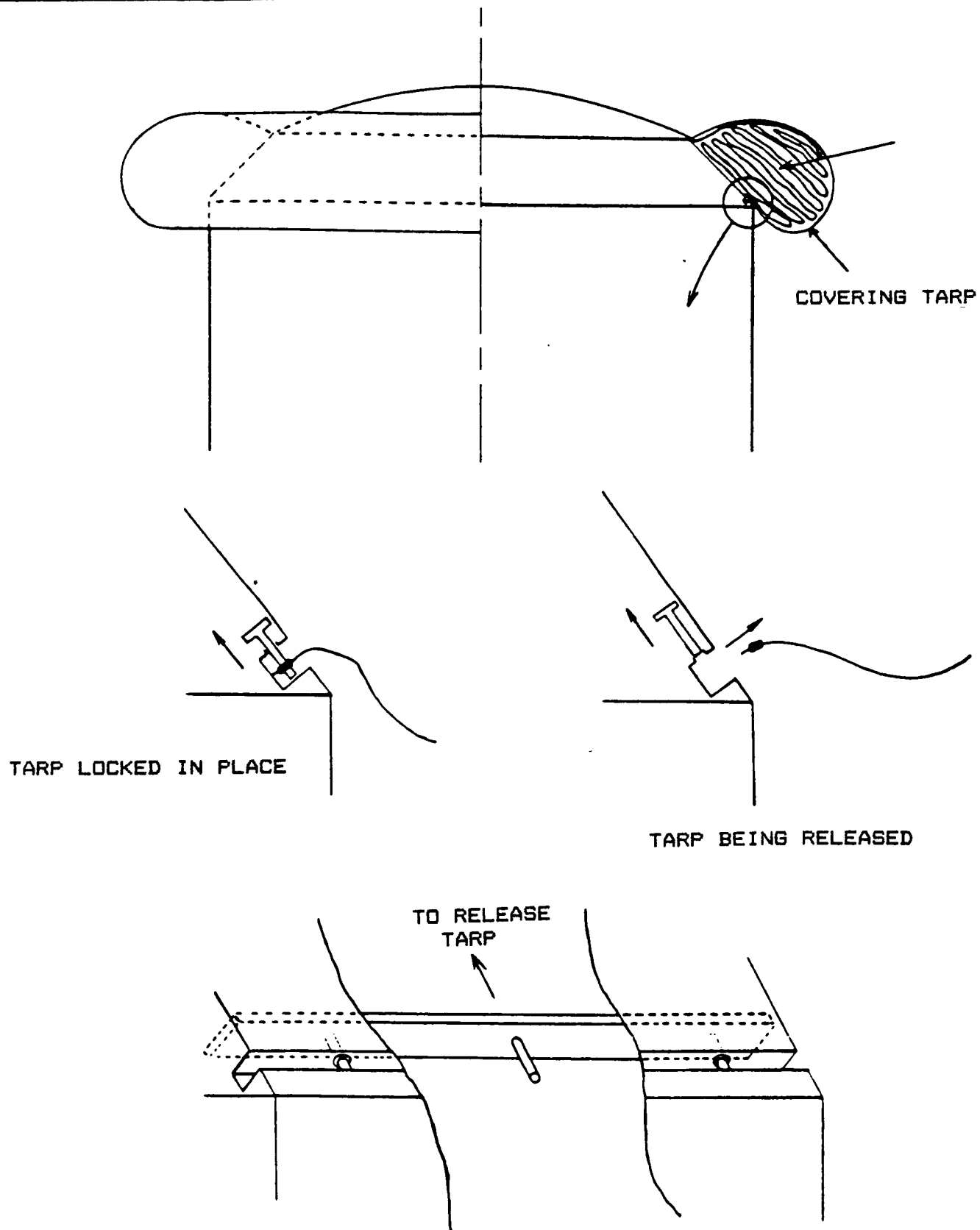
TO RELEASE
TARP

FIGURE 8.29 - COVERING TARP AND RELEASE

MALE-FEMALE LOCKS

PAYLOAD

SHIP

CAP

N$_2$ JACK

GUIDANCE TRACKS
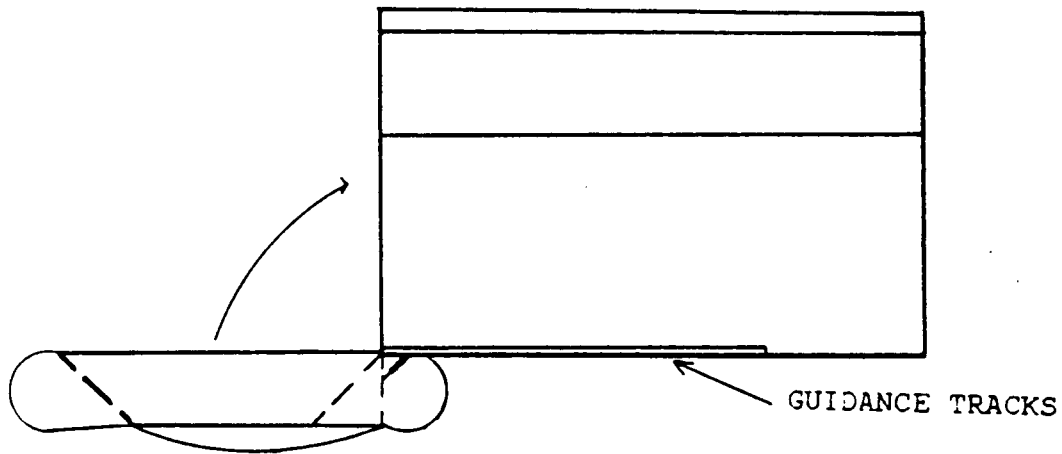
CAP LOCKED
INTO PLACE

N2 JACK

FIGURE 8.30 - CAP POSITIONING SEQUENCE
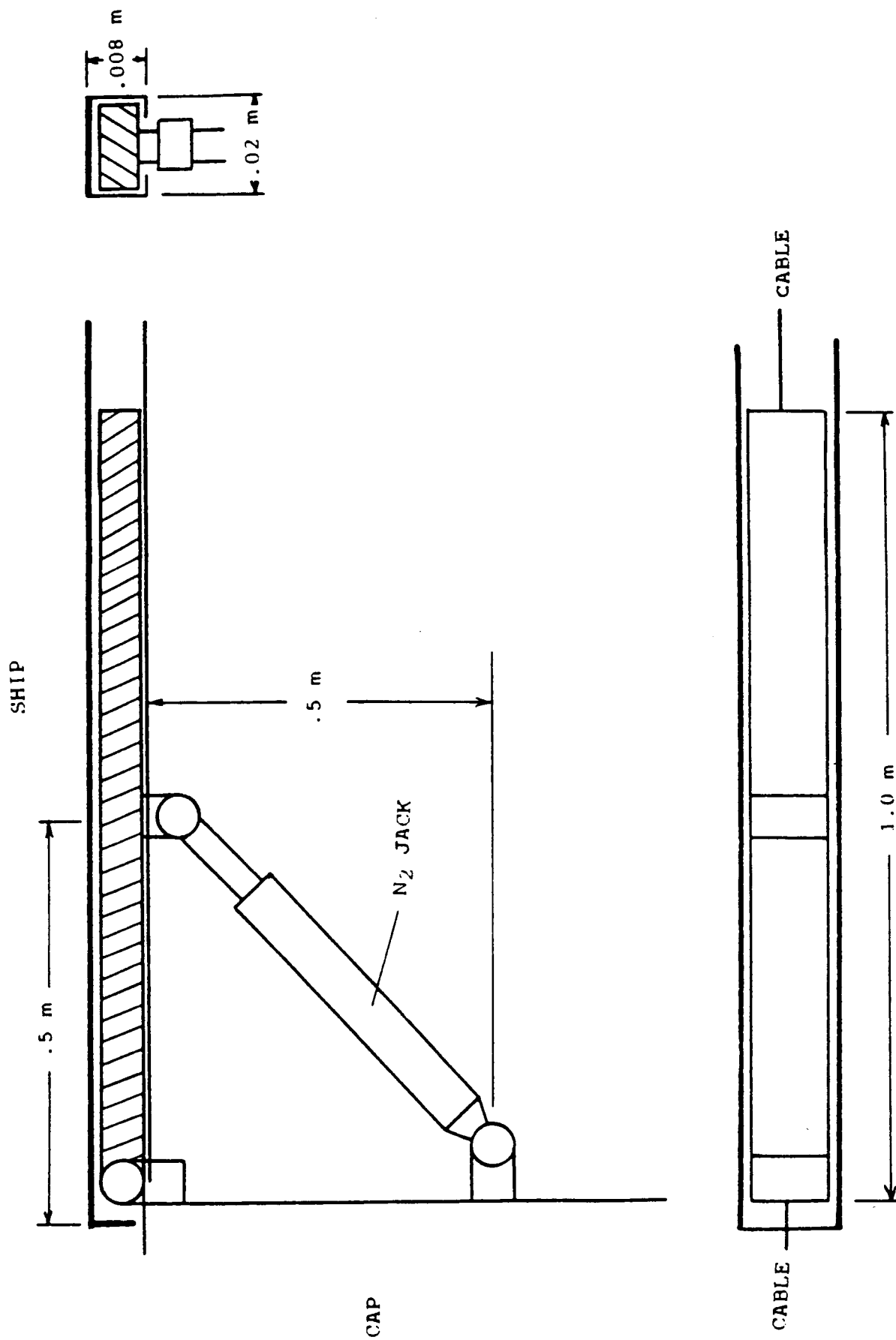
FIGURE 8.31 - MECHANISM FOR SLIDING CAP

BLEED VALVE
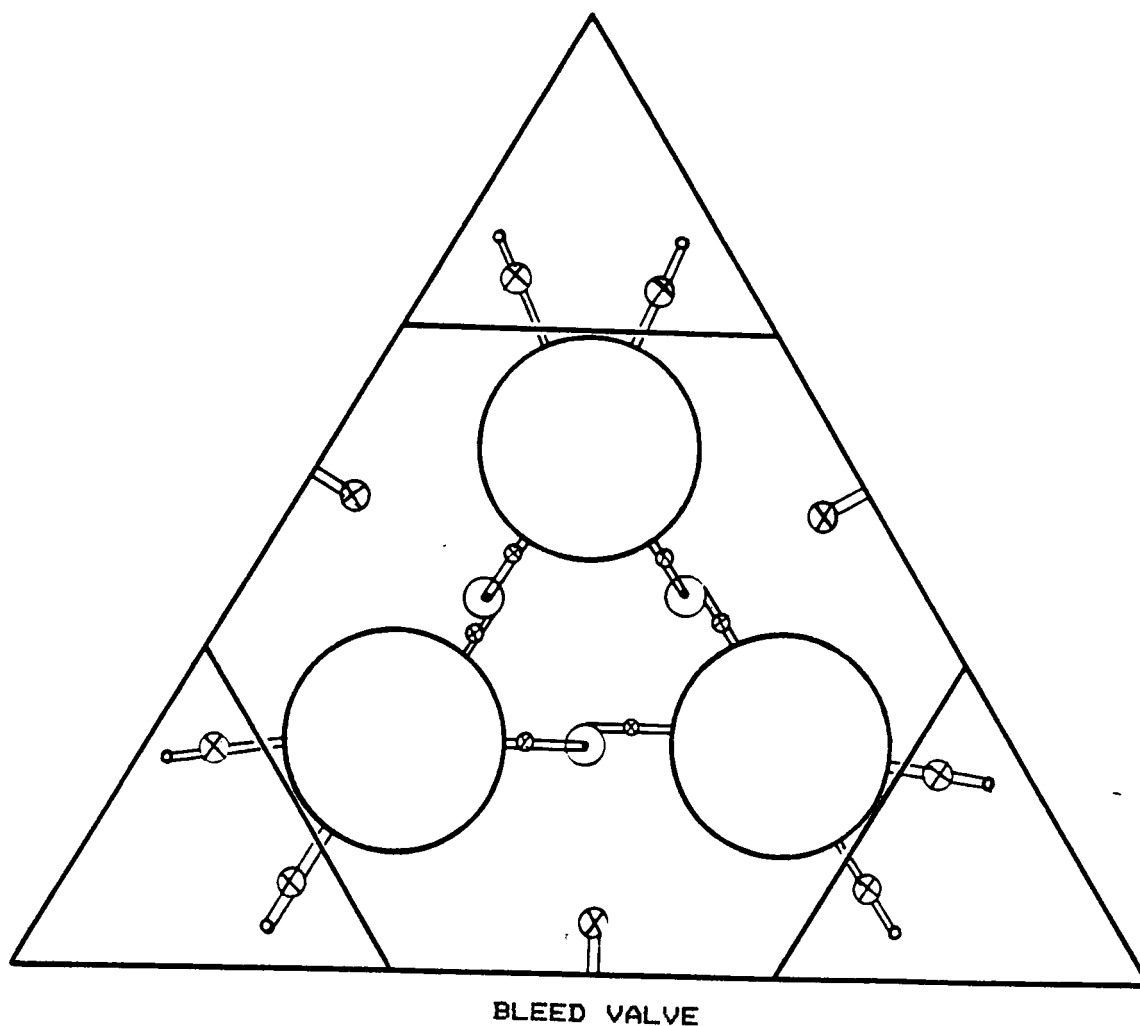
⊗ VALVES: - ONE PLACED AT START OF PIPE

          - ONE PLACED AT END OF PIPE

          - 2 WAY PUMP

o   - CONNECTION TO BALLUTE

FIGURE 8.32   VALVE AND PUMP SYSTEM FOR N2 TANKS

179

8.8 REFERENCES

1. Boeing. <u>Orbital Transfer Vehicle Concept Definition and System Analysis Study.</u> D180-29108-2-2. Vol. 2, Book 2. Seattle, Washington: 1986.

2. Boeing. D180-29108-2-3

3. Brauer, G.L. <u>Final Report Program to Optimize Simulated Trajectories (POST)</u>. Martin Marietta Corporation.

4. Collins, J.A. <u>Failure of Materials in Mechanical Design.</u> New York: John Wiley and Sons, 1981

5. Dieter, George E. <u>Mechanical Metallurgy</u>. New York: McGraw-Hill Inc., 1986.

6. Holman, J.P. <u>Heat Transfer</u>. New York: McGraw-Hill, Inc., 1986.

7. Jones, G.R., GRuszczynski, M.J., Whitehead, K.D. <u>Design Parameters and Environmental Considerations for a Reusable Aeroassisterd Orbital Transfer Vehicle</u>. Thermal Control General Dynamics Space Systems Division. San Diego, CA.

8. Jones, Robert M. <u>Mechanics of Composite Materials</u>. New York: Hemisphere Publishing Corporation, 1975.

9. Leiser, Daniel B., Smith, Marnell and Stewart, David A. <u>Options for Improving Rigidized Ceramic Heatshields</u>. NASA Ames Research Center. Moffett Field, CA.

10. Menees, Gene P. et al. <u>Aerothermodynamic Heating Analysis of Aerobraking and Aeromaneuvering Orbital Transfer Vehicles</u>.

11. Park, Chul. <u>Theory of Idealized Two-Dimensional Ballute in Newtonian Hypersonic Flow</u>. AIAA-86-0301. AIAA 24th Aerospace Sciences Meeting. Reno, Nevada: 19866.

12. Savage, R.T., Love, W., Bloetscher, F. <u>High Temperature Performance of Flexible Thermal Protection Materials.</u> NASA Ames Research Center. Moffett Field, CA.

9. ELECTRICAL POWER SYSTEM

Electrical power requirements for the LOTV are listed in Table 9.1. Two main types of power sources were considered: photovoltaic cells and fuel cells.

The photovoltaic cells were too unwieldy and restrictive. They produce only 40 W of electrical power per square meter of solar panel. For the required total power of 4.57 kW, the size of the solar array would be approximately 115 m^2. In addition, accomodations must be made to ensure that the panels are positioned properly to receive the sunlight.

A fuel cell, however, operates by exchanging chemical energy of a fuel and oxidant to electrical energy. Hydrogen is commonly used as the fuel, and since hydrogen is already being carried on the LOTV, it would be convenient to store this with the fuel for the main engine. Also, the oxygen can be stored with the oxygen for the RCS system.

Presently, the Allis-Chalmers 5 kW hydrogen-oxygen fuel cell produces enough power for both the non-aerobraked and aerobraked versions of the LOTV, and has been tested for over 2,000 hours without failure. Its dimensions are .28mx.92mx.31m; its mass is 68 kg, and it consumes approximately 250 kg of hydrogen during the trip.

However, this is just an example to show the feasibility of using a fuel cell. Fuel cell technology is growing rapidly. In the near future, a 5 kW fuel cell is projected to have a mass of 25 kg and a volume of .028 m^3 as compared to .080 m^3 for the above Allis-Chalmers fuel cell (Reference 9.3).

Table 9.1 LOTV Electrical Power Requirements

Component	Power
Turbopump start-up	2700 W
Gyros	1200 W
Computer	200 W
Communication system	100 W
Pointing/Tracking system	300 W
Turntable	20 W
Optical train	50 W
Total power (All-propulsive LOTV)	4570 W

ADDITIONAL AEROBRAKE REQUIREMENTS

3 Liquid Nitrogen Pumps	74.6 W each
Cap Positioning Motor	4.8 W
3 Tarp Release Mechanisms	1.0 W each
9 Valve Controls	1.5 W each
Sensors	5.0 W
Total additional aerobraked power	250 W

Total Power (Aerobraked LOTV)	4820 W

MASSES:

Fuel Cell	30 kg
Power Distribution and Regulation	20 kg
Total	50 kg

9.2 REFERENCES

1. Angrist, Stanley W.; Direct Energy Conversion, Fourth Ed.; Allyn and Bacon, Inc., 1982

2. Bockris and Srinivasan; Fuel Cells, McGraw-Hill Book Company, 1969

3. Williams, K. R.; An Introduction to Fuel Cells, Elsevier Publishing Co., New York, 1966

10. LOTV LIFE CYCLE COST ANALYSIS

A life cycle cost model of the laser powered orbital transfer vehicle has been developed as a tool to evaluate the relative effectivenesses of the alternate LOTV configurations and mission scenarios. In the model development several assumptions were made concerning specific LOTV cost categories. While these assumptions may result in crude estimates of specific cost magnitudes, they were applied uniformly to the three LOTV configurations being developed and thus valid relative life cycle cost comparisons can be made between them. While it is desireable that the magnitudes of the various cost estimates be in the neighborhood of the actual cost magnitudes, a high degree of cost magnitude accuracy is not required for the comparative nature of this analysis. In the complete analysis the three alternate LOTV configurations, (non-aerobraked-LEO-GEO, aerobraked-LEO-GEO, aerobraked-LEO-LLO), are compared on a life cycle cost basis for mission frequencies of five and ten per year and earth to LEO transportation costs of $1500/lbm, $500/lbm and $150/lbm. The results of the cost analysis for five missions per year are not presented here as the trends exhibited are identical to those for the ten mission per year case. The complete LOTV life cycle cost analysis may be found in reference 3.

10.1 LOTV LIFE CYCLE COST ASSUMPTIONS

The basic assumptions applied to the LOTV life cycle cost analysis are as follows:

1) All costs are reported in millions of current dollars.
2) One LOTV replacement component fails for every two missions.
3) The cost of astronaut labor in orbit, at the space station is $100,000 per hour in the extravehicular activity (EVA) mode and $25,000 per hour in the intravehicular activity (IVA) mode.
4) The LOTV is assumed to have a usefull operational life of twenty years.
5) The life cycle cost analysis is performed for of five and ten LOTV missions per year.
6) LOTV overhauls are performed once every 20 missions for the aerobrake configurations and once every 30 missions for the non-aerobrake configuration.
7) The LOTV life cycle cost analysis is performed for transportation costs, (from earth to low earth orbit), of $1500/lbm, $500/lbm and $150/lbm.
8) The average LOTV replacement (repair) module has a mass of 50 lbm and a cost of $310,000.
9) There are 25 unique replacement module types and four of each type will be initially procured and delivered to the space station for storage and use.
10) The LOTV will have no salvage value at the end of its 20 year life.

10.2 LOTV COST CATEGORIES

In this analysis, all costs can be grouped into two general categories; intital acquisition and deployment costs and operation and support costs. The LOTV cost breakdown structure shown in figure 10.1 forms the basis for the life cycle cost analysis.

10.2.1 ACQUISITION AND DEPLOYMENT COSTS

The LOTV acquisition and deployment costs as shown in figure 10.1 are divided into the following sub-categories:

1) LOTV subsystem unit costs (UC).
2) LOTV subsystem design, development, test and evaluation costs (DDTEC).
3) Ground support equipment costs (GSEC).
4) Systems engineering and integration costs for the DDTE phase of the LOTV development proces, (SEIC).
5) Pro.ram management costs for the DDTE phase (PMC).
6) Installation, checkout and assembly cost for the DDTE phase (ICAC).
7) Systems engineering and integration cost for the production phase (SEIP).
8) Program management cost for the production phase (PMCP).
9) Cost of orbital support equipment at the space station (OSEC).
10) Cost of initial LOTV delivery to low earth orbit (IDC).
11) Cost of initial LOTV assembly and checkout at the space station (IACC).
12) Cost of intial LOTV spares at the space station (ISC).

Thus the total initial LOTV acquisition and deployment cost (TADC) is given by:

$$TADC = UC + DDTEC + GSEC + SEIC + PMC + ICAC + SEIP + PMCP + \\ + OSEC + IDC + IACC + ISC$$

183
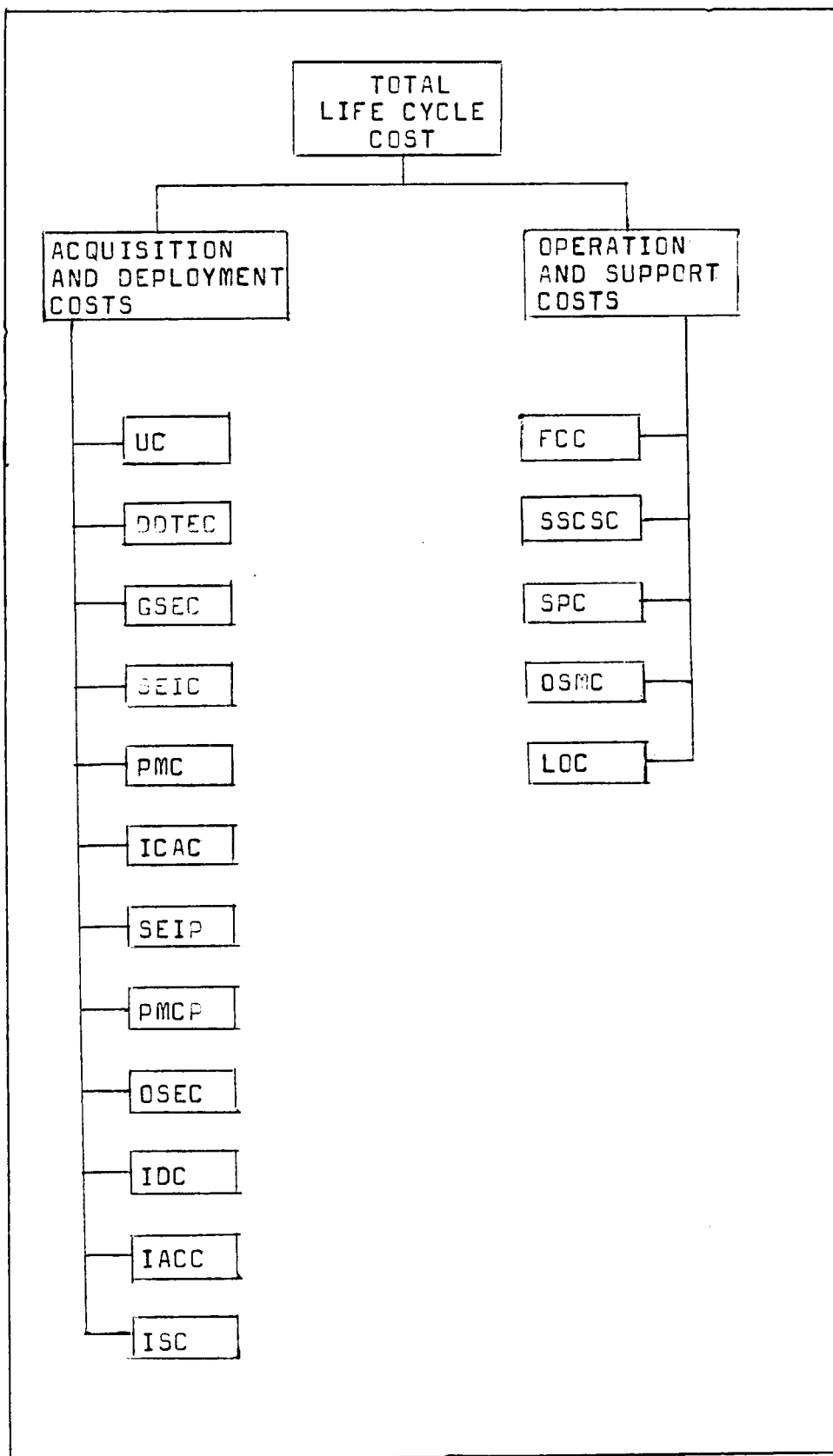
Figure 10.1   LOTV cost breakdown structure.

10.2.2 OPERATION AND SUPPORT COSTS

As shown in figure 10.1 the operation and support costs are divided into the following sub-categories.

1) Cost of fuel and cryogens, including cost of transport to LEO (FCC).
2) Cost of space station crew support and labor (SSCSC).
3) Spare parts repair and repalcement costs (SPC).
4) Cost of operations and support administrative management (OSMC).
5) Cost of LOTV overhauls (LOC).

Thus the the total operation and support costs (TOSC) without including the time value of money is:

$$TOSC = FCC + SSCSLC + SPRRC + OSAMC + LOC$$

10.3 ESTIMATION OF SUB-COST CATEGORIES

Now that the LOTV cost breakdown structure has been defined, it remains to develop cost estimates for each of the sub-categories.

10.3.1 UNIT, DESIGN, DEVELOPMENT, TEST AND EVALUATION COSTS

Cost estimating relationships (CER's) obtained from references 1 and 2 were used to calculate estimates for the unit or material cost (UC) and the design, development, test and evaluation costs (DDTEC) for each of the eleven LOTV subsystems. The CER's have the form of linear and nonlinear regression equations and were developed based on subsystem costs for past spacecraft programs. The CER's for each LOTV subsystem are as follows:

1) **LOTV Structures and Mechanisms:** This includes the main LOTV hull truss, end fittings, optical turntable and truss, mirror arm, docking mechanism and the detachable payload module. The cost estimating relationships (CER's) for this subsystem are:

$$UC = 0.064 \times STRUC^{0.545}$$
$$DDTEC = 0.821 \times STRUC^{0.437}$$

Where STRUC is the mass of the structures and mechanisms in pounds mass.

2) **Thermal Control Subsystem:** This subsystem rejects LOTV waste heat into the vacuum of space. The CER's for this subsystem are:

$$UC = 0.064 \times THERM^{0.545}$$
$$DDTEC = 0.821 \times THERM^{0.437}$$

Where THERM is the mass of the thermal control subsystem in pounds mass.

3) **Propulsion Subsystem:** This subsystem includes all propellant tanks, fuel lines and pumps and the reaction control subsystem. It does not include the LOTV main engine. The CER's for this subsystem are:

$$UC = 0.43 \times PROP^{0.494}$$
$$DDTEC = 1.668 + 0.126 \times PROP$$

Where PROP is the mass of the propulsion subsystem in pounds mass.

4) **Electric Power Subsystem:** This subsystem includes all electric power generating, storage, distribution and regulation equipment. The CER's for this subsystem are:

$$UC = 0.042 \times EPS^{0.0784}$$
$$DDTEC = 0.597 \times EPS^{0.584}$$

Where EPS is the mass of the electric power subsystem in pounds mass.

5) Guidance Navigation and Control Subsystem: This subsystem interfaces with the reaction control subsystem and the control moment gyros to provide instructions for LOTV translation, rotation and stabilization in orbit. The CER's for this subsystem are:

$$UC = 0.5763 \times GNC^{0.494}$$
$$DDTEC = 3.08 \times GNC^{0.516}$$

Where GNC is the mass of the guidance, navigation and control subsystem in pounds mass.

6) Data Management and Communications Subsystem: This subsystem processes information on the LOTV, stores and transmits data to earth and the space station and receives and executes commands from earth and the space station. The CER's for this subsystem are:

$$UC = 0.053 \times DMC^{0.917}$$
$$DDTEC = 0.615 \times DMC^{0.653}$$

Where DMC is the mass of the data management and control subsystem in pounds mass.

7) LOTV Aerobrake: Two of the proposed LOTV configurations make use of an aerobrake to decelerate in the earth's upper atmosphere for insertion into low earth orbit (LEO) after descending from geosynchronous orbit (GEO). There is both a rigid permenant structure and an inflatable ballute which is disposed of after each mission. The costs for each aerobrake part are calculated seperately as the cost of the disposable ballute is required when calculating the LOTV operating costs. The CER's for the aerobrake are:

$$UC = 0.064 \times ABRK^{0.545}$$
$$DDTEC = 0.821 \times ABRK^{0.437}$$

Where ABRK is the mass of the aerobrake in pounds mass.

8) Laser Powered Main Engine: This is the LOTV main engine which is powered by a laser beam transmitted from a large solar pumped laser station orbiting at 3984 miles altitude. The laser beam is focused into the engine plasma chamber by means of the optical subsystem. In the plasma chamber hydrogen is heated and then expanded through a nozzle to produce thrust. The CER's for the laser powered engine are:

$$UC = 1.963 + 0.000103 \times THRUST$$
$$DDTEC = 306.25 + 0.0029 \times THRUST$$

Where THRUST is the maximum propulsive force produced by the engine in pounds force.

9) Primary Mirror: This is the large mirror that captures the laser beam from the solar pumped laser station and redirects it to the secondary mirrors for focusing into the main engine plasma chamber. For the aerobraked configurations the mirror is foldable for storage during the aerobrake manuever. The mirror for the non- aerobraked configuration is fixed and rigid. The CER's for both mirror types are:

Non-Aerobrake Configuration
$$UC = 0.064 \times PM^{0.545}$$
$$DDTEC = 0.821 \times PM^{0.437}$$

Aerobrake Configurations
$$UC = 0.064 \times PM^{0.545}$$
$$DDTEC = 1.642 \times PM^{0.437}$$

Where PM is the mass of the primary mirror in pounds mass.

10) **Secondary Mirrors:** There are three secondary mirrors which consecutively receive the laser beam from the primary mirror and redirect and refocus it into the main engine plasma chamber. The CER's for the secondary mirrors are:

$$UC = 0.01 \ x \ SM$$
$$DDTEC = 0.04 \ x \ SM$$

Where SM is the mass of the secondary mirrors in pounds mass.

11) **Control Moment Gyros (CMG):** These are massive gyroscopes each spinning around one of the LOTV's three directional axes. They are used to control the LOTV's orientation during orbital operations. The CER's for the CMG's are:

$$UC = 0.00667 \ x \ CMG$$
$$DDTEC = 0.0267 \ x \ CMG$$

To obtain the unit and DDTE costs for the entire LOTV, the respective UC and DDTEC values for each LOTV subsystem are summed.

10.3.2 COST OF INITIAL LOTV DELIVERY TO LEO (IDC)

This sub-category cost is obtained by multiplying the total LOTV dry mass (in lbm) by the respective costs of transport ($1500/lbm, $500/lbm or $150/lbm) from earth to low earth orbit (LEO).

10.3.3 GROUND SUPPORT EQUIPMENT COST (GSEC)

This category includes facilities for processing, repairing and storing spare parts for return to the space station. It also includes ground tracking and communications facilities, launch center processing facilities and all of the associated management, operations and support personnel. This cost is assumed to be equal to ten percent of the total LOTV DDTE cost or:

$$GSEC = 0.1 \ x \ DDTEC_{total}$$

10.3.4 SYSTEMS ENGINEERING AND INTEGRATION COST FOR THE DDTE PHASE (SEIC)

This cost is equal to ten percent of DDTEC and GSEC or:

$$SEIC = 0.1 \ x \ (DDTEC_{total} + GSEC)$$

10.3.5 PROGRAM MANAGEMENT COSTS FOR THE DDTE PHASE (PMC)
This cost is equal to five percent of DDTEC, GSEC and SEIC or:

$$PMC = 0.05 \ x \ (DDTEC_{total} + GSEC + SEIC)$$

10.3.6 INSTALLATION, CHECKOUT AND ASSEMBLY COST FOR THE DDTE PHASE (ICAC)
This cost is equal to twenty percent of the total LOTV unit cost or:

$$ICAC = 0.2 \ x \ UC_{total}$$

10.3.7 SYSTEMS ENGINEERING AND INTEGRATION COST IN THE PRODUCTION PHASE (SEIP)
This cost is equal to ten percent of UC and ICAC or:

$$SEIP = 0.1 \ x \ (UC_{total} + ICAC)$$

10.3.8 PROGRAM MANAGEMENT COSTS FOR PRODUCTION (PMPC)
This cost is equal to five percent of UC, ICAC and SEIP or:

$$PMPC = 0.05 \ x \ (UC_{total} + ICAC + SEIP)$$

10.3.9 ORBITAL SUPPORT EQUIPMENT COST (OSEC)

This category includes a servicing and docking bay for the LOTV, refueling equipment, test and servicing tools and equipment and spare parts storage facilities. This cost is equal to ten percent of UC, DDTEC and IDC or:

$$OSEC = 0.1 \ x \ (UC_{total} + DDTEC_{total} + IDC)$$

10.3.10 COST OF INITIAL LOTV ASSEMBLY AND CHECKOUT AT THE SPACE STATION (IACC)

This cost is calculated on the basis of the number of astronaut IVA and EVA labor hours required for LOTV assembly at the space station. Where the cost of astronaut IVA and EVA time is given in the assumptions section. The estimated IVA and EVA labor hours required for each LOTV configuration are as follows:

Non-Aerobrake - LEO-GEO
IVA - 200 hours
EVA - 300 hours
Aerobrake - LEO-GEO
IVA - 250 hours
EVA - 350 hours
Aerobrake - LEO-LLO
IVA - 300 hours
EVA - 400 hours

10.3.11 COST OF INITIAL LOTV SPARE COMPONENTS AT THE SPACE STATION (ISC)

This cost is calculated based on the previously stated assumptions that the average LOTV replacement component has a mass of 50 lbm and has a unit cost of $310,000. It was also stated that there are 25 unique replacement component types and that four of each type would be initially procured for delivery to the space station. Thus the total cost of the initial spares is the sum of the number of initial spares procured multiplied by the average unit cost of a spare plus the cost of delivering the initial spares to the space station.

10.3.12 COST OF FUEL AND CRYOGENS (FCC)

The fuel and cryogen costs are calculated on a per mission basis and then multiplied by the number of missions per year to obtain the yearly cost of fuel and cryogens. This cost consists of the cost of transporting the fuel and cryogens to LEO plus the material costs. The costs of transport to LEO are as stated in the assumptions section and the material cost of the fuel and cryogens is assumed to be $5/lbm.

10.3.13 SPACE STATION CREW SUPPORT COSTS (SSCSC)

This cost is based on the number of EVA and IVA astronaut manhours required at the space station to support each LOTV mission. This includes scheduled and uscheduled maintenance activities, refueling activities, spare parts and inventory management and space station crew monitoring of the LOTV during missions. The required numbers of EVA and IVA manhours per mission for the three alternate LOTV configurations are as follows:

Non-Aerobrake - LEO-GEO
EVA - 50 hours
IVA - 100 hours
Aerobrake - LEO-GEO
EVA - 60 hours
IVA - 120 hours
Aerobrake - LEO-LLO
EVA - 70 hours
IVA - 130 hours

Where the cost of EVA and IVA labor is as stated in the assumptions section.

10.3.14 SPARE PARTS COST (SPC)

Once every two LOTV missions a spare part replacement will be required due to component failures. It is assumed that the failed part will be returned to earth for repair and that the cost of

repair will be equal to the unit cost of the part. Thus the spares cost every two LOTV missions will equal the average spare unit cost plus the cost of redelivering the spare to the space station for reuse.

10.3.15 LOTV OVERHAUL COSTS (OC)

One LOTV overhaul will be performed every 30 missions for the non-aerobrake configuration and once every 20 missions for the aerobrake configurations. The aerobrake configurations require more frequent overhauls due to the fact that they are subjected to more severe thermal and mechanical stresses during the aerobrake maneuvers. The cost of an LOTV overhaul is equal to five percent of the initial LOTV unit, DDTE and deployment costs or:

$$OC = 0.05 \times (UC_{total} + DDTEC_{total} + IDC)$$

10.4 CALCULATIONS

All calculations performed in the life cycle cost analysis were carried out in tabular form using the Super Calc III spreadsheet software package and are contained in appendix D of this report. The Super Calc III graphics capability was used to generate the life cycle cost graphs that appear in this report.

The LOTV unit and design, development, test and evaluation costs are calculated for all three LOTV configurations in tables 10.1 through 10.3 These costs were calculated using the cost estimating relationships presented in section 10.3.1.

The total initial LOTV acquisition and deployment costs are calculated in tables 10.4 to 10.6. The calculations show that the non-aerobrake, LEO-GEO LOTV configuration has the lowest initial acquisition cost, that the aerobrake, LEO-LLO configuration has the highest cost and that the aerobrake, LEO-GEO is about $15 million more expensive to acquire and deploy than the non-aerobrake configuration.

The operation and support costs for all three LOTV configurations are calculated in tables 10.7 through 10.9 assuming an earth to LEO transportation cost of $1500/lbm. The operation and support costs are recalculated in tables 10.10 through 10.12, this time assuming an earth to LEO cost of $500/lbm. Finally the operation and support costs are calculated in tables 10.13 through 10.15 assuming an earth to LEO transportation cost of $150/lbm.

A summary of the over-all life cycle cost calculations for the three LOTV configurations for ten missions per year, assuming an earth to LEO transportation cost of $1500/lbm, is contained in table 10.16. The life cycle costs for the three configurations are recalculated in table 10.17 for ten missions per year, this time assuming an earth to LEO transportation cost of $500/lbm. Finally, in table 10.18 the life cycle costs for the three configuration are calculated for ten missions per year assuming an earth to LEO cost of $150/lbm.

10.5 RESULTS AND DISCUSSION

As shown in figures 10.2 and 10.3, the aerobrake, LEO-GEO LOTV configuration has the lowest life cycle cost of the three LOTV configurations, assuming a $1500/lbm earth to LEO transportation cost. This is true even though the aerobrake configuration disposes of its ballute after every mission and the fact that its initial acquisition and deployment costs are higher than those for the non-aerobrake configuration. Thus it is apparent that the difference in life cycle costs is due to the operation and support costs. Closer inspection of the operation and support costs for the two LEO-GEO configurations shows that the aerobrake configuration has fuel and cryogen costs that are 30% lower than the fuel and cryogen cost for the non-aerobrake configuration.

It is not meaningful to compare the life cycle cost of the LEO-LLO configuration with those for the two LEO-GEO configurations because of its different and more advanced mission capabilities. However, as expected it has a significantly greater life cycle cost than either of the LEO-GEO vehicle configurations. It should also be noted that the non-aerobrake, LEO-GEO, LOTV configuration and the aerobrake, LEO-GEO, LOTV configuration have the same mission objectives and cababilities and thus life cycle cost comparisons between them are meaningful.

Closer inspection of the LOTV life cycle cost categories shows that the largest cost cotributor for all three configurations is the cost of transportation from earth to LEO. Fortunately this cost category has a high potential for reduction in the near future. The current generation of launch vehicles can launch objects into low earth orbit for a cost of $1500/lbm. It is projected that this cost may be recuded by as much as one third with the next generation of launch vehicles and by as much as one tenth when the National Aerospace Plane becomes operational. Thus life cycle cost analyses are also performed for the three LOTV configuration for earth to LEO transportation costs of $500/lbm and $150/lbm.

Figures 10.4 and 10.5 show that for an earth to LEO transportation cost of $500/lbm, the aerobrake configuration is still the prefered option for the LEO-GEO mission scenario by virtue of its lower life cycle cost. However the difference between the life cycle costs for the aerobrake and non-aerobrake configurations has decreased.

Figures 10.6 and 10.7 show that for an earth to LEO transportation cost of $150/lbm the non-aerobrake configuration becomes the perfered option for the LEO-GEO mission scenario for both five and ten missions per year, based on its lower life cycle cost. Thus as the cost of transportation from earth to LEO decreases the cost advantage of the aerobrake configuration decreases for the LEO-GEO mission until at some point between $500/lbm and $150/lbm the non-aerobrake configuration becomes the lowest life cycle cost option.

10.6 CONCLUSIONS
For the current earth to LEO transportation cost of $1500/lbm the aerobrake LOTV configuration is clearly prefered, on a life cycle cost basis, over the non-aerobrake configuration for the LEO-GEO mission scenario. This is almost completely due its 30% savings in fuel transportation costs. However as the cost of transport from earth to LEO decreases (in the future), the cost advantages of the aerobrake cofiguration begin to diminish until at some point between $500/lbm and $150/lbm for earth to LEO transportation, the non-aerobrake configuration becomes the perfered LOTV configuration for the LEO-GEO mission scenario, based on its lower life cycle cost.

Discounted Life Cycle Cost (i=10%)
(10 missions per year)

Legend:
- Non-Aero (LEO-GEO)
- Aerobrake (LEO-GEO)
- Aerobrake (LEO-LLO)

9454.32

7600.29

6299.20

Figure 10.2 Discounted life cycle cost for 10 missions/year and a transport cost of $1500/lbm.

Cumm. Discounted Life Cycle Cost (i=10%)
(10 missions per year)

Legend:
- Non-Aero (LEO-GEO)
- Aerobrake (LEO-GEO)
- Aerobrake (LEO-LLO)

Figure 10.3 Cumulative life cycle cost for 10 missions/year and a transport cost of $1500/lbm.

191

Discounted Life Cycle Cost (i=10%)
(10 missions per year)

ORIGINAL PAGE IS OF POOR QUALITY

Legend:
- Non-Aero (LEO-GEO)
- Aerobrake (LEO-GEO)
- Aerobrake (LEO-LLO)

3854.32 — 3677.02 — 5146.45

Figure 10.4 Discounted life cycle cost for 10 missions/year and a transport cost of $500/lbm.

Cumm. Discounted Life Cycle Cost (i=10%)
(10 missions per year)

Legend:
- Non-Aero (LEO-GEO)
- Aerobrake (LEO-GEO)
- Aerobrake (LEO-LLO)

Figure 10.5 Cummulative life cycle cost for 10 missions/year and a transport cost of $500/lbm.

Discounted Life Cycle Cost (i=10%)
(10 missions per year)

Legend:
- Non-Aero (LEO–GEO)
- Aerobrake (LEO–GEO)
- Aerobrake (LEO–LLO)

Values shown: 2543.23, 2759.26, 3638.70

Figure 10.6 Discounted life cycle cost for 10 missions/year and a transport cost of $150/lbm.

Cumm. Discounted Life Cycle Cost (i=10%)
(10 missions per year)

Legend:
- Non-Aero (LEO–GEO)
- Aerobrake (LEO–GEO)
- Aerobrake (LEO–LLO)

Figure 10.7 Cumulative life cycle cost for 10 missions/year and a transport cost of $150/lbm.

193

REFERENCES

1) Cathcart, J.A., Et. Al., **Advanced Orbit Transfer Vehicle Propulsion System Study**, Martin Marietta Aerospace, Denver, CO, February 1985.

2) DeYoung, R.H., Et. Al., **Preliminary Design and Cost of a 1-Megawatt Solar-Pumped Iodide Laser Space to Space Transmission Station**, NASA Technical Memorandum 4002, Langley Research Center, Hampton, VA, September 1987.

3) Boyer, D.J., **Case Study of Life Cycle Engineering in Aerospace Design Education**, Final Project Report at Virginia Polytechnic Institute and State University, May 1988.

11. DESIGN SUMMARY/CONCLUDING REMARKS

This report presents a conceptual design study of laser-powered orbital transfer vehicles to be used for transfering cargo between LEO and either GEO or LLO. The starting date for the operation of the LOTV is assumed to be the early twenty-first century.

During the design process it was decided to develop three versions of the LOTV: an aerobraked and a non-aerobraked version for the LEO/GEO scenario and an aerobraked version for the LEO/LLO scenario. Concentration was, however, placed on the LEO/GEO scenarios, with only some initial calculations made for the LEO/LLO scenario. All three versions will use similar propulsion systems for which energy will be supplied by a direct solar pumped iodide laser orbiting at an altitude of one Earth radius. For the LEO/LLO scenario a second laser located on the Moon's surface will be available. The laser beam, which will be captured and redirected by way of a four mirror optical system, will create seven plasmas in the thrust chamber, which in turn convert the laser beam energy into thermal energy to produce thrust.

The major considerations that were kept in mind throughout the design process were to maximize the ratios of the payload mass to the propellant mass and to the dry vehicle mass, to design the LOTV to be flexible in cargo and fuel capacity, to be reusable and reliable, and to keep the LOTV at reasonable costs. Furthermore, the purpose of designing both a non-aerobraked version and an aerobraked version for the LEO/GEO scenario was to compare the two and find out which one is more economical.

The key design and performance characteristics of the two workable designs of the LOTV are listed in tables 11.1 and 11.2. Results of this study indicate that the LOTV is a very attractive candidate for cargo transportation around the Earth and in an Earth-Moon system. With laser propulsion, the payload mass ratio values are at least twice as high as with the baseline chemical propulsion system. The life cycle cost analysis shows that the aerobraked configuration may have an economic advantage over the all-propulsive one as long as the cost of the propellant launching to LEO is higher than about $500/kg in current dollars.

11.1 FUTURE RECOMMENDATIONS

Although many aspects of the LOTV were considered and studied in this conceptual design, some were not investigated to the depth that they should have been due to time limitations, and others could not be solved with present technology. Before the LOTV can become a viable choice for development, however, these aspects must be carefully researched and evaluated. Some of the aspects which received only cursory attention include a heat rejection system, data management and communication systems, a vibrational analysis, the effects of folding and unfolding on the reflective

material of the wrap-rib mirror, and the gimballing of the laser engine nozzle.

The main technical problems associated with the laser propulsion seem to be: (a) thermal control of the laser engine window to prevent material fracture due to thermal shock, (b) improving the laser-to-jet energy conversion efficiency by minimizing reradiation from the plasmas, and (c) tracking accuracy over distances greater than about 50000 km. It is expected that these problems will be fully overcome by the end of this century.

Although all aspects were not studied, a large amount of information was covered, revealing that the LOTV is a very attractive candidate for transporting cargo between orbits and thereby justifying a continued design effort to make laser propulsion a reality.

Table 11.1 Characteristics of the All-Propulsive LOTV

Characteristic	Standard Option	All-Return Option
Propulsion:		
Overall efficiency of the optical train	92.5%	92.5%
Thermal conversion efficiency	50%	50%
Specific impulse	1500 sec	1500 sec
Propellant flow rate	0.136 kg/s	0.136 kg/s
Thrust	2000 N	2000 N
Masses:		
Vehicle dry mass, M_s	3855 kg	4065 kg
LEO-to-GEO payload, $M_{pl\uparrow}$	16000 kg	16000 kg
GEO-to-LEO payload, $M_{pl\downarrow}$	5000 kg	16000 kg
Initial propellant at LEO (for round trip, including RCS and reserve)	14000 kg	20200 kg
Overall initial mass	33855 kg	40265 kg
Initial propellant at GEO (for (return trip)	3750 kg	8000 kg
Propellant used for LEO-GEO leg $M_{p\uparrow}$	9600 kg	11500 kg
Propellant used for GEO-LEO leg $M_{p\downarrow}$	3350 kg	7500 kg
Inital mass at GEO	12605 kg	28065 kg
Performance:		
No. of spirals on LEO-GEO leg	20	26
LEO-to-GEO trip time	6.4 days	9 days
GEO-to-LEO trip time	5 days	7 days
LEO-to-GEO payload mass ratio, $M_{pl\uparrow}/(M_{p\uparrow} + M_s)$	1.19	1.03
GEO-to-LEO payload mass ratio, $M_{pl\downarrow}/(M_{p\downarrow} + M_s)$	0.69	1.38
Overall structural coefficient, $M_s/(M_{p\uparrow\downarrow} + M_s)$	0.22	0.17

Table 11.2 Characteristics of the Aerobraked (LEO/GEO) LOTV

Characteristic	Standard Option	All-Return Option
Propulsion:		
Overall efficiency of the optical train	87.9%	87.9%
Thermal conversion efficiency	50%	50%
Specific impulse	1500 sec	1500 sec
Propellant flow rate	0.129 kg/s	0.129 kg/s
Thrust	1900 N	1900 N
Masses:		
Vehicle dry mass at LEO, $M_{S\uparrow}$	4843 kg	4971 kg
Vehicle dry mass at GEO, $M_{S\downarrow}$	4317 kg	4445 kg
LEO-to-GEO payload, $M_{pl\uparrow}$	16000 kg	16000 kg
GEO-to-LEO payload, $M_{pl\downarrow}$	5000 kg	16000 kg
Initial propellant at LEO (for round trip, including RCS and reserve)	12500 kg	16400 kg
Overall initial mass (LEO)	33443 kg	37371 kg
Initial propellant at GEO (for (return trip)	2400 kg	4800 kg
Propellant used for LEO-GEO leg $M_{p\uparrow}$	9700 kg	11000 kg
Propellant used for GEO-LEO leg $M_{p\downarrow}$	2000 kg	4300 kg
Inital mass at GEO	11717 kg	25245 kg
Performance:		
No. of spirals on LEO-GEO leg	21	
LEO-to-GEO trip time	7.5 days	
GEO-to-LEO trip time	1.5 days	
LEO-to-GEO payload mass ratio, $M_{pl\uparrow}/(M_{p\uparrow} + M_S)$	1.1	1.0
GEO-to-LEO payload mass ratio, $M_{pl\downarrow}/(M_{p\downarrow} + M_S)$	0.79	1.83

APPENDIX A. STRUCTURES CALCULATIONS

A.1 CENTER OF GRAVITY CALCULATIONS

The center of gravity in all the configurations was measured from a reference point on the bottom front of the ship along the centerline of the cross-section. Since the ships are all symmetric around the centerline of the cross-section, zbar is always zero except when the mirror is rotated to either side. The three following equations were used for these calculations.

(XBAR)*(TOTAL MASS)=SUM [(XBAR OF COMPONENT)*(MASS OF COMPONENT)]
(YBAR)*(TOTAL MASS)=SUM [(YBAR OF COMPONENT)*(MASS OF COMPONENT)]
(ZBAR)*(TOTAL MASS)=SUM [(ZBAR OF COMPONENT)*(MASS OF COMPONENT)]

The summation includes all components of the ship, along with everything else that adds mass to the ship for the loading being considered, such as payload.

A.2 MOMENTS OF INERTIA CALCULATIONS

The moments of inertia were calculated with x,y and z measured from the previously calculated center of gravity. Several of the components were assumed to be of a simplified shape, as noted in the main text. The moments of inertia used for these shapes are as follows.

    Slender Rod: Iy=Iz=1/12*(mass)*(length)*(length)
                    x measured along the length of the rod

    Thin Rectangular Plate: Ix=1/12*(mass)*(b*b+c*c)
                    Iy=1/12*(mass)*c*c
                    Iz=1/12*(mass)*b*b
                    x measured through thickness
                    b is dimension along y axis
                    c is dimension along z axis

    Rectangular Prism: Ix=1/12*(mass)*(b*b+c*c)
                    Iy=1/12*(mass)*(c*c+a*a)
                    Iz=1/12*(mass)*(a*a+b*b)
                    a is dimension along x axis
                    b is dimension along y axis
                    c is dimension along z axis

    Thin Disk: Ix=1/2*(mass)*(radius squared)
                    Iy=Iz=1/4*(mass)*(radius squared)
                    x measured through thickness

    Circular Cylinder: Ix=1/2*(mass)*a*a
                    Iy=Iz=1/12*(mass)*(3*a*a+length)
                    x measured along length
                    a is the radius

```
Circular Cone:  Ix=3/10*(mass)*a*a
                Iy=Iz=3/5*(mass)*(.25*a*a+h*h)
                x measured along centerline
                a is radius of base
                l is lenth of centerline

Sphere:         Ix=Iy=Iz=2/5*(mass)*a*a
                a is radius
```

These values were considered as Ixbar,Iybar and Izbar and used in the following equations.

```
                Ix=Ixbar+mass*(y*y+z*z)
                Iy=Iybar+mass*(x*x+z*z)
                Iz=Izbar+mass*(x*x+y*y)
```

Ix, Iy and Iz were found for each component of the ship and summed to get the final result.

APPENDIX B. OPTICS CALCULATIONS

B.1 OPTICAL SUPPORT STRUCTURE CALCULATIONS

B.1.1 Calculation of max allowable deflection:

$\triangle A < .1\% \times A$

$A = PI \times r^2 = (3.14) \times (.5)^2$
$A = .7854$ sq m
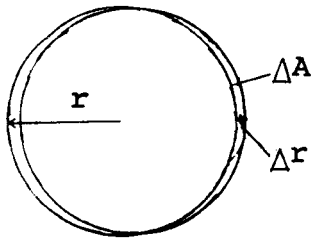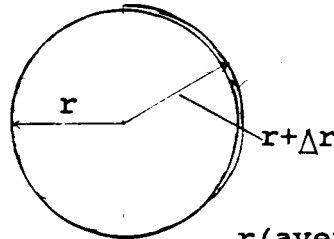
$r(average) = r + \triangle r/2$

$$\triangle A \approx \frac{PIx((r+\triangle r(average))^2 - r^2)}{2}$$

$$\frac{2 * \triangle A}{PI} = (r + \triangle r(average))^2 - r^2$$

$$= r^2 + 2\triangle r(avg)r + \triangle r(avg)^2 - r^2$$

$$\triangle r(avg)^2 + 2r\triangle r(avg) - \frac{2\triangle A}{PI} = 0$$

$\triangle A = (.001) \times (.7854) = .0007854$, $\frac{2\triangle A}{PI} = .0005$

$\triangle r(avg)^2 + \triangle r(avg) - .0005 = 0$

by pathagorean theorem $\triangle r(avg) = .0005$ m

maximun $\triangle r = 2\triangle r(avg) = .001$ m

$\triangle r = d \times theta$, $theta = \frac{\triangle r}{d} = .000065$ radians

y

$$theta = \frac{delta}{X}$$

$delta = X \times theta = (5.75)(.000065)$
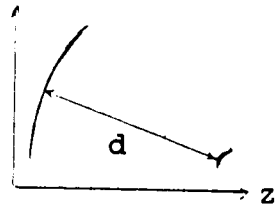
$delta = .00037$ m

maximum allowable deflection $= .00037$ m

B.1.2 Calculation of section masses:

mass = length x area x density

Section 1: upper and lower triangles-
    mass = (187.2 m)x(.00009 m^2)x(2490 kg/m^3)=41.9 kg

    diagonals-
    mass = (75.7 m)x(.00013 m^2)x(2490 kg/m^3)= 24.44 kg

    core-
    mass = (89.52 m)x(.00015 m^2)x(2490 kg/m^3)= 33.4 kg

    total mass = 99.75 kg

Section 2:
    mass = (131.16 m)x(.000643 m^2)x(2490 kg/m^3)=210 kg

Section 3:
    mass = (72.6 m)x(.00022 m^2)x(2490 kg/m^3) = 39.8 kg

B.1.3 Truss structural analysis:

The truss structural analysis was done on an IBM PC using the software package "Structural Analysis Software for Microcomputers" , 2nd edition, by B. J. Korites

This software uses the direct stiffness method to set up a system of equations governing the behavior of the structure under applied loads. The Gauss-Jordan technique is then used to determine the direct solution of the system of equations.

The analysis had to be run in three sections, truss sections 1,2, & 3, because of the size of the structure and the limitations of the software.

The results of the analysis indicated that the outer edge of the primary mirror was deflected .000334 m in the direction parallel to the beam. The maximum allowable deflection was computed as .00037 m.

$$\frac{.000334}{.00037} = .9027$$

Therefore, the deflection was 90.27 % of that allowed.

APPENDIX C. AEROBRAKE CALCULATIONS

C.1 EQUATIONS OF THE SHAPE

The shape of the ballute was modeled by hybrid blending of a hyperbola and an ellipse.

xhm = maximum hyperbolic x
yhm = maximum hyperbolic y
xm = maximum elliptical x
ym = maximum elliptical y

On x ϵ [a,xhm] the shape is given by:

$$\frac{x^2}{a^2} - \frac{y^2}{b^2} = 1$$

where a and b are constants. The value of b was chosen to approximately the cap radius, therefore, the turn-down angle (θ) could be approximated by:

$$\theta = \tan^{-1}(b/a)$$

since the hyperbola asymptoted to this angle near this point (see the figure below).

On x ϵ [xhm,xm] the shape is given by:

$$\frac{(x-xm)^2}{be^2} + \frac{y^2}{ym^2} = 1$$

where be, xm, and ym are constants. ym is prescribed as the ballute diameter. xm and be are determeined by blending the slopes of the shape equations at the intersection.
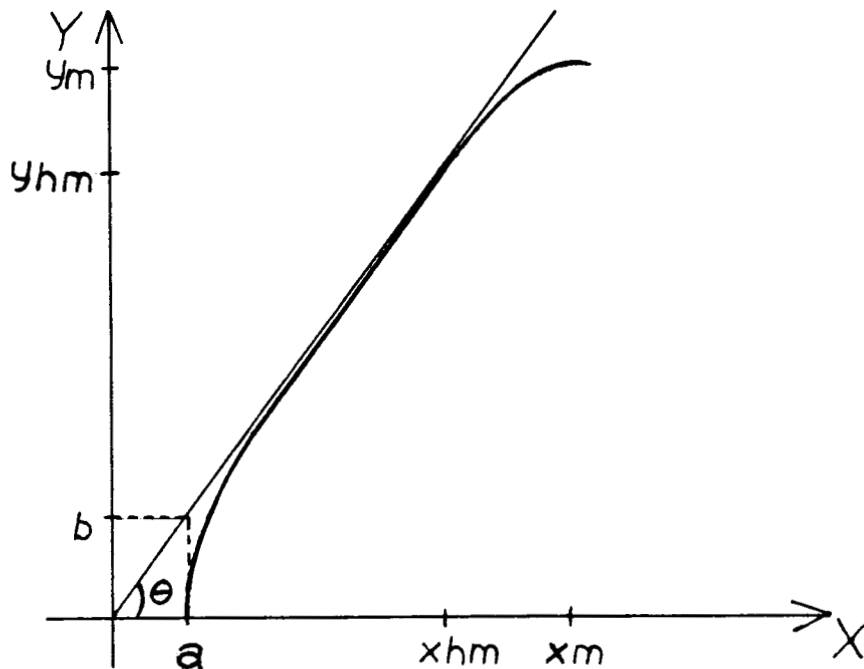
C.2 PRESSURE DISTRIBUTION

The pressure distribution on the front of the aerobrake was determined using modified Newtonian Theory;

$$C_P = C_P)_{max} (d \cdot n)^2$$

where C_P = coefficient of pressure = $(p - p_\infty)/q_\infty$

$C_P)_{max} = (p_0 - p_\infty)/q_\infty$

d = unit vector in the direction of the velocity.
   = $\cos\alpha\cos\beta \, i + \sin\alpha\sin\beta \, j + \sin\beta \, k$

α = angle of attack.

β = side-slip angle.

n = unit outward normal to the surface of the aerobrake.

For the hyperbolic portion,

$$n = \frac{- (x/a^2)i + (y/b^2)j + (z/b^2)k}{(\, (x^2/a^4) + (y^2 + z^2)/b^4 \,)^{1/2}}$$

For the elliptic portion,

$$n = \frac{((x - xm)/be^2)i + (y/ym^2)j + (z/ym^2)k}{(\, ((x - xm)^2/be^4) + (y^2 + z^2)/ym^4 \,)^{1/2}}$$

For the pressure distribution on the back of the aerobrake, it was assumed that the flow was separated and that the pressure on the back was uniform and equal to the free stream pressure.

C.3 RESULTANT FORCE CALCULATIONS

The total force resulting from the aerodynamic load is given by

$$F = - \iint_S P \, n \, dS = - \iint_S P \, n \, dS - \iint_S P_\infty \, n \, dS$$

where the integral is taken over both the front and back surfaces of the aerobrake and the second integral on the right hand side

203

is equal to zero. Therefore,

$$F = -\iint\limits_{Sf} (P - P_\infty)\, n\, dS$$

and the integral is taken over only the front surface since $(P - P_\infty)$ is equal to zero on the back surface.

The axial force, defined as the force acting in the x - direction, fixed relative to the body of the aerobrake is equal to

$$F_A = F \cdot i$$

$$= -\iint\limits_{Sf} (P - P_\infty)\, n \cdot i\, dS$$

Similatly, the side and tangential forces are defined as

$$F_T = -\iint\limits_{Sf} (P - P_\infty)\, n \cdot j\, dS \; ; \; F_Z = -\iint\limits_{Sf} (P - P_\infty)\, n \cdot k\, dS$$

Deviding each term by the dynamic pressure and the frontal surface area yeilds:

$$C_A = -\frac{1}{A} \iint\limits_{Sf} C_p\, n \cdot i\, dS$$

$$C_T = -\frac{1}{A} \iint\limits_{Sf} C_p\, n \cdot j\, dS$$

$$C_Z = -\frac{1}{A} \iint\limits_{Sf} C_p\, n \cdot k\, dS$$

Using C_p, and n as derived above, these intgrations were done numerically.

The coefficients for lift, drag and side force were then determined by

$$C_D = C_A \cos\alpha \cos\beta + C_T \sin\alpha \cos\beta + C_Z \sin\beta$$

$$C_L = -C_A \sin\alpha + C_T \cos\alpha$$

$$C_S = -C_A \cos\alpha \sin\beta - C_T \sin\alpha \sin\beta + C_Z \cos\beta$$

C.4 CALCULATION OF THE PITCHING MOMENT

The total moment (taken about the origin) caused by the aerodynamic load is equal to

$$M = -\iint_{S} P \, (r \times n) \, dS \ = \ -\iint_{Sf} (P - P_\infty) \, (r \times n) \, dS$$

where $r = xi + yj + zk$

Deviding by the dynamic pressure and the frontal area yields

$$C_m * c = \frac{1}{A} \iint_{Sf} C_P (r \times n) \, dS$$

where c is a characteristic chord length.
The coefficient of the pitching moment is the k component of this expression.

C.5 AERODYNAMIC ANALYSIS

DIAMETER = 20 m
TURN-DOWN ANGLE = 60 DEGREES

ALPHA	CA	CT	CD	CL	L/D	CMle*chord
-25	0.929	-0.086	0.878	0.315	0.359	-1.518
-20	0.990	-0.072	0.955	0.271	0.284	-1.274
-15	1.040	0.056	1.019	0.215	0.211	-0.991
-10	1.077	-0.038	1.067	0.149	0.140	-0.678
-5	1.099	-0.019	1.097	0.077	0.070	-0.344
0	1.077	0.000	1.107	0.000	0.000	0.000
5	1.099	0.019	1.097	-0.077	-0.070	0.344
10	1.077	0.038	1.067	-0.149	-0.140	0.678
15	1.040	0.056	1.019	-0.215	-0.211	0.991
20	0.990	0.072	0.955	-0.271	-0.284	1.274
25	0.929	0.086	0.878	-0.315	-0.359	1.518

TURN-DOWN ANGLE = 47.5 DEGREES

ALPHA	CA	CT	CD	CL	L/D	CMle*chord
-25	0.626	-0.126	0.621	0.150	0.242	-1.512
-20	0.661	-0.106	0.657	0.127	0.193	-1.269
-15	0.689	-0.082	0.687	0.099	0.144	-0.987
-10	0.709	-0.056	0.708	0.068	0.096	-0.675
-5	0.722	-0.029	0.722	0.035	0.048	-0.343
0	0.726	0.000	0.726	0.000	0.000	0.000
5	0.722	0.029	0.722	-0.035	-0.048	0.343
10	0.709	0.056	0.708	-0.068	-0.096	0.675
15	0.689	0.082	0.687	-0.099	-0.144	0.987
20	0.661	0.106	0.657	-0.127	-0.193	1.269
25	0.626	0.126	0.621	0.150	-0.242	1.512

DIAMETER = 20 m
TURN-DOWN ANGLE = 60 DEGREES

BETA	CSIDE	CN*chord
-25	0.447	-1.021
-20	0.387	-0.856
-15	0.308	-0.666
-10	0.214	-0.456
-5	0.110	-0.231
0	0.000	0.000
5	-0.110	0.231
10	-0.214	0.456
15	-0.308	0.666
20	-0.387	0.856
25	-0.447	1.021

TURN-DOWN ANGLE = 47.5 DEGREES

	CSIDE	CN*chord
-25	0.359	-0.868
-20	0.309	-0.729
-15	0.245	-0.567
-10	0.170	-0.388
-5	0.087	-0.197
0	0.000	0.000
5	-0.087	0.197
10	-0.170	0.388
15	-0.245	0.567
20	-0.309	0.729
25	-0.359	0.868

APPENDIX D. LIFE CYCLE COST CALCULATION TABLES

LOTV Life Cycle Cost Analysis
Unit and DDTE costs ($ millions)
(Non-Aerobrake)
(LEO-GEO)

	Dep. Var. (metric) (kg or N)	Dep. Var. (english) (lbm or lbf)	Unit Cost (UC) ($ mil)	DDTE Cost (DDTEC) ($ mil)
Structure & Mech (mass in lbm)	1365.00	3003.00	5.03	27.17
Thermal Cntr Sys (mass in lbm)	200.00	440.00	1.77	11.74
Propulsion System ex. main eng. (mass in lbm)	871.00	1916.20	17.99	243.11
Electric Pwr Sys (mass in lbm)	100.00	220.00	.06	13.93
Guide, Nav & Cntr (mass in lbm)	50.00	110.00	5.88	34.83
Data Mngmt & Comm (mass in lbm)	50.00	110.00	3.95	13.24
Aerobrake(fixed) (mass in lbm)	.00	.00	.00	.00
Aerobrake(dspsbl) (mass in lbm)	.00	.00	.00	.00
Main Engine (thrust in lbf)	2000.00	449.60	2.01	307.80
Primary Mirror (mass in lbm)	500.00	1100.00	5.82	17.52
Mirrors 2,3 & 4 (mass in lbm)	256.00	563.20	5.63	22.53
Cmg's (mass in lbm)	291.00	640.20	4.23	16.90
Total			52.35	708.76

Table 10.1 Unit and DDTE cost for the non-aerobrake configuration.

LOTV Life Cycle Cost Analysis
Unit and DDTE costs ($ millions)
(Aerobrake)
(LEO-GEO)

	Dep. Var. (metric) (kg or N)	Dep. Var. (english) (lbm or lbf)	Unit Cost (UC) ($ mil)	DDTE Cost (DDTEC) ($ mil)
Structure & Mech (mass in lbm)	1956.00	4303.20	6.12	31.79
Thermal Cntr Sys (mass in lbm)	200.00	440.00	1.77	11.74
Propulsion System ex. main eng. (mass in lbm)	734.00	1614.80	16.53	205.13
Electric Pwr Sys (mass in lbm)	100.00	220.00	.06	13.93
Guide, Nav & Cntr (mass in lbm)	50.00	110.00	5.88	34.83
Data Mngmt & Comm (mass in lbm)	50.00	110.00	3.95	13.24
Aerobrake(fixed) (mass in lbm)	660.00	1452.00	3.38	19.78
Aerobrake(dspsbl) (mass in lbm)	90.00	198.00	1.14	8.28
Main Engine (thrust in lbf)	2000.00	449.60	2.01	307.80
Primary Mirror (mass in lbm)	200.00	440.00	3.53	23.07
Mirrors 2,3 & 4 (mass in lbm)	256.00	563.20	5.63	22.53
Cmg's (mass in lbm)	291.00	640.20	4.23	16.90
Total			54.22	709.42

Table 10.2 Unit and DDTE cost for the aerobrake, LEO-GEO configuration.

9202.60

LOTV Life Cycle Cost Analysis
Unit and DDTE costs ($ millions)
(Aerobrake)
(LEO-LLO)

	Dep. Var. (metric) (kg or N)	Dep. Var. (english) (lbm or lbf)	Unit Cost (UC) ($ mil)	DDTE Cost (DDTEC) ($ mil)
Structure & Mech (mass in lbm)	2650.00	5830.00	7.22	36.30
Thermal Cntr Sys (mass in lbm)	250.00	550.00	1.99	12.94
Propulsion System ex. main eng. (mass in lbm)	891.00	1960.20	18.19	248.65
Electric Pwr Sys (mass in lbm)	100.00	220.00	.06	13.93
Guide, Nav & Cntr (mass in lbm)	50.00	110.00	5.88	34.83
Data Mngmt & Comm (mass in lbm)	50.00	110.00	3.95	13.24
Aerobrake(fixed) (mass in lbm)	700.00	1540.00	3.49	20.29
Aerobrake(dspsbl) (mass in lbm)	400.00	880.00	2.58	15.89
Main Engine (thrust in lbf)	2000.00	449.60	2.01	307.80
Primary Mirror (mass in lbm)	1400.00	3080.00	10.20	54.94
Mirrors 2,3 & 4 (mass in lbm)	512.00	1126.40	11.26	45.06
Cmg's (mass in lbm)	291.00	640.20	4.23	16.90
Total			71.06	820.77

Table 10.3 Unit and DDTE cost for the aerobrake, LEO-LLO configuration.

LOTV Life Cycle Cost Analysis: Initial Acquisition Cost
(Non-Aerobrake, LEO-GEO)

	($ millions)
Total LOTV dry weight (lbm)	
LOTV unit or material cost (UC)	52.35
LOTV design, development, test and evaluation cost (DDTEC)	708.76
Cost of initial LOTV delivery to LEO (IDC)	13.80
Ground support equipment cost (GSEC)	70.88
Systems engineering and integration cost for the DDTE phase (SEIC)	77.96
Program management cost for the DDTE phase (PMC)	42.88
Installation, checkout and assembly cost for the DDTE phase (ICAC)	10.47
Systems engineering and integration cost for the production phase (SEIPC)	6.28
Program management cost for the production phase (PMPC)	3.46
Orbital support equipment cost (OSEC)	77.49
Cost of initial spares (ISC)	38.50
Cost of initial LOTV system assembly at the space station (IAC)	35.00
Total initial LOTV system acquisition cost (TAC)	1137.83

Table 10.4 Initial acquisition and deployment cost for the non-aerobrake configuration.

LOTV Life Cycle Cost Analysis: Initial Acquisition Cost (Aerobrake, LEO-GEO)

Total LOTV dry weight (lbm)   11191.40

	($ millions)
LOTV unit or material cost (UC)	54.22
LOTV design, development, test and evaluation cost (DDTEC)	709.42
Cost of initial LOTV delivery to LEO (IDC)	16.79
Ground support equipment cost (GSEC)	70.94
Systems engineering and integration cost for the DDTE phase (SEIC)	78.04
Program management cost for the DDTE phase (PMC)	42.92
Installation, checkout and assembly cost for the DDTE phase (ICAC)	10.84
Systems engineering and integration cost for the production phase (SEIPC)	6.51
Program management cost for the production phase (PMPC)	3.58
Orbital support equipment cost (OSEC)	78.04
Cost of initial spares (ISC)	38.50
Cost of initial LOTV system assembly at the space station (IAC)	41.25
Total inital LOTV system acquisition cost (TAC)	1151.05

Table 10.5   Initial acquisition and deployment cost for the aerobrake, LEO-GEO configuration.

LOTV Life Cycle Cost Analysis: Initial Acquisition Cost (Aerobrake, LEO-LLO)

Total LOTV dry weight (lbm)   17146.80

	($ millions)
LOTV unit or material cost (UC)	71.06
LOTV design, development, test and evaluation cost (DDTEC)	820.77
Cost of initial LOTV delivery to LEO (IDC)	25.72
Ground support equipment cost (GSEC)	82.08
Systems engineering and integration cost for the DDTE phase (SEIC)	90.28
Program management cost for the DDTE phase (PMC)	49.66
Installation, checkout and assembly cost for the DDTE phase (ICAC)	14.21
Systems engineering and integration cost for the production phase (SEIPC)	8.53
Program management cost for the production phase (PMPC)	4.69
Orbital support equipment cost (OSEC)	91.76
Cost of initial spares (ISC)	38.50
Cost of initial LOTV system assembly at the space station (IAC)	47.50
Total inital LOTV system acquisition cost (TAC)	1344.75

Table 10.6   Initial acquisition and deployment cost for the aerobrake, LEO-LLO configuration.

LOTV Life Cycle Cost Analysis   (Non-Aerobrake, LEO-GEO)
Operation and Support Costs per Mission

Mass of Fuel and Other Cryogens (lbm)   44000.00

($ millions)

Fuel and Cryogen Cost (FCC)	66.22
Space Station Crew Support Cost (SSCSC)	7.50
Spare Parts Cost (SPC)	.20
Operations and Support Management Costs (OSMC)	.86
Total Operation and Support Cost per Mission (TOSC)	74.78
LOTV Overhaul Cost (OC) (performed once every 30 missions)	38.75

LOTV Life Cycle Cost Analysis   (Aerobrake, LEO-GEO)
Operation and Support Costs per Mission

Mass of Fuel and Other Cryogens (lbm)   30800.00

($ millions)

Fuel and Cryogen Cost (FCC)	46.35
Space Station Crew Support Cost (SSCSC)	9.00
Spare Parts Cost (SPC)	.20
Operations and Support Management Costs (OSMC)	.86
Cost of New Ballute for Each Mission (BC)	2.27
Total Operation and Support Cost per Mission (TOSC)	58.68
LOTV Overhaul Cost (OC) (performed once every 20 missions)	39.02

Table 10.7 Operation and support costs for the non-aerobrake configuration with a transport cost of $1500/lbm.

Table 10.8 Operation costs for the aerobrake, LEO-GEO configuration with a transport cost of $1500/lbm.

LOTV Life Cycle Cost Analysis   (Aerobrake, LEO-LLO)
Operation and Support Costs per Mission

Mass of Fuel and Other Cryogens (1bm)   50600.00

($ millions)

Fuel and Cryogen Cost (FCC)   76.15

Space Station Crew Support Cost (SSCSC)   10.25

Spare Parts Cost (SPC)   .30

Operations and Support Management Costs (OSMC)   .96

Cost of New Ballute for Each Mission (BC)   5.49

Total Operation and Support Cost per Mission (TOSC)   93.15

LOTV Overhaul Cost (OC) (performed once every 20 missions)   65.88

Table 10.9 Operation and support costs for the aerobrake, LEO-LLO configuration with a transport cost of $1500/lbm.

LOTV Life Cycle Cost Analysis   (Non-Aerobrake, LEO-GEO)
Operation and Support Costs per Mission

Mass of Fuel and Other Cryogens (1bm)   44600.00

($ millions)

Fuel and Cryogen Cost (FCC)   22.22

Space Station Crew Support Cost (SSCSC)   7.50

Spare Parts Cost (SPC)   .20

Operations and Support Management Costs (OSMC)   .86

Total Operation and Support Cost per Mission (TOSC)   30.78

LOTV Overhaul Cost (OC) (performed once every 30 missions)   38.75

Table 10.10 Operation and support costs for the non-aerobrake configuration with a transport cost of $500/lbm.

LOTV Life Cycle Cost Analysis (Aerobrake, LEO LEO)
Operation and Support Costs per Mission

Mass of Fuel and Other Cryogens (lbm)	3x00.00
	($ millions)
Fuel and Cryogen Cost (FCC)	25.55
Space Station Crew Support Cost (SSCSC)	10.25
Spare Parts Cost (SPC)	.30
Operations and Support Management Costs (OSMC)	.96
Cost of New Ballute for Each Mission (BC)	3.49
Total Operation and Support Cost per Mission (TOSC)	42.55
LOTV Overhaul Cost (OC) (performed once every 20 missions)	45.88

Table 10.12 Operation and support costs for the aerobrake, LEO-GEO configuration with a transport cost of $500/lbm.

LOTV Life Cycle Cost Analysis (Aerobrake, LEO-GEO)
Operation and Support Costs per Mission

Mass of Fuel and Other Cryogens (lbm)	30800.00
	($ millions)
Fuel and Cryogen Cost (FCC)	15.55
Space Station Crew Support Cost (SSCSC)	9.00
Spare Parts Cost (SPC)	.20
Operations and Support Management Costs (OSMC)	.86
Cost of New Ballute for Each Mission (BC)	2.27
Total Operation and Support Cost per Mission (TOSC)	27.88
LOTV Overhaul Cost (OC) (performed once every 20 missions)	39.02

Table 10.11 Operation and support costs for the aerobrake, LEO-GEO configuration with a transport cost of $1500/lbm.

LOTV Life Cycle Cost Analysis (Non-Aerobrake, LEO-GEO)
Operation and Support Costs per Mission

Mass of Fuel and Other Cryogens (lbm)   44000.00

($ millions)

Fuel and Cryogen Cost (FCC)	6.82
Space Station Crew Support Cost (SSCSC)	7.50
Spare Parts Cost (SPC)	.20
Operations and Support Management Costs (OSMC)	.86
Total Operation and Support Cost per Mission (TOSC)	15.38
LOTV Overhaul Cost (OC) (performed once every 30 missions)	38.75

Table 10.13 Operation and support costs for the non-aerobrake configuration with a transport cost of $150/lbm.

LOTV Life Cycle Cost Analysis (Aerobrake, LEO-GEO)
Operation and Support Costs per Mission

Mass of Fuel and Other Cryogens (lbm)   30800.00

($ millions)

Fuel and Cryogen Cost (FCC)	4.77
Space Station Crew Support Cost (SSCSC)	9.00
Spare Parts Cost (SPC)	.20
Operations and Support Management Costs (OSMC)	.86
Cost of New Bellute for Each Mission (BC)	2.27
Total Operation and Support Cost per Mission (TOSC)	17.10
LOTV Overhaul Cost (OC) (performed once every 20 missions)	39.02

Table 10.14 Operation and support costs for the aerobrake, LEO-GEO configuration with a transport cost of $150/lbm.

LOTV Life Cycle Cost Analysis (Aerobrake, LEO-LLO)
Operation and Support Costs per Mission

	($ millions)
Mass of Fuel and Other Cryogens (lbm)	50600.00
Fuel and Cryogen Cost (FCC)	7.84
Space Station Crew Support Cost (SSCSC)	10.25
Spare Parts Cost (SPC)	.30
Operations and Support Management Costs (OSMC)	.96
Cost of New Ballute for Each Mission (BC)	5.49
Total Operation and Support Cost per Mission (TOSC)	24.86
LOTV Overhaul Cost (OC) (performed once every 20 missions)	85.88

Table 10.15 Operation and support costs for the aerobrake, LEO-LLO configuration with a transport cost of $150/lbm.

Cumulative Discounted Life Cycle Cost ($ millions)

YEAR	Non-Aero (LEO-GEO)	Aerobrake (LEO-GEO)	Aerobrake (LEO-LLO)
0	1137.83	1151.05	1344.75
1	1817.65	1684.50	2191.57
2	2435.66	2201.71	2999.32
3	3026.61	2642.58	3699.17
4	3537.37	3070.03	4366.73
5	4001.69	3434.38	4945.12
6	4445.68	3787.64	5496.83
7	4829.42	4088.76	5974.83
8	5178.27	4380.71	6430.79
9	5511.85	4629.57	6825.84
10	5800.16	4870.85	7202.66
11	6062.26	5076.52	7529.14
12	6312.88	5275.93	7840.57
13	6529.49	5445.90	8110.39
14	6726.41	5610.70	8367.76
15	6914.70	5751.18	8590.76
16	7077.44	5887.37	8803.46
17	7225.39	6003.47	8987.76
18	7366.86	6116.03	9163.55
19	7489.13	6211.98	9315.85
20	7600.29	6299.20	9454.32	→ Total life cycle cost

Table 10.16 10 missions/year at $1500/lbm.

213

Cummulative Discounted Life Cycle Cost ($ millions)

YEAR	Non-Aero (LEO-GEO)	Aerobrake (LEO-GEO)	Aerobrake (LEO-LLO)
0	1137.83	1151.05	1344.75
1	1417.65	1404.50	1731.57
2	1672.03	1667.17	2121.14
3	1932.40	1876.63	2440.82
4	2142.63	2093.71	2762.78
5	2333.75	2266.82	3026.98
6	2529.37	2446.22	3293.07
7	2687.32	2589.29	3511.41
8	2830.91	2737.56	3731.32
9	2977.88	2855.79	3911.77
10	3096.55	2978.33	4093.51
11	3204.43	3076.04	4242.64
12	3314.85	3177.31	4392.84
13	3404.01	3258.07	4516.09
14	3485.06	3341.76	4640.22
15	3568.03	3408.51	4742.08
16	3635.01	3477.67	4844.67
17	3695.91	3532.83	4928.85
18	3758.24	3589.99	5013.63
19	3808.57	3635.58	5083.20
20	3854.32	3677.02	5146.45

Total life cycle cost

Table 10.17   10 missions/year at $500/lbm.

Cummulative Discounted Life Cycle Cost ($ millions)

YEAR	Non-Aero (LEO-GEO)	Aerobrake (LEO-GEO)	Aerobrake (LEO-LLO)
0	1137.83	1151.05	1344.75
1	1277.65	1306.50	1570.57
2	1404.76	1480.07	1813.77
3	1549.42	1608.55	2000.40
4	1654.47	1752.00	2201.40
5	1749.97	1858.17	2355.64
6	1858.66	1976.72	2521.75
7	1937.58	2064.47	2649.22
8	2009.33	2162.45	2786.50
9	2090.99	2234.97	2891.85
10	2150.29	2315.94	3005.30
11	2204.19	2375.88	3092.37
12	2265.54	2442.80	3186.13
13	2310.09	2492.33	3258.09
14	2350.59	2547.63	3335.58
15	2396.69	2588.57	3395.04
16	2430.16	2634.28	3459.09
17	2460.53	2668.11	3508.23
18	2490.22	2705.88	3561.16
19	2520.37	2733.84	3601.78
20	2543.23	2759.26	3638.70

Total life cycle cost

Table 10.18   10 missions/year at $150/lbm.